From single proteins to supercomplexes: a proteomic view on plant mitochondria

Von der Naturwissenschaftlichen Fakultät der

Gottfried Wilhelm Leibniz Universität Hannover

zur Erlangung des Grades

Doktor der Naturwissenschaften (Dr. rer. nat.)

genehmigte Dissertation

von

Nils Rugen, M.Sc.

2019

Referent: Prof. Dr. rer. nat. Hans-Peter Braun

Korreferent: Dr. rer. nat. Sascha Offermann

Tag der Promotion: 14.11.2019

The following publications contributed to this thesis:

1. Senkler, J., **Rugen, N**., Eubel, H., Hegermann, J., & Braun, H.-P. (2018)

   Absence of Complex I Implicates Rearrangement of the Respiratory Chain in European Mistletoe.

   Current Biology, *28*(10), 1606-1613.

2. **Rugen, N**., Straube, H., Franken, L. E., Braun, H.-P., & Eubel, H. (2019).

   Complexome profiling reveals association of PPR proteins with ribosomes in the mitochondria of plants.

   Molecular & Cellular Proteomics, *18*, 1345–1362.

3. Fuchs, P.*, **Rugen, N*.**, Carrie, C., Elsässer, M., Finkemeiner, I., Giese, J., Hildebrandt, T.M., Kühn, K., Maurio, V.G., Ruberti, C., Schallenberg-Rüdinger, M., Steinbeck, J., Braun, H.-P., Eubel, H., Meyer, E.H., Müller-Schüssele, S.J., Schwarzländer, M. (2019)

   Single organelle function and organization as estimated from Arabidopsis mitochondrial proteomics.

   The Plant Journal, in press, DOI: 10.1111/tpj.14534

   * co-first authorship

Abstract

The primary function of plant mitochondria is respiration, which is why they are often referred to as "powerhouses of the cell". Besides their central role in energy metabolism, plant mitochondria are also involved in the photorespiratory C2 cycle and in the provision of carbon skeletons to support efficient nitrogen assimilation. All these functions are catalyzed by mitochondrial proteins. Their composition, abundance and interactions in plant mitochondria are the subject of this thesis. In yeast, Trypanosomes, and several mammalian cell types, mitochondria are organized as extensive mitochondrial networks, resulting in a situation where a cell only hosts few but large mitochondria. In plants, hundreds of small mitochondria are only connected by fusion and fission over time but not physically. Hence, the organelles form individual, functional units. Paradoxically, their biochemical and physiological characterization focuses on large organelle populations and thereby disregards the properties of the individual mitochondrion. This partially is based on the fact that cell biological approaches capturing structural features of plant mitochondria often are of limited value for understanding their physiological properties. **Chapter 2.1** of this thesis models the protein content of a single mitochondrion by combining proteomics with classical cell biology. Besides other insights into the function of a single plant mitochondrion, it could be shown that proteins involved in ATP synthesis and transport make up nearly half of the plant mitochondrial proteome. The five protein complexes of the OXPHOS system contribute most to this segment of the mitochondrial proteome, underlining the overall importance of mitochondrial ATP synthesis for the entire plant cell. Despite the central function of OXHPOS components in plants, certain unicellular parasites and yeasts apparently do not need a complete OXPHOS system. Intriguingly, it recently has been reported that the mitochondrial genome of the multicellular parasitic flowering plant *Viscum album* (European mistletoe) is reduced and lacks the genes encoding the mitochondrially encoded subunits of complex I. This implies that the corresponding genes either have been lost or, alternatively, were transferred to the nuclear genome. The consequences for the mitochondrial respiratory chain were so far unknown. **Chapter 2.2** presents data suggesting that *V. album* indeed lacks mitochondrial complex I. The absence of complex I is accompanied by a rearrangement of the respiratory chain including (i) stable supercomplexes composed of complexes III_2 and IV, and (ii) the occurrence of numerous alternative oxidoreductases. Mitochondria of *V. album* also possess less cristae than mitochondria from non-parasitic plants, which can be explained by low amounts of ATP synthase dimers. The mitochondrial proteome consists of proteins encoded in the nucleus or in the rudimentary mitochondrial genome. The few proteins encoded on the mitochondrial genome are translated by mitochondrial ribosomes. While structure and composition of these mitoribosomes are well established in yeast and mammals, the current knowledge of plant mitoribosomes is negligible. Isolation of plant mitoribosomes is difficult due to their sedimentation coefficient, which is very close to that of cytosolic ribosomes, their interaction with the inner mitochondrial membrane, and the attachment of cytosolic ribosomes to the mitochondrial surface. As part of this dissertation, plant mitoribosomes were analyzed via a novel *complexome profiling* strategy (**chapter 2.3**). This revealed an unconventional molecular mass of the small ribosomal subunit of plants. In addition, several pentatricopeptide repeat (PPR) proteins were discovered to form part of both, the large and the small mitoribosomal subunit.

Keywords: Plant mitochondria, proteomics, protein complexes

Zusammenfassung

Die Hauptfunktion von Mitochondrien ist Respiration, weshalb sie häufig als „Kraftwerke der Zelle“ bezeichnet werden. Neben ihrer zentralen Rolle im Energiestoffwechsel sind Pflanzenmitochondrien auch am photorespiratorischen C2 Zyklus und an der Bereitstellung von Kohlenstoffgerüsten beteiligt, um effiziente Stickstoffassimilation zu unterstützen. All diese Funktionen werden dabei von mitochondrialen Proteinen katalysiert. Diese Dissertation handelt von ihrer Zusammensetzung, Häufigkeit und Interaktion in pflanzlichen Mitochondrien. In Hefen, Trypanosomen und mehreren Säugetier-Zelltypen liegen Mitochondrien als ausgedehnte mitochondriale Netzwerke vor was zur Folge hat, dass eine einzelne Zelle nur wenige, sehr große Mitochondrien in sich trägt. In Pflanzen sind hunderte kleine Mitochondrien durch Fusions- und Fissionsprozesse nur über die Zeit, nicht aber physikalisch miteinander verbunden. Die einzelnen Organellen bilden daher individuelle, funktionale Einheiten. Paradoxerweise konzentriert sich die biochemische und physiologische Untersuchung pflanzlicher Mitochondrien meist auf große Organellen-Populationen und vernachlässigt dabei die Eigenschaften der einzelnen Organellen. Dies beruht zum Teil darauf, dass zellbiologische Ansätze, die strukturelle Eigenschaften von Pflanzenmitochondrien abbilden, nur von begrenztem Wert für das Verständnis ihrer physiologischen Eigenschaften sind. **Kapitel 2.1** dieser Arbeit modelliert den Proteingehalt eines einzelnen Mitochondriums durch die Kombination von Proteomik mit klassischer Zellbiologie. Neben weiteren Einblicken in die Funktion eines einzelnen Pflanzenmitochondrions konnte herausgefunden werden, dass Proteine, die an der Synthese und dem Transport von ATP beteiligt sind, etwa die Hälfte des pflanzlichen mitochondrialen Proteoms ausmachen. Die fünf Proteinkomplexe des OXPHOS-Systems tragen dabei am meisten zu diesem Teil des Proteoms bei, was die Bedeutung der mitochondrialen ATP-Synthese für die gesamte Zelle unterstreicht. Trotz dieser zentralen Funktion der OXPHOS-Komponenten in Pflanzen scheinen einige einzellige Parasiten und Hefen kein komplettes OXPHOS-System zu benötigen. Interessanterweise wurde kürzlich berichtet, dass das mitochondriale Genom der mehrzelligen, parasitären Pflanze *Viscum Album* (Europäische Mistel) stark reduziert ist und keine Gene für die mitochondrial-kodierten Untereinheiten von Komplex I enthält. Dies impliziert, dass die entsprechenden Gene entweder verloren oder, alternativ, in das Kerngenom transferiert wurden. Die Auswirkungen auf die mitochondriale Atmungskette waren bis dato unklar. **Kapitel 2.2** präsentiert Daten die nahelegen, dass *V. album* tatsächlich keinen mitochondrialen Komplex I besitzt. Das Fehlen von Komplex I wird begleitet von einer umgeordneten Atmungskette, die sich durch (i) stabile Superkomplexe bestehend aus Komplex III_2 und IV und (ii) das Vorkommen zahlreicher alternativer Oxidoreduktasen auszeichnet. *V. Albu*m Mitochondrien besitzen außerdem weniger Cristae als Mitochondrien nicht-parasitärer Pflanzen, was durch kleinere Mengen von ATP-Synthase-Dimeren erklärt werden kann. Das mitochondriale Proteom besteht aus Proteinen, die im Zellkern oder im mitochondrialen Rest-Genom kodiert sind. Die wenigen mitochondrial-kodierten Proteine werden an mitochondrialen Ribosomen synthetisiert. Während Struktur und Zusammensetzung dieser Mitoribosomen in Hefe und Säugetieren bereits erforscht sind, ist der Wissensstand über pflanzliche Mitoribosomen überschaubar. Ihre Isolation wird erschwert durch ihren Sedimentationskoeffizienten der dem cytosolischer Ribosomen sehr ähnlich ist, durch ihre Interaktion mit der inneren mitochondrialen Membrane und durch die Bindung cytosolischer Ribosomen an die mitochondriale Oberfläche. Als Teil dieser Dissertation wurden pflanzliche Mitoribosomen mittels einer neuen *Complexome Profiling* Strategie analysiert (**Kapitel 2.3**). Es konnte dadurch gezeigt werden, dass die kleine ribosomale Untereinheit pflanzlicher Ribosomen eine ungewöhnliche molekulare Masse hat. Darüber hinaus wurden mehrere „Pentatricopeptide Repeat“ (PPR) Proteine als Teil der kleinen sowie auch der großen mitoribosomalen Untereinheit identifiziert.

Schlüsselbegriffe: Pflanzliche Mitochondrien, Proteomik, Proteinkomplexe

Contents

Abbreviations

2-PG	2-phosphoglycolate
3-PGA	3-phosphoglycerate
BCKDH	branched chain α-ketoacid dehydrogenase
BN-PAGE	blue native polyacrylamide gel electrophoresis
CA	carbonic anhydrase
ccm	cytochrome c maturation
CMS-S	S-type cytoplasmic male sterility
Cryo-ET	cryoelectron tomography
cyt c	cytochrome c
FAS	fatty acid synthase
GDC	glycine decarboxylase complex
H_2pterin	6-hydroxymethyl-7,8-dihydropterin
iBAQ	intensity-based absolute quantification
IMM	inner mitochondrial membrane
IMS	intermembrane space
LC-MS/MS	liquid chromatography coupled tandem mass spectrometry
LECA	Last Eukaryotic Common Ancestor
mb	megabases
mETC	mitochondrial electron transport chain
mtDNA	mitochondrial DNA
mtLSU	large subunit of the mitochondrial ribosome
mtSSU	small subunit of the mitochondrial ribosome
OMM	outer mitochondrial membrane
p-ABA	p-amino benzoic acid
PPR	pentatricopeptide repeat
PUMP	plant uncoupling mitochondrial protein
Q	ubiquinone
QH_2	ubiquinol
ROS	reactive oxygen species
rRNA	ribosomal RNA
RubisCO	ribulose 1,5-bisphosphate carboxylase-oxygenase
RuBP	ribulose-1,5-bisphosphate
SHMT	serine hydroxymethyltransferase
THF	tetrahydrofolate
TPR	tetratricopeptide repeat
tRNA	transfer RNA
UCP	uncoupling protein

Chapter 1: Introduction

This chapter provides the reader with the theoretical background with respect to this thesis. It is divided into three parts: the first part describes general mitochondrial features, such as structure, gene expression, and metabolic function. Part two focuses on the oxidative phosphorylation (OXPHOS) system and describes its special features in plant mitochondria. The third and final part discusses PPR proteins and RNA editing, and their connection with mitochondrial translation. It also provides a review of the protein composition of plant mitochondrial ribosomes.

1.1 Mitochondrial features & functions

1.1.1 Mitochondrial Structure

It is widely accepted that the mitochondria originate in bacterial endosymbiosis (Sagan, 1967) and that the primordial mitochondrion descends from the α-proteobacterial clade (Burger et al., 2013; Gray, 2012; Gray and Doolittle, 1982). Still, there are several divergent symbiogenetic models for the mitochondrial organelle evolution, describing different ways of how the mitochondrial ancestor entered the host and the nature of this host. Another yet unresolved question is the origin of the bulk of the mitochondrial proteome, which does seem to be of α-proteobacterial origin, indicating that the mitochondrial compartment itself is of bacterial origin while its' different functions may have more than a single origin (Cavalier-Smith, 1987). More research is necessary to untangle the exact origin of the mitochondrion and its numerous functions (reviewed in Gray, 2017). Mitochondria and α-proteobacteria are of comparable appearance with respect to size and shape, but mitochondria have developed several structural features distinguishing them from bacteria.

Mitochondria frequently undergo dynamic fusion and fission events that control mitochondrial size, shape, the number of mitochondria per cell and allow equal distribution of the mitochondrial genome (Arimura et al., 2004; Logan, 2003; Sheahan et al., 2004, 2005). Fusion and fission enables mitochondria to exist as single, individual organelles or to form large mitochondrial networks leading to cells hosting only a few large mitochondria in mammals or even a single mitochondrion like it is found in some parasitic protists (Hoitzing et al., 2015; de Souza et al., 2009; Vincent et al., 2019; Zamponi et al., 2018). In higher plants like *Arabidopsis thaliana*, cells contain hundreds of individual mitochondria which clearly sets them apart from many other eukaryotes (Logan, 2006). The number depends on factors like cell size, cell type and the cells' physiological state with young leaves hosting approximately 300 and mature leaves 450 mitochondria per cell (Preuten et al., 2010). Most of the single mitochondria in *Arabidopsis thaliana* typically have either a spherical or elongated shape and possess a variable diameter of 0.5 – 1.0 µm and a length of ~ 3.0 µm (Douce, 1985).

Due to their endosymbiont origin, mitochondria possess a double membrane with each membrane being equipped with a specific set of proteins. The outer mitochondrial membrane (OMM) envelopes the inner mitochondrial membrane (IMM) which is characterized by pleomorphic invaginations, the so-called "cristae", which are connected to the IMM via narrow tubular segments also known as "crista junctions". With the formation of cristae, the IMM is functionally divided into the inner boundary membrane and the cristae membrane. The inner boundary membrane surrounds the aqueous matrix, which houses enzymes belonging to the pyruvate dehydrogenase complex (PDC), the TCA cycle, glycine decarboxylation in the frame of photorespiration and other enzymes. The cristae membrane encloses the intercristal space. While the inner boundary membrane is equipped with transport proteins for metabolites and ADP/ATP, the cristae membrane mainly hosts the high abundant complexes of the oxidative phosphorylation (OXPHOS) system (Logan, 2006; Mannella, 2006). The cristae structure is most likely not just a result of random invagination of the inner membrane. Instead, the respiratory complex V (ATP synthase) forms dimers that assemble into rows which introduce membrane

curvatures ultimately shaping the cristae (Davies et al., 2012; Dudkina et al., 2005a; Hahn et al., 2016). Complex V dimers, reconstituted into liposomes, spontaneously assemble into rows and start bending the liposome lipid bilayer. The authors suggest that this spontaneous self-assembly is the first step in mitochondrial cristae formation (Blum et al., 2019).

OMM and IMM are separated by the “intermembrane space”, but the two membranes are connected via so-called “contact sites”, first described by Charles R. Hackenbrock in 1968 (Hackenbrock, 1968). By application of chemical fixation and electron microscopy he could show sites with no identifiable space between OMM and IMM. Today we know that there is at least one more type of contact site besides the one described by Hackenbrock. In this type, inner and outer membrane are connected via bridge-like structures (“Intermembrane bridges” or just “bridges”) maintaining a constant distance and separation between both membranes (Perkins et al., 2001; Senda and Yoshinaga-Hirabayashi, 1998). Hackenbrock suggested that the close proximity of OMM and IMM in the contact sites might be used for the direct transport of small molecules between cytosol and the mitochondrial matrix (Hackenbrock, 1968; Logan, 2006) while Senda and Yoshinaga-Hirabayashi suggested that intermembrane bridges maintain mitochondrial structure and organization by keeping OMM and IMM apart and thereby keeping the intermembrane space an perceivable compartment (Logan, 2006; Senda and Yoshinaga-Hirabayashi, 1998).

Several studies also indicate that contact sides are involved in protein import. Cytosolic 80S ribosomes selectively attach to OMM regions which are in contact with the IMM but are not detectable in OMM areas that are not in close proximity to the IMM (Kellems et al., 1975). Precursor proteins stuck during translocation were identified in both OMM and IMM, leading to the term “translocation contact sites” (Schleyer and Neupert, 1985; Schwaiger et al., 1987). Arrested translocation intermediates allow the co-isolation of the translocase of the outer membrane (TOM) complex and the preprotein translocase of the inner membrane (TIM) complex, indicating the necessity for close proximity of TOM and TIM for the coordinated performance of both complexes (Dekker et al., 1997; Schülke et al., 1999). In plant mitochondria, TIM-17 connects both OMM and IMM via a c-terminal domain that is also necessary for correct protein import (Murcha et al., 2005). To date, it is not clarified if all contact sites are translocation contact sites or if different types of contact sites have their own specific function (reviewed in Logan, 2006).

1.1.2 Biogenesis of mitochondria

Due to the fact that mitochondria are semiautonomous organelles containing their own genome, they are not synthesized *de novo*. Mitochondrial biogenesis can be defined as the increase in mitochondrial number but also in mass (Millar et al., 2008). During seed germination, “new and complete” mitochondria originate from fission of already existing, unstructured “promitochondria” (based on the "maturation model" by Plattner et al., 1970) which lack typical mitochondrial features like cristae structures or high respiratory activity and which have to undergo conversion into fully active mitochondria (Howell et al., 2006, 2007; Logan et al., 2001).

Since the mitochondrial genome of flowering plants only contains between 20 and 40 protein coding genes (Kubo and Newton, 2008; Morley and Nielsen, 2017), the bulk of mitochondrial proteins is synthesized within the cytosol and imported into the mitochondria afterwards. The biogenesis as well as maintenance of mitochondria therefore require coordination of both, the mitochondrial and the nuclear genome and comprise several steps involving the expression of mitochondrial and nuclear genes, protein targeting, import and -where necessary- assembly into protein complexes or insertion into membranes, the synthesis of lipids and nucleic acids and finally the regulation of fusion and fission (Howell et al., 2007; Millar et al., 2008). Reflecting the central role of mitochondria, their biogenesis is

regulated by several pathways that translate external and internal stimuli ore reflect the developmental stage of the cell (Carrie et al., 2013; Welchen et al., 2014).

As outlined above, most mitochondrial proteins necessary for establishing metabolically active mitochondria have to be imported. This is reflected by the ordered assembly of mitochondrial components shortly after imbibition. The import apparatus required for translocation of nuclear encoded proteins is established first and is followed by components of the TCA cycle and the OXPHOS system (Howell et al., 2006). During the period of TCA cycle and OXPHOS establishment, ATP can be produced by glycolysis or extra-mitochondrial β-oxidation of fatty acids, which leads to accumulation of cytosolic NADH. External alternative NADH dehydrogenases can oxidize the cytosolic NADH to generate ATP, prevent overaccumulation of cytosolic NADH and build up mitochondrial membrane potential supporting mitochondrial protein import (Logan et al., 2001). In *A. thaliana*, 12 hours after imbibition under continuous light conditions mitochondria of typical size and shape can be observed (Law et al., 2012).

1.1.3 Plant mitochondrial genome

The size of the angiosperm mitochondrial genome (mitogenome) usually ranges between 200 and 700 kb but may be significantly larger, reaching 11 megabases (mb) in *Silene conica* (Sloan et al., 2012a). Compared to the size of mammalian mitogenomes (15-17 kb) or the genomes found in yeast mitochondria (19,4 & 78,9 kb for *Schizosaccharomyces pombe* and *Saccharomyces cerevisiae*, respectively), plant mitogenomes are the largest mitogenomes reported so far (Gualberto and Newton, 2017; Morley and Nielsen, 2017). The extreme difference in genome size is not reflected by a matching increase in genes since *Arabidopsis thaliana* contains 57 mitochondrial genes (Unseld et al., 1997), whereas humans possess 37 (Anderson et al., 1981) and *S. cerevisiae* 34 (Nakao et al., 2009). The mitochondrial DNA (mtDNA) primarily encodes essential components of the OXPHOS complexes I – V of the electron transport chain. In addition to this, genes of ribosomal RNA (rRNA), transfer RNA (tRNA), cytochrome c maturation (CCM) proteins and -depending on the species- a variable number of ribosomal proteins (Kubo and Newton, 2008) are found as well on the plant mitochondrial genome. Instead, the genome contains numerous non-conserved, noncoding sequences. Although some of these sequences were perhaps introduced via mitochondrial horizontal gene transfer (Bergthorsson et al., 2003; Gualberto and Newton, 2017) and a part of the mitogenome can be considered to be descended from chloroplast or nuclear DNA (Alverson et al., 2010, 2011a), the origin of most of these sequences is unclear.

Besides the non-coding regions mentioned above, plant mitogenomes are characterized by sequence repeats of different size and number. Based on their size, they are classified as either large repeats (> 500 base pairs, high recombination frequency), intermediate-sized repeats (100 – 500 base pairs, involved in infrequent recombination events) and small repeats (> 50 base pairs, involved in rare or no recombination events) (Alverson et al., 2011a). Being sites of frequent intramolecular recombination events, the large repeats are the foundation of the structural diversity in the plant mitogenome (Lonsdale et al., 1984; Stern and Palmer, 1984). Knowledge about this connection led to the postulation of the “master circle model”: a circular chromosome (the master circle chromosome) contains all genetic information of the mitochondrial genome. By intramolecular recombination, the master circle is converted into a set of equimolar subgenomic circles. (Lonsdale et al., 1984; Palmer and Shields, 1984; Sloan, 2013). As a consequence, the plant mitochondrial genome would not exist as a single, circular chromosome but rather as a population of structurally different molecules interconverting between the master circle conformation and the subgenomic circles (Gualberto and Newton, 2017; Sloan, 2013). This model is supported by restriction-based mapping, often leading to the prediction of circular chromosomes (Gualberto and Newton, 2017). However, several approaches to visualize the *in vivo* structure of plant mtDNA via gel-based techniques or electron microscopy showed that rather

linear and branched mtDNA molecules are the predominating structures of the plant mitogenome (Backert and Börner, 2000; Manchekar et al., 2006; Oldenburg and Bendich, 1996; Sloan, 2013). The existence of a linear mitochondrial genome was shown in the S-type cytoplasmic male sterility (CMS-S) genotype of maize (Schardl et al., 1984; Zabala et al., 1997). A linear state would require protection of the DNA from degradation and it could be shown that linear mtDNA molecules are indeed protected by terminally attached proteins (Gabay-Laughnan et al., 2009). Recent efforts to sequence the mitogenomes of *Mimulus guttatus* produced also data that are not reconcilable with a model only comprising a master circle and its subgenomic circles (Mower et al., 2012). All these findings support the view that not circular but noncircular mtDNA is the rule and that the circular mtDNA found in animals is an exception. As such, the plant mitogenome consists of several linear, partially overlapping concatameric chromosomes that are circularly permutable and thus can map a circular genome. Alternatively, the linear concatamers are larger than the full genome which would allow circular mapping. Both versions show structural similarities to the genome of certain bacteriophages (Bendich, 1993; Gualberto and Newton, 2017; Sloan, 2013).

Genome sequencing revealed that the plant mitochondrial genome may also exist as multichromosomal genome. The existence of plant multichromosomal genomes was first observed in mitochondria of *Cucumis sativus*, where two additional, autonomous chromosomes were identified (Alverson et al., 2011b). The number of chromosomes can exceed 100 chromosomes per genome as shown in genus *Silene* (Sloan et al., 2012b). Many of these chromosomes do not carry identifiable genes and can be lost or gained (Wu et al., 2015). The empty chromosomes may not serve any important function and could reflect an ongoing process of whole-genome loss. Wu et al. propose that this might be regarded as an ongoing selection process aimed at maintaining gene-carrying chromosomes while sorting out empty chromosomes (Wu et al., 2015).

The mitogenome of *Arabidopsis thaliana* was completely sequenced in 1997. It has a length of 366,924 nucleotides and contains 57 genes (Unseld et al., 1997). The mitogenome structure was physically mapped in 1993 and comprises five DNA molecules. Three different molecules contain the complete genome (367 kb) and can be split into two subgenomic molecules (233 and 134 kb) (Klein et al., 1994).

1.1.4 Mitochondrial function

Mitochondria host many functions essential to the cell. These functions are implemented by mitochondrial proteins. The following paragraphs give an introduction to some of the many different functions executed by mitochondria.

Participation in Photorespiration

Ribulose 1,5-bisphosphate carboxylase-oxygenase (RubisCO) catalyzes the first step of photosynthetic carbon fixation in C3 plants. A molecule CO_2 is added onto the C_5 molecule ribulose-1,5-bisphosphate (RuBP) to form the unstable C_6 molecule 3-keto-2-carboxyarabinitol-1,5-bisphosphate. This molecule decays into two C_3 molecules 3-phosphoglycerate (3-PGA) which can be used to synthesize trioses and other sugars by the Calvin cycle.

Besides for CO_2, RubisCO also has a (weaker) affinity for molecular oxygen. If RubisCO binds oxygen instead of CO_2, one molecule 3-PGA and one C_2 molecule 2-phosphoglycolate (2-PG) is generated, the latter of which is toxic.

Together with chloroplasts and peroxisomes, plant mitochondria are involved in the photorespiratory C2 cycle (often named “photorespiration”) which is able to convert two molecules 2-PG into one molecule 3-phosphoglycerate (3-PGA).

In the frame of this metabolic pathway, two mitochondrial enzymes, the glycine decarboxylase complex (GDC) and the serine hydroxymethyltransferase (SHMT), catalyze the conversion of two molecules of glycine to one molecule of serine (Bauwe et al., 2010). SHMT as well as all four proteins of the GDC are nuclear encoded and are found to be of high abundance in the matrix of green leaf mitochondria (Douce et al., 2001).

The GDC is a multi-enzyme system consisting of four types of proteins termed the P-, H-, T-, and L-proteins. Together, they serve in decarboxylating and deaminating glycine imported from the peroxisome (Peterhansel et al., 2010). The p-protein decarboxylates glycine releasing CO_2 and transferring the remaining amino methylene part to lipoamide arm of the H protein which does not function as an enzyme but as a cofactor interacting with P-, and L-protein (Bauwe and Kolukisaoglu, 2003; Douce et al., 2001). The T-protein (an aminomethyltransferase) further metabolizes the amino methylene releasing NH_3 and transferring the remaining methylene group to tetrahydrofolate (THF) yielding N^5,N^{10}-methylene tetrahydrofolate (CH_2-THF) (Bauwe and Kolukisaoglu, 2003; Douce and Neuburger, 1999). The reduced H-protein is finally reoxidized via the L-protein and electrons are transferred to FAD. The reduced $FADH_2$ is finally re-oxidized by NAD^+, which is reduced to NADH. The complex can now metabolize the next glycine molecule. The L-protein is also known as E3 subunit, which additionally forms part of the pyruvate dehydrogenase complex (PDC) and the 2-oxogluterate complex (OGDC) found in the mitochondrial TCA cycle (Bourguignon et al., 1992, 1996) as well as in the branched chain α-ketoacid dehydrogenase (BCKDH) complex (Peng et al., 2015). The importance of GDC for other processes not related to photorespiration is underlined by functional knockouts that lead to lethality even under non-photorespiratory conditions (Engel et al., 2007). It has been proposed that GDC also plays an important role for C1 metabolism by recycling glycine originating from the cytosol as part of a proposed “serine-glycine cycle” (Mouillon et al., 1999).

The mitochondrial SHMT combines CH_2-THF with a second glycine molecule to form serine and regenerate THF for GDC. Serine is transported back into the peroxisome where it is further metabolized. A bulk of the NADH generated by GDC can be oxidized and recycled within the mitochondrion by the electron transport chain. In this case, the reduction of the large amounts of NADH is mainly uncoupled from ATP synthesis via uncoupling proteins (Sweetlove et al., 2006), alternative NADH dehydrogenases and alternative oxidases (Rasmusson et al., 2004) to enable continuous flow of the respiratory C2 cycle and ultimately efficient photosynthesis (Fernie et al., 2004) (For more details, see section 1.2.3 Alternative respiratory enzymes and additional functions of the plant OXPHOS system). The remaining non-oxidized NADH can be exported via malate export into the peroxisomes where it can be used for subsequent steps of the photorespiratory cycle (Hanning and Heldt, 1993; Sweetlove et al., 2006; Zoglowek et al., 1988). At the same time, respiratory complex I knockouts in tobacco indicate that intact mitochondrial respiration is essential for optimal photosynthetic performance under photorespiratory conditions despite the operation of alternative NAD(P)H dehydrogenases (Dutilleul et al., 2003).

Also, the export of the large amounts of generated CO_2 can be linked to complexes of the respiratory chain. Under photorespiratory conditions, the high activity of RubisCO and GDC lead to imbalanced CO_2 ratio between chloroplasts and mitochondria. Passive diffusion of CO_2 across the organellar membranes potentially reduces mitochondrial CO_2 concentration and increases the CO_2 within chloroplast. Alternatively, it was suggested that CO_2 released in mitochondria could be transformed into bicarbonate by complex I-integrated carbonic anhydrases (CAs) (See also section 1.2.2. Organization of OXPHOS complexes and **Figure *2***). In this form, it could be actively transported out of the mitochondrion and into the chloroplast by bicarbonate transporters. Within the chloroplast, the bicarbonate could be re-converted into CO_2 and subsequently be fixed by RubisCO (Braun and Zabaleta, 2007).

Degradation of amino acids

Beyond being building blocks for protein synthesis, amino acids serve as electron donors to supply the electron transport chain and represent an alternative energy source during germination (Galili et al., 2014) and extended darkness (Durgud et al., 2018), as compatible osmolytes during abiotic stress conditions (Batista-Silva et al., 2019), as precursor for phytohormone synthesis (Amir, 2010) or immune signaling molecules (Hartmann et al., 2018). On the other hand, amino acids like lysine also have toxic properties that the cell needs to deal with (Batista-Silva et al., 2019). Hence, the level of amino acids within the cell have to be strictly regulated by controlled amino acid synthesis and catabolism.

While the biosynthesis of amino acids has been frequently investigated and is mainly located within chloroplasts, current knowledge about plant amino acid catabolism is rather incomplete. The major sites of the catabolic reaction are the cytosol and the mitochondria (Hildebrandt et al., 2015). Given that carbon skeletons are usually converted into TCA cycle precursors or intermediates, this localization allows effective generation of energy-rich compounds from amino acid. Before being fed into the TCA cycle, amino acids need to be deaminated. This requires presence of several aminotransferases that transfer the amino group to 2-oxogluterate (2OG), thereby producing glutamate. Regeneration of 2OG is accomplished by the mitochondrial glutamate dehydrogenase (Hildebrandt et al., 2015).

Plant mitochondria as a central hub of cofactor synthesis

Lipoic acid is an indispensable sulfur-containing cofactor for the decarboxylating activity of enzyme complexes such as GDC (See 1.1.4 Mitochondrial function for more information), PDC, OGDC and the BCKDH complex. Conveniently, mitochondria are equipped with a lipoic acid synthase (Yasuno and Wada, 1998) which adds two sulfur atoms to the octanoyl group bound to an acyl carrier protein (ACP) forming lipoyl-ACP (Douce et al., 2001; Miller et al., 2000). The final transfer to the different apoprotein subunits of the dehydrogenase complexes is performed via a lipoyltransferase (Wada et al., 2001). In parallel, chloroplasts also host a lipoic acid synthase isoform allowing them to efficiently supply the plastidic PDC with lipoic acid. While the complete pathway of mitochondrial lipoic acid biosynthesis is not fully described, there are studies indicative of a relation between the biosynthesis of fatty acids and lipoic acid in plant mitochondria. Fatty acid synthesis is initiated by malonate which can be activated in malonyl-acyl carrier protein. The fatty acid synthase (FAS) can catalyze the transformation into octanoyl-ACP, which then can be used to form lipoyl-ACP (Gueguen et al., 2000; Wada et al., 1997, 2001).

Tetrahydrofolate (5,6,7,8-tetrahydropteroyl-polyglutamate, H4PteGlun) is derivate of folate (Vitamin B9) and plays an important role as a carrier for the C1 metabolism and less frequently as an electron donor. In contrast to animals, plants can *de novo* synthesize tetrahydrofolate from 6-hydroxymethyl-7,8-dihydropterin (H_2pterin) and p-amino benzoic acid (p-ABA) within their mitochondria. Five sequential enzymes are required for this pathway: 6-hydroxymethyl-7,8-dihydropterin pyrophosphate kinase (HPPK), 7,8-dihydropteroate synthase (DHPS), dihydrofolate synthetase (DHFS), dihydrofolate reductase (DHFR) and a folylpolyglutamate synthetase (FPGS). The mitochondrial localization of all five proteins was shown in pea leaves (Neuburger et al., 1996). GFP-fusion assays and western blot analyses could also show that DHFS is only located in mitochondria (Ravanel et al., 2001). Taken together, these results strongly indicate that mitochondria are the only site of tetrahydrofolate synthesis.

Biotin (Vitamin H) is exclusively generated by the plant mitochondria. It functions as a cofactor for a small number of carboxylase enzymes involved in the frame of decarboxylation, carboxylation and transcarboxylation reactions related to the carbohydrate and fatty acid metabolism (Alban et al., 2000). Biotin is synthesized from pimeloyl-CoA in four steps, the first one being located within

peroxisomes and the last three taking place in mitochondria (Bitonti et al., 2012). The first two mitochondrial enzymes, DAPA synthase and dethiobiotin synthase (Bio1 and Bio3 in *Arabidopsis thaliana*) can also exist as a fusion protein (Millar et al., 2008). The function of biotin synthase (Bio2 in *Arabidopsis thaliana*), the enzyme catalyzing the final step in biotin synthesis, relies on three mitochondrial accessory proteins: Adrenodoxin, adrenodoxin reducatse and cysteine desulfurase (Picciocchi, 2001; Picciocchi et al., 2003). Involvement of cysteine desulfurase indicates that cysteine is a major sulfur donor linking amino acid degradation and biotin synthesis (Hildebrandt et al., 2015; Picciocchi et al., 2003).

Mitochondrial respiration

The primary function of plant mitochondria is respiration, which is why they are often referred to as "powerhouses of the cell". In mitochondria, catabolism of organic compounds is linked to the synthesis of ATP via oxidative phosphorylation (OXPHOS). The mitochondrial TCA cycle oxidizes organic acids such as pyruvate or malate to reduce NAD^+ and FAD which fuel the electron transport chain (ETC), ultimately reducing oxygen and producing a proton gradient that can be used for the formation of ATP.

The TCA cycle fulfills more functions than just generating NADH and $FADH_2$ to fuel ATP synthesis by the electron transport chain and can be seen as a central hub that is embedded in a larger metabolic network which allows it to contribute to several metabolic pathways (Sweetlove et al., 2010). In green tissue the TCA cycle provides carbon skeletons for biosynthetic processes like nitrogen assimilation (Hodges, 2002) and produces malate to export NADH via the malate-oxaloacetate shuttle to provide reducing power outside the mitochondria (Hanning and Heldt, 1993; Sweetlove et al., 2010). In both cases, a non-cyclic flux mode of the TCA cycle is required while the classical cyclic flux mode is probably only necessary during high demands for ATP that can be found in heterotrophic cells (Sweetlove et al., 2010).

The predominant flux mode depends on the metabolic circumstances of the cell. While the non-cyclic flux mode is the dominant form during the day to support nitrogen assimilation, it is the full cycle during the night to support mitochondrial ATP synthesis and export. How the mitochondrial metabolism is regulated to fit the current metabolic situation surrounding the mitochondria is not completely understood. Since the diurnal circle follows a predictable pattern, the rotation of protein synthesis and protein degradation does not seem reasonable but rather energetically unfavorable since the biosynthesis of proteins consumes high amounts of GTP. Comparison of the mitochondrial proteome at different time points during the diurnal cycle showed that changes in protein abundance barely contribute to flux regulation (Lee et al., 2010). Therefore, other mechanisms regulating enzyme activity like post-translational modifications (PTMs) or dynamic protein:protein interactions (PPIs) might constitute the regulatory basis of dynamic mitochondrial function. Recently, a study combining isotope-dilution experiments and several protein:protein interaction assays reported the interaction of TCA cycle proteins and substrate channeling of TCA cycle substrates *in vivo*, indicating the existence of TCA cycle metabolons in plant mitochondria (Zhang et al., 2017).

1.1.5 The proteome of a single plant mitochondrion

Plant mitochondria are organized as single, individual entities, which undergo dynamic fusion and fission events. Despite the fact that plant mitochondria operate as individual organelles and that nearly every mitochondrial function is constrained by the limitations of the individual organelle, most physiological and biochemical assessments are based on experiments considering bulk phase mitochondria. With the aim to get new insights into the functional and structural organization of plant mitochondria, a proteomic approach to determine the proteome of an average individual mitochondrion was designed: the protein content of a single *Arabidopsis thaliana* mitochondrion was modeled based on experimental data and theoretical considerations (**chapter 2.1**).

The generated proteome of an average single mitochondrion possesses about 1.5 million proteins and 913 different mitochondrial protein species. Proteins involved in the production and transport of ATP contributed nearly half (46%) to the total proteome (**Figure *1***). The OXPHOS complexes contributed most to this content, reflecting the importance of these protein complexes for mitochondrial function.

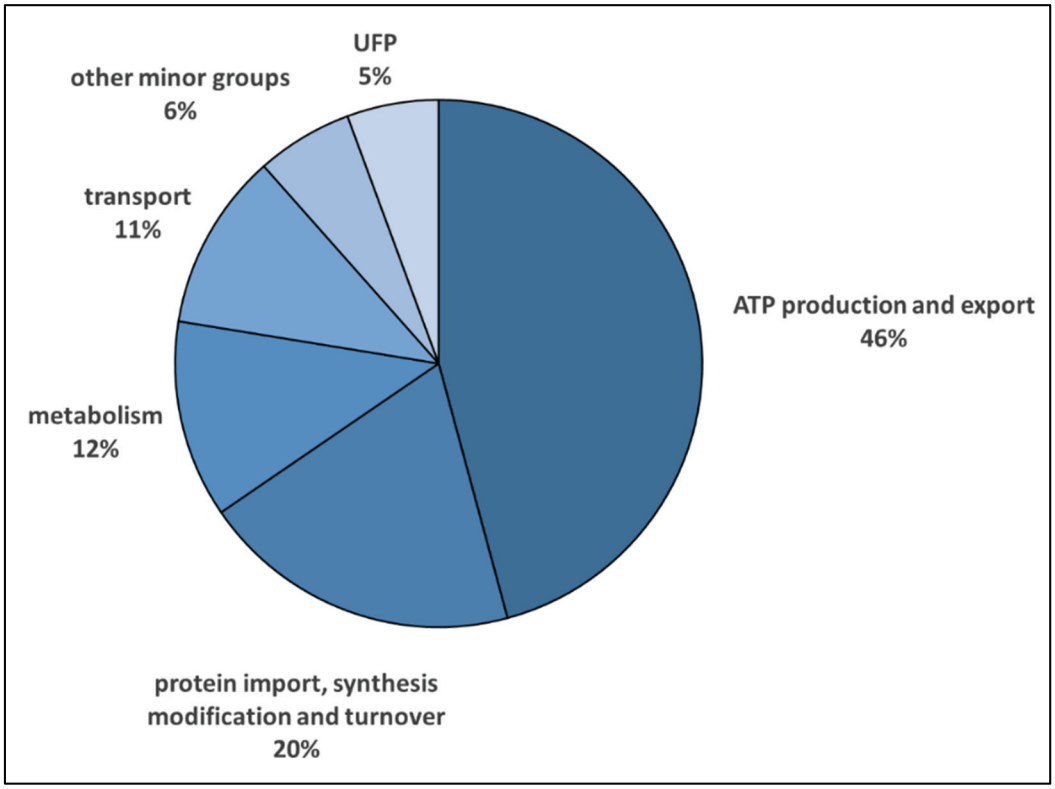

Figure 1: Proteome composition of the single mitochondrial proteome classified by meta-categories.
The contribution of each meta-category displayed with respect to total copy number contribution of the 913 proteins with mitochondrial location as identified by SUBAcon (Hooper et al., 2014). UFP: Unknown function protein.

1.2 The oxidative phosphorylation (OXPHOS) system

1.2.1 General structure and ATP synthesis

The mitochondrial electron transport chain (mETC) consists of the mitochondrial complexes I – IV and the two electron transport molecules ubiquinone and cytochrome c (Cyt c). Together with the ATP synthase (mitochondrial complex V), they form the mitochondrial oxidative phosphorylation (OXPHOS) system (**Figure *2***). In general, this system of protein complexes catalyzes oxidation of NADH and $FADH_2$ to reduce the terminal electron acceptor, oxygen. This electron flow is coupled to the translocation of protons from the matrix into the mitochondrial intermembrane space (IMS) which fuels the production of ATP (Millar et al., 2011)

Mitochondrial Complex I, the NADH dehydrogenase complex, oxidizes NADH to NAD^+ and transfers two electrons from NADH to ubiquinone (Q), thereby reducing it to ubiquinol (QH_2). Oxidation of $FADH_2$ to FAD is catalyzed by mitochondrial complex II, the succinate dehydrogenase complex (also part of the TCA cycle) which also leads to the transfer of two electrons to ubiquinone but without transfer of protons across the cristae membrane. Complex II oxidizes succinate to fumarate and reduces FAD back to $FADH_2$. Ubiquinone is lipid-soluble and functions as a mobile electron carrier within the inner mitochondrial membrane (IMM), allowing the transport of electrons from complex I and II to mitochondrial complex III_2, the ubiquinol:cytochrome c-oxidoreductase complex. Electrons are transported via the small protein cytochrome c to mitochondrial complex IV, the cytochrome-c:O_2-oxidoreductase complex. Complex IV uses four electrons to reduce one molecule of oxygen. The reduced oxygen reacts with protons located in the mitochondrial matrix and forms water. Electron transport is coupled to proton translocation into the IMS, mediated by complex I, III_2 and IV. This creates a transmembrane proton gradient and the resulting proton motive force, which can be used by mitochondrial complex V, the ATP synthase complex, to phosphorylate ADP, yielding ATP. This final step of oxidative phosphorylation transfers the protons back into the mitochondrial matrix and reduces the proton motive force (Millar et al., 2011).

1.2.2 Organization of OXPHOS complexes

During the last century, two models describing the organization of the respiratory complexes were subject of intense discussions: the “solid state” and the “fluid state” model. The solid state model predicts that individual respiratory complexes catalyzing all the reaction of the pathway assemble into functional solid state units allowing efficient catalysis of the whole pathway. These units are connected via the electron transporters ubiquinone and cytochrome c that follow enclosed, pre-defined routes allowing efficient electron transfer without electron leakage towards the outside (Fowler and Richardson, 1963; Keilin and Hartree, 1947). The liquid state model on the other hand is based on the assumption that all complexes exist as individual entities that randomly diffuse within the membrane and that ubiquinone and cytochrome c do not follow pre-defined paths between the respiratory complexes (Hackenbrock et al., 1986).

Over many years, the fluid state model was generally accepted, until Hermann Schägger and Kathy Pfeiffer could biochemically show the existence of yeast and mammalian respiratory complex assemblies, nowadays known as “respiratory supercomplexes”. Their findings also indicated existence of units catalyzing the entire process of the respiratory chain, the so-called respirasomes (Schägger and Pfeiffer, 2000). These large supercomplexes consist of the complexes I, III_2, and IV, and owe their name to the fact that they theoretically could catalyze the complete ETC reaction provided that ubiquinone and cytochrome c are available. Initially often waved aside as artifacts caused by solubilization with the mild detergents digitonin and dodecylmaltoside and protein coating with Coomassie Brilliant Blue, Schäggers and Pfeiffers findings were soon supported by experiments using

a variety of other detergents and different separation techniques like ultracentrifugation on sucrose density gradients. Simultaneously, supercomplexes were also found in other lifeforms like bacteria (Stroh et al., 2004) and plants (Eubel et al., 2003).

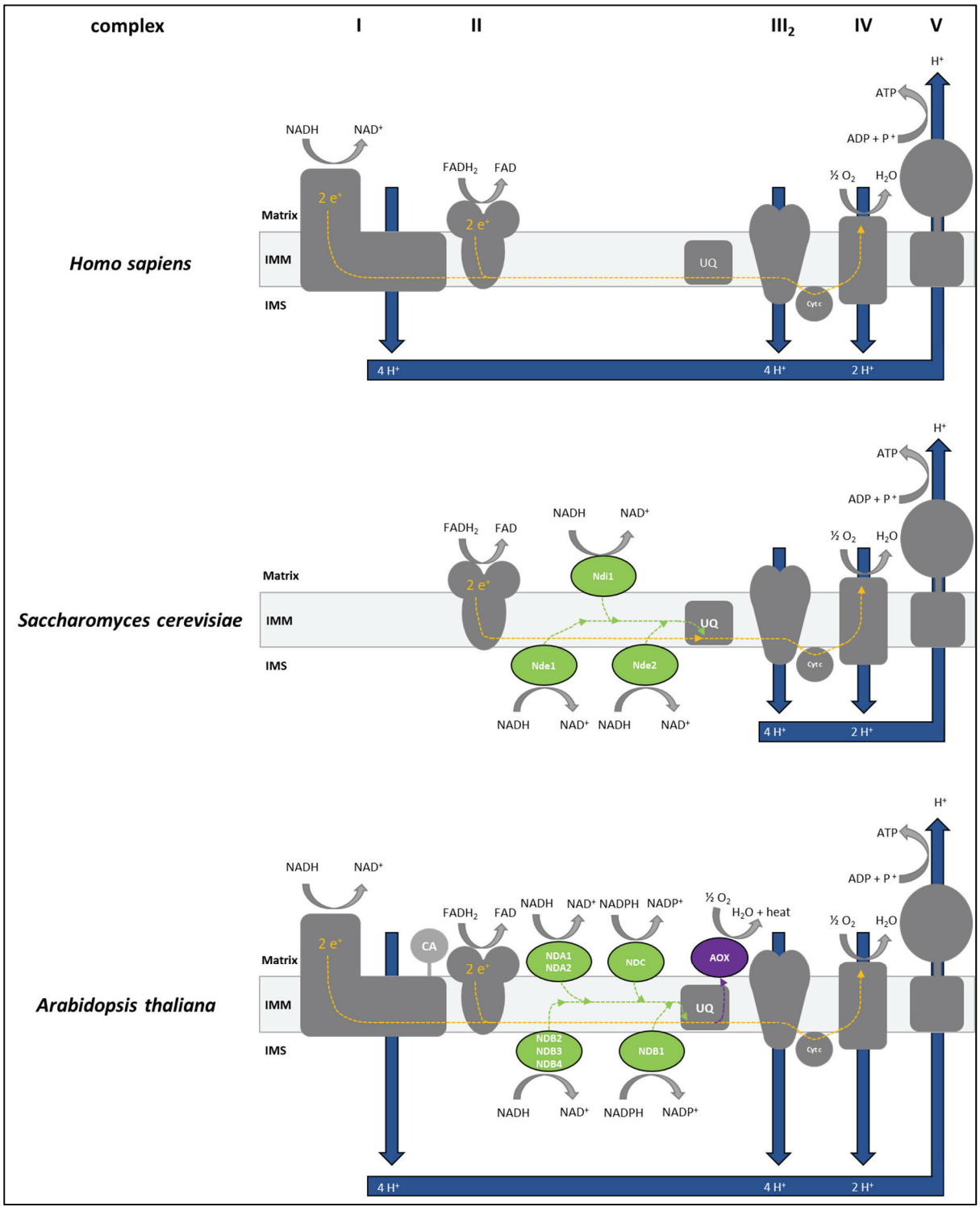

Figure 2: OXPHOS systems of *Homo sapiens*, *Saccharomyces cerevisiae* and *Arabidopsis thaliana*.
The mammalian OXPHOS system consists of the classical complexes I – V. Complex I and II oxidize NADH and FADH respectively. Electrons (orange line) are transported via ubiquinone (UQ), complex III_2, cytochrome c (cyt c) to complex IV, where molecular oxygen (O_2) is reduced to water. The coupled proton translocation from the matrix across the inner mitochondrial membrane (IMM) into the inter membrane space (IMS) (depicted as blue arrows) is used to fuel ATP synthesis at complex V. In baker's yeast, complex I is absent and three alternative NADH dehydrogenases (Ndi1, Nde1 and Nde2, in green) oxidize NADH without coupled proton translocation. In plants, numerous alternative NAD(P)H dehydrogenases (NDA1-2, NDB1-4 and NDC, green) occur and additionally an alternative oxidase (AOX, purple), which can reduce oxygen in situations of low ADP availability. CA = Plant specific carbonic anhydrase domain.

First insights into the structural organization of respiratory supercomplexes came from a study investigating the Arabidopsis I+III_2 supercomplex by negative stain single particle electron microscopy (Dudkina et al., 2005b). It could be demonstrated that the individual respiratory complexes within supercomplexes are put together in a defined way, which supports functioning of the ETC. The structures of other OXPHOS supercomplexes were resolved shortly later (summarized in Boekema and Braun, 2007). Furthermore, OXPHOS supercomplexes were also observed in the absence of detergents by cryoelectron tomography (Cryo-ET), a procedure which allows analyzing complete mitochondria (Davies et al., 2011; Dudkina et al., 2010). To date, the occurrence of respiratory supercomplexes is generally accepted.

It is currently believed that singular respiratory complexes and respiratory supercomplexes co-exist in the inner mitochondrial membrane. This conclusion is based on the reported variation of supercomplex abundance and composition under different physiological conditions (Helbig et al., 2009). In this "plasticity model", the mitochondrial electron transport chain has a rather plastic organization which allows to balance the distribution between free respiratory complexes and supercomplexes to achieve optimal performance and adjust to cellular needs (Acin-Perez and Enriquez, 2014).

Higher levels of conserved supramolecular organization of complex I and V, showing their spatial segregation in mammals, fungi and also plants, were recently described (Davies et al., 2011). While (dimeric) complex V forms long rows in the curved regions of the cristae membrane, complex I is irregularly distributed on the adjacent flat membrane regions of the cristae. This conserved arrangement generates a local proton gradient in the cristae space and thus optimizes mitochondrial ATP synthesis (Davies et al., 2011). These data underline another model of OXPHOS organization, the so-called "compartment model" (Magalon and Alberge, 2016).

1.2.3 Alternative respiratory enzymes and additional functions of the plant OXPHOS system

Being sessile organisms, plants have to adapt to abiotic or biotic stress factors like drought, metal toxicity, salinity, hypoxia, pathogen attack, extreme temperatures or phases of high light intensity. To manage these diverse challenges, plants developed several build-in mechanisms for stress perception, stress tolerance, and stress avoidance.

During high light conditions, plant leaf cells have to fight the accumulation of phosphoglycolate (2-PG) generated by RubisCO by recycling it via the photorespiratory C_2 cycle (see section 1.1.4 Mitochondrial function; section Participation in Photorespiration). This causes a drastic increase in electron insertion into the respiratory chain and coupled to this an increase in proton gradient formation. However, the mitochondrial capacity of generating ATP is limited by ADP availability. During low ADP availability, the glycine breakdown can lead to overreduction of the ETC followed by increased generation of reactive oxygen species (ROS) at complex I, II and III_2 (Brand, 2010; Jardim-Messeder et al., 2015). ROS molecules like superoxide are also produced during normal ETC operation, but at lower higher concentrations. ROS can react with and damage proteins, DNA and lipids (Foyer et al., 1997; Saed-Moucheshi et al., 2014; Suzuki et al., 2012) and at the same time function as signal molecules associated with the execution of programmed cell death or the response to pathogens (Huang et al., 2016; Møller and Sweetlove, 2010).

Besides the "classical" OXPHOS system, plant mitochondria are therefore equipped with a set of proteins that allows them to avoid increased ROS production by redirecting the electron flow through alternative, "non-phosphorylating" (non-proton-gradient-forming) pathways: alternative Type 2 NAD(P)H dehydrogenases and alternative oxidase (AOX) (Huang et al., 2016) (**Figure *2***). These enzymes

introduce additional branches into the electron transport chain that transform the “classical”, rather linear electron transport chain into a more flexible, branched system.

Alternative NAD(P)H dehydrogenases can be found in plants, protists, fungi, some bacteria, but not in animals (Rasmusson et al., 2008). In *Arabidopsis thaliana*, alternative NAD(P)H dehydrogenases are encoded by seven nuclear genes that can be divided into three subgroups: NDA (1-2), NDB (1-4) and NDC (Michalecka et al., 2003). NDA1, NDA2 and NDC are attached to the inner mitochondrial membrane, facing the mitochondrial matrix while NDB1, NDB2, NDB3 and NDB4 are attached to the inner mitochondrial membrane facing the IMS (Elhafez et al., 2006). Besides their different localizations within the inner mitochondrial membrane, the alternative NAD(P)H dehydrogenases also show different substrate specificities: NDB1 (Ca^{2+} dependent) and NADC1 show NADPH dehydrogenase activity, whereas NDB2 (Ca^{2+} stimulated), NDB3, NDB4 as well as NDA1 and NDA2 use NADH as substrate (Geisler et al., 2007). In contrast to mitochondrial complex I, oxidation of NAD(P)H via the alternative dehydrogenases is not linked to proton translocation and thus independent of available ADP (Rasmusson and Wallström, 2010). Hence, the alternative dehydrogenases allow constant NAD(P)H oxidation and ETC electron flow, thus preventing ROS formation (Waszczak et al., 2018). Several studies reported light-dependent regulation of alternative NAD(P)H dehydrogenases, indicating their role in supporting the mitochondrial transport chain in NAD(P)H oxidation during phases of high photosynthetic activity (Rasmusson and Escobar, 2007).

The alternative NAD(P)H dehydrogenase introduce an additional branch to the electron transport chain by offering alternative electron entry points and thus bypassing complex I and the proton translocation connected to it. The electrons gained from oxidation of NADH or NADPH are transferred on the ubiquinone pool, which thus becomes reduced. In the classical ETC, electrons would be transferred to complex III_2, cytochrome c, complex IV and finally reach the terminal electron acceptor molecular oxygen. Electron flow via complexes III_2 and IV in general is coupled with proton translocation across the inner mitochondrial membrane. Still, in phases of low demand for ATP (or low ADP availability), production of ROS could occur by overreduction of ubiquinone, complexes III_2 and IV. To also bypass the complexes III_2 and IV, plants mitochondria possess the alternative oxidases (AOX), which directly catalyzes electron transfer from ubiquinol onto molecular oxygen. The free energy of this reaction is transmitted as heat (Rogov and Zvyagilskaya, 2015). In *Arabidopsis thaliana*, five differentially synthesized alternative oxidases (AOX1a-AOX1d and AOX2) are located within the inner mitochondrial membrane, all facing the mitochondrial matrix (Saisho et al., 2001; Thirkettle-Watts et al., 2003).

Transcription of the genes encoding *AOX1* and *AOX2* is induced by several stimulants (Saha et al., 2016). One of the major stimuli is dysfunction of the respiratory chain complexes I, II and IV (Juszczuk et al., 2012; Vanlerberghe and McIntosh, 1994). Therefore, any factor disturbing the activity of the cytochrome pathway is a potential AOX inducer (Saha et al., 2016). It was also reported that AOX transcript and protein levels increase during drought, probably to oxidize excess reductants accumulating within the chloroplast during light conditions to preserve photosynthetic activity (Vanlerberghe et al., 2016). Several stress conditions as the ones described above do not just lead to increased AOX transcription but also ROS formation. Consequently, AOX is also induced by ROS (Vanlerberghe and McIntosh, 1994).

However, AOX activity is not only genetically controlled, but also biochemically. AOX forms homodimers and the linkage between the two monomers modulates AOX activity (Saha et al., 2016). When the monomers are non-covalently connected, AOX is in its reduced, active form while covalently bond monomers lead to the oxidized, inactive state (Rhoads et al., 1998). It was shown that the transition from the inactive to active form as well as an increase in AOX protein abundance can be induced by drought stress (Bartoli et al., 2005). In the active form, AOX activity is further adjusted by

secondary regulatory mechanisms which are not yet fully understood. Two conserved cysteine residues (Cys_I & Cys_{II}) can interact with α-keto acids like pyruvate (Cys_I) and glyoxylate (Cys_I & Cys_{II}) and modulate AOX activity (Umbach et al., 2002, 2006). Depending on whether a cysteine or a serine is present in the conserved position, AOX can be either activated by pyruvate or by succinate (Pu et al., 2015).

Besides the alternative NAD(P)H dehydrogenases, plant mitochondria include several additional proteins acting as electron donors for the ETC, like dihydroorotate dehydrogenase (DHODH), glycerol-3-phosphate dehydrogenase (G3-PDH), proline dehydrogenase (ProDH) and electron transfer flavoprotein ubiquinone oxidoreductase (ETFQO). All these enzymes catalyse electron transfer from different electron donors to the UQ pool. Similar enzymes are also present in the mitochondria from fungi and animals. Finally, cytochrome c is another entry point for electrons coming from other biochemical pathways. D-lactate dehydrogenase (DLDH) and L-galactone-1,4-lactone dehydrogenase (GLDH) transfer electrons to cytochrome c and provide an additional force driving the reduction of complex IV (Schertl and Braun, 2014).

Alternative NAD(P)H dehydrogenases and AOX help mitochondria to maintain a steady electron flow in the presence of a high proton gradient. The so-called uncoupling proteins (UCPs) or plant uncoupling mitochondrial proteins (PUMPs) are an alternative energy dissipating system to circumvent block of the electron transport chain that is caused by a high proton gradient. UCPs are integral membrane proteins of the inner mitochondrial membrane that catalyze proton translocation across the inner mitochondrial membrane from the IMS into the mitochondrial matrix. Unlike respiratory complex V, translocation via UCPs is not coupled the ATP synthesis. Instead, the energy is dissipated as heat (Vercesi et al., 2006). So, instead of avoiding proton translocation, UCPs can decrease the proton gradient itself and thereby discharge the electron transport chain and display a second level of regulation: While AOX mediates redox-potential dissipation (electrons), UCPs mediate proton electrochemical potential-dissipation.

Since UCP activity generates heat, one would expect that one of the major functions of UCPs is thermogenesis. Until now, this physiological role has only been demonstrated for mammals (Silva, 2006). While UCPs can make up to 5% of the overall mitochondrial protein content in mammals, their abundance in plants is much lower. This low abundance most likely indicates other functional roles of plant UCPs (Vercesi et al., 2006). Sweetlove et al. showed in *ucp1* knockouts that the uncoupling activity of UCP1 is essential for the mitochondrial steps of photorespiration and that it works in combination with nonphosphorylating bypasses mediated by alternative NAD(P)H dehydrogenases and AOX to uncouple mitochondria during photorespiratory conditions (Sweetlove et al., 2006). Since UCP activity is enhanced by ROS (Smith et al., 2004), the authors suggest that it is ROS accumulation during photorespiratory conditions at over-reduced ETC components which causes increased UCP activity. As a consequence, proton translocation dissipation would lead to a relieve of the thermodynamic constraint interfering with respiratory electron flow and prevent further ROS formation.

1.2.4 Life without OXPHOS?

The mitochondrial OXPHOS system is highly conserved in eukaryotes since it plays an essential role for ATP synthesis. Plants like *Arabidopsis thaliana* are equipped with a complete OXPHOS system (Complex I, II, III_2, IV and V) which is augmented by alternative oxidoreductases to balance the plant cell redox state during photosynthesis (and photorespiration) and stress situation (see chapters above & Millar et al., 2011; Schertl and Braun, 2014). Genetic manipulation to dissect the impact of the loss of functional complex I in *A. thaliana* revealed that plants can survive without complex I, but exhibit a dramatically disturbed metabolism and development. The mutants display induced abundance of

proteins involved in glycolysis, TCA cycle, and several OXPHOS components to compensate for reduced ATP synthesis caused by missing electron transport and proton translocation at complex I (Fromm et al., 2016; Kühn et al., 2015). However, due to presence of the numerous alternative respiratory enzymes, the plants can survive but are non-fertile.

Lack of complex I can occur naturally in unicellular eukaryotes. A well-known example lacking complex I is baker's yeast (*Saccharomyces cerevisiae*) (Foury et al., 1998; Gabaldón et al., 2005) (**Figure *2***). *S. cerevisiae* is a facultative anaerobic organism, which is able use fermentation to produce ATP. Similar to plants and bacteria, *S. cerevisiae* possesses alternative NADH dehydrogenases that can partially substitute complex I (but lack the proton translocating activity; Marcet-Houben et al., 2009; Matus-Ortega et al., 2015; de Vries and Grivell, 1988).

An even more reduced OXPHOS system can be found in *Chromera velia*, a unicellular phototrophic relative of the parasitic apicomplexans. This organism is equipped with a considerably reduced mitochondrial ETC, lacking complexes I and III_2. The respiratory chain of *Chromera* is divided into two disconnected parts: complex II, together with an alternative NADH dehydrogenase (NDH2) and other electron donors, reduces ubiquinone which transfers electrons onto AOX. No protons are pumped across the crista membrane by these enzymes. In addition, orthologs of L- and D-lactate:cytochrome c oxidoreductases transfer electrons from lactate to cytochrome c, bypassing the lacking complex III_2. Cytochrome c is finally oxidized by complex IV. Regeneration of lactate is performed by a bidirectional NADH dependent D-lactate dehydrogenase reducing pyruvate. Since the mitochondrial genome of *Chromera* only carries two genes (*cox1* and *cox3*), is has the lowest protein-coding capacity reported so far (Flegontov et al., 2015). Recently, a comparably reduced OXPHOS system was discovered in the dinoflagellate Amoebophyra *ceratii* (John et al., 2019). Intriguingly, the mitochondrial genome seems to be completely absent, but nevertheless mitochondria are present and active. According to a current model, all mitochondrial genes encoding subunits of the OXPHOS system were transferred into the cell nucleus; furthermore, the complexes I and III_2 were lost (John et al., 2019). Biochemical proof of this model is pending.

Some other eukaryotes even completely lack an OXPHOS system. The unicellular obligate intracellular parasites of the *Microsporidia* division possess no OXPHOS components and TCA cycle, indicating strong degeneration of their mitochondria and ATP synthesis by substrate-level phosphorylation (Katinka et al., 2001; Marcet-Houben et al., 2009). During proliferation, microsporidia can recruit host mitochondria to their membrane, which may serve in the uptake of host ATP. This prediction is supported by the identification of four genes coding for ADP/ATP transporters. The ability of microsporidia to drain host-ATP was linked to their mitochondrial degeneration (James et al., 2013) and it was reported that *Microsporidia* only possess rudimentary genome-less organelles with unknown function termed "mitosomes" (James et al., 2013; Williams et al., 2002).

The core mitochondrial functions of the four respiratory complexes and ATP synthase are dispensable in environments in which ATP can be synthesized by other means like substrate-level phosphorylation. Such environments are mostly inhabited by parasites (Muller et al., 2012). The genomes of parasites are often characterized by the loss of genes and functions, reflecting the increasing dependence of the parasite on the host.

Parasitism also exists in the plant kingdom. Well-known representatives are mistletoes, which are obligate hemiparasitic flowering plants that grow on various trees. Recently, two research groups reported and characterized the mitogenomes of different mistletoe species. Interestingly, all investigated genomes lack genes encoding complex I subunits (Petersen et al., 2015; Skippington et al., 2017; Skippingtona et al., 2015). Lack of mitochondrial genes coding for complex I subunits in mistletoe may follow the same ratio as suggested for *A. ceratii* (John et al., 2019). Alternatively,

mistletoe might truly lack complex I, which would be the first case of missing complex I in the mitochondria of a multicellular organism.

To gain further insights into the OXPHOS composition of the *Viscum album* (European mistletoe), mitochondria were isolated from leaves of the species and systematically analyzed by blue native (BN) polyacrylamide gel electrophoresis (PAGE) in combination with protein identification by mass spectrometry (**Chapter 2.2**). While the mitochondrial complexes II, III_2, IV and V were all identified, complex I clearly was absent. Occurrence of several alternative NAD(P)H dehydrogenases and an alternative oxidase seem to compensate for the lack of complex I. Rearrangement of the OXPHOS system in V. album is also evident by the presence of very stable supercomplexes formed by complexes III_2 and IV. However, dimerization of complex V could not be observed. As a consequence, the mitochondria of *Viscum album* feature comparatively few cristae. Further insights into the molecular adaptations caused by “life without complex I” are given in **chapter 2.2**.

1.3 Mitochondrial gene expression

1.3.1 Why is there still a mitochondrial genome?

Following the endosymbiotic event that gave rise to the development of mitochondria, the gene content in the mitochondrial genome was continuously reduced. Most genes of the original endosymbiont genome were either lost or transferred to the nucleus during evolution of endosymbiosis. Each of the diverse eukaryotic lineages that developed from the original eukaryote carried out this reductive evolutionary process independently, which eventually lead to the diverse mitochondrial genomes we observe today (Roger et al., 2017).

Maintaining such an extra genome next the nuclear genome is accompanied by high energetic costs for genome maintenance and duplication, transcription, mRNA maturation and finally mRNA translation (Christian and Spremulli, 2012). So, why do eukaryotes still invest so much energy in a genome, that encodes less than 5% of the mitochondrial proteome (Giegé et al., 2005)? Several predictions were made to explain why mitochondria still need their own genome (Allen, 2015; Roger et al., 2017). A possible explanation for preserving the mitochondrial genome is to enable local gene expression control in response to local redox states within mitochondria (Allen, 2015). Another rather simple explanation would be that the continuous existence of the mitogenome does not serve a specific function but rather is a consequence of the circumstance that it is difficult to synthesize highly hydrophobic proteins in the cytosol and import them into the mitochondria since they either cannot cross the mitochondrial membrane (Claros et al., 1995) or are directed to the ER and not the mitochondria because of their hydrophobic transmembrane domains (Björkholm et al., 2015, 2017; von Heijne, 1986).

1.3.2 PPR proteins and RNA Editing

The so-called pentatricopeptide repeat (PPR) proteins play a central role in plant organellar gene expression (Giegé, 2013). They are found to be involved in processes like transcription, RNA splicing, RNA editing, RNA end maturation and also translation itself. Interestingly, their presence among eukaryotes is unequal with relative small number in fungi and animals and very high numbers in higher plants (Giegé, 2013). In *Arabidopsis thaliana*, over 496 of PPR were identified, representing ~1% of the coding capacity of the nuclear genome (Aubourg et al., 2000; Cheng et al., 2016).

Depending on the motifs they carry, PPR proteins are categorized in the P and PLS subfamilies. The P family, only carrying the P motif, is involved in RNA stabilization, cleavage splicing and translation (Barkan and Small, 2014). PPR proteins of the P subfamily can also bind RNA sequences to prevent RNA degradation and modify the secondary RNA structure to recruit additional proteins (Shikanai, 2015). The PLS family is further divided into PLS, E, E^+ and DYW subgroups, which is based on the C-terminal extension of each protein. It is specifically this family, which is involved in RNA editing. RNA editing describes a deamination reaction on mRNA that leads to the conversion of cytidine residues to uridine and thereby modifies the genetic information of the mRNA. In higher plants, this process nearly exclusively takes place in plastids and mitochondria (Shikanai, 2015). Evidence for the interaction of several RNA editing factors in *Arabidopsis thaliana* lead to the suggestion that PPR proteins form “editiosomes”. Here, E^+-type PPR proteins like SLO2 mediate RNA target recognition while P-type PPR proteins like NUWA establish interaction between SLO2 and DYW2, a PPR protein possessing a DYW domain which contains the catalytic editing domain (Andrés-Colás et al., 2017; Guillaumot et al., 2017). It was recently confirmed that the DYW domain functions as a cytidine deaminase which mediates C-to-U RNA editing (Oldenkott et al., 2019). Interestingly, the analyzed DYW-type PPR protein was able to edit RNA sites without any additional proteins indicating that formation of an editosome was not necessary. Since this study focuses on PPR protein of moss *Physcomitrella patens*, the authors suggest

that the development of complex editosomes in flowering plants became necessary because several editing factors seem to have lost their catalytic DYW domain (Oldenkott et al., 2019). Consequently, DYW2 probably plays an important role for RNA editing of several sites. This is reflected by its relatively high copy number when compared to other PPR proteins (**chapter 2.1**).

So why do plants edit RNA? It is still not clear why plants possess this huge subfamily of PPR genes and several attempts were made to explain why plants have retained them instead of "simply repairing" their genomes (Chateigner-Boutin and Small, 2010; Shikanai, 2015). RNA editing might be a regulatory mechanism. In the early days of RNA editing research partial editing of some sites was detected indicating that proteins might exist in edited and unedited conformation (Lu and Hanson, 1992). This "protein polymorphism" was indeed shown for ribosomal protein S12 by immunoblot analysis (Lu et al., 1996; Phreaner et al., 1996). In a more recent study, mass spectrometry could also prove the existence of polymorphic NDHB proteins within the chloroplast NAD(P)H dehydrogenase complex and a study applying ribosome profiling proved that mitoribosomes do not discriminate between edited and unedited mRNAs (Okuda et al., 2010; Planchard et al., 2018). The editing sites in the former study are probably silent since the authors could not find any functional or phenotypic difference between the complexes containing the edited or the unedited protein (Okuda et al., 2010). It is compelling to speculate that some proteins exist in one, two or even more forms with different functions or activity. To the best of the author's knowledge, this has never been shown so far. However, while many partial editing sites are silent, mutants that lack editing of these sites can show strong phenotypes (Chateigner-Boutin et al., 2008). A further argument indicating the regulatory role of RNA editing is the observation that partially edited sites are differentially edited when compared between different growth conditions, different organs or after environmental stress (Chateigner-Boutin and Small, 2010). RNA editing regulates the translation of a plastid encoded subunit of the plastid NADH dehydrogenase, which has a partially editing site at its start codon. Only the edited codon is recognized by the plastid ribosome and it seems that the extend of editing depends on developmental and environmental conditions (Hirose and Sugiura, 1997). Messenger RNAs loaded on mitoribosomes showed an increase in the editing level at partially edited sites (Planchard et al., 2018). This increase could be explained by the strong RNA helicase activity of the mitoribosome, making the editing sites more accessible for PPR proteins.

1.3.3 Mitochondrial ribosomes

Despite all the information indicating a connection between PPR proteins, RNA editing and translation, the exact role of PPR proteins during protein synthesis is still unclear. PPR proteins were proposed to be involved in plant mitochondrial translation, and two PPR proteins could be identified in mitochondrial high-molecular weight fractions harboring ribosomes which might indicate that they present interaction partners or even components of the mitochondrial ribosome (Hammani et al., 2011; Uyttewaal et al., 2008). Indeed, TPR and PPR were identified as components of trypanosomal mitochondrial ribosomes (Ramrath et al., 2018). These results indicate that TPR/PPR proteins might also be structural components of plant mitoribosomes.

Mitochondrial ribosomes mostly resemble 70S ribosomes in bacteria, which can be explained by the α-proteobacterial origin of mitochondria. Despite having a different sedimentation coefficient than their bacterial counterparts, mitoribosomes are still of comparable size (Hamilton and O'Brien, 1974). Interestingly, the mitoribosome of the Last Eukaryotic Common Ancestor (LECA) was probably larger than bacterial ribosomes and contained many additional proteins in both subunits, indicating that eukaryotic mitoribosomes underwent a very dynamic and diverse evolutionary history including loss of ribosomal genes or their transfer into the host nucleus and the acquisition of novel mitoribosomal components (Desmond et al., 2011). Many of these drastic changes were probably conducted to better fit the needs of a mitochondrion. One such example is the highly hydrophobic polypeptide exit tunnel

of the mammalian large mitoribosomal subunit (mtLSU), which probably facilitates export of the hydrophobic membrane proteins of the respiratory chain that are produced within mitochondria (Brown et al., 2014). Furthermore, yeast and mammalian mitoribosomes were shown to interact with the inner mitochondrial membrane where the respiratory chain complexes are finally located. Yeast mitoribosomes also interact with the membrane insertion machinery which would allow co-translational membrane insertion of the hydrophobic OXPHOS components (Liu and Spremulli, 2000; Pfeffer et al., 2015).

Cryo-EM of yeast and mammalian mitoribosomes also showed that there is a general trend of structural rRNA reduction in mitoribosomes when compared to bacterial ribosomes (Amunts et al., 2015; Desai et al., 2017; Greber et al., 2015). At the same time, mitoribosomes are also comparatively protein rich. This can be observed at the contact sites between the large and small subunits of the mammalian mitoribosome which is not dominated by RNA-RNA interactions as observed for cytosolic ribosomes, but by protein-protein interactions instead (Sharma et al., 2003). In animals, a tRNA also replaces the structural 5S rRNA, leaving only the 16S and 12S rRNA (Brown et al., 2014; Chrzanowska-Lightowlers et al., 2017). Consequently, mammalian mitoribosomes possess more than 30 proteins which are absent in bacterial ribosomes, reflecting a general trend to substitute rRNA by proteins (Amunts et al., 2015; Greber et al., 2014).

While the mitochondrial ribosomes of mammals, yeast and even trypanosomes are well characterized at near-atomic resolution (Amunts et al., 2015; Desai et al., 2017; Ramrath et al., 2018), our knowledge of the structure and the composition of plant mitoribosomes is negligible. The mitoribosomes of higher plants possess three rRNAs: The 18S rRNA in the small subunit (mtSSU) and 5S and 26S rRNA in the large subunit (mtLSU). While the rRNA content in the mitoribosomes of different plant species is quite comparable, the protein composition can differ: In potato, 68 proteins were identified as mitoribosomal components while in broad bean approximately 80 proteins were found (Maffey et al., 1997; Pinel et al., 1986; Vasconcelos and Bogorad, 1971). However, these studies were conducted before highly sensitive protein identification techniques like mass spectrometry became available. Therefore, many of the proteins could not be identified and it cannot be ruled out that the mitoribosomal fractions were not contaminated by cytosolic ribosomes. Even with the technologies available today, it still is difficult to determine the protein composition of plant mitochondrial ribosomes since their purification is complicated for several reasons: (i) the sedimentation coefficient of mitoribosomes is very close to the coefficient reported for cytosolic ribosomes (77-78S to 80S) (Leaver and Harmey, 1976), (ii) the low solubility of mitoribosomes, which is caused by their attachment to the inner mitochondrial membrane (Liu and Spremulli, 2000; Pfeffer et al., 2015), and (iii) the attachment of cytosolic ribosomes to the mitochondrial surface (Gold et al., 2017).

To get a better insight into the protein composition of plant mitochondrial ribosomes, chemical cross-linking was combined with complexome profiling (**Chapter 2.3**). The presence of several PPR proteins was observed in both ribosomal subunit clusters, substantiating a potential involvement of PPR proteins in mitochondrial protein synthesis. Surprisingly, the small ribosomal subunit has an unusually large size, which even surpasses that of the large subunit. These discoveries can only be partly explained by plant-specific mtSSU components. Instead, formation of mtSSU dimers for regulatory reasons is proposed, as previously discussed for bacteria.

1.4. References

Acin-Perez, R., and Enriquez, J.A. (2014). The function of the respiratory supercomplexes: The plasticity model. Biochim. Biophys. Acta - Bioenerg. *1837*, 444–450.

Alban, C., Job, D., and Douce, R. (2000). BIOTIN METABOLISM IN PLANTS. Annu. Rev. Plant Physiol. Plant Mol. Biol. *51*, 17–47.

Allen, J.F. (2015). Why chloroplasts and mitochondria retain their own genomes and genetic systems: Colocation for redox regulation of gene expression. Proc. Natl. Acad. Sci. *112*, 10231–10238.

Alverson, A.J., Wei, X., Rice, D.W., Stern, D.B., Barry, K., and Palmer, J.D. (2010). Insights into the evolution of mitochondrial genome size from complete sequences of citrullus lanatus and cucurbita pepo (Cucurbitaceae). Mol. Biol. Evol. *27*, 1436–1448.

Alverson, A.J., Zhuo, S., Rice, D.W., Sloan, D.B., and Palmer, J.D. (2011a). The Mitochondrial Genome of the Legume Vigna radiata and the Analysis of Recombination across Short Mitochondrial Repeats. PLoS One *6*, e16404.

Alverson, A.J., Rice, D.W., Dickinson, S., Barry, K., and Palmer, J.D. (2011b). Origins and Recombination of the Bacterial-Sized Multichromosomal Mitochondrial Genome of Cucumber. Plant Cell *23*, 2499–2513.

Amir, R. (2010). Current understanding of the factors regulating methionine content in vegetative tissues of higher plants. Amino Acids *39*, 917–931.

Amunts, A., Brown, A., Toots, J., Scheres, S.H.W., and Ramakrishnan, V. (2015). The structure of the human mitochondrial ribosome. Science (80-.). *348*, 95–98.

Anderson, S., Bankier, A.T., Barrell, B.G., de Bruijn, M.H.L., Coulson, A.R., Drouin, J., Eperon, I.C., Nierlich, D.P., Roe, B.A., Sanger, F., et al. (1981). Sequence and organization of the human mitochondrial genome. Nature *290*, 457–465.

Andrés-Colás, N., Zhu, Q., Takenaka, M., De Rybel, B., Weijers, D., and Van Der Straeten, D. (2017). Multiple PPR protein interactions are involved in the RNA editing system in Arabidopsis mitochondria and plastids . Proc. Natl. Acad. Sci. *114*, 8883–8888.

Arimura, S., Yamamoto, J., Aida, G.P., Nakazono, M., and Tsutsumi, N. (2004). Frequent fusion and fission of plant mitochondria with unequal nucleoid distribution. Proc. Natl. Acad. Sci. U. S. A. *101*, 7805–7808.

Aubourg, S., Boudet, N., Kreis, M., and Lecharny, A. (2000). In Arabidopsis thaliana, 1% of the genome codes for a novel protein family unique to plants. Plant Mol. Biol. *42*, 603–613.

Backert, S., and Börner, T. (2000). Phage T4-like intermediates of DNA replication and recombination in the mitochondria of the higher plant Chenopodium album (L.). Curr. Genet. *37*, 304–314.

Barkan, A., and Small, I. (2014). Pentatricopeptide Repeat Proteins in Plants. Annu. Rev. Plant Biol. *65*, 415–442.

Bartoli, C.G., Gomez, F., Gergoff, G., Guiamét, J.J., and Puntarulo, S. (2005). Up-regulation of the mitochondrial alternative oxidase pathway enhances photosynthetic electron transport under drought conditions. J. Exp. Bot. *56*, 1269–1276.

Batista-Silva, W., Heinemann, B., Rugen, N., Nunes-Nesi, A., Araújo, W.L., Braun, H.P., and Hildebrandt, T.M. (2019). The role of amino acid metabolism during abiotic stress release. Plant Cell Environ. *42*, 1630–1644.

Bauwe, H., and Kolukisaoglu, Ü. (2003). Genetic manipulation of glycine decarboxylation. J. Exp. Bot. *54*, 1523–1535.

Bauwe, H., Hagemann, M., and Fernie, A.R. (2010). Photorespiration: players, partners and origin. Trends Plant Sci. *15*, 330–336.

Bendich, A.J. (1993). Reaching for the ring: the study of mitochondrial genome structure. Curr. Genet. *24*, 279–290.

Bergthorsson, U., Adams, K.L., Thomason, B., and Palmer, J.D. (2003). Widespread horizontal transfer of mitochondrial genes in flowering plants. Nature *424*, 197–201.

Bitonti, M., Seaver, D., Henry, C.S., and Hanson, D. (2012). B vitamin pathways and their compartmentation : a In Posidonia oceanica cadmium induces changes in DNA guide for the and perplexed methylation chromatin patterning. *63*, 5379–5395.

Björkholm, P., Harish, A., Hagström, E., Ernst, A.M., and Andersson, S.G.E. (2015). Mitochondrial genomes are retained by selective constraints on protein targeting. Proc. Natl. Acad. Sci. U. S. A. *112*, 10154–10161.

Björkholm, P., Ernst, A.M., Hagström, E., and Andersson, S.G.E. (2017). Why mitochondria need a genome revisited. FEBS Lett. *591*, 65–75.

Blum, T.B., Hahn, A., Meier, T., Davies, K.M., and Kühlbrandt, W. (2019). Dimers of mitochondrial ATP synthase induce membrane curvature and self-assemble into rows. Proc. Natl. Acad. Sci. *116*, 4250–4255.

Boekema, E.J., and Braun, H.P. (2007). Supramolecular structure of the mitochondrial oxidative phosphorylation system. J. Biol. Chem. *282*, 1–4.

Bourguignon, J., MACHEREL, D., NEUBURGER, M., and DOUCE, R. (1992). Isolation, characterization, and sequence analysis of a cDNA clone encoding L-protein, the dihydrolipoamide dehydrogenase component of the glycine cleavage system from pea-leaf mitochondria. Eur. J. Biochem. *204*, 865–873.

Bourguignon, J., Merand, V., Rawsthorne, S., Forest, E., and Douce, R. (1996). Glycine decarboxylase and pyruvate dehydrogenase complexes share the same dihydrolipoamide dehydrogenase in pea leaf mitochondria: evidence from mass spectrometry and primary-structure analysis. Biochem. J. *313 (Pt 1)*, 229–234.

Brand, M.D. (2010). The sites and topology of mitochondrial superoxide production. Exp. Gerontol. *45*, 466–472.

Braun, H.P., and Zabaleta, E. (2007). Carbonic anhydrase subunits of the mitochondrial NADH dehydrogenase complex (complex I) in plants. Physiol. Plant. *129*, 114–122.

Brown, A., Amunts, A., Bai, X.C., Sugimoto, Y., Edwards, P.C., Murshudov, G., Scheres, S.H.W., and Ramakrishnan, V. (2014). Structure of the large ribosomal subunit from human mitochondria. Science (80-.). *346*, 718–722.

Burger, G., Gray, M.W., Forget, L., and Lang, B.F. (2013). Strikingly bacteria-like and gene-richmitochondrial genomes throughout jakobid protists. Genome Biol. Evol. *5*, 418–438.

Carrie, C., Murcha, M.W., Giraud, E., Ng, S., Zhang, M.F., Narsai, R., and Whelan, J. (2013). How do plants make mitochondria? Planta *237*, 429–439.

Cavalier-Smith, T. (1987). The Simultaneous Symbiotic Origin of Mitochondria, Chloroplasts, and Microbodies. Ann. N. Y. Acad. Sci. *503*, 55–71.

Chateigner-Boutin, A.L., and Small, I. (2010). Plant RNA editing. RNA Biol. *7*, 213–219.

Chateigner-Boutin, A.L., Ramos-Vega, M., Guevara-García, A., Andrés, C., Gutiérrez-Nava, M.D.L.L., Cantero, A., Delannoy, E., Jiménez, L.F., Lurin, C., Small, I., et al. (2008). CLB19, a pentatricopeptide

repeat protein required for editing of rpoA and clpP chloroplast transcripts. Plant J. *56*, 590–602.

Cheng, S., Gutmann, B., Zhong, X., Ye, Y., Fisher, M.F., Bai, F., Castleden, I., Song, Y., Song, B., Huang, J., et al. (2016). Redefining the structural motifs that determine RNA binding and RNA editing by pentatricopeptide repeat proteins in land plants. Plant J. *85*, 532–547.

Christian, B.E., and Spremulli, L.L. (2012). Mechanism of protein biosynthesis in mammalian mitochondria. Biochim. Biophys. Acta - Gene Regul. Mech.

Chrzanowska-Lightowlers, Z., Rorbach, J., and Minczuk, M. (2017). Human mitochondrial ribosomes can switch structural tRNAs – but when and why? RNA Biol. *14*, 1668–1671.

Claros, M.G., Perea, J., Shu, Y., Samatey, F.A., Popot, J.-L., and Jacq, C. (1995). Limitations to in vivo Import of Hydrophobic Proteins into Yeast Mitochondria. The Case of a Cytoplasmically Synthesized Apocytochrome b. Eur. J. Biochem. *228*, 762–771.

Davies, K.M., Strauss, M., Daum, B., Kief, J.H., Osiewacz, H.D., Rycovska, A., Zickermann, V., and Kühlbrandt, W. (2011). Macromolecular organization of ATP synthase and complex I in whole mitochondria. Proc. Natl. Acad. Sci. U. S. A. *108*, 14121–14126.

Davies, K.M., Anselmi, C., Wittig, I., Faraldo-Gómez, J.D., and Kühlbrandt, W. (2012). Structure of the yeast F1Fo-ATP synthase dimer and its role in shaping the mitochondrial cristae. Proc. Natl. Acad. Sci. U. S. A. *109*, 13602–13607.

Dekker, P.J.T., Martin, F., Maarse, A.C., Bömer, U., Müller, H., Guiard, B., Meijer, M., Rassow, J., and Pfanner, N. (1997). The Tim core complex defines the number of mitochondrial translocation contact sites and can hold arrested preproteins in the absence of matrix Hsp70-Tim44. EMBO J. *16*, 5408–5419.

Desai, N., Brown, A., Amunts, A., and Ramakrishnan, V. (2017). The structure of the yeast mitochondrial ribosome. Science *355*, 528–531.

Desmond, E., Brochier-Armanet, C., Forterre, P., and Gribaldo, S. (2011). On the last common ancestor and early evolution of eukaryotes: reconstructing the history of mitochondrial ribosomes. Res. Microbiol. *162*, 53–70.

Douce, R. (1985). Mitochondria in higher plants : structure, function, and biogenesis (Academic Press).

Douce, R., and Neuburger, M. (1999). Biochemical dissection of photorespiration. Curr. Opin. Plant Biol. *2*, 214–222.

Douce, R., Bourguignon, J., Neuburger, M., and Rébeillé, F. (2001). The glycine decarboxylase system: A fascinating complex. Trends Plant Sci. *6*, 167–176.

Dudkina, N. V., Heinemeyer, J., Keegstra, W., Boekema, E.J., and Braun, H.P. (2005a). Structure of dimeric ATP synthase from mitochondria: An angular association of monomers induces the strong curvature of the inner membrane. FEBS Lett. *579*, 5769–5772.

Dudkina, N. V., Oostergetel, G.T., Lewejohann, D., Braun, H.P., and Boekema, E.J. (2010). Row-like organization of ATP synthase in intact mitochondria determined by cryo-electron tomography. Biochim. Biophys. Acta - Bioenerg. *1797*, 272–277.

Dudkina, N. V, Eubel, H., Keegstra, W., Boekema, E.J., and Braun, H.-P. (2005b). Structure of a mitochondrial supercomplex formed by respiratory-chain complexes I and III. Proc. Natl. Acad. Sci. U. S. A. *102*, 3225–3229.

Durgud, M., Gupta, S., Ivanov, I., Omidbakhshfard, M.A., Benina, M., Alseekh, S., Staykov, N., Hauenstein, M., Dijkwel, P.P., Hörtensteiner, S., et al. (2018). Molecular Mechanisms Preventing

Senescence in Response to Prolonged Darkness in a Desiccation-Tolerant Plant. Plant Physiol. *177*, 1319–1338.

Dutilleul, C., Driscoll, S., Cornic, G., De Paepe, R., Foyer, C.H., and Noctor, G. (2003). Functional Mitochondrial Complex I Is Required by Tobacco Leaves for Optimal Photosynthetic Performance in Photorespiratory Conditions and during Transients. Plant Physiol. *131*, 264–275.

Elhafez, D., Murcha, M.W., Clifton, R., Soole, K.L., Day, D.A., and Whelan, J. (2006). Characterization of mitochondrial alternative NAD(P)H dehydrogenases in arabidopsis: Intraorganelle location and expression. Plant Cell Physiol. *47*, 43–54.

Engel, N., van den Daele, K., Kolukisaoglu, Ü., Morgenthal, K., Weckwerth, W., Pärnik, T., Keerberg, O., and Bauwe, H. (2007). Deletion of Glycine Decarboxylase in Arabidopsis Is Lethal under Nonphotorespiratory Conditions. Plant Physiol. *144*, 1328–1335.

Eubel, H., Jänsch, L., and Braun, H.-P. (2003). New Insights into the Respiratory Chain of Plant Mitochondria. Supercomplexes and a Unique Composition of Complex II. Plant Physiol. *133*, 274 LP – 286.

Fernie, A.R., Carrari, F., and Sweetlove, L.J. (2004). Respiratory metabolism: Glycolysis, the TCA cycle and mitochondrial electron transport. Curr. Opin. Plant Biol.

Flegontov, P., Michálek, J., Janouškovec, J., Lai, D.-H., Jirků, M., Hajdušková, E., Tomčala, A., Otto, T.D., Keeling, P.J., Pain, A., et al. (2015). Divergent Mitochondrial Respiratory Chains in Phototrophic Relatives of Apicomplexan Parasites. Mol. Biol. Evol. *32*, 1115–1131.

Foury, F., Roganti, T., Lecrenier, N., and Purnelle, B. (1998). The complete sequence of the mitochondrial genome of Saccharomyces cerevisiae. FEBS Lett. *440*, 325–331.

Fowler, L.R., and Richardson, S.H. (1963). Studies on the electron transfer system. L. On the mechanism of reconstitution of the mitochondrial electron transfer system. J. Biol. Chem. *238*, 456–463.

Foyer, C.H., Lopez-Delgado, H., Dat, J.F., and Scott, I.M. (1997). Hydrogen peroxide- and glutathione-associated mechanisms of acclimatory stress tolerance and signalling. Physiol. Plant. *100*, 241–254.

Fromm, S., Senkler, J., Eubel, H., Peterhänsel, C., and Braun, H.P. (2016). Life without complex I: Proteome analyses of an Arabidopsis mutant lacking the mitochondrial NADH dehydrogenase complex. J. Exp. Bot. *67*, 3079–3093.

Gabaldón, T., Rainey, D., and Huynen, M.A. (2005). Tracing the evolution of a large protein complex in the eukaryotes, NADH:ubiquinone oxidoreductase (Complex I). J. Mol. Biol. *348*, 857–870.

Gabay-Laughnan, S., Kuzmin, E. V, Monroe, J., Roark, L., and Newton, K.J. (2009). Characterization of a novel thermosensitive restorer of fertility for cytoplasmic male sterility in maize. Genetics *182*, 91–103.

Galili, G., Avin-Wittenberg, T., Angelovici, R., and Fernie, A.R. (2014). The role of photosynthesis and amino acid metabolism in the energy status during seed development. Front. Plant Sci. *5*, 1–6.

Geisler, D.A., Broselid, C., Hederstedt, L., and Rasmusson, A.G. (2007). Ca2+-binding and Ca2+-independent respiratory NADH and NADPH dehydrogenases of Arabidopsis thaliana. J. Biol. Chem. *282*, 28455–28464.

Giegé, P. (2013). Pentatricopeptide repeat proteins: a set of modular RNA-specific binders massively used for organelle gene expression. RNA Biol. *10*, 1417–1418.

Giegé, P., Sweetlove, L.J., Cognat, V., and Leaver, C.J. (2005). Coordination of Nuclear and Mitochondrial Genome Expression during Mitochondrial Biogenesis in Arabidopsis. Plant Cell *17*,

1497–1512.

Gold, V.A., Chroscicki, P., Bragoszewski, P., and Chacinska, A. (2017). Visualization of cytosolic ribosomes on the surface of mitochondria by electron cryo-tomography. EMBO Rep. *18*, 1786–1800.

Gray, M.W. (2012). Mitochondrial Evolution. Cold Spring Harb. Perspect. Biol. *4*, a011403–a011403.

Gray, M.W. (2017). Lynn Margulis and the endosymbiont hypothesis: 50 years later. Mol. Biol. Cell *28*, 1285–1287.

Gray, M.W., and Doolittle, W.F. (1982). Has the endosymbiont hypothesis been proven? Microbiol. Rev. *46*, 1–42.

Greber, B.J., Boehringer, D., Leitner, A., Bieri, P., Voigts-Hoffmann, F., Erzberger, J.P., Leibundgut, M., Aebersold, R., and Ban, N. (2014). Architecture of the large subunit of the mammalian mitochondrial ribosome. Nature *505*, 515–519.

Greber, B.J., Bieri, P., Leibundgut, M., Leitner, A., Aebersold, R., Boehringer, D., and Ban, N. (2015). The complete structure of the 55S mammalian mitochondrial ribosome. Science (80-.). *348*, 303–308.

Gualberto, J.M., and Newton, K.J. (2017). Plant Mitochondrial Genomes: Dynamics and Mechanisms of Mutation. Annu. Rev. Plant Biol. *68*, 225–252.

Gueguen, V., Macherel, D., Jaquinod, M., Douce, R., and Bourguignon, J. (2000). Fatty acid and lipoic acid biosynthesis in higher plant mitochondria. J. Biol. Chem. *275*, 5016–5025.

Guillaumot, D., Lopez-Obando, M., Baudry, K., Avon, A., Rigaill, G., Falcon de Longevialle, A., Broche, B., Takenaka, M., Berthomé, R., De Jaeger, G., et al. (2017). Two interacting PPR proteins are major Arabidopsis editing factors in plastid and mitochondria. Proc. Natl. Acad. Sci. *114*, 201705780.

Hackenbrock, C.R. (1968). Chemical and physical fixation of isolated mitochondria in low-energy and high-energy states. 1–8.

Hackenbrock, C.R., Chazotte, B., and Gupte, S.S. (1986). The random collision model and a critical assessment of diffusion and collision in mitochondrial electron transport. J. Bioenerg. Biomembr. *18*, 331–368.

Hahn, A., Parey, K., Bublitz, M., Mills, D.J., Zickermann, V., Vonck, J., Kühlbrandt, W., and Meier, T. (2016). Structure of a Complete ATP Synthase Dimer Reveals the Molecular Basis of Inner Mitochondrial Membrane Morphology. Mol. Cell *63*, 445–456.

Hamilton, M.G., and O'Brien, T.W. (1974). Ultracentrifugal characterization of the mitochondrial ribosome and subribosomal particles of bovine liver. Molecular size and composition. Biochemistry *13*, 5400–5403.

Hammani, K., Gobert, A., Hleibieh, K., Choulier, L., Small, I., and Giegé, P. (2011). An Arabidopsis Dual-Localized Pentatricopeptide Repeat Protein Interacts with Nuclear Proteins Involved in Gene Expression Regulation . Plant Cell *23*, 730–740.

Hanning, I., and Heldt, H.W. (1993). On the Function of Mitochondrial Metabolism during Photosynthesis in Spinach (Spinacia oleracea L.) Leaves (Partitioning between Respiration and Export of Redox Equivalents and Precursors for Nitrate Assimilation Products). Plant Physiol. *103*, 1147–1154.

Hartmann, M., Zeier, T., Bernsdorff, F., Reichel-Deland, V., Kim, D., Hohmann, M., Scholten, N., Schuck, S., Bräutigam, A., Hölzel, T., et al. (2018). Flavin Monooxygenase-Generated N-Hydroxypipecolic Acid Is a Critical Element of Plant Systemic Immunity. Cell.

von Heijne, G. (1986). Why mitochondria need a genome. FEBS Lett. *198*, 1–4.

Helbig, A.O., de Groot, M.J.L., van Gestel, R.A., Mohammed, S., de Hulster, E.A.F., Luttik, M.A.H., Daran-Lapujade, P., Pronk, J.T., Heck, A.J.R., and Slijper, M. (2009). A three-way proteomics strategy allows differential analysis of yeast mitochondrial membrane protein complexes under anaerobic and aerobic conditions. Proteomics *9*, 4787–4798.

Hildebrandt, T.M., Nunes Nesi, A., Araújo, W.L., and Braun, H.P. (2015). Amino Acid Catabolism in Plants. Mol. Plant *8*, 1563–1579.

Hirose, T., and Sugiura, M. (1997). Both RNA editing and RNA cleavage are required for translation of tobacco chloroplast ndhD mRNA: apossible regulatory mechanism for the expression of a chloroplast operon consisting of functionally unrelated genes. EMBO J. *16*, 6804–6811.

Hodges, M. (2002). Enzyme redundancy and the importance of 2-oxoglutarate in plant ammonium assimilation. In Journal of Experimental Botany, (Narnia), pp. 905–916.

Hoitzing, H., Johnston, I.G., and Jones, N.S. (2015). What is the function of mitochondrial networks? A theoretical assessment of hypotheses and proposal for future research. BioEssays *37*, 687–700.

Hooper, C.M., Tanz, S.K., Castleden, I.R., Vacher, M.A., Small, I.D., and Millar, A.H. (2014). SUBAcon: A consensus algorithm for unifying the subcellular localization data of the Arabidopsis proteome. Bioinformatics *30*, 3356–3364.

Howell, K.A., Millar, A.H., and Whelan, J. (2006). Ordered Assembly of Mitochondria During Rice Germination Begins with Promitochondrial Structures Rich in Components of the Protein Import Apparatus. Plant Mol. Biol. *60*, 201–223.

Howell, K.A., Millar, A.H., and Whelan, J. (2007). Building the Powerhouse: What are the Signals Involved in Plant Mitochondrial Biogenesis? Plant Signal. Behav. *2*, 428–430.

Huang, S., Van Aken, O., Schwarzländer, M., Belt, K., and Millar, A.H. (2016). The Roles of Mitochondrial Reactive Oxygen Species in Cellular Signaling and Stress Response in Plants. Plant Physiol. *171*, 1551–1559.

James, T.Y., Pelin, A., Bonen, L., Ahrendt, S., Sain, D., Corradi, N., and Stajich, J.E. (2013). Shared signatures of parasitism and phylogenomics unite cryptomycota and microsporidia. Curr. Biol. *23*, 1548–1553.

Jardim-Messeder, D., Caverzan, A., Rauber, R., de Souza Ferreira, E., Margis-Pinheiro, M., and Galina, A. (2015). Succinate dehydrogenase (mitochondrial complex II) is a source of reactive oxygen species in plants and regulates development and stress responses. New Phytol. *208*, 776–789.

John, U., Lu, Y., Wohlrab, S., Groth, M., Janouškovec, J., Kohli, G.S., Mark, F.C., Bickmeyer, U., Farhat, S., Felder, M., et al. (2019). An aerobic eukaryotic parasite with functional mitochondria that likely lacks a mitochondrial genome. Sci. Adv. *5*, eaav1110.

Juszczuk, I.M., Szal, B., and Rychter, A.M. (2012). Oxidation-reduction and reactive oxygen species homeostasis in mutant plants with respiratory chain complex I dysfunction. Plant, Cell Environ. *35*, 296–307.

Katinka, M.D., Duprat, S., Cornillot, E., Méténier, G., Thomarat, F., Prensier, G., Barbe, V., Peyretaillade, E., Brottier, P., Wincker, P., et al. (2001). Genome sequence and gene compaction of the eukaryote parasite Encephalitozoon cuniculi. Nat. 2001 4146862 *414*, 450.

Keilin, D., and Hartree, E.F. (1947). Activity of the cytochrome system in heart muscle preparations. Biochem. J. *41*, 500–502.

Kellems, R.E., Allison, V.F., and Butow, R.A. (1975). Cytoplasmic type 80S ribosomes associated with yeast mitochondria. IV. Attachment of ribosomes to the outer membrane of isolated mitochondria. J. Cell Biol. *65*, 1–14.

Klein, M., Eckert-Ossenkopp, U., Schmiedeberg, I., Brandt, P., Unseld, M., Brennicke, A., and Schuster, W. (1994). Physical mapping of the mitochondrial genome of Arabidopsis thaliana by cosmid and YAC clones. Plant J. *6*, 447–455.

Kubo, T., and Newton, K.J. (2008). Angiosperm mitochondrial genomes and mutations. Mitochondrion *8*, 5–14.

Kühn, K., Obata, T., Feher, K., Bock, R., Fernie, A.R., and Meyer, E.H. (2015). Complete Mitochondrial Complex I Deficiency Induces an Up-Regulation of Respiratory Fluxes That Is Abolished by Traces of Functional Complex I. Plant Physiol. *168*, 1537–1549.

Law, S.R., Narsai, R., Taylor, N.L., Delannoy, E., Carrie, C., Giraud, E., Millar, A.H., Small, I., and Whelan, J. (2012). Nucleotide and RNA Metabolism Prime Translational Initiation in the Earliest Events of Mitochondrial Biogenesis during Arabidopsis Germination. Plant Physiol. *158*, 1610–1627.

Leaver, C.J., and Harmey, M.A. (1976). Higher-plant mitochondrial ribosomes contain a 5S ribosomal ribonucleic acid component. Biochem. J. *157*, 275–277.

Lee, C.P., Eubel, H., and Millar, a H. (2010). Diurnal changes in mitochondrial function reveal daily optimization of light and dark respiratory metabolism in Arabidopsis. Mol. Cell. Proteomics *9*, 2125–2139.

Liu, M., and Spremulli, L. (2000). Interaction of mammalian mitochondrial ribosomes with the inner membrane. J. Biol. Chem. *275*, 29400–29406.

Logan, D.C. (2003). Mitochondrial dynamics. New Phytol. *160*, 463–478.

Logan, D.C. (2006). The mitochondrial compartment. J. Exp. Bot. *57*, 1225–1243.

Logan, D.C., Millar, A.H., Sweetlove, L.J., Hill, S.A., and Leaver, C.J. (2001). Mitochondrial biogenesis during germination in maize embryos. Plant Physiol. *125*, 662–672.

Lonsdale, D.M., Hodge, T.P., and Fauron, C.M.-R. (1984). The physical map and organisatlon of the mitochondrial genome from the fertile cytoplasm of maize. Nucleic Acids Res. *12*, 9249–9261.

Lu, B., and Hanson, M.R. (1992). A single nuclear gene specifies the abundance and extent of RNA editing of a plant mitochondrial transcript. Nucleic Acids Res. *20*, 5699–5703.

Lu, B., Wilson, R.K., Phreaner, C.G., Mulligan, R.M., and Hanson, M.R. (1996). Protein polymorphism generated by differential RNA editing of a plant mitochondrial rps12 gene. Mol. Cell. Biol. *16*, 1543–1549.

Maffey, L., Degand, H., and Boutry, M. (1997). Partial purication of mitochondrial ribosomes from broad bean and identi ® cation of proteins encoded by the mitochondrial genome. 365–371.

Magalon, A., and Alberge, F. (2016). Distribution and dynamics of OXPHOS complexes in the bacterial cytoplasmic membrane. Biochim. Biophys. Acta - Bioenerg. *1857*, 198–213.

Manchekar, M., Scissum-Gunn, K., Song, D., Khazi, F., McLean, S.L., and Nielsen, B.L. (2006). DNA recombination activity in soybean mitochondria. J. Mol. Biol.

Mannella, C.A. (2006). The relevance of mitochondrial membrane topology to mitochondrial function. Biochim. Biophys. Acta - Mol. Basis Dis. *1762*, 140–147.

Marcet-Houben, M., Marceddu, G., and Gabaldán, T. (2009). Phylogenomics of the oxidative phosphorylation in fungi reveals extensive gene duplication followed by functional divergence. BMC Evol. Biol. *9*, 295.

Matus-Ortega, M.G., Cárdenas-Monroy, C.A., Flores-Herrera, O., Mendoza-Hernández, G., Miranda, M., González-Pedrajo, B., Vázquez-Meza, H., and Pardo, J.P. (2015). New complexes containing the

internal alternative NADH dehydrogenase (Ndi1) in mitochondria of Saccharomyces cerevisiae. Yeast *32*, 629–641.

Michalecka, A.M., Svensson, Å.S., Johansson, F.I., Agius, S.C., Johanson, U., Brennicke, A., Binder, S., and Rasmusson, A.G. (2003). Arabidopsis Genes Encoding Mitochondrial Type II NAD(P)H Dehydrogenases Have Different Evolutionary Origin and Show Distinct Responses to Light. Plant Physiol. *133*, 642–652.

Millar, A.H., Small, I.D., Day, D.A., and Whelan, J. (2008). Mitochondrial biogenesis and function in Arabidopsis. Arab. B. *6*, e0111.

Millar, A.H., Whelan, J., Soole, K.L., and Day, D.A. (2011). Organization and Regulation of Mitochondrial Respiration in Plants. Annu. Rev. Plant Biol. *62*, 79–104.

Miller, J.R., Busby, R.W., Jordan, S.W., Cheek, J., Henshaw, T.F., Ashley, G.W., Broderick, J.B., Cronan, J.E., and Marletta, M.A. (2000). Escherichia coli lipA is a lipoyl synthase: In vitro biosynthesis of lipoylated pyruvate dehydrogenase complex from octanoyl-acyl carrier protein. Biochemistry *39*, 15166–15178.

Møller, I.M., and Sweetlove, L.J. (2010). ROS signalling - specificity is required. Trends Plant Sci.

Morley, S.A., and Nielsen, B.L. (2017). Plant mitochondrial DNA. Front. Biosci. (Landmark Ed. *22*, 1023–1032.

Mouillon, J.M., Aubert, S., Bourguignon, J., Gout, E., Douce, R., and Rébeillé, F. (1999). Glycine and serine catabolism in non-photosynthetic higher plant cells: Their role in C1 metabolism. Plant J. *20*, 197–205.

Mower, J.P., Case, A.L., Floro, E.R., and Willis, J.H. (2012). Evidence against equimolarity of large repeat arrangements and a predominant master circle structure of the mitochondrial genome from a monkeyflower (Mimulus guttatus) lineage with cryptic CMS. Genome Biol. Evol. *4*, 670–686.

Muller, M., Mentel, M., van Hellemond, J.J., Henze, K., Woehle, C., Gould, S.B., Yu, R.-Y., van der Giezen, M., Tielens, A.G.M., and Martin, W.F. (2012). Biochemistry and Evolution of Anaerobic Energy Metabolism in Eukaryotes. Microbiol. Mol. Biol. Rev. *76*, 444–495.

Murcha, M.W., Elhafez, D., Millar, A.H., and Whelan, J. (2005). The C-terminal region of TIM17 links the outer and inner mitochondrial membranes in Arabidopsis and is essential for protein import. J. Biol. Chem. *280*, 16476–16483.

Nakao, Y., Kanamori, T., Itoh, T., Kodama, Y., Rainieri, S., Nakamura, N., Shimonaga, T., Hattori, M., and Ashikari, T. (2009). Genome Sequence of the Lager Brewing Yeast, an Interspecies Hybrid. DNA Res. An Int. J. Rapid Publ. Reports Genes Genomes *16*, 115.

Neuburger, M., Rébeillé, F., Jourdain, A., Nakamura, S., and Douce, R. (1996). Mitochondria are a major site for folate and thymidylate synthesis in plants. J. Biol. Chem. *271*, 9466–9472.

Okuda, K., Hammani, K., Tanz, S.K., Peng, L., Fukao, Y., Myouga, F., Motohashi, R., Shinozaki, K., Small, I., and Shikanai, T. (2010). The pentatricopeptide repeat protein OTP82 is required for RNA editing of plastid ndhB and ndhG transcripts. Plant J. *61*, 339–349.

Oldenburg, D.J., and Bendich, A.J. (1996). Size and Structure of Replicating Mitochondrial DNA in Cultured Tobacco Cells. Plant Cell *8*, 447–461.

Oldenkott, B., Yang, Y., Lesch, E., Knoop, V., and Schallenberg-Rüdinger, M. (2019). Plant-type pentatricopeptide repeat proteins with a DYW domain drive C-to-U RNA editing in Escherichia coli. Commun. Biol. *2*, 1–8.

Palmer, J.D., and Shields, C.R. (1984). Tripartite structure of the Brassica campestris mitochondrial

genome. Nature *307*, 437–440.

Peng, C., Uygun, S., Shiu, S.-H., and Last, R.L. (2015). The Impact of the Branched-Chain Ketoacid Dehydrogenase Complex on Amino Acid Homeostasis in Arabidopsis. Plant Physiol. *169*, pp.00461.2015.

Perkins, G., Renken, C.W., Klei, I.J. van der, Ellisman, M.H., Neupert, W., and Frey, T.G. (2001). Electron tomography of mitochondria after the arrest of protein import associated with Tom19 depletion. Eur. J. Cell Biol. *80*, 139–150.

Peterhansel, C., Horst, I., Niessen, M., Blume, C., Kebeish, R., Kürkcüoglu, S., and Kreuzaler, F. (2010). Photorespiration. 1–24.

Petersen, G., Cuenca, A., Møller, I.M., and Seberg, O. (2015). Massive gene loss in mistletoe (Viscum, Viscaceae) mitochondria. Sci. Rep. *5*, 17588.

Pfeffer, S., Woellhaf, M.W., Herrmann, J.M., and Förster, F. (2015). Organization of the mitochondrial translation machinery studied in situ by cryoelectron tomography. Nat. Commun. *6*, 6019.

Phreaner, C.G., Williams, M.A., and Mulligan, R.M. (1996). Incomplete Editing of rps12 Transcripts Results in the Synthesis of Polymorphic Polypeptides in Plant Mitochondria. Plant Cell *8*, 107.

Picciocchi, A. (2001). Biochemical Characterization of the Arabidopsis Biotin Synthase Reaction. The Importance of Mitochondria in Biotin Synthesis. Plant Physiol. *127*, 1224–1233.

Picciocchi, A., Douce, R., and Alban, C. (2003). The plant biotin synthase reaction. Identification and characterization of essential mitochondrial accessory protein components. J. Biol. Chem. *278*, 24966–24975.

Pinel, C., Douce, R., and Mache, R. (1986). A study of mitochondrial ribosomes from the higher plant Solanum tuberosum L. Mol. Biol. Rep. *11*, 93–97.

Planchard, N., Bertin, P., Quadrado, M., Dargel-Graffin, C., Hatin, I., Namy, O., and Mireau, H. (2018). The translational landscape of Arabidopsis mitochondria. Nucleic Acids Res. *46*, 6218–6228.

Plattner, H., Salpeter, M.M., Saltzgaber, J., and Schatz, G. (1970). Promitochondria of Anaerobically Grown Yeast, IV. Conversion into Respiring Mitochondria. Proc. Natl. Acad. Sci. *66*, 1252–1259.

Preuten, T., Cincu, E., Fuchs, J., Zoschke, R., Liere, K., and Börner, T. (2010). Fewer genes than organelles: extremely low and variable gene copy numbers in mitochondria of somatic plant cells. Plant J. *64*, 948–959.

Pu, X., Lv, X., Tan, T., Fu, F., Qin, G., and Lin, H. (2015). Roles of mitochondrial energy dissipation systems in plant development and acclimation to stress. Ann. Bot. *116*, 583–600.

Ramrath, D.J.F., Niemann, M., Leibundgut, M., Bieri, P., Prange, C., Horn, E.K., Leitner, A., Boehringer, D., Schneider, A., and Ban, N. (2018). Evolutionary shift toward protein-based architecture in trypanosomal mitochondrial ribosomes. Science (80-.). *362*, eaau7735.

Rasmusson, A.G., and Escobar, M.A. (2007). Light and diurnal regulation of plant respiratory gene expression. Physiol. Plant. *129*, 57–67.

Rasmusson, A.G., and Wallström, S.V. (2010). Involvement of mitochondria in the control of plant cell NAD(P)H reduction levels. Biochem. Soc. Trans. *38*, 661–666.

Rasmusson, A.G., Soole, K.L., and Elthon, T.E. (2004). Alternative Nad(P)H Dehydrogenases of Plant Mitochondria. Annu. Rev. Plant Biol. *55*, 23–39.

Rasmusson, A.G., Geisler, D.A., and Møller, I.M. (2008). The multiplicity of dehydrogenases in the electron transport chain of plant mitochondria. Mitochondrion *8*, 47–60.

Ravanel, S., Cherest, H., Jabrin, S., Grunwald, D., Surdin-Kerjan, Y., Douce, R., and Rébeillé, F. (2001). Tetrahydrofolate biosynthesis in plants: Molecular and functional characterization of dihydrofolate synthetase and three isoforms of folylpolyglutamate synthetase in Arabidopsis thaliana. Proc. Natl. Acad. Sci. *98*, 15360–15365.

Rhoads, D.M., Umbach, A.L., Sweet, C.R., Lennon, A.M., Rauch, G.S., and Siedow, J.N. (1998). Regulation of the cyanide-resistant alternative oxidase of plant mitochondria: Identification of the cysteine residue involved in α-keto acid stimulation and intersubunit disulfide bond formation. J. Biol. Chem. *273*, 30750–30756.

Roger, A.J., Muñoz-Gómez, S.A., and Kamikawa, R. (2017). The Origin and Diversification of Mitochondria. Curr. Biol. *27*, R1177–R1192.

Rogov, A.G., and Zvyagilskaya, R.A. (2015). Physiological role of alternative oxidase (from yeasts to plants). Biochem. *80*, 400–407.

Saed-Moucheshi, A., Shekoofa, A., and Pessarakli, M. (2014). Reactive Oxygen Species (ROS) Generation and Detoxifying in Plants. J. Plant Nutr. *37*, 1573–1585.

Sagan, L. (1967). On the origin of mitosing cells. J. Theor. Biol. *14*, 225-IN6.

Saha, B., Borovskii, G., and Panda, S.K. (2016). Alternative oxidase and plant stress tolerance. Plant Signal. Behav. *11*, e1256530.

Saisho, D., Nakazono, M., Lee, K.-H., Tsutsumi, N., Akita, S., and Hirai, A. (2001). The gene for alternative oxidase-2 (AOX2) from Arabidopsis thaliana consists of five exons unlike other AOX genes and is transcribed at an early stage during germination. Genes Genet. Syst. *76*, 89–97.

Schägger, H., and Pfeiffer, K. (2000). Supercomplexes in the respiratory chains of yeast and mammalian mitochondria. EMBO J. *19*, 1777–1783.

Schardl, C.L., Lonsdale, D.M., Pring, D.R., and Rose, K.R. (1984). Linearization of maize mitochondrial chromosomes by recombination with linear episomes. Nature *310*, 292–296.

Schertl, P., and Braun, H.-P. (2014). Respiratory electron transfer pathways in plant mitochondria. Front. Plant Sci. *5*, 163.

Schleyer, M., and Neupert, W. (1985). Transport of proteins into mitochondria: Translocational intermediates spanning contact sites between outer and inner membranes. Cell *43*, 339–350.

Schülke, N., Sepuri, N.B., Gordon, D.M., Saxena, S., Dancis, A., and Pain, D. (1999). A multisubunit complex of outer and inner mitochondrial membrane protein translocases stabilized in vivo by translocation intermediates. J. Biol. Chem. *274*, 22847–22854.

Schwaiger, M., Herzog, V., and Neupert, W. (1987). Characterization of translocation contact sites involved in the import of mitochondrial proteins. J. Cell Biol. *105*, 235–246.

Senda, T., and Yoshinaga-Hirabayashi, T. (1998). Intermembrane bridges within membrane organelles revealed by quick-freeze deep-etch electron microscopy. Anat. Rec. *251*, 339–345.

Sharma, M.R., Koc, E.C., Datta, P.P., Booth, T.M., Spremulli, L.L., and Agrawal, R.K. (2003). Structure of the Mammalian Mitochondrial Ribosome Reveals an Expanded Functional Role for Its Component Proteins. Cell *115*, 97–108.

Sheahan, M.B., Rose, R.J., and McCurdy, D.W. (2004). Organelle inheritance in plant cell division: the actin cytoskeleton is required for unbiased inheritance of chloroplasts, mitochondria and endoplasmic reticulum in dividing protoplasts. Plant J. *37*, 379–390.

Sheahan, M.B., McCurdy, D.W., and Rose, R.J. (2005). Mitochondria as a connected population: ensuring continuity of the mitochondrial genome during plant cell dedifferentiation through massive

mitochondrial fusion. Plant J. *44*, 744–755.

Shikanai, T. (2015). RNA editing in plants: Machinery and flexibility of site recognition. Biochim. Biophys. Acta - Bioenerg.

Silva, J.E. (2006). Thermogenic Mechanisms and Their Hormonal Regulation. Physiol. Rev. *86*, 435–464.

Skippington, E., Barkman, T.J., Rice, D.W., and Palmer, J.D. (2017). Comparative mitogenomics indicates respiratory competence in parasitic Viscum despite loss of complex I and extreme sequence divergence, and reveals horizontal gene transfer and remarkable variation in genome size. BMC Plant Biol. *17*, 49.

Skippingtona, E., Barkman, T.J., Ricea, D.W., and Palmera, J.D. (2015). Miniaturized mitogenome of the parasitic plant viscum scurruloideum is extremely divergent and dynamic and has lost all nad genes. Proc. Natl. Acad. Sci. U. S. A. *112*, E3515–E3524.

Sloan, D.B. (2013). One ring to rule them all? Genome sequencing provides new insights into the 'master circle' model of plant mitochondrial DNA structure. New Phytol. *200*, 978–985.

Sloan, D.B., Alverson, A.J., Chuckalovcak, J.P., Wu, M., McCauley, D.E., Palmer, J.D., and Taylor, D.R. (2012a). Rapid evolution of enormous, multichromosomal genomes in flowering plant mitochondria with exceptionally high mutation rates. PLoS Biol. *10*, e1001241.

Sloan, D.B., Alverson, A.J., Chuckalovcak, J.P., Wu, M., McCauley, D.E., Palmer, J.D., and Taylor, D.R. (2012b). Rapid evolution of enormous, multichromosomal genomes in flowering plant mitochondria with exceptionally high mutation rates. PLoS Biol. *10*.

Smith, A.M.O., Ratcliffe, R.G., and Sweetlove, L.J. (2004). Activation and function of mitochondrial uncoupling protein in plants. J. Biol. Chem. *279*, 51944–51952.

de Souza, W., Attias, M., and Rodrigues, J.C.F. (2009). Particularities of mitochondrial structure in parasitic protists (Apicomplexa and Kinetoplastida). Int. J. Biochem. Cell Biol. *41*, 2069–2080.

Stern, D.B., and Palmer, J.D. (1984). Recombination sequences in plant mitochondrial genomes: diversity and homologies to known mitochondrial genes. Nucleic Acids Res. *12*, 6141–6157.

Stroh, A., Anderka, O., Pfeiffer, K., Yagi, T., Finel, M., Ludwig, B., and Schägger, H. (2004). Assembly of respiratory complexes I, III, and IV into NADH oxidase supercomplex stabilizes complex I in Paracoccus denitrificans. J. Biol. Chem. *279*, 5000–5007.

Suzuki, N., Koussevitzky, S., Mittler, R., and Miller, G. (2012). ROS and redox signalling in the response of plants to abiotic stress. Plant, Cell Environ. *35*, 259–270.

Sweetlove, L.J., Lytovchenko, A., Morgan, M., Nunes-nesi, A., Taylor, N.L., Baxter, C.J., Eickmeier, I., and Fernie, A.R. (2006). Mitochondrial uncoupling protein is required for efficient photosynthesis. *103*, 3–8.

Sweetlove, L.J., Beard, K.F.M., Nunes-Nesi, A., Fernie, A.R., and Ratcliffe, R.G. (2010). Not just a circle: Flux modes in the plant TCA cycle. Trends Plant Sci. *15*, 462–470.

Thirkettle-Watts, D., McCabe, T.C., Clifton, R., Moore, C., Finnegan, P.M., Day, D.A., and Whelan, J. (2003). Analysis of the Alternative Oxidase Promoters from Soybean. Plant Physiol. *133*, 1158–1169.

Umbach, A.L., Gonzàlez-Meler, M.A., Sweet, C.R., and Siedow, J.N. (2002). Activation of the plant mitochondrial alternative oxidase: insights from site-directed mutagenesis. Biochim. Biophys. Acta - Bioenerg. *1554*, 118–128.

Umbach, A.L., Ng, V.S., and Siedow, J.N. (2006). Regulation of plant alternative oxidase activity: A tale of two cysteines. Biochim. Biophys. Acta - Bioenerg. *1757*, 135–142.

Unseld, M., Marienfeld, J.R., Brandt, P., and Brennicke, A. (1997). The mitochondrial genome of Arabidopsis thaliana contains 57 genes in 366,924 nucleotides. Nat. Genet. *15*, 57–61.

Uyttewaal, M., Mireau, H., Rurek, M., Hammani, K., Arnal, N., Quadrado, M., and Giegé, P. (2008). PPR336 is Associated with Polysomes in Plant Mitochondria. J. Mol. Biol. *375*, 626–636.

Vanlerberghe, G.C., and McIntosh, L. (1994). Mitochondrial electron transport regulation of nuclear gene expression. Studies with the alternative oxidase gene of tobacco. Plant Physiol. *105*, 867–874.

Vanlerberghe, G.C., Martyn, G.D., and Dahal, K. (2016). Alternative oxidase: a respiratory electron transport chain pathway essential for maintaining photosynthetic performance during drought stress. Physiol. Plant. *157*, 322–337.

Vasconcelos, A.C.L., and Bogorad, L. (1971). Proteins of cytoplasmic, chloroplast, and mitochondrial ribosomes of some plants. Biochim. Biophys. Acta - Nucleic Acids Protein Synth. *228*, 492–502.

Vercesi, A.E., Borecký, J., Maia, I. de G., Arruda, P., Cuccovia, I.M., and Chaimovich, H. (2006). Plant Uncoupling Mitochondrial Proteins. Annu. Rev. Plant Biol. *57*, 383–404.

Vincent, A.E., White, K., Davey, T., Philips, J., Ogden, R.T., Lawless, C., Warren, C., Hall, M.G., Ng, Y.S., Falkous, G., et al. (2019). Quantitative 3D Mapping of the Human Skeletal Muscle Mitochondrial Network. Cell Rep. *26*, 996-1009.e4.

de Vries, S., and Grivell, L.A. (1988). Purification and characterization of a rotenone-insensitive NADH: Q6 oxidoreductase from mitochondria of Saccharomyces cerevisiae. Eur. J. Biochem. *176*, 377–384.

Wada, H., Shintani, D., and Ohlrogge, J. (1997). Why do mitochondria synthesize fatty acids? Evidence for involvement in lipoic acid production. Proc. Natl. Acad. Sci. U. S. A. *94*, 1591–1596.

Wada, M., Yasuno, R., Jordan, S.W., Cronan Jr., J.E., and Wada, H. (2001). Lipoic Acid Metabolism in Arabidopsis thaliana: Cloning and Characterization of a cDNA Encoding Lipoyltransferase. Plant Cell Physiol. *42*, 650–656.

Waszczak, C., Carmody, M., and Kangasjärvi, J. (2018). Reactive Oxygen Species in Plant Signaling. Annu. Rev. Plant Biol. *69*, 209–236.

Welchen, E., García, L., Mansilla, N., and Gonzalez, D.H. (2014). Coordination of plant mitochondrial biogenesis: keeping pace with cellular requirements. Front. Plant Sci. *4*, 551.

Williams, B.A.P., Hirt, R.P., Lucocq, J.M., and Embley, T.M. (2002). A mitochondrial remnant in the microsporidian Trachipleistophora hominis. Nature *418*, 865–869.

Wu, Z., Cuthbert, J.M., Taylor, D.R., and Sloan, D.B. (2015). The massive mitochondrial genome of the angiosperm Silene noctiflora is evolving by gain or loss of entire chromosomes . Proc. Natl. Acad. Sci. *112*, 10185–10191.

Yasuno, R., and Wada, H. (1998). Biosynthesis of lipoic acid in Arabidopsis: cloning and characterization of the cDNA for lipoic acid synthase. Plant Physiol. *118*, 935–943.

Zabala, G., Gabay-Laughnan, S., Laughnan, J.R., Roark, L., Oddiraju, S., Lin, G.N., Meyer, L., Sun, H., Kim, K., Wang, C., et al. (1997). The nuclear gene Rf3 affects the expression of the mitochondrial chimeric sequence R implicated in S-type male sterility in maize. Genetics *147*, 847–860.

Zamponi, N., Zamponi, E., Cannas, S.A., Billoni, O. V, Helguera, P.R., and Chialvo, D.R. (2018). Mitochondrial network complexity emerges from fission/fusion dynamics. Sci. Rep. *8*, 363.

Zhang, Y., Beard, K.F.M., Swart, C., Bergmann, S., Krahnert, I., Nikoloski, Z., Graf, A., George Ratcliffe, R., Sweetlove, L.J., Fernie, A.R., et al. (2017). Protein-protein interactions and metabolite channelling in the plant tricarboxylic acid cycle. Nat. Commun. *8*, 15212.

Zoglowek, C., Krömer, S., and Heldt, H.W. (1988). Oxaloacetate and Malate Transport by Plant Mitochondria. Plant Physiol. *87*, 109–115.

Chapter 2: Publications & Manuscripts

Publication 1

2.1 Single organelle function and organization as estimated from Arabidopsis mitochondrial proteomics

Philippe Fuchs[1,2,#], Nils Rugen[3,#], Chris Carrie[4], Marlene Elsässer[1,2,5], Iris Finkemeier[1], Jonas Giese[1], Tatjana M. Hildebrandt[3], Kristina Kühn[6], Veronica G. Maurino[7], Cristina Ruberti[1], Mareike Schallenberg-Rüdinger[5], Janina Steinbeck[1], Hans-Peter Braun[3,§], Holger Eubel[3,§], Etienne H. Meyer[6,§], Stefanie J. Müller-Schüssele[2,§], Markus Schwarzländer[1,§]

[1] Institut für Biologie und Biotechnologie der Pflanzen (IBBP), Westfälische Wilhelms-Universität, Schlossplatz 7-8, 48143 Münster, Germany

[2] Institut für Nutzpflanzenforschung und Ressourcenschutz (INRES), Rheinische Friedrich-Wilhelms-Universität Bonn, Friedrich-Ebert-Allee 144, 53113 Bonn, Germany

[3] Institut für Pflanzengenetik, Leibniz Universität Hannover, Herrenhäuser Str. 2, 30419 Hannover, Germany

[4] Department Biologie I - Botanik, Ludwig-Maximilians Universität München, Grosshadernerstr. 2-4, 82152 Planegg-Martinsried, Germany

[5] Institut für Zelluläre und Molekulare Botanik (IZMB), Rheinische Friedrich-Wilhelms-Universität Bonn, Kirschallee 1, 53115 Bonn, Germany

[6] Institut für Biologie, Martin-Luther-Universität Halle-Wittenberg, Weinbergweg 10, 06120 Halle/Saale, Germany

[7] Institute of Developmental and Molecular Biology of Plants, and Cluster of Excellence on Plant Sciences (CEPLAS), Heinrich Heine University Düsseldorf, Universitätsstraße 1, 40225 Düsseldorf, Germany.

[#] authors contributed equally, [§] authors contributed equally
Correspondence: markus.schwarzlander@uni-muenster.de

Type of authorship:	Shared first author
Type of article:	Research article
Share of the work:	10%
Contribution to the publication:	Planed and performed experiments, analyzed data
Journal:	The Plant Journal
Impact factor:	5.72
Number of citations (Web of Science):	0
Date of Publication:	September 14, 2019
DOI:	10.1111/tpj.14534

* Note that the supplementary files for chapter 2.1 are not included in the printed version of this dissertation (but included on the accompanied compact disc).

the plant journal

SEB SOCIETY FOR EXPERIMENTAL BIOLOGY

The Plant Journal (2019) doi: 10.1111/tpj.14534

RESOURCE

Single organelle function and organization as estimated from Arabidopsis mitochondrial proteomics

Philippe Fuchs[1,2,†], Nils Rugen[3,†], Chris Carrie[4], Marlene Elsässer[1,2,5], Iris Finkemeier[1], Jonas Giese[1], Tatjana M. Hildebrandt[3], Kristina Kühn[6], Veronica G. Maurino[7], Cristina Ruberti[1], Mareike Schallenberg-Rüdinger[5], Janina Steinbeck[1], Hans-Peter Braun[3,††], Holger Eubel[3,††], Etienne H. Meyer[6,††], Stefanie J. Müller-Schüssele[2,††] and Markus Schwarzländer[1,*††]

[1]*Institut für Biologie und Biotechnologie der Pflanzen (IBBP), Westfälische Wilhelms-Universität, Schlossplatz 7-8, 48143 Münster, Germany,*

[2]*Institut für Nutzpflanzenforschung und Ressourcenschutz (INRES), Rheinische Friedrich-Wilhelms-Universität Bonn, Friedrich-Ebert-Allee 144, 53113 Bonn, Germany,*

[3]*Institut für Pflanzengenetik, Leibniz Universität Hannover, Herrenhäuser Str. 2, 30419 Hannover, Germany,*

[4]*Department Biologie I - Botanik, Ludwig-Maximilians-Universität München, Grosshadernerstr. 2-4, 82152 Planegg-Martinsried, Germany,*

[5]*Institut für Zelluläre und Molekulare Botanik (IZMB), Rheinische Friedrich-Wilhelms-Universität Bonn, Kirschallee 1, 53115 Bonn, Germany,*

[6]*Institut für Biologie, Martin-Luther-Universität Halle-Wittenberg, Weinbergweg 10, 06120 Halle/Saale, Germany, and*

[7]*Institute of Developmental and Molecular Biology of Plants, and Cluster of Excellence on Plant Sciences (CEPLAS), Heinrich Heine University Düsseldorf, Universitätsstraße 1, 40225 Düsseldorf, Germany*

Received 12 June 2019; revised 23 August 2019; accepted 28 August 2019.
*For correspondence (e-mail markus.schwarzlander@uni-muenster.de).
†These authors contributed equally to this work.
††These authors contributed equally to this work.

In memory of Axel Brennicke (1953–2017).

SUMMARY

Mitochondria host vital cellular functions, including oxidative phosphorylation and co-factor biosynthesis, which are reflected in their proteome. At the cellular level plant mitochondria are organized into hundreds of discrete functional entities, which undergo dynamic fission and fusion. It is the individual organelle that operates in the living cell, yet biochemical and physiological assessments have exclusively focused on the characteristics of large populations of mitochondria. Here, we explore the protein composition of an individual average plant mitochondrion to deduce principles of functional and structural organisation. We perform proteomics on purified mitochondria from cultured heterotrophic Arabidopsis cells with intensity-based absolute quantification and scale the dataset to the single organelle based on criteria that are justified by experimental evidence and theoretical considerations. We estimate that a total of 1.4 million protein molecules make up a single Arabidopsis mitochondrion on average. Copy numbers of the individual proteins span five orders of magnitude, ranging from >40 000 for Voltage-Dependent Anion Channel 1 to sub-stoichiometric copy numbers, i.e. less than a single copy per single mitochondrion, for several pentatricopeptide repeat proteins that modify mitochondrial transcripts. For our analysis, we consider the physical and chemical constraints of the single organelle and discuss prominent features of mitochondrial architecture, protein biogenesis, oxidative phosphorylation, metabolism, antioxidant defence, genome maintenance, gene expression, and dynamics. While assessing the limitations of our considerations, we exemplify how our understanding of biochemical function and structural organization of plant mitochondria can be connected in order to obtain global and specific insights into how organelles work.

Keywords: plant mitochondrion, single organelle, proteomics, intensity-based absolute quantification, oxidative phosphorylation, TCA cycle, antioxidant defence, cofactor synthesis, mitochondrial genome, RNA editing, mitochondrial fission, *Arabidopsis thaliana*.

© 2019 The Authors.
The Plant Journal published by Society for Experimental Biology and John Wiley & Sons Ltd
This is an open access article under the terms of the Creative Commons Attribution License, which permits use, distribution and reproduction in any medium, provided the original work is properly cited.

INTRODUCTION

Mitochondria are central to complex life. Their evolutionary, genetic, biophysical, biochemical, and cell biological characteristics have been studied intensely. However, the resulting views of the organelle have remained remarkably separated between disciplines in several cases. Mitochondria were recognized early as organelles that exist as multiple individual entities in cells (Altmann, 1890). Those entities were later identified as the location of respiration, based on morphological considerations (Kingsbury, 1912), and dissected in their architecture by electron microscopy, and, more recently, super-resolution microscopy techniques (Sjostrand, 1953; Jakobs and Wurm, 2014; Chen *et al.*, 2018). Edmund V. Cowdry recognized the intrinsic limitation of pure morphological investigations as early as 1924 by pointing out that

> it is quite obvious that the investigation of mitochondria will never achieve the usefulness which it deserves as an instrument for advance in biology and medicine until we know much more of their chemical constitution as the only accurate basis for interpretation of our findings. In other words, we must wait up on the slow development of direct, quantitative cellular chemistry. (Cowdry, 1924)

In parallel, mitochondrial functions, such as their respiratory or biosynthetic features, were analysed across large numbers of mitochondria in organisms and tissues, or isolated from those sources (Utter *et al.*, 1958; Ohnishi and Hagihara, 1964; Weiss *et al.*, 1970; Werner and Neupert, 1972). The fundamental divide between cell biological and biochemical approaches to mitochondria has left a void at the centre of organelle biology, leaving the question open of how exactly the individual mitochondrion carries out its functions as a physically discrete unit.

How the individual mitochondrion, as the smallest unit of mitochondrial populations in cells, works is relevant across eukaryotic organisms. Several organisms contain extensive mitochondrial networks (Hoitzing *et al.*, 2015) resulting in a situation of a single cell containing only a few large mitochondria or even a single physically discrete mitochondrion. Examples are mitochondria in yeast, trypanosomes or several mammalian cell types (de Souza *et al.*, 2009; Rafelski, 2013; Zamponi *et al.*, 2018; Vincent *et al.*, 2019). At the opposite end of this spectrum, small, highly fragmented mitochondria are present, for instance, in mammalian neurons and flowering plant cells. Cells of flowering plants, such as the reference organism *Arabidopsis thaliana*, typically contain several hundred of discrete organelles per cell, which are connected over time by fusion and fission (Sheahan *et al.*, 2005). The organizational structure of plant mitochondria has been described as a 'discontinuous whole' (Logan, 2006), to emphasize that the organelles form a continuous network that does not exist in space but over time. However, nearly all mitochondrial function occurs at the level of the individual mitochondrion and is constrained by the physical properties of the individual unit.

A realistic understanding of the processes that occur at the single organelle level requires *in vivo* analysis. This has become possible for specific parameters through fluorescent sensors, and has provided initial insights into heterogeneity in composition and function between single mitochondria, e.g. with respect to mtDNA content and bioenergetics (Arimura *et al.*, 2004b; Schwarzländer *et al.*, 2012). Yet, imaging-based approaches to explore the properties of individual mitochondria remain cumbersome, are typically limited to only a small set of parameters and leave a large proportion of mitochondrial functions inaccessible. Very recently, an imaging-based approach was used to estimate stoichiometry and protein copy numbers in carboxysomes (Sun *et al.*, 2019) raising hopes that analogous approaches may become available for other organelles in the future.

The development of increasingly sensitive and sophisticated proteomic approaches has allowed the identification of proteins in mitochondrial extracts and to infer functional characteristics of mitochondria (Kruft *et al.*, 2001; Millar *et al.*, 2001; Heazlewood *et al.*, 2004). Also a limited number of quantitative proteomic datasets of plant mitochondria have been reported (Nelson *et al.*, 2013; Mueller *et al.*, 2014; Salvato *et al.*, 2014; Wagner *et al.*, 2015; Senkler *et al.*, 2017) and relative protein abundances have been linked to specific mitochondrial pathways (Taylor *et al.*, 2011). Generating proteomic datasets from a single mitochondrion of any organism remains impossible due to technical constraints. Important insights into the proteome of a single mitochondrion come from a recent study in yeast (Morgenstern *et al.*, 2017). High quality quantitative proteomic datasets allowed the extraction of absolute copy numbers of the individual mitochondrial proteins under the assumption that each yeast cell hosts a single mitochondrion. The fragmented nature of plant mitochondria, with hundreds of small and discrete units per cell adds a further layer of complexity. An elegant first step towards the protein inventory of a single plant mitochondrion has recently been taken through a theoretical appraisal (Møller, 2016).

Our motivation to explore the composition of a single mitochondrion is based on the question if new insights into organelle biology can be obtained by applying the geometrical constraints under which the individual mitochondria function to biochemical data generated from a population of mitochondria. Normalization of quantitative proteomic data allows scaling down from the population

© 2019 The Authors.

to the averaged individual, which may already deliver decisive benefits.

In this article, we explore the proteomic makeup of a single mitochondrion and what that might imply for its structure and function as an individual unit. We use shotgun proteomics of isolated mitochondria from heterotrophic Arabidopsis cell suspension culture in combination with intensity-based absolute quantification (iBAQ). We normalize the proteomic dataset to derive average copy numbers of individual proteins in a single mitochondrion using reasonable assumptions based on experimental evidence about the physical properties of a typical plant mitochondrion. We make use of the protein copy numbers per mitochondrion to explore the potential added value of considering the single organelle to gain meaningful insights into plant mitochondrial properties and processes. We unite expertise from several current fields of plant research to explore the implications of a single organelle perspective on a range of specific biological questions. We develop hypotheses and devise several thought experiments, based on available data, to synthesize an original perspective that illustrates how individual mitochondria operate. The approach exemplifies a strategy that may be used also for other organisms, cells and organelles.

RESULTS AND DISCUSSION

Towards the protein inventory of a single mitochondrion

A single mitochondrion is made up by about 1.4 million proteins. We aimed at estimating the total protein number per single mitochondrion. This requires assumptions about mitochondrial size and shape, both of which are variable in plant mitochondria. Based on literature micrographs, our own experience with live fluorescence microscopy as well as transmission electron microscopy of *A. thaliana* mitochondria (Figure 1a), a sphere of 0.8 μm in diameter represents a reasonable approximation of an average mitochondrion from a living heterotrophic Arabidopsis cell (de Virville *et al.*, 1998; Logan and Leaver, 2000; Eubel *et al.*, 2007). Most Arabidopsis mitochondria are spherical to bean-shaped within a diameter range of 0.4–2.0 μm, with the exception of slender, extended individuals, which are typically underrepresented. Mitochondrial density previously measured experimentally at 1.2 g ml^{-1} (Glas and Bahr, 1966), allows estimating the weight of a single hydrated plant mitochondrion of 0.8 μm in diameter at 322 fg (see Dataset S1, worksheet #2). The dry mass contribution to hydrated mitochondrial weight was determined at 26–35%, but was subsequently criticized as a gross underestimation (Glas and Bahr, 1966; Berthet and Baudhuin, 1967). Assuming 25% protein content, which is justified by the additional presence of lipids, metabolites, RNA and DNA, a single mitochondrion contains 80.4 fg of protein (Dataset S1, worksheet #2).

To estimate how many protein copies a mitochondrion is comprised of, we calculated the abundance-adjusted weight of an average protein in our proteomic samples (as introduced below), equalling 38 350 Da (6.37×10^{-20} g), closely reflecting the values retrieved from the SUBAcon database (39 247 Da) (Hooper *et al.*, 2014) (Dataset S1, worksheet #4). Considering that an N-terminal targeting peptide of a large proportion of proteins, encoded in the nuclear genome, is proteolytically cleaved after import, we subtracted 3514 Da (abundance-weighted average mitochondrial target peptide size, corrected for frequency of occurrence, see Dataset S1, worksheet #5) (Kmiec *et al.*, 2014; Ghifari *et al.*, 2019). Accordingly, a mass of 34 836 Da (5.78×10^{-20} g) was estimated for a mature mitochondrial protein on average, resulting in 1 390 777 protein molecules that constitute a single mitochondrion. This is in line with previous estimations (10^6 protein copies for a small mitochondrion; 1.6×10^6 for a mitochondrion of the size considered here) derived from a different set of assumptions (Møller, 2016).

Intensity-based quantitative proteomics to estimate protein copy numbers per mitochondrion. To exemplify our approach, we chose isolated mitochondria from Arabidopsis dark-cultured cell suspensions for shotgun proteomics. The cell suspensions provide the technical advantage of fast growth and low contamination with photosynthetic plastid proteins. They do not represent any specialized tissue and are not synchronized for cell cycle progression, minimizing bias from specialized functions or a dominating effect of biogenesis. While specific functions, such as the support of photosynthesis, are unlikely to be represented by this material, it will be straightforward to adjust the approach to any other source of mitochondria.

Four biological replicates from separate mitochondrial protein isolations were analyzed by liquid chromatography coupled with tandem mass spectrometry (LC-MS/MS). At least one unique peptide was required for a protein to be considered as identified. An intensity-based absolute quantification (iBAQ) score was used as a quantitative estimate for each identified protein, for which only unique peptides and razor peptides were taken into account (Arike *et al.*, 2012). We normalized the iBAQ scores against the sum of all iBAQ values in each replicate, calculated the median iBAQ score per protein across the four replicates and renormalized against the sum of all iBAQ scores. The resulting normalized median iBAQ scores indicate the fraction of the quantitative contribution of each protein to the proteome. Multiplication of this score for each protein by the total number of protein molecules per single mitochondrion (1 390 777; see above) provided an estimate of the copy number of each protein species per mitochondrion (Figure 1a). This approach provides meaningful estimates of protein copy number across the proteome overall, but is

© 2019 The Authors.
The Plant Journal published by Society for Experimental Biology and John Wiley & Sons Ltd,
The Plant Journal, (2019), doi: 10.1111/tpj.14534

(a)

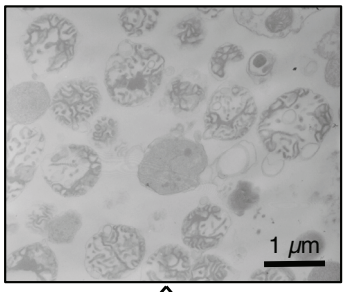

LC-MS/MS

MaxQuant analysis

iBAQ values

normalisation
averaging
re-normalisation

individual abundance in relation to the whole proteome

volume of one mitochondrion

density
protein content

weight of proteins in one mitochondrion

weight of an average mature mitochondrial protein

number of proteins per mitochondrion

copy number of each protein per mitochondrion

(b)

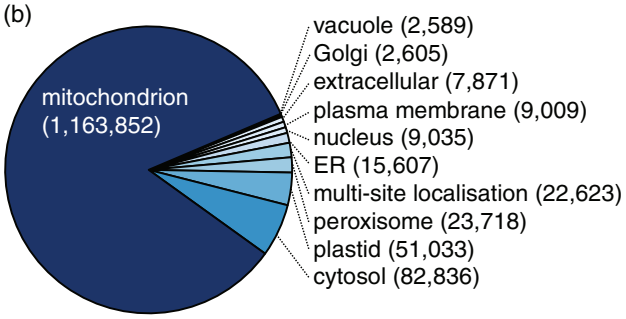

(c)

functional meta-category	copy number	protein species	rel. abundance
ATP production and export	557,063	141	47.9%
protein import, synthesis, modification and turnover	221,372	365	19.0%
metabolism	139,798	123	12.0%
transport	125,845	45	10.8%
UFP	60,903	193	5.2%
other minor groups	58,871	50	5.1%
total	1,163,852	917	100%

Figure 1. The proteome of a single mitochondrion.
(a) Overview of our approach summarizing the proteomics and the calculations made to obtain copy numbers. Steps marked with blue background represent assumptions; all others are based on experimental findings, physical constraints and calculations. See Dataset S1, worksheet #2, for all calculation details. The electron micrograph was obtained from a mitochondrial preparation from heterotrophic Arabidopsis cell suspension culture. Liquid chromatography coupled with tandem mass spectrometry (LC-MS/MS); Intensity-Based Absolute Quantification (iBAQ).
(b) Subcellular location of identified proteins. In total 2934 protein species were identified and classified according to their likely subcellular location based on SUBAcon (Hooper *et al.*, 2014). The cumulated copy number of all protein species allocated to a subcellular compartment is provided in brackets and displayed as a percentage of the total copy number of all proteins.
(c) Functional meta-categories for 917 proteins with mitochondrial localisation as identified by SUBAcon (finer classification into functional sub-categories is shown in Table S1); Unknown function protein (UFP).

© 2019 The Authors.

limited by the intrinsic shortcomings of proteomic analysis of biological samples and iBAQ quantitation, such as the individual biochemical peptide properties affecting ionisation and detection characteristics (Schwanhäusser *et al.*, 2011; Fabre *et al.*, 2014; Krey *et al.*, 2014). To exemplify the principle in the following sections we treat the calculated copy numbers from the datasets as precise values.

Critical appraisal of the single mitochondrion proteome dataset. In total, 2934 protein species were identified and quantified across the four biological replicates (Dataset S1, worksheet #1). More than two-thirds of these were detected in all four samples (Figure S1a), indicating that the dataset is coherent with respect to both protein content and technical reproducibility.

Organelles isolated from disrupted cells often contain proteins attributed to other cellular components, which may reflect contaminations or shared components. We used the SUBAcon algorithm (Hooper *et al.*, 2014) which unambiguously assigned 2799 proteins to a single cellular location, based on weighted experimental evidence and predictions. One third of these (917 proteins) are annotated as mitochondrial, while most of the remaining proteins were annotated as plastidic (597 proteins) or cytosolic (564 proteins, Figure S1b). Protein abundance (as deduced from normalized iBAQ values; Dataset S1, worksheet #1) revealed that 84% of the protein content in the mitochondrial isolates are of mitochondrial origin (1 163 852 copies out of 1 390 777 copies in total; Figure 1b), which matches in range the purity of isolated Arabidopsis mitochondria used for quantitative proteomics reported previously (Klodmann *et al.*, 2010; Senkler *et al.*, 2017).

One of the four replicates contained a higher amount of plastid contamination as indicated by the strongly increased abundance of the marker proteins RbcL, AccD, ClpP1, and Rps11, which are encoded by the plastid genome (Dataset S1, worksheet #1). We consciously decided to use the full dataset without applying additional selection criteria, because many mitochondrial proteins are expected to be present at low abundance and would be lost if more stringent parameters were applied. In addition, the use of median instead of mean for our calculations of the normalized iBAQ values largely balanced the effects originating from an individual outlier (i.e. one replicate with higher contamination levels). For the specific goals pursued here limiting the risk of excluding mitochondrial proteins of low abundance outweighs the benefit of stringent exclusion of contaminants. Another limitation is the inherent incompleteness of proteomic datasets. Thus, several mitochondrial proteins, such as the intron maturase MatR or the OXPHOS subunit Atp9, which are encoded in the mitochondrial genome, were not identified. Although they may not be expressed (or very lowly) in the cells we analysed, their absence in our dataset is more likely due to their biochemical properties preventing their identification by mass spectrometry. Out of the different groups of mitochondrial proteins, the oxidative phosphorylation (OXPHOS) complexes are particularly prone to underestimation partly because they are enriched in protein subunits with unfavourable properties for mass spectrometry, such as small size and high hydrophobicity.

Considerations about the mitochondrion as an individual

Almost half of the mitochondrial proteome serves cellular ATP provision. When the 917 mitochondrial protein species are broadly classified according to their annotated functions (Table S1; Figure 1c; Figure S1c,d; Hooper *et al.*, 2014), the group of proteins involved in ATP production and transport makes up 557 063 copies, which is almost 48% of the total mitochondrial protein content. The 97 proteins involved in OXPHOS (105 when complex II is included) contribute most of the copies. Interestingly, 53 944 protein copies (10% of copies within this group) belong to only five ATP transporters (AAC1, AAC2, AAC3, APC2, ADNT1), mirroring the extremely high ATP fluxes that a mitochondrion is able to maintain. The combined copy number of all remaining mitochondrial transporters identified for the inner membrane (IMM) and outer membrane (OMM; 125 845 copies in total) belong to distinctively more protein species (45 protein species).

Protein import, synthesis, modification and turnover, are carried out by 221 372 protein molecules (19% of the total mitochondrial protein content, Figure 1c). The high number of 365 protein species in this meta-group that includes the functional groups 'protein import', 'RNA processing', 'protein synthesis' and 'protein fate' (Table S1), is mainly due to the high number of proteins related to RNA processing (135 protein species), most of which are pentatricopeptide repeat (PPR) proteins. Metabolism not related to cellular respiration uses only 139 798 molecules (12% of the mitochondrial protein content) and is mainly related to amino acid metabolism (44 of 123 protein species in this meta-group).

The makeup of the outer and inner mitochondrial membranes is dominated by few protein species. The mitochondrion is delimited by a double membrane system and each membrane contains a specific set of proteins. The protein with the highest copy number in the mitochondrion is the Voltage-dependent anion channel 1 (VDAC1: 44 381 copies), which resides in the OMM and constitutes the main passage between the cytosol and the intermembrane space (IMS) for a large variety of compounds (Colombini, 2004). In a single Arabidopsis mitochondrion, 80 760 monomers of the five VDAC isoforms (VDAC1–5) are present, which equals a density of 40 167 VDAC channels per μm^2 (OMM surface: 2.0 μm^2) (Dataset S2, worksheet #1). Assuming that the dimensions of the Arabidopsis VDACs are similar to

© 2019 The Authors.
The Plant Journal published by Society for Experimental Biology and John Wiley & Sons Ltd,
The Plant Journal, (2019), doi: 10.1111/tpj.14534

those found for the human VDAC crystal structure (Bayrhuber *et al.*, 2008; 8.5 nm^2 lipid-displacing area), 34.2% of the OMM surface consist of VDAC proteins (Figure 2; Dataset S2, worksheet #1), making VDACs a major building block of the OMM. Considering that VDAC conductance is regulated (Zizi *et al.*, 1994; Hodge and Colombini, 1997; Mlayeh *et al.*, 2010), the VDAC proteins not only provide a high degree of permeability to the OMM, but also effectively functionalise the membrane to act as a conditional *nano-sieve*. Gating of metabolite fluxes by VDACs is likely to play an important regulatory role to adjust organelle metabolism, physiology and volume (Liu and Colombini, 1992). *Pits* and *in-plane subunits* of proteins that occur at sufficiently high density to adopt crystalline array

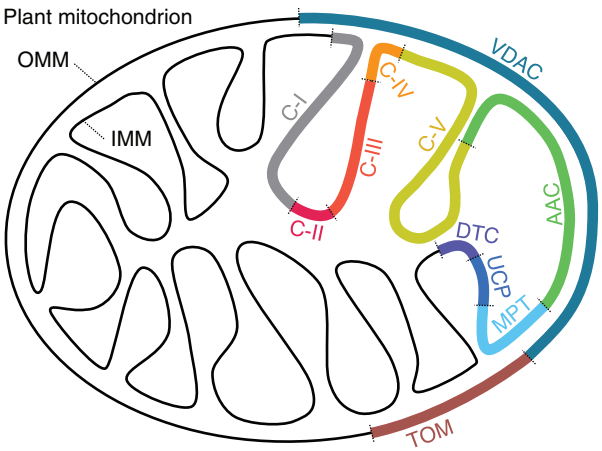

Protein family/complex	area of OMM
VDAC	34.2%
TOM	12.1%
Protein family/complex	**area of IMM**
Complex I (C-I)	5.0%
Complex II (C-II)	0.8%
Complex III (C-III)	2.7%
Complex IV (C-IV)	1.2%
Complex V (C-V)	8.4%
AAC	6.2%
MPT	2.5%
UCP	1.0%
DTC	0.8%
remaining proteins	~1.1%

Figure 2. Proportions of mitochondrial membrane areas constituted by individual protein families.
Schematic representation of the outer mitochondrial membrane (OMM) and the inner mitochondrial membrane (IMM) of a typical plant mitochondrion in a 1:3 ratio (membrane area represented as lines). Colour-coded membrane segments represent the proportional constitution of OMM or IMM by highly abundant protein families and protein complexes in % of total membrane area occupied as shown in the table inset. VDAC (voltage-dependent anion-selective channel protein), TOM (translocase of the outer membrane), C-I (NADH:ubiquinone oxidoreductase), C-II (succinate dehydrogenase), C-III (cytochrome bc_1 complex), C-IV (cytochrome *c* oxidase), C-V (ATP-synthase), AAC (ADP/ATP carrier), MPT (mitochondrial phosphate carrier protein), UCP (uncoupling protein), DTC (mitochondrial dicarboxylate/tricarboxylate carrier).

organisation were already found in early electron micrographs and by X-ray diffraction of plant OMM preparations (Parsons, 1965; Mannella and Bonner, 1975; Mannella, 1982). They can be retrospectively identified as VDAC. A density of 20 000 molecules per μm^2 OMM was calculated by Mannella and Bonner, 1975, corresponding to 40 000 VDAC proteins per mitochondrion, or 20% of OMM for the mitochondrial dimensions adopted here. Both estimates (34.2% and 20%) turn out similar, considering that they are derived from independent approaches and different assumptions. A second major constituent of the OMM is the Translocase of the Outer Membrane (TOM) complex that covers an additional 12.1% of the OMM surface area (Figure 2; Dataset S2, worksheet #6) and is discussed in further detail in the next section.

In contrast to the domination of the OMM by the protein families of VDAC and TOM, the IMM protein inventory is made up by a large number of different proteins of which a large proportion groups into the OXPHOS complexes (17 258 complexes; Dataset S2, worksheet #2) and carrier proteins (97 980 copies) (Dataset S2, worksheet #3; Figure 2). Assuming a OMM:IMM ratio of 1:3 as reported for rat liver mitochondria (Schwerzmann *et al.*, 1986), complex I (~120 nm^2 lipid-displacing area; Zickermann *et al.*, 2015) alone constitutes 5% of the IMM (6 μm^2), while complex II (~16 nm^2 lipid-displacing area; Sun *et al.*, 2005), III_2 (~50 nm^2 lipid-displacing area; Zhang *et al.*, 1998) and IV (~38 nm^2 lipid-displacing area; Dudkina *et al.*, 2011) together add up to another 4.7% (0.8%, 2.7% and 1.2%, respectively) (Dataset S2, worksheet #2). The estimated mitochondrial electron transport chain (ETC) complex density ranges for the complexes I to IV (413, 523, 542, and 318 complexes per μm^2, respectively) are in general agreement with previous reports for mammalian mitochondria (277, 535, 812, and 1880 complexes per μm^2, respectively) (Gupte *et al.*, 1984). Conceivably, packing high amounts of bulky ETC complexes, particularly complex I, into the membrane impacts on the overall IMM architecture. This concept is well-established for ATP-synthase dimers, which introduce the curvature required for cristae formation (Dudkina *et al.*, 2005; Davies *et al.*, 2012; Hahn *et al.*, 2016). In our dataset, the total area of the ATP-synthase membrane-integral part amounts to 8.4% area of the IMM, which nearly equals the area composed of complexes I–IV (9.7% of IMM area). Overall the OXPHOS complexes make up 18.1% of the IMM, which is in line with ATP production as a defining mitochondrial function (Figure 2; Dataset S2, worksheet #2).

OXPHOS relies on bulk substrate availability in the mitochondrial matrix, which needs to be supplied from the cytosol by high flux rates through IMM carriers. The necessity for high transport capacity is mirrored by high copy numbers of transporters mediating the exchange of ADP/ATP, Pi/H$^+$, di- and tricarboxylates and the uncoupling of

© 2019 The Authors.

the H^+-gradient at 53 065 (mitochondrial ADP/ATP carrier 1–3; AAC1–3), 21 325 (mitochondrial phosphate transporter 2 and 3; MPT2 and MPT3), 6836 (mitochondrial dicarboxylate/tricarboxylate carrier, DTC) and 8595 (uncoupling proteins 1 and 3; UCP1 and UCP3) copies (Dataset S2, worksheet #3). These transporters make up 10.5% of IMM area assuming a lipid-displacing area of ~7 nm^2 as estimated from the bovine AAC crystal structure (Pebay-Peyroula *et al.*, 2003) (AAC 6.2%, MPT 2.5%, DTC 0.8% and UCP 1%; Figure 2; Dataset S2, worksheet #3). In contrast to the transporters that mediate the bulk fluxes of energy metabolism, all remaining identified carriers together amount to 1.1% of IMM area. Note that this is based on the curated list of IMM transporters in Dataset S2 (worksheet #3), and not the global, but less precise, SUBAcon classification, which includes proteins, such as GET3c or MICU that are not membrane transporters. In total, the OXPHOS and carriers account for ~30% of the IMM area, corresponding to 41.4% of the IMM weight (Dataset S2, worksheet #4), which is about half of what has been previously estimated (~80 weight-%) (Krauss, 2001). While the concept of proteins dominating the makeup of the IMM is supported by our estimations, the difference to previous numbers is likely due to the underestimation of OXPHOS proteins by the MS-based approach. This effect may be illustrated taking complex I as an example, which is made up of a matrix arm and a membrane arm at a 1:1 stoichiometry. Averaging the number of matrix arm proteins results in 3932 matrix arm copies, but averaging the number of membrane arm proteins results in only 1841 membrane arm copies. There is no experimental indication, however, of a significant amount of unassembled matrix arm subunits in the mitochondrion (Meyer *et al.*, 2007). Instead matrix arm proteins are typically found in the membrane fraction, i.e. assembled with the membrane arm and set in stoichiometry. This inconsistency suggests that the copy numbers of the membrane arm proteins are systematically underestimated by the mass spectrometry approach. The number of complex I particles per mitochondrion may be more realistically estimated based on the matrix arm only, which would increase the estimation from 2491 complex I copies (averaged across all subunits) to 3932 complex I copies (average of matrix arm subunits only) (Dataset S3, worksheet #2). An analogous effect is to be expected for other OXPHOS complexes, but it is hard to account for this effect systematically due to the individual biochemical properties of the complex subunits involved. The rough assumption of doubling the OXPHOS complex copy numbers increases the protein area of the IMM to 48%, corresponding to 62% of the membrane weight, which closes the gap to previous reports using independent approaches (Krauss, 2001).

A maximum of 18 crista sheets can be stacked in the typical Arabidopsis mitochondrion, based on the dimensions of the OXPHOS complexes (here specifically complex I and complex V) (Dataset S2, worksheet #5). Assuming that those cristae are organized as flat sheet structures that span the entire available diameter of the matrix, the summed-up length of the cristae ridges, where rows of ATP synthase dimers provide curvature (Blum *et al.*, 2019), adds up to 32.5 μm. Considering a diameter of about 10 nm per ATP synthase dimer in the row of dimers (Zickermann *et al.*, 2015), 3253 dimers are required to constitute the cristae ridges. This requirement matches the number of ATP synthase molecules present in the single mitochondrion (6426 monomers, 3213 dimers) (Dataset S3, worksheet #2). This remains a rough estimate since the cristae may adopt different sizes and more complex shapes, which would then decrease or increase, respectively, the number of dimers required. The presence of the 18 crista sheets is an upper limit, since it would leave insufficient space for large protein complexes, such as the pyruvate decarboxylase complex (PDC), 2-oxoglutarate dehydrogenase complex (OGDC) and the glycine decarboxylase complex (GDC), in the matrix (discussed in the sections on TCA cycle and GDC). Furthermore, 18 cristae would result in an IMM surface area of 12 μm^2, or an IMM:OMM surface area ratio of 6:1 instead of 3:1, as used for the estimations above (Schwerzmann *et al.*, 1986). In the presence of less cristae, a surplus of ATP-synthase molecules may exist as monomers that do not introduce membrane curvature (Blum *et al.*, 2019), or as dimers to introduce more complex cristae structures.

The protein import machinery could double the mitochondrial proteome in under 7 h. Of all mitochondrial protein copies, 12% are involved in protein import and protein fate, including maturation, folding, and degradation (221 372 protein copies; Figure 1c; Table S1). The components of the import apparatus are of particular importance since the vast majority of mitochondrial proteins are encoded by nuclear genes, synthesized in cytosolic ribosomes, and must be imported.

The main entry gate into mitochondria is the translocase of the outer membrane (TOM) complex and almost all proteins entering mitochondria must pass through it. The TOM complex is by far the most abundant import complex found in a single mitochondrion with 8139 TOM40 copies (Dataset S2, worksheet #6). Previous work on mammalian and yeast mitochondria have demonstrated that the TOM complex is triangular (containing 3 TOM40 channels) measuring 14.5 nm on edge and that between 8 and 14 TOM complexes cluster together in assemblies of approximately 30–40 nm in diameter (Model *et al.*, 2008; Wurm *et al.*, 2011). Assuming these values are similar for plant TOM complexes, a single plant mitochondrion contains 247 TOM complex clusters on average (assuming 11 TOM complexes per cluster), accounting for 12.1% of the OMM surface area as noted above (Dataset S2, worksheet #6;

© 2019 The Authors.

Figure 2). These numbers match previous observations in yeast, which contains approximately 100 active import sites per μm^2 of OMM surface area (Gold *et al.*, 2014).

The two translocases of the inner membrane, the TIM23 and TIM22 complexes, are present at much lower numbers. Assuming that both complexes exist as dimers (Bauer *et al.*, 1996), only 175 TIM22 complex dimers (349 copies of TIM22) and 370 TIM23 complex dimers (740 copies of TIM17 and 852 copies of TIM23) are present per mitochondrion (compared to the 2713 TOM complexes) (Figure S2). In yeast, the stoichiometry of TOM40:TIM23:TIM22 proteins was calculated to be 5:1:0.2 (Sirrenberg *et al.*, 1997), in plant mitochondria we found a very similar stoichiometry 7.3:1:0.5. TOM complexes are found in excess over the inner membrane translocases and this may reflect the fact that the TOM complexes must import, in addition to proteins of the inner membrane and the matrix, proteins destined for the OMM and the IMS. TIM22 is only present at 349 copies per mitochondrion, while one of the many TIM22 substrates, the ATP/ADP carrier 1 protein (AAC1), is present at 39 984 copies. The TIM23 complex imports proteins containing pre-sequences, equalling approximately 70% of protein copies (973 544 copies) per mitochondrion. How long would it take one mitochondrion to double the copy number of all TIM23 substrates? Assuming a translocation rate of 40 amino acids per second (based on Sec pathway measurements in bacteria, (Fessl *et al.*, 2018), an average protein length of 353 amino acids and 370 active import sites per mitochondrion (assuming that the TIM23 complex is the limiting step), it would take approximately 6 h and 27 min to double the number of TIM23 substrate proteins in a single mitochondrion.

Composition and function of the OXPHOS system. The OXPHOS system of plants consists of the complexes I–V, cytochrome *c*, the alternative oxidase (AOX) and alternative NAD(P)H dehydrogenases (NDs) (Meyer *et al.*, 2019). Overall, 115 proteins that represent subunits of OXPHOS components were identified in the course of a recent complexome profiling approach in Arabidopsis and additional 21 proteins were identified by other investigations (Senkler *et al.*, 2017 and discussion within). If isoforms are subtracted, the Arabidopsis OXPHOS system—according to current knowledge—consists of 105 distinct protein species. Only three of these proteins are not covered by our proteome datasets (the SDH8 subunit of complex II and the c-subunit of the ATP synthase complex, both of which are very small and hydrophobic, and the AOX1B protein; Dataset S3, worksheet #2). Copy numbers of proteins forming part of the same protein complex vary to a degree (Dataset S3, worksheet #2), which may be due to biological reasons (e.g., multiple copies of some subunits per complex [e.g., α- and β-subunit of complex V], non-assembled subunits) or technical reasons (e.g., dependence of the iBAQ score on the hydrophobicity of a protein). Average copy numbers of OXPHOS components were calculated by averaging copy numbers of all the identified subunits (corrected for specific subunits if they are present in more than one copy per complex) (Dataset S3, worksheet #2). The result likely represents a lower estimate of the number of OXPHOS complexes. An account of the limits of this approach is provided above in the section "*Critical appraisal of the single mitochondrion proteome dataset*".

The ATP synthase (complex V; 6426 particles per mitochondrion) and complex III (6537 complex III monomers, corresponding to 3268 complex III dimers) are the most abundant OXPHOS components, which correlates well with results from blue native PAGE (Senkler *et al.*, 2017). About 2491 copies of complex I, 3156 copies of complex II and 1916 copies of complex IV are present per mitochondrion. These numbers explain why supercomplex formation of complex I and dimeric complex III leads to drastic reduction of monomeric complex I particles, while complex III dimers remain abundant (Dudkina *et al.*, 2005). The copy number of cytochrome *c* (2252) lies in between the copy numbers of dimeric complex III and complex IV. Complex IV of plants can also form part of respiratory supercomplexes together with dimeric complex III or dimeric complex III plus monomeric complex I (Eubel *et al.*, 2004). Respiratory supercomplexes that include the complexes I, III_2 and IV are also designated "respirasomes", because they can autonomously carry out the entire reaction of the ETC (assuming cytochrome *c* and ubiquinone are present). The copy number of complex IV in a single mitochondrion of Arabidopsis suggests that complex IV is limiting respirasome formation in plant mitochondria. There is a current consensus that supramolecular assemblies of respiratory supercomplexes and singular (monomeric) respiratory complexes co-exist under *in vivo* conditions and that the degree of supercomplex formation varies depending on physiological conditions of plant cells (Ramírez-Aguilar *et al.*, 2011). In total, 222 136 proteins form part of the four *classical* protein complexes of the respiratory chain (complexes I–IV), 52.9% (117 427) belonging to complex I. In Arabidopsis, complex I contains a carbonic anhydrase (CA) domain that includes gamma-type CA subunits (Fromm *et al.*, 2016b). This domain consists of three CA subunits of the five known plant CA/CAL proteins (CA1, CA2, CA3, CAL1 and CAL2) in combinations that are not precisely defined so far (Fromm *et al.*, 2016b). With the realistic assumption that these five proteins have similar biochemical properties and therefore their copy numbers can be interpreted in term of stoichiometry, our results show that the CA2 protein is clearly the most prominent CA/CAL protein (47% of all CA/CAL proteins). Summed up copy numbers for CA1 and CA3 only account for 31% and the ones for CAL1 and CAL2 for 22%. This provides a plausible

© 2019 The Authors.

explanation for the particularly drastic reduction of complex I in mutants lacking CA2 (Wang *et al.*, 2012; Fromm *et al.*, 2016a).

Assuming a respiratory activity of 200 nmol O_2 min^{-1} mg $protein^{-1}$ that is typical for isolated Arabidopsis mitochondria (Eubel *et al.*, 2007; Wagner *et al.*, 2015) and an ADP/O ratio of 2.5, we estimated that a single mitochondrion produces 968 658 ATP molecules per second, corresponding to 151 ATP molecules by each of the 6426 ATP synthase complexes (Dataset S2, worksheet #7). This synthesis rate corresponds to a rotation rate of ATP synthase of 50 sec^{-1}, which is consistent in range with the 130 sec^{-1} measured for the ATP hydrolysis activity of a prokaryotic ATP-synthase at saturating ATP supply (Yasuda *et al.*, 2001). Assuming that all export of the ATP that the mitochondrion synthesizes is mediated by AAC1–3, each of the 53 065 AAC protein copies (Dataset S2, worksheet #3) needs to transport 18 ATP molecules per second. The combined activities of the 6426 ATP-synthase motors deliver 103 fW of power per mitochondrion (assuming $\Delta G(ATP)$ at -64 kJ mol^{-1} under physiological conditions). This means that less than a 2-cl shot glass worth of respiring mitochondria (18.2 ml) turn over the equivalent of the power consumption of a modern 7W LED, that replaces the traditional 60W light bulb (Dataset S2, worksheet #8).

TCA cycle proteins make up over 80% of the matrix protein volume. The tricarboxylic acid (TCA) cycle is a central hub of primary plant metabolism, serving biosynthesis, catabolism and energy conversion. Its integrative role in the cellular metabolic network requires unique flexibility of TCA cycle flux in plants, and several different flux modes, both cyclic and non-cyclic, have been reported depending on the physiological circumstances (Sweetlove *et al.*, 2010). In heterotrophic Arabidopsis cells a cyclic flux mode can be anticipated. The ten enzymatic steps of the TCA cycle (including pyruvate dehydrogenase and NAD-malic enzyme) are represented by 176 358 protein copies per mitochondrion, corresponding to 12.7% of mitochondrial protein content (Table S1). Assuming that the matrix volume takes up 50% of the total mitochondrial volume (Møller, 2016), and estimating the protein volume from available protein crystal structures of non-plant species (Dataset S2, worksheet #9, TCA cycle proteins are well-conserved), the TCA cycle enzymes occupy 16.8% of the matrix volume (0.0225 μm^3 out of 0.134 μm^3, Figure 3; Dataset S2, worksheet #9). This equals 80.5% of the protein volume of the matrix (assuming similar average density of the proteins as of the mitochondrion overall and similar weight contribution of proteins to matrix as to whole mitochondrion). The two large multi-enzyme complexes PDC (*Mr* ~10^7) and 2-oxoglutarate dehydrogenase (OGDC; *Mr* ~4×10^6) alone account for 11.2% of the total matrix volume (10.2% and 1.0%, respectively, corresponding to 49.0% and 4.7% of matrix protein volume) (Figure 3; Dataset S2, worksheet #9). The total number of PDC and OGDC is as small as 222 and 181, respectively, as multiple functional enzymes are organised in these megacomplexes (Zhou *et al.*, 2001) (active units E1, E2 and E3 in 5:5:2 stoichiometry; PDC: 14 204 protein copies, OGDC: 12 998

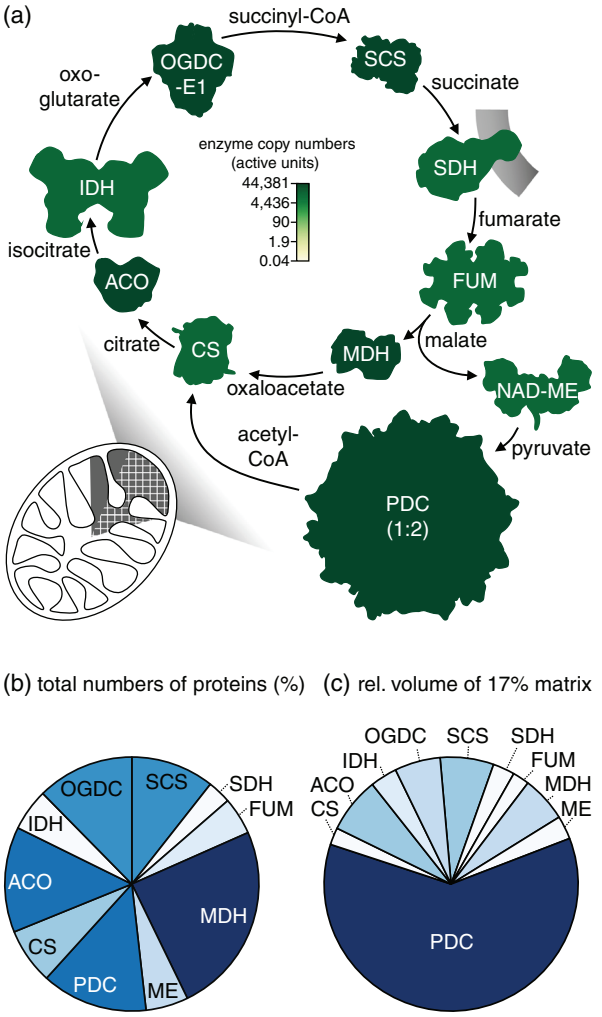

Figure 3. TCA cycle enzymes.
(a) Matrix volume occupied by all matrix proteins shaded in grey (20.8%), contribution of TCA cycle enzymes grid patterned (16.8%). Enzyme structures show physiologically relevant oligomerisation (active enzymes): citrate synthase (CS) as dimer, aconitase (ACO) as monomer, isocitrate dehydrogenase (IDH) as hetero-octamer of four outer catalytic and four inner regulatory subunits, pyruvate dehydrogenase complex (PDC) scaled down in displayed size by half (1:2) compared to all other enzymes and the 2-oxoglutarate dehydrogenase (OGDC)-E1 subunit as homodimer, succinyl-CoA-synthase (SCS) as heterotetramer (two α- and two β-subunits), succinate dehydrogenase (SDH) as monomer, fumarase (FUM) as tetramer, malate dehydrogenase (MDH) as homodimer, NAD-malic enzyme (NAD-ME) as homodimer.
Pie charts show (b) the proportion of enzymes (active units in %) to the total numbers of TCA cycle proteins (physiologically active units: 105 135) and (c) the contribution of each TCA enzyme relative to the TCA enzyme-occupied matrix space (%).

© 2019 The Authors.
The Plant Journal published by Society for Experimental Biology and John Wiley & Sons Ltd,
The Plant Journal, (2019), doi: 10.1111/tpj.14534

protein copies). Aconitase (ACO) and malate dehydrogenase (MDH) are both comparatively small proteins, but high in abundance (14 121 and 25 684 copies), contributing 1.2% and 1.0% of the total matrix volume, each. Succinate dehydrogenase (SDH) is the only integral membrane protein linking the TCA cycle with the respiratory electron transport chain. Its matrix-exposed part accounts for 0.5% total matrix volume, while it makes up 0.8% of the IMM area (assuming an IMM:OMM ratio of 3:1, Schwerzmann *et al.*, 1986). SDH makes the smallest contribution to the total number of TCA cycle enzymes (3156 SDH complex monomers). The large contribution of TCA cycle enzymes to fill the crowded matrix volume makes substrate diffusion between enzymes extremely efficient and the discrimination of functional protein–protein interactions for metabolon formation from more random interactions particularly challenging (Zhang *et al.*, 2017).

A mitochondrion has the capacity to metabolize its own mass worth in malate within 1 h. Different from mammals where pyruvate is the primary TCA cycle substrate, the main substrate can vary between metabolic states in plants and malate plays a particularly prominent role (Sweetlove *et al.*, 2010). Malate is metabolized through two different reactions catalyzed by NAD-malic enzyme (NAD-ME) and malate dehydrogenase (MDH) (Figure 3) (Maurino and Engqvist, 2015). NAD-ME1 and NAD-ME2 associate to form active homo- and heterodimers to metabolize malate to pyruvate. A single mitochondrion contains similar amounts of NAD-ME1 (2632 copies) and NAD-ME2 (3061 copies) (Dataset S1, worksheet #1 and S2, worksheet #10). In a heterotrophic organ, such as roots, the total NAD-ME activity is composed of 8% NAD-ME1 homodimers, 32% NAD-ME2 homodimers, and 60% heterodimers (Tronconi *et al.*, 2008). Applying those contributions to the single mitochondrion, there are 155 NAD-ME1 homodimers (310 NAD-ME1 copies), and 2322 heterodimers (2322 NAD-ME1 copies). Analogously, 1065 copies of NAD-ME2 are present in 532 homodimers, and 1996 copies contribute to 1996 heterodimers. The independent consideration of NAD-ME1 and 2 result in similar copy numbers involved in heterodimers (2322 versus 1996) in line with their 1:1 stoichiometry in the complex. Based on the enzymatic turnover numbers determined *in vitro* for the three different dimer types (Tronconi *et al.*, 2010), a single mitochondrion has a total NAD-ME capacity to metabolize 224 852 malate molecules per second (Dataset S2, worksheet #10).

An analogous estimation for mitochondrial MDH (13 190 copies of MDH1; 10 826 copies of MDH2; Dataset S2, worksheet #10 and S3, worksheet #4) suggests that total MDH capacity is at 183 625 malate molecules per second (Dataset S2, worksheet #10). This estimation is based on the *in vitro* turnover numbers for the reverse reaction of OAA to malate and the consideration that MDH1 and MDH2 have 80-fold and 34-fold higher maximal activity for OAA than for malate as substrate (Hüdig *et al.*, 2015). The capacities of NAD-ME and MDH for malate turnover appear to be similar and add up to 408 477 molecules of malate per second. This equals a mass of 54.8 MDa per second adding up to the mass of the entire single mitochondrion over the course of 59 min (Dataset S2, worksheet #10). This remarkable capacity appears highly above of what is typically required for malate oxidation *in vivo*, but is generally consistent with previous indications that MDH (but not NAD-ME) is present at > 100-fold excess (Hagedorn *et al.*, 2004). Carbon flux through MDH and NAD-ME will certainly be constrained by several influences, including malate uptake into the matrix, efficient product removal, and recycling of NAD^+, but the high combined capacity of MDH and NAD-ME emphasizes the significance of malate metabolism in plant mitochondria.

The copy numbers of glycine decarboxylase and serine hydroxymethyltransferase proteins mirror metabolic demands of the cell. The glycine decarboxylase complex (GDC) acts together with the serine hydroxymethyltransferase (SHMT) to convert glycine to serine, which is an essential step in the photorespiratory cycle (Bauwe *et al.*, 2010; Peterhänsel *et al.*, 2010) and in N^5,N^{10}-methylene tetrahydrofolate provision for one-carbon metabolism (Engel *et al.*, 2007; Maurino and Peterhänsel, 2010).

The GDC is a multi-enzyme system of four loosely associated P-, H-, T- and L-proteins (Bauwe and Kolukisaoglu, 2003; Peterhänsel *et al.*, 2010). The four proteins are present in unequal molar amounts, but the exact stoichiometric composition of the Arabidopsis complex is not yet established. The GDC components in the heterotrophic Arabidopsis cell suspension culture mitochondria, in which photorespiration is not active, accounts for only a small fraction (0.18%) of the mitochondrial proteome mass (Dataset S2, worksheet #11). This is consistent with the idea that the abundance of the GDC proteins positively correlates with the photosynthetic activity (Bourguignon *et al.*, 1993; Mouillon *et al.*, 1999). GDC contributes up to 32% of the total matrix protein in photosynthetically active pea leaves (Oliver *et al.*, 1990). In the heterotrophic cell suspension culture mitochondria only 0.57% of the total matrix space is occupied by GDC (Dataset S2, worksheet #11). We found 807 copies of GDC-P, 2503 copies of GDC-H, 2577 copies of GDC-T, 14 990 copies of GDC-L (MTLPD1: 4876; MTLPD2: 10 114) per mitochondrion (Datasheet S1, worksheet #1; Dataset S3, worksheet #5). The excess of the L-proteins detected may be explained by the additional participation as E3 subunits of the pyruvate and 2-oxoglutarate dehydrogenase complexes assuming that both L-proteins are shared between GDC, PDC, OGDC and

© 2019 The Authors.

branched-chain α-ketoacid dehydrogenase (BCKDH) (Bourguignon *et al.*, 1992, 1996; Lutziger and Oliver, 2001). The shared contribution of the L-proteins to the former three dehydrogenase complexes was considered in the calculations (Dataset S2, worksheets #9 and #11). Assuming that the turnover rates of the P-proteins from Arabidopsis are similarly low as those of *Synechocystis* (Hasse *et al.*, 2007), the GDC has the capability of converting only 115 molecules glycine per second in the cell suspension culture single mitochondrion (Dataset S2, worksheet #11).

Serine hydroxymethyltransferase (SHMT) is present at higher copy numbers than GDC, which is mainly due to SHMT2 (3885 copies; SHMT1: 38 copies). The low representation of SHMT1 can be explained by its involvement in photorespiration, which is not active in the heterotrophic mitochondrion (Somerville and Ogren, 1981; Engel *et al.*, 2011), while SHMT2 is typically not present in photosynthetically active cells (McClung *et al.*, 2000; Bauwe and Kolukisaoglu, 2003). Assuming that the turnover numbers of SHMT1 and 2 are similar to that of the plastidial isoform (Zhang *et al.*, 2010), the heterotrophic mitochondrion has the capability of producing 61 989 molecules of serine and tetrahydrofolate per second (Dataset S2, worksheet #11), indicating active one-carbon metabolism.

High copy numbers reflect the essential functions of mitochondrial amino acid catabolism enzymes. Beyond glycine catabolism, mitochondria are a major site of amino acid degradation. The different catabolic pathways give rise to several intermediates of mitochondrial carbon metabolism (Hildebrandt *et al.*, 2015). The proteome here generated includes almost all presently known mitochondrial steps of the amino acid catabolic pathways, i.e. the enzymes catalyzing the degradation of branched-chain amino acids, Pro and Arg, Cys, as well as Ser/Gly metabolism (Dataset S3, worksheet #6).

The degradation pathways of most amino acids require transfer of the amino group to 2-oxoglutarate catalyzed by a diverse set of aminotransferases followed by oxidative deamination of Glu by glutamate dehydrogenase (GDH) (Hildebrandt *et al.*, 2015). Consistently, GDH2 is the most abundant amino acid metabolic enzyme and with 12 933 copies per mitochondrion it is the twelfth most abundant protein of the mitochondrion overall. GDH1 is present at 4269 copies further boosting the enzymatic capacity of GDH. Several aminotransferases operating upstream of GDH are also present at high copy numbers, the most abundant being GABA transaminase (5418 copies), aspartate aminotransferase 1 (5347 copies) and alanine aminotransferase 1 (4728 copies).

The prominence of mitochondrial Cys metabolism, as a hub of several downstream pathways is emphasized by high copy numbers of mitochondrial O-acetylserine (thiol) lyase (OASC; 3571 copies) required for Cys synthesis and regulation (Wirtz *et al.*, 2012), the Cys desulfurase NifS (4265 copies) involved in the synthesis of iron-sulfur clusters and of β-cyanoalanine synthase (CAS; 12 218 copies). CAS catalyzes the substitution of the Cys sulfhydryl group with cyanide to produce the β-cyanoalanine and H_2S (Hatzfeld *et al.*, 2000). The main physiological function of CAS is thought to be the detoxification of cyanide produced during ethylene synthesis to protect cytochrome *c* oxidase from irreversible inhibition. The 12 218 copies of CAS exceed those of complex IV markedly (1916 copies, see above). Considering the fact that the flux of cyanide production in the cell is very low in comparison to respiratory flux, a very high copy number of CAS in the matrix, i.e. in direct vicinity to the active site of cytochrome *c* oxidase, reflects the potentially detrimental effect of cyanide inhibition and the importance of the activity of the cyanide-sensitive pathway of respiration.

Antioxidant enzyme capacity exceeds mitochondrial ROS production by far. The generation of reactive oxygen species (ROS) in mitochondria requires a tight balance between ROS scavenging, ROS signalling functions and redox regulation of mitochondrial metabolism. Molecular oxygen is the terminal electron acceptor of the ETC where it accepts four electrons and is fully reduced to water. In addition, and at much lower rate, single electrons can be transferred to molecular oxygen at specific sites of the ETC, which gives rise to superoxide. The rate of superoxide production can vary considerably depending on the overall respiratory activity and substrate availability in the mitochondrion (Møller, 2001; Murphy, 2009). In isolated soybean mitochondria (state II), superoxide production of up to 1.3 nmol min^{-1} mg^{-1} protein was observed when mitochondria were fed with respiratory substrates for complex I+II. Hence, it was estimated that up to 5.9% of the respiratory electron flow ends up in superoxide production (Puntarulo *et al.*, 1988). This number is likely to be smaller *in vivo*, but provides a useful upper limit. In mitochondria isolated from Arabidopsis seedlings and cell suspension culture, state III respiratory rates typically reach 200 nmol O_2 min^{-1} mg^{-1} protein (Eubel *et al.*, 2007; Wagner *et al.*, 2015), which would result in a superoxide production of up to 11.8 nmol O_2^- min^{-1} mg^{-1} protein. Superoxide itself is unstable and dismutates into hydrogen peroxide and molecular oxygen with a rate constant of 5×10^5 M^{-1} sec^{-1}. Yet, superoxide also inactivates Fe/S cluster-containing proteins, such as aconitase, with rate constants of 10^6 to 10^7 M^{-1} sec^{-1} (Halliwell and Gutteridge, 2015). Manganese superoxide dismutase (MnSOD) competes with those reactions in the mitochondrial matrix, catalysing rapid superoxide dismutation. MnSOD (MSD1) was detected among the top 30 most abundant mitochondrial proteins (11 223 copies per mitochondrion) with a similar abundance to aconitase 3 (9898 protein copies). As

© 2019 The Authors.
The Plant Journal published by Society for Experimental Biology and John Wiley & Sons Ltd,
The Plant Journal, (2019), doi: 10.1111/tpj.14534

MnSODs reach turnover numbers (k_{cat}) of 40 000 sec^{-1} and k_{cat}/K_m of 8×10^8 M^{-1} sec^{-1} (Hsu *et al.*, 1996), the SOD capacity in a single mitochondrion is sufficient to detoxify 448 932 392 molecules of superoxide per second. This rate exceeds even generous estimates of superoxide generation by a factor of 39 000-fold (Dataset S2, worksheet #12). Potentially, the large amount of MnSOD copies present can be explained by increasing the probability for each superoxide molecule generated to be detoxified by MnSOD before encountering a Fe/S cluster-containing enzyme. The enormous SOD capacity in the mitochondrial matrix matches the observation that MnSOD activity is not rate-limiting in ROS detoxification under stress (Kliebenstein *et al.*, 1998).

As superoxide dismutation leads to O_2 and hydrogen peroxide (H_2O_2) formation, it was estimated that 0.9–1.5% of consumed O_2 is converted to H_2O_2 (Puntarulo *et al.*, 1988), which would result in up to3 nmol H_2O_2 min^{-1} mg^{-1} $protein^{-1}$ at typical state III respiratory rates. Matrix peroxidases reduce H_2O_2 to water using either glutathione, ascorbate or the thioredoxin (Trx) system as electron donors. The most abundant peroxidase in the mitochondrion is peroxiredoxin II F (PrxII F) at 5787 copies, i.e. half the copy number of MnSOD. While that ratio matches the stoichiometry of H_2O_2 molecules to be detoxified per superoxide molecule (1:2), PrxII F has a much lower turnover number than MnSOD (0.67 sec^{-1} versus 40 000 sec^{-1}) (Finkemeier *et al.*, 2005) meaning that only 3877 H_2O_2 molecules can be reduced to water in a single mitochondrion per second. Induction of PrxII F protein abundance by more than 3-fold was observed in response to oxidative stress treatments (Sweetlove *et al.*, 2002), indicating that baseline PrxII F capacity can become limiting and needs to be increased under stress. Alternatively, the physiological role of PrxII F may be the oxidation of target thiols in the mitochondrial matrix, similar to the function of plastidic 2-Cys Prx (Pérez-Ruiz *et al.*, 2017; Vaseghi *et al.*, 2018). After oxidation, PrxII F has to be regenerated by glutathione or the thioredoxin (Trx) system (Finkemeier *et al.*, 2005). Both Trx-o1 (837 copies) and -o2 (20 copies) were detected in the mitochondrial proteome, as well as the mitochondrial NADPH-dependent thioredoxin reductases a (Ntra; 913 copies) and b (Ntrb; 342 copies), both of which have been found dual-targeted to the cytosol and the mitochondrial matrix (Reichheld *et al.*, 2007). A high capacity for superoxide removal and a low capacity for H_2O_2 removal mirror the different physiological roles of the two reactive species. While superoxide will be quenched efficiently in the matrix, H_2O_2 fluctuations in matrix H_2O_2 remain plausible, as well as diffusion out of the matrix, consistent with the likely roles of H_2O_2 in intracellular signalling (Huang *et al.*, 2016).

However, there are additional peroxidases with much higher turnover numbers for H_2O_2 in the mitochondrion (Dataset S3, worksheet #7). The dual-localized stromal ascorbate peroxidase (sAPX) (Chew *et al.*, 2003) was detected at 1708 copies. Assuming that all detected protein comes from the mitochondrion (rather than from plastid contaminations) and a turnover number for H_2O_2 of 1800 sec^{-1} as for the tobacco sAPX (Kitajima *et al.*, 2008), the capacity of sAPX in a single mitochondrion is 3.07 Mio molecules of H_2O_2 per second. Although this generous estimate equals less than 1% of the MnSOD capacity, it mirrors a dominant role to sAPX in quenching a major share of the H_2O_2 flux in the matrix.

Mitochondria host co-factor biogenesis including iron-sulfur clusters, biotin, lipoic acid, tetrahydrofolate and potentially the last step of heme synthesis. A key function of mitochondria is the biogenesis of essential cofactors including iron-sulfur (Fe/S) clusters, biotin, lipoic acid and tetrahydrofolate. Proteins involved in the Fe/S assembly pathway are the most abundant of this category (above the average copy number of 474 copies) whereas the enzymes involved in biotin, lipoic acid and tetrahydrofolate biogenesis are detected at much lower copy numbers (21–347 copies; Figure 4; Dataset S3, worksheet #8). Interestingly, some enzymes (NSF1, BIO2 and HPPK/DHPS2) are present in excess compared to the others involved in the same pathway. This may reflect differing enzymatic capacities per protein, protein-specific inactivation through oxidative damage and/or different roles in the control of metabolic flux through the respective pathway. Proteins involved in the delivery of the cofactors to apoenzymes are less abundant than biosynthetic enzymes (Figure 4). Electrons provided by a ferredoxin reductase/ferredoxin (FDR/MFDX) system are required in three of these biosynthetic pathways. The two isoforms of MFDX detected show very differing copy numbers (MFDX1: 73 and MFDX2: 494). Based on the respective abundances of MFDX isoforms and biosynthetic enzymes, it is tempting to speculate that MFDX1 plays a role in biotin and lipoic acid biosynthesis, whereas MFDX2 is involved in Fe/S clusters biogenesis.

In plants, the heme synthesis pathway is located in the plastids (Tanaka and Tanaka, 2007), but its last step, i.e. the chelation of iron, was proposed to be also performed in mitochondria (Chow *et al.*, 1997, 1998; Hey *et al.*, 2016), however this has been disputed (Lister *et al.*, 2001; Masuda *et al.*, 2003; Woodson *et al.*, 2011). Several proteins involved in heme biosynthesis were identified in our analysis (Dataset S3, worksheet #8), albeit at low copy numbers (<80 copies), indicating etioplast contamination of our mitochondria isolations. Remarkably, the ferrochelatase (FC1) shows a copy number (78 copies) higher than the remaining proteins of the pathway (less than 26 copies, excluding the dual-targeted glutamyl-tRNA synthase), which may support the hypothesis that the last step of heme biosynthesis is actually present in plant mitochondria.

© 2019 The Authors.

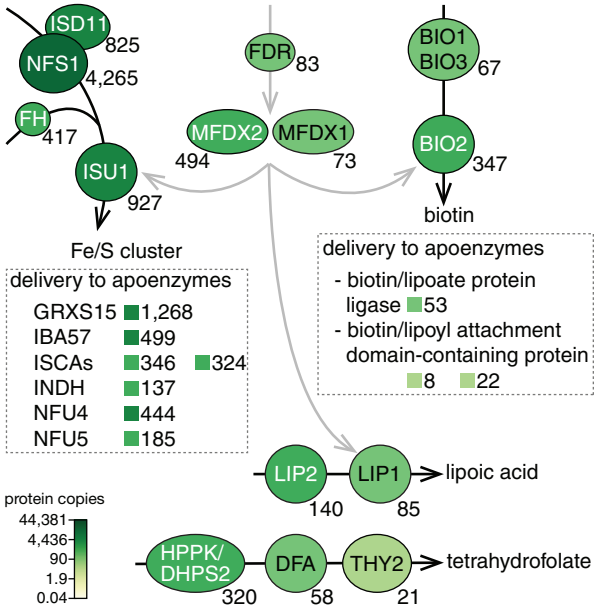

Figure 4. Cofactor biogenesis pathways.
Simplified representation of the mitochondrial steps of the biosynthesis pathways of Fe/S clusters, biotin, lipoic acid and tetrahydrofolate. Each pathway is represented with black arrows. The biosynthetic enzymes are represented as circles. The final product of the pathway is indicated in black. No substrates or intermediates are shown. The grey arrows represent electron transfers. Proteins involved in the delivery of the cofactor to the apoenzymes are indicated in dashed boxes together with their copy numbers. Cysteine desulfurase (NFS1); NFS1 interacting protein (ISD11); frataxin (FH); iron-sulfur cluster assembly protein 1 (ISU1); glutaredoxin S15 (GRXS15); iron-sulfur cluster assembly factor for biotin synthase- and aconitase-like mitochondrial proteins, with a mass of 57 kDa (IBA57); iron-sulfur cluster A-type carrier (ISCA); homologous to iron-sulfur protein required for NADH dehydrogenase (INDH); NifU-like protein (NFU); ferredoxin reductase (FDR); mitochondrial ferredoxin (MFDX); biotin synthase (BIO); lipoic acid synthase (LIP); bifunctional hydroxymethyl-dihydropterin-pyrophosphokinase and dihydropteroate synthase (HPPK/DHPS); folylpolyglutamate synthase (DFA); thymidylate synthase (THY).

Writers and erasers of several reversible protein modifications are present at low copy number in plant mitochondria. Reversible post-translational modifications play an important role for transient regulations of mitochondrial activities (Hartl and Finkemeier, 2012). Protein modifications derived from the metabolic cofactors ATP, *S*-adenosylmethionine, and acetyl-CoA as well as other acyl-CoA metabolites are present at a high abundance in mitochondria (Finkemeier and Schwarzländer, 2018). Although inventories of several of these protein modifications were reported for Arabidopsis mitochondria (Ito *et al.*, 2009; König *et al.*, 2014a; van Wijk *et al.*, 2014; Hosp *et al.*, 2017), most of the writers and erasers of these modifications are unknown.

The light-dependent inactivation of the pyruvate dehydrogenase E1 subunit by phosphorylation via pyruvate dehydrogenase kinase (PDK) represents an important example of a known writer (Mooney *et al.*, 2000). We identified 120 PDK copies and 8944 copies of its substrate, the catalytic pyruvate dehydrogenase (PDH) E1 β-subunit. Assuming the mammalian PDK kinase activity of 70 nmol min^{-1} mg^{-1} of PDH-E1 (Bowker-Kinley and Popov, 1999), the analogous phosphorylation of one site in all PDH-E1 copies (corresponding to 1.49×10^{-11} nmol) would take 26 min (Dataset S2, worksheet #13). Notably, this time range is similar to the time that it takes to dark-adapt photosynthetic tissues (20–30 min) (Murchie and Lawson, 2013).

While the PDK was already identified nearly 20 years ago, the identity of the pyruvate dehydrogenase phosphatase remains unknown. A protein phosphatase 2C family protein was identified in potato mitochondria as a candidate (Salvato *et al.*, 2014), and the Arabidopsis homologue is present at eight copies per mitochondrion (Dataset S3, worksheet #9). Similar (low) copy numbers of both the kinase and the phosphatase per mitochondrion may be regarded as further evidence for their function as a regulatory couple. Another phosphatase, SLP2, which is present in the IMS, and involved in the regulation of seed germination (Uhrig *et al.*, 2017), was detected at comparably low copy number (296 copies).

Similar to the protein phosphatases as erasers, two different protein lysine deacetylases, Sirtuin 2 (SRT2) and HDA14, were recently identified to reside in Arabidopsis mitochondria (Hartl and Finkemeier, 2012; König *et al.*, 2014b). SRT2, which functions as a lysine deacetylase of proteins, such as of the ATP/ADP carrier, at the matrix side of the IMM, was detected in this dataset with only 23 copies. It appears that SRT2 is of higher abundance in mitochondria of green Arabidopsis seedlings where around 323 copies per mitochondrion were found (König *et al.*, 2014b). The absence of SRT2 in isolated Arabidopsis mitochondria led to increased ATP export rates as mediated by increased activity of the ATP/ADP-carrier AAC1, suggesting a direct role of acetylation in modulating cellular ATP provision by the mitochondrion. Since the kinetic properties of sirtuins are highly dependent on their specific protein substrates, it is not possible to estimate catalytic capacities for the deacetylation rates of AAC1. No candidate acetyltransferase protein was identified in this dataset, which might either indicate that the acetyltransferase is of even lower abundance and below detection limit or that acetylation solely occurs non-enzymatically in the matrix, driven by alkaline conditions (König *et al.*, 2014a). All modifying enzymes detected in this study were of particular low abundance, which fits their predicted regulatory functions.

Substoichiometric amounts of mitochondrial DNA are reflected by low copy numbers of DNA-binding proteins. The plant mitochondrial genome is maintained in the organelles separately from the nuclear genome.

© 2019 The Authors.
The Plant Journal published by Society for Experimental Biology and John Wiley & Sons Ltd,
The Plant Journal, (2019), doi: 10.1111/tpj.14534

Proteome profiling identified the single-stranded DNA-binding proteins Whirly2 (WHY2), Organellar DNA-binding protein 1 (ODB1), Single-stranded DNA-binding proteins 1 and 2 (SSB1, SSB2), RecA homolog 2 (RECA2) and the enzyme DNA gyrase as the most abundant DNA-binding proteins in Arabidopsis mitochondria (Figure 5). The most abundant of these, WHY2, is present at 974 copies, corresponding to 41 24-mers (oligomeric status according to Cappadocia *et al.* (2012)). Arabidopsis mitochondria contain only one full genome per approximately three organelles, meaning that 122 kbp of mitochondrial DNA are present per mitochondrion on average (Preuten *et al.*, 2010). Based on these numbers and assuming that all protein copies of WHY2 are bound to DNA *in vivo*, WHY2 is present at three 24-mers per 10^4 bases. By comparison, the major DNA-binding protein of human mitochondria, mitochondrial Transcription factor A (TFAM), is bound to DNA at 600 molecules per 10^4 base pairs (Kukat *et al.*, 2011). Assuming that each WHY2 protomer within a 24-mer binds 9 nt of ssDNA (Cappadocia *et al.*, 2012), SSBs bind 30 or 60 nt per tetramer (Qian and Johnson, 2017), and RECA2 binds 3 nt per protomer of the RECA2 filament (Cox, 2007), these abundant proteins will cover between 7 and 11% of the mitochondrial genome. Another 3% can be estimated to be bound by ODB1 and the OSB family (Dataset S2, worksheet #14). Based on these numbers, (i) at least 80% of the Arabidopsis mitochondrial genome are "naked", i.e. not covered by protein, and (ii) 10–15% of the mitochondrial genome are kept in a single-stranded configuration by ssDNA-binding proteins. These estimates are based on the assumption that all proteomically detected DNA-binding proteins are bound to DNA *in vivo*. We might therefore underestimate the proportion of naked DNA and overestimate the proportion of ssDNA. An earlier study reported about 7% of ssDNA for mitochondria of *Chenopodium album* (Backert *et al.*, 1997).

Two DNA-binding proteins are present at extremely low copy numbers (Organellar single-stranded DNA binding protein 1 [OSB1] and MutS protein homologue [MSH1]), and a third, RECA3, was not detected. All three proteins are critical for mtDNA maintenance since their knockout causes dramatic mtDNA lesions that accumulate over generations (Zaegel *et al.*, 2006; Shedge *et al.*, 2007). Our proteomic data indicate only four copies of OSB1 and two copies of MSH1 per mitochondrion. Assuming that MSH1 functions as a dimer (Gualberto and Newton, 2017), only one functional unit of this protein is found per mitochondrion. This possibly reflects the low expression of these proteins in any tissue other than gametophytes. The DNA gyrase complex (about 400 copies) is by far the most abundant enzyme acting on mitochondrial DNA, about 100-fold more abundant than each of the DNA polymerases POL1A (five copies) and POL1B (two copies). This implies that only a minor portion of the mitochondrial DNA gyrase pool is required to relax DNA during replication. Surprisingly the RNA polymerase RPOTm, which has been considered the major RNA polymerase in dicot mitochondria owing to its loss being intolerable in Arabidopsis (Kühn *et al.*, 2009), is present at only five copies per mitochondrion. Thus, the nonessential RPOTmp, present at 31 copies per mitochondrion, may be the major RNA polymerase in dicot mitochondria. Assuming that plant mitochondrial RNA

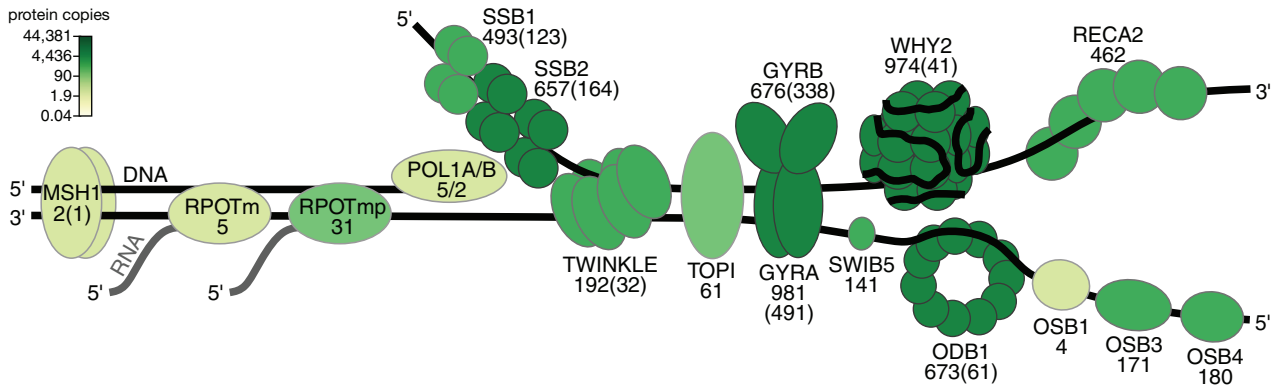

Figure 5. Proteins associated with the mitochondrial genome.
DNA-binding proteins detected are represented as binding to single-stranded or double-stranded DNA (based on findings recently reviewed by Gualberto and Kühn, 2014; Gualberto and Newton, 2017). The DNA polymerases 1A (POL1A) and 1B (POL1B) are summarized by a single symbol. For proteins known or assumed to be present in homo- or hetero-oligomers the inferred number of complexes is shown in brackets. For DNA gyrase composed of two DNA gyrase A (GYRA) and two DNA gyrase B (GYRB) subunits each, the subunits are of similar abundance (981 versus 676), which allows estimating about 400 enzyme complexes per mitochondrion. RecA homolog 2 (RECA2); MutS homolog 1 (MSH1); organellar DNA-binding protein 1 (ODB1); organellar single-stranded DNA-binding protein (OSB1, OSB3, OSB4); T3/T7 bacteriophage-type RNA polymerase, mitochondrial (RPOTm); T3/T7 bacteriophage-type RNA polymerase, mitochondrial/plastidial (RPOTmp); mitochondrial single-stranded DNA-binding protein (SSB1, SSB2); SWI/SNF protein complex B protein 5 (SWIB5); Type-IA DNA topoisomerase (TOPI), twinkle-like DNA primase-helicase (TWINKLE); Whirly 2 (WHY2). Not included in the figure: homolog of bacterial RecG (RECG1, four copies), DNA repair protein RadA-like protein (RADA, 34 copies); protein related to *Escherichia coli* RuvC, involved in homologous recombination (Gualberto and Newton, 2017) (eight copies); DNA Ligase I (47 copies).

© 2019 The Authors.
The Plant Journal published by Society for Experimental Biology and John Wiley & Sons Ltd,
The Plant Journal, (2019), doi: 10.1111/tpj.14534

polymerases elongate at a rate of 50 nucleotides per second, which is the average rate reported for bacterial and nuclear enzymes (Vogel and Jensen, 1994; Bubulya and Spector, 2004; Pérez-Ortín *et al.*, 2007), RPOTm and RPOTmp together can transcribe 108 kb of DNA per minute. This is in the range of the DNA present per mitochondrion (see above), and about three times the transcribed part of that DNA, according to transcriptome data indicating that about 30% of the Arabidopsis mitochondrial genome are transcribed.

Most RNA-processing and RNA-editing PPR proteins are present at low copy numbers. The RNA-binding and -processing PPR proteins constitute one of the largest gene families in the nuclear genome of *A. thaliana* (496 genes, Cheng *et al.*, 2016). The majority, 278 members, are mitochondrial localized as identified by SUBAcon (Hooper *et al.*, 2014). Out of these, 107 were detected here (Dataset S3, worksheet #11). It is reasonable to interpret the relatively low detection coverage as a reflection of the generally low copy number of the PPR proteins per mitochondrion. This is supported by the observation that more than 60% of the identified PPR proteins were represented by less than 20 copies per mitochondrion (Figure 6; Dataset S3, worksheet #11). Although PPR proteins contributed only 1.4% of the complete proteome mass, they represented 4.7% of the identified protein species.

Structurally, PPR proteins are classified into two different subgroups, P- and PLS-type. Most PLS-type PPR proteins act as specific C-to-U editing factors (Barkan and Small, 2014), many of them with a C-terminal DYW-domain as cytidine deaminase (Oldenkott *et al.*, 2019). They are particularly lowly abundant with protein copies ranging from 0.83 (i.e. substoichiometric) to 34. Notably, the PLS-type protein DYW2 contrasted this tendency and was present at 351 copies per mitochondrion. DYW2 lacks an extended upstream PPR array and is, in contrast to most other PLS-type PPR proteins, involved in editing of many sites providing the DYW domain *in trans* (Andrés-Colás *et al.*, 2017; Guillaumot *et al.*, 2017). The comparatively high copy numbers suggest that DYW2 constitutes a general component of the editosome in Arabidopsis. In support of that, the copy numbers of most other editing proteins like the Multiple Organellar RNA-editing Factors (MORFs, Takenaka *et al.*, 2012), the Organelle RNA Recognition Motif-containing proteins (ORRMs) or the Organellar Zinc finger proteins (OZs, Sun *et al.*, 2016), which support editing at many sites, are comparable to those of DYW2 or even higher (Figure 6; Dataset S3, worksheet #11).

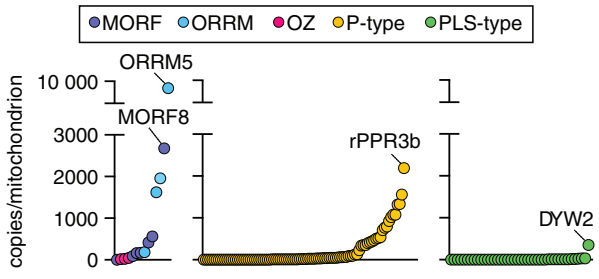

Figure 6. Copy numbers of RNA-processing and RNA-editing proteins.
The identified proteins of three different groups involved in RNA-processing and RNA-editing in particular P-type, PLS-type pentatricopeptide repeat (PPR) proteins and additional RNA-editing proteins (multiple organellar RNA-editing factors [MORFs, Takenaka *et al.*, 2012]/organelle RNA recognition motif-containing proteins [ORRMs]/organellar zinc finger proteins [OZs, Sun *et al.*, 2016]) are plotted with increasing abundance (copy number/single mitochondrion). Highlighted are the most abundant proteins of each group: P-type PPR protein rPPR3b with 2189 copies, PLS-type PPR protein DYW2 with 351 copies, ORRM5 with 7857 copies and MORF8 with 2676 copies per mitochondrion.

Of the P-type subgroup, we identified 58% of the mitochondrial-predicted proteins (95 out of 165) with copy numbers ranging from 0.6 to 2189. In contrast to most PPR proteins, all of the currently characterized and relatively highly abundant P-type PPR proteins seem not to recognize single specific RNA targets but act via less specific protein–protein or protein–rRNA interactions (Waltz *et al.*, 2019). Among them are the 10 recently identified ribosome-associated PPR proteins (Rugen *et al.*, 2019a,b; Waltz *et al.*, 2019), including two of the three most abundant PPR proteins rPPR3b (2189 copies) and PPR336 (1335 copies), and NUWA (1077 copies), which interacts with DYW2 as part of the RNA editosome (Andrés-Colás *et al.*, 2017; Guillaumot *et al.*, 2017).

However, most P- and PLS-type PPR proteins act on particular RNA targets only and are fundamental for the efficient processing of specific mitochondrial transcripts, e.g. by RNA-editing, 5′ and 3′ processing or intron splicing (Bentolila *et al.*, 2013; Barkan and Small, 2014; Brown *et al.*, 2014). Interestingly, the copy numbers for these proteins were generally very low or even substoichiometric to the mitochondrial population. This was also the case for non-PPR RNA-processing factors with specific targets like the maturases or the PORR-protein WTF9 (Brown *et al.*, 2014; Dataset S3, worksheet #11). We identified only one (nMAT2, 34 copies) of the five maturases, required for splicing of individual group II introns. The high abundance of the DEAD-box protein PMH2 (1322 copies) can be explained by its general role in RNA stabilisation (Köhler *et al.*, 2010). Low numbers of RNA-processing factors indicate that continuous mitochondrial fusion and fission may be crucial to ensure proper function of the gene products that require post-transcriptional modification.

The copy numbers of proteins involved in mitochondrial dynamics indicate frequent, but heterogenic, fission events. The balance between mitochondrial fusion and fission events controls mitochondrial genome distribution, mitochondrial size, shape and number within a cell, and mitochondrial segregation between the daughter cells

© 2019 The Authors.
The Plant Journal published by Society for Experimental Biology and John Wiley & Sons Ltd,
The Plant Journal, (2019), doi: 10.1111/tpj.14534

during cell division (Arimura *et al.*, 2004b; Sheahan *et al.*, 2004, 2005; Logan and Paszkiewicz, 2017). While the genetic components of the fusion machinery are unknown in plants, several proteins involved in fission have been identified (Arimura *et al.*, 2004b; Logan and Paszkiewicz, 2017). All established components of the fission machinery were found in the proteomic dataset (Figure 7; Dataset S2, worksheet #12), with the exception of Fission1b (FIS1B) and Elongated mitochondria 2 (ELM2), whose contribution in the mitochondrial division seems to be marginal (Arimura *et al.*, 2017), and FRIENDLY, which is a cytosolic protein only transiently associated with the mitochondria (El Zawily *et al.*, 2014). A total of 2108 copies of proteins involved in mitochondrial fission were identified per mitochondrion, with Elongated mitochondria 1 (ELM1), and Peroxisomal and mitochondrial division factors (PMD2 and PMD1) being the most abundant (286, 1300 and 402 copies, respectively). ELM1 is a plant-specific adapter protein directing dynamin-related proteins (DRP3) to fission sites while putatively interacting with the outer mitochondrial membrane tail-anchored Fission1 (FIS1) proteins (Arimura *et al.*, 2008; Scott and Logan, 2011). However, DRP3A localisation to mitochondria occurred independent of ELM1 in cold-induced mitochondrial fission (Arimura *et al.*, 2017). Here, FIS1A (53 copies) was detected at a similar copy number to that of the sum of the two Dynamin-related protein 3 (DRP3A, B) isoforms (67 copies), while the ELM1 copy number was 4 times higher (286 copies). The reason for the excess of ELM1 is unclear and suggests FIS-independent functions or that yet unknown, plant-specific membrane proteins are involved in the recruitment of ELM1 to the outer mitochondrial membrane.

During fission DRP3A and DRP3B are recruited to the outer mitochondrial membrane and form a contractible ring (Arimura *et al.*, 2008; Fujimoto *et al.*, 2009). DRP3A and DRP3B isoforms co-localise to mitochondrial fission sites and to tips of mitochondria after division. Their GTPase activity is required for the mitochondrial fission to proceed (Arimura *et al.*, 2004b; Arimura, 2018). The crystal structure of the human mitochondrial fission dynamin-related protein DNM1L was resolved and current models show a dimer as the basic unit with higher order assemblies (Fröhlich *et al.*, 2013). A current assembly model predicts 48 tetramers (192 monomers) to be required for the formation of a contractible ring around a membrane tubule with a diameter of 0.11 μm (0.35 μm circumference). Assuming similar protein structures and oligomerisation for Arabidopsis DRP3, for a cylindrical-shaped elongated plant mitochondrion with a diameter of 0.4 μm (i.e. half of the 0.8 μm diameter assumed for a normal, spherical mitochondrion) and a resulting circumference of 1.26 μm, 175 tetramers or 700 DRP3 protein copies would be necessary to assemble into a ring around the constriction site (Dataset S2, worksheet #15). As we estimate 67 copies in total for DRP3A and DRP3B per mitochondrion, this could be interpreted as one out of ten mitochondria is undergoing fission at a given time point, under the assumption that DRP3 also forms tetramers in Arabidopsis (Figure 7). This is in line with high fission rates of Arabidopsis mitochondria (Arimura *et al.*, 2004b), and reflects the observation that not every plant mitochondrion displays a constriction site (Arimura *et al.*, 2004a).

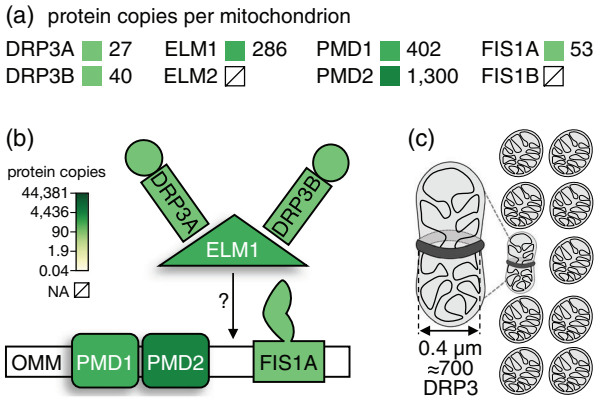

Figure 7. Components of the mitochondrial fission machinery.
(a) Protein copies per mitochondrion of protein species involved in mitochondrial fission. Dynamin-related protein (DRP), elongated mitochondria (ELM), peroxisomal and mitochondrial division factor (PMD), fission (FIS).
(b) Localization and interactions between fission-related proteins. Recruitment of DRP3 isoforms to the outer mitochondrial membrane (OMM) can be ELM1-dependent or -independent (Arimura *et al.*, 2017; Arimura, 2018).
(c) If approximately 700 DRP3 copies are necessary to span a constriction site with a diameter of 0.4 μm, and assuming all DRP3 copies are localized at such a site, the number of DRP3 copies present could support a constriction site at every 10th mitochondrion at a time.

CONCLUSIONS AND OUTLOOK

To gain insights into the makeup and function of individual subcellular compartments, we scaled a quantitative proteomic dataset from isolated Arabidopsis mitochondria to protein copy numbers present in a theoretical single organelle. That enabled us to assess structural and functional features of mitochondria in the context of the geometrical, biochemical and physical constraints of the single organelle. We needed to make several assumptions, and several intrinsic limitations of quantitative proteomics remain. The accuracy of our estimations may be improved in the future through development of the field as well as experimental refinement. Our calculations may then be straightforwardly adjusted and the consequences on the copy numbers and the overall picture revisited. For instance, 5.2% of the protein copies present in the dataset are not functionally annotated (Table S1), which means that the amount of protein copies in the specified functional categories likely represent underestimations. Despite all required caution, the picture that several of our thought experiments deliver is generally consistent with conclusions drawn independently from

© 2019 The Authors.

previous experimental analyses. This provides confidence that our assumptions are reasonable, and that the approach is valid and informative overall.

We provide an innovative and coherent perspective of how a plant mitochondrion works and are able to deduce unanticipated details of mitochondrial biology. By combining quantitative proteomics with cell biology, we exemplify insights into the local environment that a mitochondrial protein might encounter and provide quantitative estimates to further define the roles that individual protein species, families or complexes play as part of the individual mitochondrion. Although we cover diverse examples of mitochondrial function and organisation, we regard the dataset as a resource to be exploited by the community and encourage our colleagues to make use of it for specific questions and thought experiments.

A single mitochondrion only contains an estimated amount of about 80 fg of protein (Dataset S1, worksheet #2). Hence, assessing the proteome of a single mitochondrion directly is currently technically not feasible. Our approach provides an indirect alternative, but does not allow any insight into the potential heterogeneity between mitochondria with respect to their size, metabolic state or biochemical makeup. Overcoming technical sensitivity limitations would allow an assessment of the differences between individual single mitochondrial proteomes. Heterogeneity in mitochondrial populations likely carries biological significance, especially for those proteins present at very low or even substoichiometric copy numbers. Micromanipulation- or MALDI imaging-based approaches to resolve individual mitochondria may provide an avenue for proteins with larger copy numbers and favourable properties for mass spectrometry analysis (Yajima *et al.*, 2018; Zhang *et al.*, 2018). Innovative single cell proteomic approaches and single molecule approaches, such as nanopore sequencing of proteins (Budnik *et al.*, 2018; Restrepo-Pérez *et al.*, 2018) may open the door to the first single organelle proteomes with quantitative protein coverage.

EXPERIMENTAL PROCEDURES

Cultivation of a heterotrophic Arabidopsis cell suspension culture and isolation of mitochondria

A heterotrophic Arabidopsis cell suspension culture was established as described previously (Sunderhaus *et al.*, 2006; Schikowsky *et al.*, 2017). Cells were sub-cultured on a weekly basis after which their mass increased by a factor of three. Mitochondria isolations were performed after 7 days of culture and used a combination of differential centrifugation and isopycnic Percoll (GE Healthcare, Solingen, Germany; https://www.gelifesciences.com/en/de/shop/cell-therapy/media/percoll-density-gradient-media-p-05823) gradient centrifugation as described by Werhahn *et al.* (2001). Isolated mitochondria were washed, pelleted and re-suspended to yield a concentration of 100 mg mitochondria per mL and stored at −80°C. Four independent mitochondria isolations were performed.

Mass spectrometry

For each mitochondria isolation, a volume corresponding to 50 μg of protein (according to Bradford) was mixed with the same volume of 2x Laemmli buffer (125 mM Tris HCl [pH 6.8], 4% [w/v] SDS, 10% [v/v] β-mercaptoethanol, 0.1% [w/v] bromophenol blue). Solubilized proteins were purified, concentrated, and digested in a glycine-SDS gel. The resulting peptides were subsequently extracted as previously described (Thal *et al.*, 2018) and resuspended in 20 μl of 5% [v/v] ACN, 0.1% [v/v] TFA. LC-MS/MS was primarily performed as described in (Thal *et al.*, 2018) with minor differences. Peptide solution (1 μl) was loaded on a 2-cm C18 reversed phase trap column (Acclaim PepMap100, diameter: 100 μm, granulometry: 5 μm, pore size: 100 Å; Thermo Fisher Scientific, Waltham, MA, USA; https://www.thermofisher.com/order/catalog/product/164567#/164567) and further separated on a 50-cm C18 reversed phase analytical column (Acclaim PepMap100, diameter: 75 μm, granulometry: 3 μm, pore size: 100 Å; Thermo Fisher Scientific). Peptides were eluted by a non-linear 5–36% [v/v] acetonitrile gradient in 0.1% [v/v] formic acid over a period of 240 min at 33°C.

Processing of MS data

Acquired LC-MS/MS spectra were queried against an in-house modified TAIR10 database comprising protein models of the mitochondrial and plastid genomes after RNA editing using MaxQuant 1.6.0.1 (Cox and Mann, 2008). Editing site information was based on the PREPACT database (Lenz *et al.*, 2018) and a published RNA-seq analysis (Bentolila *et al.*, 2013). Sites that are edited at more than 50% efficiency were considered. The search parameters were set to: carbamidomethylation (C) as fixed modification, oxidation (M) and acetylation (protein N-term) as variable modifications. The specific digestion mode was set to trypsin (P) and a maximum of two missed cleavage sites was allowed. FDR at the protein and PSM level was set to 1%. For maximum proteome coverage, the minimum number of unique peptides per protein group was 1. Unique and razor peptides were used for protein quantification. The iBAQ function of MaxQuant was enabled, "log fit" disabled.

To increase the number of quantifiable proteins between the four replicates, we used retention time alignment and peptide identification transfer via the "match between runs" feature of MaxQuant with a match time windows of 0.7 min and an alignment time window of 20 min (Cox *et al.*, 2014).

Estimating the average single mitochondrion protein inventory

The considerations are provided in the Results section and the calculations are detailed in Dataset S1 (worksheet #2). In brief, the volume and mass of a mitochondrion of 0.8 μm in diameter was calculated assuming a spherical shape and a mitochondrial density of 1.2 g ml^{-1} (Glas and Bahr, 1966). Of the mitochondrial mass 25% were considered protein. Total protein mass was divided by the mass of the abundance-adjusted average mitochondrial protein to calculate the total protein copies per mitochondrion. The copy number of each individual protein species was estimated by multiplying the normalized median iBAQ score with the total protein copies.

DATA STATEMENT

The mass spectrometry proteomics data are openly accessible. They have been deposited to the ProteomeXchange Consortium via the PRIDE partner repository (Vizcaino *et al.*, 2013) with the dataset identifier PXD014292.

© 2019 The Authors.
The Plant Journal published by Society for Experimental Biology and John Wiley & Sons Ltd,
The Plant Journal, (2019), doi: 10.1111/tpj.14534

ACKNOWLEDGEMENTS

We thank Michael Senkler (Hannover) for excellent bioinformatics support. We further thank Ian Max Møller (Aarhus) and José Gualberto (Strasbourg), as well as both anonymous reviewers for critical reading and very helpful comments that have strengthened this manuscript. This work was enabled through the collaborative DFG research grant PAK918 (EU54/4-1, IF1655/3-1, MA2379/14-1, MU4137/1-1, SCHA1953/3-1, SCHW1719/5-1) as part of the 'Plant Mitochondria in New Light' initiative.

CONFLICT OF INTEREST

The authors declare no conflict of interest.

AUTHOR CONTRIBUTIONS

H-PB, PF and MS conceived the project in active discussion with all co-authors. HE and NR performed the itochondrial isolations, the proteomic experiments, and nalyzed the proteomic data. IF advised on MaxQuant ata search and iBAQ evaluation. PF performed the scaling to protein copy numbers with input from MS, H-PB, HE, SJMS and EHM. All co-authors contributed to the writing of the individual sections including individual data analyses. The first draft of the manuscript was assembled by PF, EHM, SJMS and MS. All co-authors contributed to finalizing the manuscript.

SUPPORTING INFORMATION

Additional Supporting Information may be found in the online version of this article.

Figure S1. Characteristics of the proteomic dataset.

Figure S2. Copy numbers of proteins involved in plant mitochondrial protein import and sorting.

Table S1. Functional sub-categories for 917 proteins with mitochondrial localisation as identified based on SUBAcon.

Dataset S1. Proteomic dataset and calculation of protein copy numbers.

Dataset S2. Calculations for specific examples discussed.

Dataset S3. Subsets of proteins discussed in the individual sections.

REFERENCES

Altmann, R. (1890) *Die Elementarorganismen und ihre Beziehungen zu den Zellen*. 1st ed. Leipzig: Veit. Available at: http://www.deutschestextarchiv.de/book/show/altmann_elementarorganismen_1890.

Andrés-Colás, N., Zhu, Q., Takenaka, M., De Rybel, B., Weijers, D. and Van Der Straeten, D. (2017) Multiple PPR protein interactions are involved in the RNA editing system in *Arabidopsis* mitochondria and plastids. *Proc. Natl Acad. Sci. USA*, **114**, 8883–8888.

Arike, L., Valgepea, K., Peil, L., Nahku, R., Adamberg, K. and Vilu, R. (2012) Comparison and applications of label-free absolute proteome quantification methods on *Escherichia coli*. *J. Proteomics*, **75**, 5437–5448.

Arimura, S. (2018) Fission and fusion of plant mitochondria, and genome maintenance. *Plant Physiol.* **176**, 152–161.

Arimura, S., Aida, G.P., Fujimoto, M., Nakazono, M. and Tsutsumi, N. (2004a) *Arabidopsis* dynamin-like protein 2a (ADL2a), like ADL2b, is involved in plant mitochondrial division. *Plant Cell Physiol.* **45**, 236–242.

Arimura, S., Yamamoto, J., Aida, G.P., Nakazono, M. and Tsutsumi, N. (2004b) Frequent fusion and fission of plant mitochondria with unequal nucleoid distribution. *Proc. Natl Acad. Sci. USA*, **101**, 7805–7808.

Arimura, S., Fujimoto, M., Doniwa, Y., Kadoya, N., Nakazono, M., Sakamoto, W. and Tsutsumi, N. (2008) Arabidopsis ELONGATED MITOCHONDRIA1 is required for localization of DYNAMIN-RELATED PROTEIN3A to mitochondrial fission sites. *Plant Cell*, **20**, 1555–1566.

Arimura, S.-I., Kurisu, R., Sugaya, H., Kadoya, N. and Tsutsumi, N. (2017) Cold treatment induces transient mitochondrial fragmentation in *Arabidopsis thaliana* in a way that requires DRP3A but not ELM1 or an ELM1-like homologue, ELM2. *Int. J. Mol. Sci.* **18**, 2161.

Backert, S., Lurz, R., Oyarzabal, O.A. and Börner, T. (1997) High content, size and distribution of single-stranded DNA in the mitochondria of *Chenopodium album* (L.). *Plant Mol. Biol.* **33**, 1037–1050.

Barkan, A. and Small, I. (2014) Pentatricopeptide repeat proteins in plants. *Annu. Rev. Plant Biol.* **65**, 415–442.

Bauer, M.F., Sirrenberg, C., Neupert, W. and Brunner, M. (1996) Role of Tim23 as voltage sensor and presequence receptor in protein import into mitochondria. *Cell*, **87**, 33–41.

Bauwe, H. and Kolukisaoglu, Ü. (2003) Genetic manipulation of glycine decarboxylation. *J. Exp. Bot.* **54**, 1523–1535.

Bauwe, H., Hagemann, M. and Fernie, A.R. (2010) Photorespiration: players, partners and origin. *Trends Plant Sci.* **15**, 330–336.

Bayrhuber, M., Meins, T., Habeck, M. *et al.* (2008) Structure of the human voltage-dependent anion channel. *Proc. Natl Acad. Sci. USA*, **105**, 15370–15375.

Bentolila, S., Oh, J., Hanson, M.R. and Bukowski, R. (2013) Comprehensive high-resolution analysis of the role of an *Arabidopsis* gene family in RNA editing. *PLoS Genet.* **9**, e1003584.

Berthet, J. and Baudhuin, P. (1967) A remark about the determination of the water content of mitochondria. *J. Cell Biol.* **34**, 701–702.

Blum, T.B., Hahn, A., Meier, T., Davies, K.M. and Kühlbrandt, W. (2019) Dimers of mitochondrial ATP synthase induce membrane curvature and self-assemble into rows. *Proc. Natl Acad. Sci. USA*, **116**, 4250–4255.

Bourguignon, J., Macherel, D., Neuburger, M. and Douce, R. (1992) Isolation, characterization, and sequence analysis of a cDNA clone encoding L-protein, the dihydrolipoamide dehydrogenase component of the glycine cleavage system from pea-leaf mitochondria. *Eur. J. Biochem.* **204**, 865–873.

Bourguignon, J., Vauclare, P., Merand, V., Forest, E., Neuburger, M. and Douce, R. (1993) Glycine decarboxylase complex from higher plants. Molecular cloning, tissue distribution and mass spectrometry analyses of the T protein. *Eur. J. Biochem.* **217**, 377–386.

Bourguignon, J., Merand, V., Rawsthorne, S., Forest, E. and Douce, R. (1996) Glycine decarboxylase and pyruvate dehydrogenase complexes share the same dihydrolipoamide dehydrogenase in pea leaf mitochondria: evidence from mass spectrometry and primary-structure analysis. *Biochem. J.* **313**, 229–234.

Bowker-Kinley, M. and Popov, K.M. (1999) Evidence that pyruvate dehydrogenase kinase belongs to the ATPase/kinase superfamily. *Biochem. J.* **344**, 47–53.

Brown, G.G., Colas des Francs-Small, C. and Ostersetzer-Biran, O. (2014) Group II intron splicing factors in plant mitochondria. *Front. Plant Sci.* **5**, 35.

Bubulya, P.A. and Spector, D.L. (2004) On the movements of nuclear components in living cells. *Exp. Cell Res.* **296**, 4–11.

Budnik, B., Levy, E., Harmange, G. and Slavov, N. (2018) SCoPE-MS: mass spectrometry of single mammalian cells quantifies proteome heterogeneity during cell differentiation. *Genome Biol.* **19**, 161.

Cappadocia, L., Parent, J.-S., Zampini, É., Lepage, É., Sygusch, J. and Brisson, N. (2012) A conserved lysine residue of plant Whirly proteins is necessary for higher order protein assembly and protection against DNA damage. *Nucleic Acids Res.* **40**, 258–269.

Chen, Q., Jin, C., Shao, X. *et al.* (2018) Super-resolution tracking of mitochondrial dynamics with an Iridium(III) luminophore. *Small*, **14**, e1802166.

Cheng, S., Gutmann, B., Zhong, X. *et al.* (2016) Redefining the structural motifs that determine RNA binding and RNA editing by pentatricopeptide repeat proteins in land plants. *Plant J.* **85**, 532–547.

Chew, O., Whelan, J. and Millar, A.H. (2003) Molecular definition of the ascorbate-glutathione cycle in *Arabidopsis* mitochondria reveals dual targeting of antioxidant defenses in plants. *J. Biol. Chem.* **278**, 46869–46877.

Chow, K.-S., Singh, D.P., Roper, J.M. and Smith, A.G. (1997) A single precursor protein for ferrochelatase-I from *Arabidopsis* is imported *in vitro* into both chloroplasts and mitochondria. *J. Biol. Chem.* **272**, 27565–27571.

© 2019 The Authors.

Chow, K.S., Singh, D.P., Walker, A.R. and Smith, A.G. (1998) Two different genes encode ferrochelatase in *Arabidopsis*: mapping, expression and subcellular targeting of the precursor proteins. *Plant J.* **15**, 531–541.

Colombini, M. (2004) VDAC: the channel at the interface between mitochondria and the cytosol. *Mol. Cell. Biochem.* **256–257**, 107–115.

Cowdry, E.V. (1924) Mitochondria, Golgi apparatus and chromidial substance. In *General Cytology* (Cowdry, E.V., ed). Chicago, IL: The University of Chicago Press, pp. 311–382.

Cox, M.M. (2007) Motoring along with the bacterial RecA protein. *Nat. Rev. Mol. Cell Biol.* **8**, 127–138.

Cox, J. and Mann, M. (2008) MaxQuant enables high peptide identification rates, individualized p.p.b.-range mass accuracies and proteome-wide protein quantification. *Nat. Biotechnol.* **26**, 1367–1372.

Cox, J., Hein, M.Y., Luber, C.A., Paron, I., Nagaraj, N. and Mann, M. (2014) Accurate proteome-wide label-free quantification by delayed normalization and maximal peptide ratio extraction, termed MaxLFQ. *Mol. Cell Proteomics*, **13**, 2513–2526.

Davies, K.M., Anselmi, C., Wittig, I., Faraldo-Gomez, J.D. and Kühlbrandt, W. (2012) Structure of the yeast F1Fo-ATP synthase dimer and its role in shaping the mitochondrial cristae. *Proc. Natl Acad. Sci. USA*, **109**, 13602–13607.

Dudkina, N.V., Heinemeyer, J., Keegstra, W., Boekema, E.J. and Braun, H.-P. (2005) Structure of dimeric ATP synthase from mitochondria: an angular association of monomers induces the strong curvature of the inner membrane. *FEBS Lett.* **579**, 5769–5772.

Dudkina, N.V., Kudryashev, M., Stahlberg, H. and Boekema, E.J. (2011) Interaction of complexes I, III, and IV within the bovine respirasome by single particle cryoelectron tomography. *Proc. Natl Acad. Sci. USA*, **108**, 15196–15200.

El Zawily, A.M., Schwarzländer, M., Finkemeier, I. *et al.* (2014) FRIENDLY regulates mitochondrial distribution, fusion, and quality control in *Arabidopsis*. *Plant Physiol.* **166**, 808–828.

Engel, N., van den Daele, K., Kolukisaoglu, U., Morgenthal, K., Weckwerth, W., Parnik, T., Keerberg, O. and Bauwe, H. (2007) Deletion of glycine decarboxylase in *Arabidopsis* is lethal under nonphotorespiratory conditions. *Plant Physiol.* **144**, 1328–1335.

Engel, N., Ewald, R., Gupta, K.J., Zrenner, R., Hagemann, M. and Bauwe, H. (2011) The presequence of *Arabidopsis* serine hydroxymethyltransferase SHM2 selectively prevents import into mesophyll mitochondria. *Plant Physiol.* **157**, 1711–1720.

Eubel, H., Heinemeyer, J. and Braun, H.P. (2004) Identification and characterization of respirasomes in potato mitochondria. *Plant Physiol.* **134**, 1450–1459.

Eubel, H., Lee, C.P., Kuo, J., Meyer, E.H., Taylor, N.L. and Millar, A.H. (2007) Free-flow electrophoresis for purification of plant mitochondria by surface charge: isolation of plant mitochondria by FFE. *Plant J.* **52**, 583–594.

Fabre, B., Lambour, T., Bouyssié, D., Menneteau, T., Monsarrat, B., Burlet-Schiltz, O. and Bousquet-Dubouch, M.-P. (2014) Comparison of label-free quantification methods for the determination of protein complexes subunits stoichiometry. *EuPA Open Proteomics*, **4**, 82–86.

Fessl, T., Watkins, D., Oatley, P. *et al.* (2018) Dynamic action of the Sec machinery during initiation, protein translocation and termination. *eLife*, **7**, e35112.

Finkemeier, I. and Schwarzländer, M. (2018) Mitochondrial regulation and signalling in the photosynthetic cell: principles and concepts. In *Annual Plant Reviews online*. (Roberts, J.A., ed). Chichester, UK: John Wiley & Sons Ltd, pp. 185–226.

Finkemeier, I., Goodman, M., Lamkemeyer, P., Kandlbinder, A., Sweetlove, L.J. and Dietz, K.-J. (2005) The mitochondrial type II peroxiredoxin F is essential for redox homeostasis and root growth of *Arabidopsis thaliana* under stress. *J. Biol. Chem.* **280**, 12168–12180.

Fröhlich, C., Grabiger, S., Schwefel, D., Faelber, K., Rosenbaum, E., Mears, J., Rocks, O. and Daumke, O. (2013) Structural insights into oligomerization and mitochondrial remodelling of dynamin 1-like protein. *EMBO J.* **32**, 1280–1292.

Fromm, S., Braun, H.-P. and Peterhänsel, C. (2016a) Mitochondrial gamma carbonic anhydrases are required for complex I assembly and plant reproductive development. *New Phytol.* **211**, 194–207.

Fromm, S., Senkler, J., Zabaleta, E., Peterhänsel, C. and Braun, H.-P. (2016b) The carbonic anhydrase domain of plant mitochondrial complex I. *Physiol. Plantarum*, **157**, 289–296.

Fujimoto, M., Arimura, S., Mano, S. *et al.* (2009) *Arabidopsis* dynamin-related proteins DRP3A and DRP3B are functionally redundant in mitochondrial fission, but have distinct roles in peroxisomal fission. *Plant J.* **58**, 388–400.

Ghifari, A.S., Huang, S. and Murcha, M.W. (2019) The peptidases involved in plant mitochondrial protein import. *J. Exp. Bot.* https://doi.org/10.1093/jxb/erz365

Glas, U. and Bahr, G.F. (1966) Quantitative study of mitochondria in rat liver: dry mass, wet mass, volume, and concentration of solids. *J. Cell Biol.* **29**, 507–523.

Gold, V.A.M., Ieva, R., Walter, A., Pfanner, N., van der Laan, M. and Kühlbrandt, W. (2014) Visualizing active membrane protein complexes by electron cryotomography. *Nat. Commun.* **5**, 4129.

Gualberto, J.M. and Kühn, K. (2014) DNA-binding proteins in plant mitochondria: implications for transcription. *Mitochondrion*, **19**, 323–328.

Gualberto, J.M. and Newton, K.J. (2017) Plant mitochondrial genomes: dynamics and mechanisms of mutation. *Annu. Rev. Plant Biol.* **68**, 225–252.

Guillaumot, D., Lopez-Obando, M., Baudry, K. *et al.* (2017) Two interacting PPR proteins are major *Arabidopsis* editing factors in plastid and mitochondria. *Proc. Natl Acad. Sci. USA*, **114**, 8877–8882.

Gupte, S., Wu, E.S., Hoechli, L., Hoechli, M., Jacobson, K., Sowers, A.E. and Hackenbrock, C.R. (1984) Relationship between lateral diffusion, collision frequency, and electron transfer of mitochondrial inner membrane oxidation-reduction components. *Proc. Natl Acad. Sci. USA*, **81**, 2606–2610.

Hagedorn, P.H., Flyvbjerg, H. and Møller, I.M. (2004) Modelling NADH turnover in plant mitochondria. *Physiol. Plant.* **120**, 370–385.

Hahn, A., Parey, K., Bublitz, M., Mills, D.J., Zickermann, V., Vonck, J., Kühlbrandt, W. and Meier, T. (2016) Structure of a complete ATP synthase dimer reveals the molecular basis of inner mitochondrial membrane morphology. *Mol. Cell*, **63**, 445–456.

Halliwell, B. and Gutteridge, J.M.C. (2015) *Free Radicals in Biology and Medicine*. New York, NY: Oxford University Press.

Hartl, M. and Finkemeier, I. (2012) Plant mitochondrial retrograde signaling: post-translational modifications enter the stage. *Front. Plant Sci.* **3**, 253.

Hasse, D., Mikkat, S., Thrun, H.-A., Hagemann, M. and Bauwe, H. (2007) Properties of recombinant glycine decarboxylase P- and H-protein subunits from the cyanobacterium *Synechocystis* sp. strain PCC 6803. *FEBS Lett.* **581**, 1297–1301.

Hatzfeld, Y., Maruyama, A., Schmidt, A., Noji, M., Ishizawa, K. and Saito, K. (2000) β-Cyanoalanine synthase is a mitochondrial cysteine synthase-like protein in spinach and *Arabidopsis*. *Plant Physiol.* **123**, 1163–1172.

Heazlewood, J.L., Tonti-Filippini, J.S., Gout, A.M., Day, D.A., Whelan, J. and Millar, A.H. (2004) Experimental analysis of the *Arabidopsis* mitochondrial proteome highlights signaling and regulatory components, provides assessment of targeting prediction programs, and indicates plant-specific mitochondrial proteins. *Plant Cell*, **16**, 241–256.

Hey, D., Ortega-Rodes, P., Fan, T., Schnurrer, F., Brings, L., Hedtke, B. and Grimm, B. (2016) Transgenic tobacco lines expressing sense or antisense FERROCHELATASE 1 RNA show modified ferrochelatase activity in roots and provide experimental evidence for dual localization of ferrochelatase 1. *Plant Cell Physiol.* **57**, 2576–2585.

Hildebrandt, T.M., Nunes Nesi, A., Araújo, W.L. and Braun, H.-P. (2015) Amino acid catabolism in plants. *Mol. Plant*, **8**, 1563–1579.

Hodge, T. and Colombini, M. (1997) Regulation of metabolite flux through voltage-gating of VDAC channels. *J. Membr. Biol.* **157**, 271–279.

Hoitzing, H., Johnston, I.G. and Jones, N.S. (2015) What is the function of mitochondrial networks? A theoretical assessment of hypotheses and proposal for future research. *Bioessays*, **37**, 687–700.

Hooper, C.M., Tanz, S.K., Castleden, I.R., Vacher, M.A., Small, I.D. and Millar, A.H. (2014) SUBAcon: a consensus algorithm for unifying the subcellular localization data of the *Arabidopsis* proteome. *Bioinformatics*, **30**, 3356–3364.

Hosp, F., Lassowskat, I., Santoro, V. *et al.* (2017) Lysine acetylation in mitochondria: from inventory to function. *Mitochondrion*, **33**, 58–71.

Hsu, J.L., Hsieh, Y., Tu, C., O'Connor, D., Nick, H.S. and Silverman, D.N. (1996) Catalytic properties of human manganese superoxide dismutase. *J. Biol. Chem.* **271**, 17687–17691.

Huang, S., Van Aken, O., Schwarzländer, M., Belt, K. and Millar, A.H. (2016) The roles of mitochondrial reactive oxygen species in cellular signaling and stress response in plants. *Plant Physiol.* **171**, 1551–1559.

© 2019 The Authors.
The Plant Journal published by Society for Experimental Biology and John Wiley & Sons Ltd,
The Plant Journal, (2019), doi: 10.1111/tpj.14534

Hüdig, M., Maier, A., Scherrers, I., Seidel, L., Jansen, E.E.W., Mettler-Altmann, T., Engqvist, M.K.M. and Maurino, V.G. (2015) Plants possess a cyclic mitochondrial metabolic pathway similar to the mammalian metabolic repair mechanism involving malate dehydrogenase and L-2-hydroxyglutarate dehydrogenase. *Plant Cell Physiol.* **56**, 1820–1830.

Ito, J., Taylor, N.L., Castleden, I., Weckwerth, W., Millar, A.H. and Heazlewood, J.L. (2009) A survey of the *Arabidopsis thaliana* mitochondrial phosphoproteome. *Proteomics*, **9**, 4229–4240.

Jakobs, S. and Wurm, C.A. (2014) Super-resolution microscopy of mitochondria. *Curr. Opin. Chem. Biol.* **20**, 9–15.

Kingsbury, B.F. (1912) Cytoplasmic fixation. *Anat. Rec.* **6**, 39–52.

Kitajima, S., Kurioka, M., Yoshimoto, T., Shindo, M., Kanaori, K., Tajima, K. and Oda, K. (2008) A cysteine residue near the propionate side chain of heme is the radical site in ascorbate peroxidase. *FEBS J.* **275**, 470–480.

Kliebenstein, D.J., Monde, R.A. and Last, R.L. (1998) Superoxide dismutase in *Arabidopsis*: an eclectic enzyme family with disparate regulation and protein localization. *Plant Physiol.* **118**, 637–650.

Klodmann, J., Sunderhaus, S., Nimtz, M., Jansch, L. and Braun, H.P. (2010) Internal architecture of mitochondrial complex I from *Arabidopsis thaliana*. *Plant Cell*, **22**, 797–810.

Kmiec, B., Teixeira, P.F. and Glaser, E. (2014) Shredding the signal: targeting peptide degradation in mitochondria and chloroplasts. *Trends Plant Sci.* **19**, 771–778.

Köhler, D., Schmidt-Gattung, S. and Binder, S. (2010) The DEAD-box protein PMH2 is required for efficient group II intron splicing in mitochondria of *Arabidopsis thaliana*. *Plant Mol. Biol.* **72**, 459–467.

König, A.-C., Hartl, M., Boersema, P.J., Mann, M. and Finkemeier, I. (2014a) The mitochondrial lysine acetylome of *Arabidopsis*. *Mitochondrion*, **19**, 252–260.

König, A.-C., Hartl, M., Pham, P.A. *et al.* (2014b) The *Arabidopsis* class II sirtuin is a lysine deacetylase and interacts with mitochondrial energy metabolism. *Plant Physiol.* **164**, 1401–1414.

Krauss, S. (2001) Mitochondria: structure and role in respiration. *Encyclopedia Life Sci.* 1–6.

Krey, J.F., Wilmarth, P.A., Shin, J.-B., Klimek, J., Sherman, N.E., Jeffery, E.D., Choi, D., David, L.L. and Barr-Gillespie, P.G. (2014) Accurate label-free protein quantitation with high- and low-resolution mass spectrometers. *J. Proteome Res.* **13**, 1034–1044.

Kruft, V., Eubel, H., Jänsch, L., Werhahn, W. and Braun, H.P. (2001) Proteomic approach to identify novel mitochondrial proteins in *Arabidopsis*. *Plant Physiol.* **127**, 1694–1710.

Kühn, K., Richter, U., Meyer, E.H. *et al.* (2009) Phage-type RNA polymerase RPOTmp performs gene-specific transcription in mitochondria of *Arabidopsis thaliana*. *Plant Cell*, **21**, 2762–2779.

Kukat, C., Wurm, C.A., Spahr, H., Falkenberg, M., Larsson, N.-G. and Jakobs, S. (2011) Super-resolution microscopy reveals that mammalian mitochondrial nucleoids have a uniform size and frequently contain a single copy of mtDNA. *Proc. Natl Acad. Sci. USA*, **108**, 13534–13539.

Lenz, H., Hein, A. and Knoop, V. (2018) Plant organelle RNA editing and its specificity factors: enhancements of analyses and new database features in PREPACT 3.0. *BMC Bioinformatics*, **19**, 255.

Lister, R., Chew, O., Rudhe, C., Lee, M.N. and Whelan, J. (2001) *Arabidopsis thaliana* ferrochelatase-I and -II are not imported into *Arabidopsis* mitochondria. *FEBS Lett.* **506**, 291–295.

Liu, M.Y. and Colombini, M. (1992) A soluble mitochondrial protein increases the voltage dependence of the mitochondrial channel, VDAC. *J. Bioenerg. Biomembr.* **24**, 41–46.

Logan, D.C. (2006) Plant mitochondrial dynamics. *Biochim. Biophys. Acta Mol. Cell Res.* **1763**, 430–441.

Logan, D.C. and Leaver, C.J. (2000) Mitochondria-targeted GFP highlights the heterogeneity of mitochondrial shape, size and movement within living plant cells. *J. Exp. Bot.* **51**, 865–871.

Logan, D.C. and Paszkiewicz, G. (2017) The dynamic chondriome: control of number, shape, size and motility of mitochondria. In *Annual Plant Reviews, Volume 50* (Logan, D.C., ed). Chichester, UK: John Wiley & Sons Ltd, pp. 67–109.

Lutziger, I. and Oliver, D.J. (2001) Characterization of two cDNAs encoding mitochondrial lipoamide dehydrogenase from Arabidopsis. *Plant Physiol.* **127**, 615–623.

Mannella, C. (1982) Structure of the outer mitochondrial membrane: ordered arrays of porelike subunits in outer-membrane fractions from *Neurospora crassa* mitochondria. *J. Cell Biol.* **94**, 680–687.

Mannella, C.A. and Bonner, W.D. (1975) X-ray diffraction from oriented outer mitochondrial membranes. Detection of in-plane subunit structure. *Biochim. Biophys. Acta*, **413**, 226–233.

Masuda, T., Suzuki, T., Shimada, H., Ohta, H. and Takamiya, K. (2003) Subcellular localization of two types of ferrochelatase in cucumber. *Planta*, **217**, 602–609.

Maurino, V.G. and Engqvist, M.K.M. (2015) 2-Hydroxy acids in plant metabolism. *Arabidopsis Book*, **13**, e0182.

Maurino, V.G. and Peterhänsel, C. (2010) Photorespiration: current status and approaches for metabolic engineering. *Curr. Opin. Plant Biol.* **13**, 248–255.

McClung, C.R., Hsu, M., Painter, J.E., Gagne, J.M., Karlsberg, S.D. and Salomé, P.A. (2000) Integrated temporal regulation of the photorespiratory pathway. Circadian regulation of two *Arabidopsis* genes encoding serine hydroxymethyltransferase. *Plant Physiol.* **123**, 381–392.

Meyer, E.H., Heazlewood, J.L. and Millar, A.H. (2007) Mitochondrial acyl carrier proteins in *Arabidopsis thaliana* are predominantly soluble matrix proteins and none can be confirmed as subunits of respiratory complex I. *Plant Mol. Biol.* **64**, 319–327.

Meyer, E.H., Welchen, E. and Carrie, C. (2019) Assembly of the complexes of the oxidative phosphorylation system in land plant mitochondria. *Annu. Rev. Plant Biol.* **70**, 23–50.

Millar, A.H., Sweetlove, L.J., Giegé, P. and Leaver, C.J. (2001) Analysis of the *Arabidopsis* mitochondrial proteome. *Plant Physiol.* **127**, 1711–1727.

Mlayeh, L., Chatkaew, S., Léonetti, M. and Homblé, F. (2010) Modulation of plant mitochondrial VDAC by phytosterols. *Biophys. J.* **99**, 2097–2106.

Model, K., Meisinger, C. and Kühlbrandt, W. (2008) Cryo-electron microscopy structure of a yeast mitochondrial preprotein translocase. *J. Mol. Biol.* **383**, 1049–1057.

Møller, I.M. (2001) PLANT MITOCHONDRIA AND OXIDATIVE STRESS: electron transport, NADPH turnover, and metabolism of reactive oxygen species. *Annu. Rev. Plant Physiol. Plant Mol. Biol.* **52**, 561–591.

Møller, I.M. (2016) What is hot in plant mitochondria? *Physiol. Plant.* **157**, 256–263.

Mooney, B.P., David, N.R., Thelen, J.J., Miernyk, J.A. and Randall, D.D. (2000) Histidine modifying agents abolish pyruvate dehydrogenase kinase activity. *Biochem. Biophys. Res. Commun.* **267**, 500–503.

Morgenstern, M., Stiller, S.B., Lübbert, P. *et al.* (2017) Definition of a high-confidence mitochondrial proteome at quantitative scale. *Cell Rep.* **19**, 2836–2852.

Mouillon, J.-M., Aubert, S., Bourguignon, J., Gout, E., Douce, R. and Rébeillé, F. (1999) Glycine and serine catabolism in non-photosynthetic higher plant cells: their role in C1 metabolism: role of glycine and serine in C1 metabolism. *Plant J.* **20**, 197–205.

Mueller, S.J., Lang, D., Hoernstein, S.N.W. *et al.* (2014) Quantitative analysis of the mitochondrial and plastid proteomes of the moss *Physcomitrella patens* reveals protein macrocompartmentation and microcompartmentation. *Plant Physiol.* **164**, 2081–2095.

Murchie, E.H. and Lawson, T. (2013) Chlorophyll fluorescence analysis: a guide to good practice and understanding some new applications. *J. Exp. Bot.* **64**, 3983–3998.

Murphy, M.P. (2009) How mitochondria produce reactive oxygen species. *Biochem. J.* **417**, 1–13.

Nelson, C.J., Li, L., Jacoby, R.P. and Millar, A.H. (2013) Degradation rate of mitochondrial proteins in *Arabidopsis thaliana* cells. *J. Proteome Res.* **12**, 3449–3459.

Ohnishi, T. and Hagihara, B. (1964) Preparation of yeast mitochondria. *J. Biochem.* **55**, 584–585.

Oldenkott, B., Yang, Y., Lesch, E., Knoop, V. and Schallenberg-Rüdinger, M. (2019) Plant-type pentatricopeptide repeat proteins with a DYW domain drive C-to-U RNA editing in *Escherichia coli*. *Commun. Biol.* **2**, 85.

Oliver, D.J., Neuburger, M., Bourguignon, J. and Douce, R. (1990) Interaction between the component enzymes of the glycine decarboxylase multienzyme complex. *Plant Physiol.* **94**, 833–839.

Parsons, J.A. (1965) Mitochondrial incorporation of tritiated thymidine in *Tetrahymena pyriformis*. *J. Cell Biol.* **25**, 641–645.

© 2019 The Authors.

Pebay-Peyroula, E., Dahout-Gonzalez, C., Kahn, R., Trézéguet, V., Lauquin, G.J.-M. and Brandolin, G. (2003) Structure of mitochondrial ADP/ATP carrier in complex with carboxyatractyloside. *Nature*, **426**, 39–44.

Pérez-Ortín, J.E., Alepuz, P.M. and Moreno, J. (2007) Genomics and gene transcription kinetics in yeast. *Trends Genet.* **23**, 250–257.

Pérez-Ruiz, J.M., Naranjo, B., Ojeda, V., Guinea, M. and Cejudo, F.J. (2017) NTRC-dependent redox balance of 2-Cys peroxiredoxins is needed for optimal function of the photosynthetic apparatus. *Proc. Natl Acad. Sci. USA*, **114**, 12069–12074.

Peterhänsel, C., Horst, I., Niessen, M., Blume, C., Kebeish, R., Kürkcüoglu, S. and Kreuzaler, F. (2010) Photorespiration. *Arabidopsis Book*, **8**, e0130.

Preuten, T., Cincu, E., Fuchs, J., Zoschke, R., Liere, K. and Börner, T. (2010) Fewer genes than organelles: extremely low and variable gene copy numbers in mitochondria of somatic plant cells: gene copy numbers in mitochondria. *Plant J.* **64**, 948–959.

Puntarulo, S., Sánchez, R.A. and Boveris, A. (1988) Hydrogen peroxide metabolism in soybean embryonic axes at the onset of germination. *Plant Physiol.* **86**, 626–630.

Qian, Y. and Johnson, K.A. (2017) The human mitochondrial single-stranded DNA-binding protein displays distinct kinetics and thermodynamics of DNA binding and exchange. *J. Biol. Chem.* **292**, 13068–13084.

Rafelski, S.M. (2013) Mitochondrial network morphology: building an integrative, geometrical view. *BMC Biol.* **11**, 71.

Ramírez-Aguilar, S.J., Keuthe, M., Rocha, M., Fedyaev, V.V., Kramp, K., Gupta, K.J., Rasmusson, A.G., Schulze, W.X. and van Dongen, J.T. (2011) The composition of plant mitochondrial supercomplexes changes with oxygen availability. *J. Biol. Chem.* **286**, 43045–43053.

Reichheld, J.P., Khafif, M., Riondet, C., Droux, M., Bonnard, G. and Meyer, Y. (2007) Inactivation of thioredoxin reductases reveals a complex interplay between thioredoxin and glutathione pathways in *Arabidopsis* development. *Plant Cell*, **19**, 1851–1865.

Restrepo-Pérez, L., Joo, C. and Dekker, C. (2018) Paving the way to single-molecule protein sequencing. *Nat. Nanotechnol.* **13**, 786–796.

Rugen, N., Straube, H., Franken, L.E., Braun, H.-P. and Eubel, H. (2019a) Complexome profiling reveals association of PPR proteins with ribosomes in the mitochondria of plants. *Mol. Cell. Proteomics.* **18**, 1345–1362.

Rugen, N., Straube, H., Franken, L.E., Braun, H.-P. and Eubel, H. (2019b) Correction: complexome profiling reveals association of PPR proteins with ribosomes in the mitochondria of plants. *Mol. Cell. Proteomics.* **18**, 1704.

Salvato, F., Havelund, J.F., Chen, M., Rao, R.S.P., Rogowska-Wrzesinska, A., Jensen, O.N., Gang, D.R., Thelen, J.J. and Møller, I.M. (2014) The potato tuber mitochondrial proteome. *Plant Physiol.* **164**, 637–653.

Schikowsky, C., Senkler, J. and Braun, H.-P. (2017) SDH6 and SDH7 contribute to anchoring succinate dehydrogenase to the inner mitochondrial membrane in *Arabidopsis thaliana*. *Plant Physiol.* **173**, 1094–1108.

Schwanhäusser, B., Busse, D., Li, N., Dittmar, G., Schuchhardt, J., Wolf, J., Chen, W. and Selbach, M. (2011) Global quantification of mammalian gene expression control. *Nature*, **473**, 337–342.

Schwarzländer, M., Logan, D.C., Johnston, I.G., Jones, N.S., Meyer, A.J., Fricker, M.D. and Sweetlove, L.J. (2012) Pulsing of membrane potential in individual mitochondria: a stress-induced mechanism to regulate respiratory bioenergetics in *Arabidopsis*. *Plant Cell*, **24**, 1188–1201.

Schwerzmann, K., Cruz-Orive, L.M., Eggman, R., Sänger, A. and Weibel, E.R. (1986) Molecular architecture of the inner membrane of mitochondria from rat liver: a combined biochemical and stereological study. *J. Cell Biol.* **102**, 97–103.

Scott, I. and Logan, D.C. (2011) Mitochondrial dynamics. In *Plant Mitochondria* (Kempken, F., ed.). New York, NY: Springer New York, pp. 31–63.

Senkler, J., Senkler, M., Eubel, H. *et al.* (2017) The mitochondrial complexome of *Arabidopsis thaliana*. *Plant J.* **89**, 1079–1092.

Sheahan, M.B., Rose, R.J. and McCurdy, D.W. (2004) Organelle inheritance in plant cell division: the actin cytoskeleton is required for unbiased inheritance of chloroplasts, mitochondria and endoplasmic reticulum in dividing protoplasts. *Plant J.* **37**, 379–390.

Sheahan, M.B., McCurdy, D.W. and Rose, R.J. (2005) Mitochondria as a connected population: ensuring continuity of the mitochondrial genome during plant cell dedifferentiation through massive mitochondrial fusion. *Plant J.* **44**, 744–755.

Shedge, V., Arrieta-Montiel, M., Christensen, A.C. and Mackenzie, S.A. (2007) Plant mitochondrial recombination surveillance requires unusual RecA and MutS homologs. *Plant Cell*, **19**, 1251–1264.

Sirrenberg, C., Endres, M., Becker, K., Bauer, M.F., Walther, E., Neupert, W. and Brunner, M. (1997) Functional cooperation and stoichiometry of protein translocases of the outer and inner membranes of mitochondria. *J. Biol. Chem.* **272**, 29963–29966.

Sjostrand, F.S. (1953) Electron microscopy of mitochondria and cytoplasmic double membranes. *Nature*, **171**, 30–32.

Somerville, C.R. and Ogren, W.L. (1981) Photorespiration-deficient mutants of *Arabidopsis thaliana* lacking mitochondrial serine transhydroxymethylase activity. *Plant Physiol.* **67**, 666–671.

de Souza, W., Attias, M. and Rodrigues, J.C.F. (2009) Particularities of mitochondrial structure in parasitic protists (Apicomplexa and Kinetoplastida). *Int. J. Biochem. Cell Biol.* **41**, 2069–2080.

Sun, F., Huo, X., Zhai, Y., Wang, A., Xu, J., Su, D., Bartlam, M. and Rao, Z. (2005) Crystal structure of mitochondrial respiratory membrane protein complex II. *Cell*, **121**, 1043–1057.

Sun, T., Bentolila, S. and Hanson, M.R. (2016) The unexpected diversity of plant organelle RNA editosomes. *Trends Plant Sci.* **21**, 962–973.

Sun, Y., Wollman, A., Huang, F., Leake, M. and Liu, L. (2019) Single-organelle quantification reveals the stoichiometric and structural variability of carboxysomes dependent on the environment. *Plant Cell*, **31**, 1648–1664.

Sunderhaus, S., Dudkina, N.V., Jänsch, L., Klodmann, J., Heinemeyer, J., Perales, M., Zabaleta, E., Boekema, E.J. and Braun, H.-P. (2006) Carbonic anhydrase subunits form a matrix-exposed domain attached to the membrane arm of mitochondrial complex I in plants. *J. Biol. Chem.* **281**, 6482–6488.

Sweetlove, L.J., Heazlewood, J.L., Herald, V., Holtzapffel, R., Day, D.A., Leaver, C.J. and Millar, A.H. (2002) The impact of oxidative stress on *Arabidopsis* mitochondria. *Plant J.* **32**, 891–904.

Sweetlove, L.J., Beard, K.F.M., Nunes-Nesi, A., Fernie, A.R. and Ratcliffe, R.G. (2010) Not just a circle: flux modes in the plant TCA cycle. *Trends Plant Sci.* **15**, 462–470.

Takenaka, M., Zehrmann, A., Verbitskiy, D., Kugelmann, M., Härtel, B. and Brennicke, A. (2012) Multiple organellar RNA editing factor (MORF) family proteins are required for RNA editing in mitochondria and plastids of plants. *Proc. Natl Acad. Sci. USA*, **109**, 5104–5109.

Tanaka, R. and Tanaka, A. (2007) Tetrapyrrole biosynthesis in higher plants. *Annu. Rev. Plant Biol.* **58**, 321–346.

Taylor, N.L., Heazlewood, J.L. and Millar, A.H. (2011) The Arabidopsis thaliana 2-D gel mitochondrial proteome: refining the value of reference maps for assessing protein abundance, contaminants and post-translational modifications. *Proteomics*, **11**, 1720–1733.

Thal, B., Braun, H.-P. and Eubel, H. (2018) Proteomic analysis dissects the impact of nodulation and biological nitrogen fixation on *Vicia faba* root nodule physiology. *Plant Mol. Biol.* **97**, 233–251.

Tronconi, M.A., Fahnenstich, H., Gerrard Weehler, M.C., Andreo, C.S., Flügge, U.-I., Drincovich, M.F. and Maurino, V.G. (2008) *Arabidopsis* NAD-malic enzyme functions as a homodimer and heterodimer and has a major impact on nocturnal metabolism. *Plant Physiol.* **146**, 1540–1552.

Tronconi, M.A., Maurino, V.G., Andreo, C.S. and Drincovich, M.F. (2010) Three different and tissue-specific NAD-malic enzymes generated by alternative subunit association in *Arabidopsis thaliana*. *J. Biol. Chem.* **285**, 11870–11879.

Uhrig, R.G., Labandera, A.-M., Tang, L.-Y., Sieben, N.A., Goudreault, M., Yeung, E., Gingras, A.-C., Samuel, M.A. and Moorhead, G.B.G. (2017) Activation of mitochondrial protein phosphatase SLP2 by MIA40 regulates seed germination. *Plant Physiol.* **173**, 956–969.

Utter, M.F., Keech, D.B. and Nossal, P.M. (1958) Oxidative phosphorylation by subcellular particles from yeast. *Biochem. J.* **68**, 431–440.

Vaseghi, M.-J., Chibani, K., Telman, W., Liebthal, M.F., Gerken, M., Schnitzer, H., Mueller, S.M. and Dietz, K.-J. (2018) The chloroplast 2-cysteine peroxiredoxin functions as thioredoxin oxidase in redox regulation of chloroplast metabolism. *eLife*, **7**, e38194.

Vincent, A.E., White, K., Davey, T. *et al.* (2019) Quantitative 3D mapping of the human skeletal muscle mitochondrial network. *Cell Rep.* **27**, 321.

de Virville, J.D., Alin, M.-F., Aaron, Y., Rémy, R., Guillot-Salomon, T. and Cantrel, C. (1998) Changes in functional properties of mitochondria during growth cycle of *Arabidopsis thaliana* cell suspension cultures. *Plant Physiol. Biochem.* **36**, 347–356.

Vizcaino, J.A., Cote, R.G., Csordas, A. *et al.* (2013) The Proteomics Identifications (PRIDE) database and associated tools: status in 2013. *Nucleic Acids Res.* **41**, D1063–D1069.

© 2019 The Authors.
The Plant Journal published by Society for Experimental Biology and John Wiley & Sons Ltd,
The Plant Journal, (2019), doi: 10.1111/tpj.14534

Vogel, U. and Jensen, K.F. (1994) The RNA chain elongation rate in *Escherichia coli* depends on the growth rate. *J. Bacteriol.* **176**, 2807–2813.

Wagner, S., Behera, S., De Bortoli, S. *et al.* (2015) The EF-hand Ca^{2+} binding protein MICU choreographs mitochondrial Ca^{2+} dynamics in *Arabidopsis*. *Plant Cell*, **27**, 3190–3212.

Waltz, F., Nguyen, T.-T., Arrivé, M. *et al.* (2019) Small is big in *Arabidopsis* mitochondrial ribosome. *Nat. Plants*, **5**, 106–117.

Wang, Q., Fristedt, R., Yu, X., Chen, Z., Liu, H., Lee, Y., Guo, H., Merchant, S.S. and Lin, C. (2012) The gamma-carbonic anhydrase subcomplex of mitochondrial complex I is essential for development and important for photomorphogenesis of *Arabidopsis*. *Plant Physiol.* **160**, 1373–1383.

Weiss, H., von Jagow, G., Klingenberg, M. and Bücher, T. (1970) Characterization of *Neurospora crassa* mitochondria prepared with a grind-mill. *Eur. J. Biochem.* **14**, 75–82.

Werhahn, W., Niemeyer, A., Jänsch, L., Kruft, V., Schmitz, U.K. and Braun, H. (2001) Purification and characterization of the preprotein translocase of the outer mitochondrial membrane from *Arabidopsis*. Identification of multiple forms of TOM20. *Plant Physiol.* **125**, 943–954.

Werner, S. and Neupert, W. (1972) Functional and biogenetical heterogeneity of the inner membrane of rat-liver mitochondria. *Eur. J. Biochem.* **25**, 379–396.

van Wijk, K.J., Friso, G., Walther, D. and Schulze, W.X. (2014) Meta-analysis of *Arabidopsis thaliana* phospho-proteomics data reveals compartmentalization of phosphorylation motifs. *Plant Cell*, **26**, 2367–2389.

Wirtz, M., Beard, K.F.M., Lee, C.P. *et al.* (2012) Mitochondrial cysteine synthase complex regulates O-acetylserine biosynthesis in plants. *J. Biol. Chem.* **287**, 27941–27947.

Woodson, J.D., Perez-Ruiz, J.M. and Chory, J. (2011) Heme synthesis by plastid ferrochelatase I regulates nuclear gene expression in plants. *Curr. Biol.* **21**, 897–903.

Wurm, C.A., Neumann, D., Lauterbach, M.A., Harke, B., Egner, A., Hell, S.W. and Jakobs, S. (2011) Nanoscale distribution of mitochondrial import receptor Tom20 is adjusted to cellular conditions and exhibits an inner-cellular gradient. *Proc. Natl Acad. Sci. USA*, **108**, 13546–13551.

Yajima, Y., Hiratsuka, T., Kakimoto, Y., Ogawa, S., Shima, K., Yamazaki, Y., Yoshikawa, K., Tamaki, K. and Tsuruyama, T. (2018) Region of interest analysis using mass spectrometry imaging of mitochondrial and sarcomeric proteins in acute cardiac infarction tissue. *Sci. Rep.* **8**, 7493.

Yasuda, R., Noji, H., Yoshida, M., Kinosita, K. and Itoh, H. (2001) Resolution of distinct rotational substeps by submillisecond kinetic analysis of F1-ATPase. *Nature*, **410**, 898–904.

Zaegel, V., Guermann, B., Le Ret, M., Andrés, C., Meyer, D., Erhardt, M., Canaday, J., Gualberto, J.M. and Imbault, P. (2006) The plant-specific ssDNA binding protein OSB1 is involved in the stoichiometric transmission of mitochondrial DNA in *Arabidopsis*. *Plant Cell*, **18**, 3548–3563.

Zamponi, N., Zamponi, E., Cannas, S.A., Billoni, O.V., Helguera, P.R. and Chialvo, D.R. (2018) Mitochondrial network complexity emerges from fission/fusion dynamics. *Sci. Rep.* **8**, 363.

Zhang, Z., Huang, L., Shulmeister, V.M., Chi, Y.I., Kim, K.K., Hung, L.W., Crofts, A.R., Berry, E.A. and Kim, S.H. (1998) Electron transfer by domain movement in cytochrome bc1. *Nature*, **392**, 677–684.

Zhang, Y., Sun, K., Sandoval, F.J., Santiago, K. and Roje, S. (2010) One-carbon metabolism in plants: characterization of a plastid serine hydroxymethyltransferase. *Biochem. J.* **430**, 97–105.

Zhang, Y., Beard, K.F.M., Swart, C. *et al.* (2017) Protein-protein interactions and metabolite channelling in the plant tricarboxylic acid cycle. *Nat. Commun.* **8**, 15212.

Zhang, L., Khattar, N., Kemenes, I., Kemenes, G., Zrinyi, Z., Pirger, Z. and Vertes, A. (2018) Subcellular peptide localization in single identified neurons by capillary microsampling mass spectrometry. *Sci. Rep.* **8**, 12227.

Zhou, Z.H., McCarthy, D.B., O'Connor, C.M., Reed, L.J. and Stoops, J.K. (2001) The remarkable structural and functional organization of the eukaryotic pyruvate dehydrogenase complexes. *Proc. Natl Acad. Sci. USA*, **98**, 14802–14807.

Zickermann, V., Wirth, C., Nasiri, H., Siegmund, K., Schwalbe, H., Hunte, C. and Brandt, U. (2015) Mechanistic insight from the crystal structure of mitochondrial complex I. *Science*, **347**, 44–49.

Zizi, M., Forte, M., Blachly-Dyson, E. and Colombini, M. (1994) NADH regulates the gating of VDAC, the mitochondrial outer membrane channel. *J. Biol. Chem.* **269**, 1614–1616.

© 2019 The Authors.

Publication 2

2.2 Absence of Complex I Implicates Rearrangement of the Respiratory Chain in European Mistletoe

Jennifer Senkler,[1] Nils Rugen,[1] Holger Eubel,[1] Jan Hegermann,[2] and Hans-Peter Braun[1,3,*]

[1]Institut für Pflanzengenetik, Leibniz Universität Hannover, Herrenhäuser Straße 2, 30419 Hannover, Germany

[2]Institut für Funktionelle und Angewandte Anatomie, Medizinische Hochschule Hannover, Carl-Neuberg-Straße 1, 30625 Hannover, Germany

Type of authorship:	Co-author
Type of article:	Research article
Share of the work:	20%
Contribution to the publication:	Planed and performed experiments, analyzed data
Journal:	Current Biology
Impact factor (2018):	9.13
Number of citations (Web of Science):	6
Date of Publication:	May 21, 2018
DOI:	10.1016/j.cub.2018.03.050

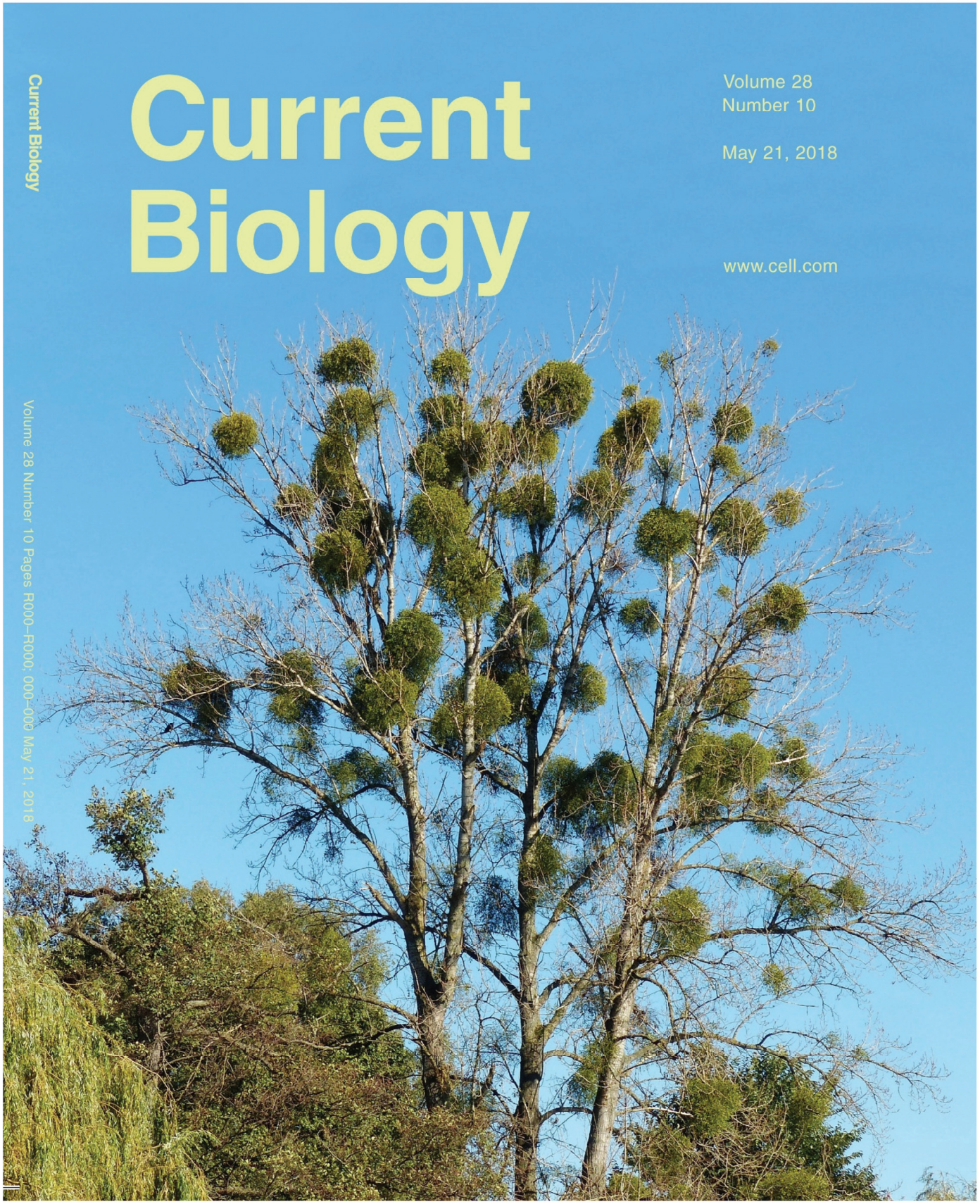

On the cover: European mistletoe (*Viscum album*) on a black poplar (*Populus nigra*) tree at the Herrenhausen Gardens in Hannover, Germany, in October 2017. *V. album* is evergreen and becomes nicely visible when the host trees lose their leaves in autumn. In this issue, Senkler et al. (pages 1606–1613) and Maclean et al. (pages 1614–1619) present evidence that *V. album* lacks the mitochondrial NADH dehydrogenase complex (complex I of the respiratory chain). This enzyme complex substantially contributes to mitochondrial ATP formation and so far was considered indispensable for multicellular life. The remaining respiratory chain is rearranged in *V. album*: complexes III and IV form a stable supercomplex, and alternative NADH dehydrogenases are present, which, however, do not contribute to mitochondrial ATP generation. As a consequence, the mitochondrial capacity for ATP production is reduced in *V. album*. These results give insights into a special operation mode of the mitochondrial respiratory chain and shed new light on the biochemistry of parasitism. Photograph © Hans-Peter Braun.

Article

Current Biology

Absence of Complex I Implicates Rearrangement of the Respiratory Chain in European Mistletoe

Graphical Abstract

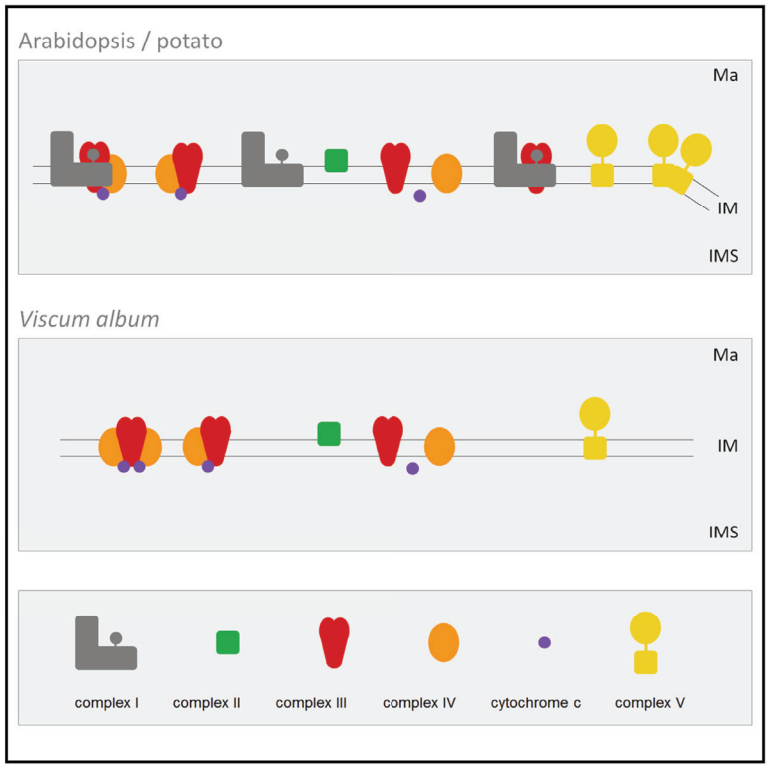

Authors

Jennifer Senkler, Nils Rugen, Holger Eubel, Jan Hegermann, Hans-Peter Braun

Correspondence

braun@genetik.uni-hannover.de

In Brief

Complex I is considered to be an essential component of the respiratory chain of all multicellular eukaryotes. Senkler et al. show that the European mistletoe, a semiparasitic flowering plant, lacks complex I. As a consequence, the respiratory chain is rearranged. It is composed of stable III+IV supercomplexes and alternative oxidoreductases.

Highlights

- Mitochondria from European mistletoe (*Viscum album*) lack complex I
- In consequence, the respiratory chain (RC) of *V. album* is rearranged
- The RC of *V. album* includes stable III+IV supercomplexes and alternative enzymes
- The ATP synthase complex is of low abundance, and crista formation is reduced

Senkler et al., 2018, Current Biology *28*, 1606–1613
May 21, 2018 © 2018 Elsevier Ltd.
https://doi.org/10.1016/j.cub.2018.03.050

CellPress

CellPress

Current Biology
Article

Absence of Complex I Implicates Rearrangement of the Respiratory Chain in European Mistletoe

Jennifer Senkler,[1] Nils Rugen,[1] Holger Eubel,[1] Jan Hegermann,[2] and Hans-Peter Braun[1,3,*]
[1]Institut für Pflanzengenetik, Leibniz Universität Hannover, Herrenhäuser Straße 2, 30419 Hannover, Germany
[2]Institut für Funktionelle und Angewandte Anatomie, Medizinische Hochschule Hannover, Carl-Neuberg-Straße 1, 30625 Hannover, Germany
[3]Lead Contact
*Correspondence: braun@genetik.uni-hannover.de
https://doi.org/10.1016/j.cub.2018.03.050

SUMMARY

The mitochondrial oxidative phosphorylation (OXPHOS) system, which is based on the presence of five protein complexes, is in the very center of cellular ATP production. Complexes I to IV are components of the respiratory electron transport chain that drives proton translocation across the inner mitochondrial membrane. The resulting proton gradient is used by complex V (the ATP synthase complex) for the phosphorylation of ADP. Occurrence of complexes I to V is highly conserved in eukaryotes, with exceptions being restricted to unicellular parasites that take up energy-rich compounds from their hosts. Here we present biochemical evidence that the European mistletoe (*Viscum album*), an obligate semi-parasite living on branches of trees, has a highly unusual OXPHOS system. *V. album* mitochondria completely lack complex I and have greatly reduced amounts of complexes II and V. At the same time, the complexes III and IV form remarkably stable respiratory supercomplexes. Furthermore, complexome profiling revealed the presence of 150 kDa complexes that include type II NAD(P)H dehydrogenases and an alternative oxidase. Although the absence of complex I genes in mitochondrial genomes of mistletoe species has recently been reported, this is the first biochemical proof that these genes have not been transferred to the nuclear genome and that this respiratory complex indeed is not assembled. As a consequence, the whole respiratory chain is remodeled. Our results demonstrate that, in the context of parasitism, multicellular life can cope with lack of one of the OXPHOS complexes and give new insights into the life strategy of mistletoe species.

INTRODUCTION

The mitochondrial electron transport chain can be biochemically divided into four functional segments, which represent protein complexes (reviewed in [1]). Complex I transfers electrons from NADH to ubiquinone, complex II from succinate to ubiquinone, complex III from ubiquinol to cytochrome *c*, and complex IV from cytochrome *c* to molecular oxygen [2]. Together with the ATP synthase complex (complex V), complexes I to IV constitute the oxidative phosphorylation (OXPHOS) system. The physiology of all five complexes has received considerable attention (reviewed in [2]). It meanwhile has become clear that the OXPHOS complexes can form defined supramolecular assemblies designated respiratory supercomplexes [3–6].

Due to its central importance for ATP production, the mitochondrial OXPHOS system is highly conserved in eukaryotes. Only a few species have a reduced OXPHOS system, and all of them are unicellular organisms (reviewed in [7]). Some species of the Microsporidia clade, which are spore-forming unicellular parasites, completely lack an OXPHOS system [8]. These organisms are able to acquire ATP from their host cells [9]. Furthermore, some dinoflagellates and chromerids have a degenerated respiratory chain [10]. In the latter clade, several species simultaneously lack complexes I and III [11]. Finally, complex I is absent in yeast and some other Saccharomycotina species [8, 12–15]. Alternative oxidoreductases can replace the classical oxidoreductase complexes, like type II NADH dehydrogenases or the alternative oxidase (AOX). However, since these enzymes do not couple electron transport and proton translocation across the inner mitochondrial membrane, they do not contribute to mitochondrial ATP formation. Plants possess a complete OXPHOS system (complexes I to V) and, in addition, alternative oxidoreductases involved in respiratory electron transport [16, 17]. The alternative oxidoreductases are considered to keep the redox system of the plant cell in a balance, which is especially relevant at high light and other stress conditions. It is probably due to the presence of these extra enzymes that some mutant plant lines can survive without complex I, but their development is dramatically disturbed [18–22].

Recently, the mitochondrial genomes of mistletoe species were characterized and found to be surprisingly divergent with respect to the mitogenomes of other angiosperms [23–25]. Several mistletoe species are obligate hemiparasitic plants that live on branches of trees and absorb water, nutrients, and organic compounds from their hosts. Parasitic life style has implications on cellular respiration. All investigated *Viscum* species lack mitochondrial genes encoding subunits of complex I [23–25]. In most angiosperms, nine subunits of complex I are encoded by the mitochondrial genome (ND1, ND2, ND3, ND4, ND4L, ND5, ND6, ND7, and ND9), and another ~40 subunits are nuclear encoded, translated in the cytoplasm, and post-translationally transported into the organelles [26]. It has been discussed that presence of a functionally active complex I in

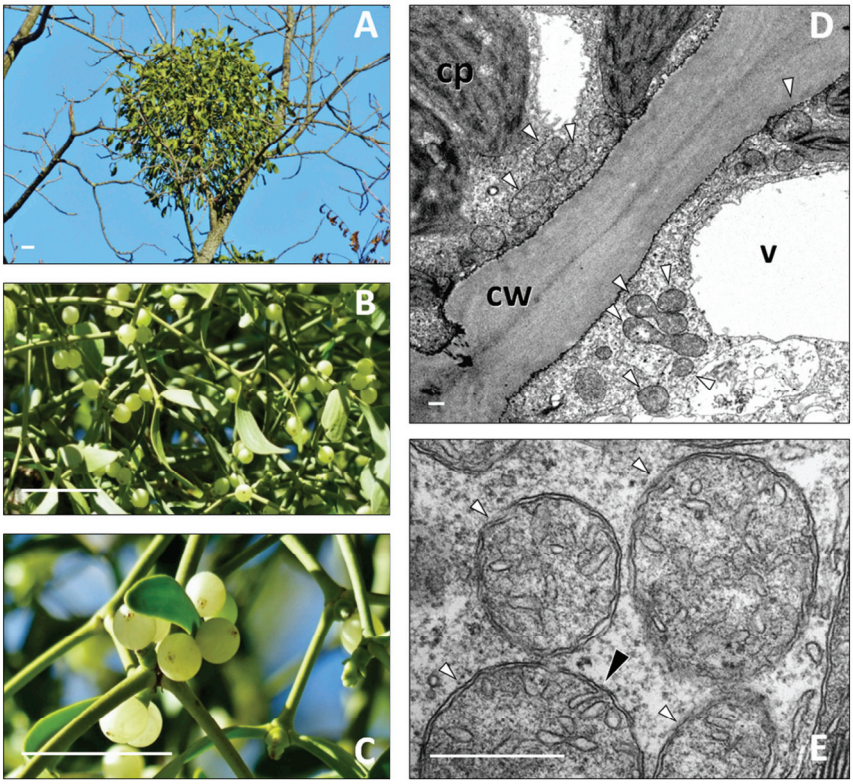

Figure 1. *Viscum album* at the Herrenhausen Gardens, Hannover, Germany

(A–C) Whole mistletoe plant on a maple tree (A), leaves (B), and white berries (C). The scale bars correspond to 5 cm. Photos were taken in October 2017.

(D and E) Transmission electron microscopy (TEM) images of parts of two mistletoe leaf cells (D) and mistletoe mitochondria (E). The scale bars correspond to 0.5 μm. White arrowheads, mitochondria; black arrowhead, invagination of the inner mitochondrial membrane. cp, chloroplast; v, vacuole; cw, cell wall.

mistletoe species would require the transfer of a whole set of mitochondrial genes to the nucleus [24]. However, such a scenario never has been found in any other Eukarya species. It therefore was speculated that *Viscum* mitochondria lack complex I [25]. This, however, also has not been described before for any multicellular Eukarya species. Furthermore, Petersen et al. [24] present evidence that *Viscum* mitochondria also lack functional genes encoding subunits of the complexes II and V. This basically would indicate respiratory deficiency of the species. However, careful re-annotation of the mitochondrial genome of *V. album* revealed evidence for the presence of a full set of functional complex II to V genes [25].

We here report a biochemical and proteomic study to define the OXPHOS system of *V. album*. Systematic analysis of mitochondrial protein complexes by blue native PAGE (BN-PAGE) combined with mass spectrometry (MS) allowed identification of complexes II, III, IV, and V. Complexes III and IV form remarkably stable supercomplexes of III_2IV_1 and III_2IV_2 composition. The ATP synthase complex is of very low abundance, and ATP synthase dimers could not be detected. Consequently, cristae formation is low in *V. album* mitochondria as shown by electron microscopy (EM) analyses. Complexome profiling revealed presence of numerous alternative NAD(P)H dehydrogenases and AOX. Our data indicate that *V. album* has a very reduced but functional OXPHOS system with unique features.

RESULTS AND DISCUSSION

Mistletoes (*V. album*) were harvested from local trees in the Herrenhausen Gardens (Hannover, Germany) in summer 2017. Typical plants have a diameter of about 80 cm (Figures 1A–1C). EM analyses of ultra-thin leaf sections were carried out to investigate the subcellular organization of *V. album* cells (Figures 1D and 1E). Mitochondria are of roundish to elongated shape and include comparatively few cristae. Mature leaves were used for mitochondrial preparations. However, standard protocols for isolating mitochondria from plants were not suitable for *V. album*. This most likely is due to the high content of secondary compounds of *V. album*, which form viscous aggregates, not only in biochemical fractions of the white berries, but also in fractions from leaves. A method for preparing *V. album* mitochondria has been developed and is given in the STAR Methods section. Evaluation of quantitative peptide identification data revealed good purity (see below).

V. album Mitochondria Exhibit an Unusual Composition of Protein Complexes

Mitochondrial protein complexes from *V. album* were next analyzed by BN-PAGE (Figure 2). Several protein complexes are visible in the 400–900 kDa range. Molecular masses of the protein complexes clearly differ from those of the model plant *Arabidopsis*. 2D SDS-PAGE was carried out to identify the protein complexes based on their subunit compositions (Figure 3). Like in *Arabidopsis*, *V. album* mitochondria contain dimeric complex III (500 kDa), as well as monomeric complex IV (200 kDa). Furthermore, two abundant 700 and 900 kDa complexes are visible that are absent in *Arabidopsis*. Both include the subunits of complexes III and IV. Subunits of complex IV are more abundant in the 900 kDa complex compared to the 700 kDa complex. We conclude that both complexes represent supercomplexes of dimeric complex III plus one or two copies of monomeric complex IV. These supercomplexes have not been detected in *Arabidopsis*, but some low amounts are present in potato tuber mitochondria [29]. In contrast, $III+IV_{1-2}$ supercomplexes are abundant in yeast and mammalian mitochondria ([30]; Figure S1). Complex I and complex I-including supercomplexes are not present in *V. album*. Furthermore, the ATP synthase (complex V) and succinate dehydrogenase (complex II) could not be identified by visual inspection of the 2D BN/SDS gels (Figure 3).

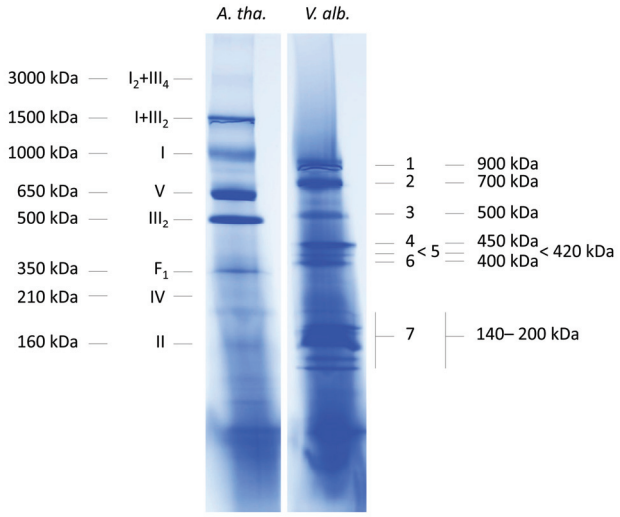

Figure 2. Analysis of Mitochondrial Protein Complexes from *Arabidopsis thaliana* and the Mistletoe *Viscum album* by 1D BN-PAGE

The gel was Coomassie stained. Identity and molecular masses (in kDa) of the OXPHOS complexes from *Arabidopsis* are given to the left of the gel. Mitochondrial protein complexes of *V. album* are numbered from 1 to 7; their apparent molecular masses are given in kDa. A. tha., *A. thaliana*; V. alb., *V. album*. Designations: I, complex I; V, complex V; III_2, dimeric complex III; F_1, F_1 part of complex V; IV, complex IV; II, complex II; $I+III_2$, supercomplex composed of complex I and dimeric complex III; I_2+III_4, megacomplex composed of two complex I monomers and two copies of dimeric complex III.

A 2D Reference Map of Mitochondrial Proteins in *V. album*

To search for protein complexes of lower abundance, 170 spots of the 2D BN/SDS gel were analyzed by MS (Figure S2A). Data evaluation using the *Arabidopsis* TAIR10 protein database (https://www.arabidopsis.org/) allowed us to identify 1,245 proteins overall in the 170 spots (427 unique proteins; Data S1). On average, only few peptides per protein were identified, reflecting the high sequence divergence between *Viscum* and other groups of angiosperms [25]. Furthermore, MS data were evaluated using *Viscum* protein sequence data available at NCBI (https://www.ncbi.nlm.nih.gov/) (Figure S2B; Data S2). MS data were also evaluated using the UniProt all plants database (http://www.uniprot.org/). However, usage of this database did not allow additional protein identifications compared to TAIR10 evaluation (data not shown). Protein identification data are summarized in Figure 4. A 2D GelMap has been created and is accessible at https://gelmap.de/1327. Most identified proteins are assigned to the mitochondrial compartment, but some chloroplast and peroxisomal proteins were also found.

Unique Composition of the Respiratory Chain in *V. album* Mitochondria

Our MS data reveal the absence of complex I but the presence of complexes II to V in *V. album*. However, complexes II and V are of low abundance. Subunits of complex V run at about 670 kDa in close proximity to the 700 kDa III_2+IV_1 supercomplex on the 2D gels (Figure 4). Additionally, subunits of the F_1 and F_0 subcomplexes of complex V run in the 300–350 kDa range. Subunits of complex II were identified at 100–200 kDa on the 2D gels (Figure 4). Six different alternative dehydrogenases were identified on the *V. album* GelMap (https://gelmap.de/1327; Data S1), including peptides identical to the AOX2, NDA1, NDA2, NDB2, NDB3, and NDC1 proteins of *Arabidopsis*. This indicates presence of numerous alternative electron transport pathways. However, the alternative enzymes do not contribute to the proton gradient across the inner mitochondrial membrane as their electron transport reactions are not coupled to proton translocation.

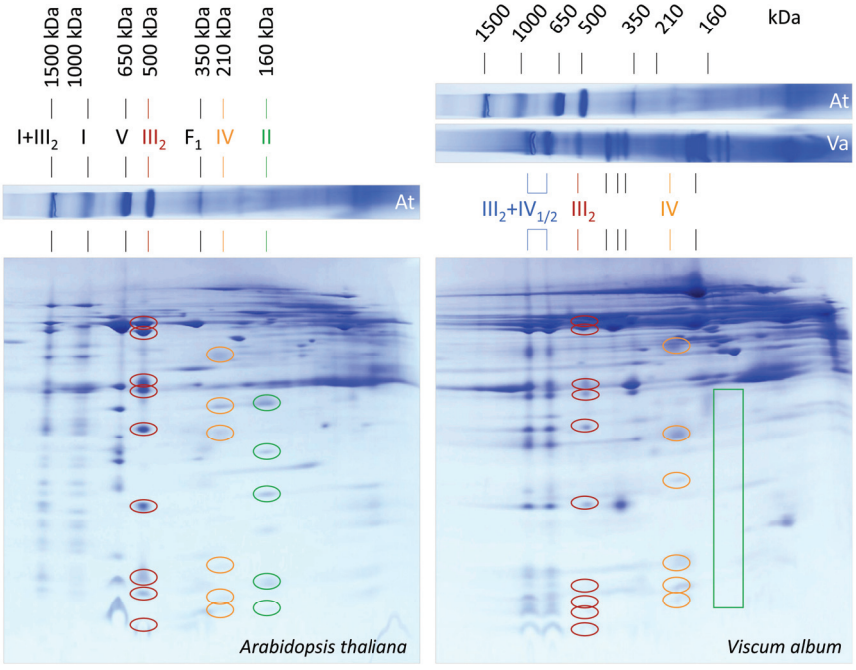

Figure 3. 2D Analyses of Mitochondrial Protein Complexes from *Arabidopsis thaliana* and *Viscum album* by BN/SDS-PAGE

The 2D gels were Coomassie stained. The corresponding stripes of the first gel dimension (BN-PAGE) are given above the 2D gels. Identities and molecular masses (in kDa) of protein complexes are given above the 1D gel stripes. At, *A. thaliana*; Va, *V. album*. Designations: I, complex I; V, complex V; III_2, dimeric complex III; F_1, F_1 part of complex V; IV, complex IV; II, complex II; $I+III_2$, supercomplex composed of complex I and dimeric complex III; $III_2+IV_{1/2}$, supercomplexes composed of dimeric complex III and either one or two copies of monomeric complex IV. Visible subunits of complex III_2 are encircled in red, complex IV subunits in orange, and complex II subunits in green. In *V. album*, complex II subunits are not visible (green box). Note that complex II has seven to eight subunits in plants [27, 28]. A comparison of mitochondrial protein complexes from *V. album* and yeast is presented in Figure S1.

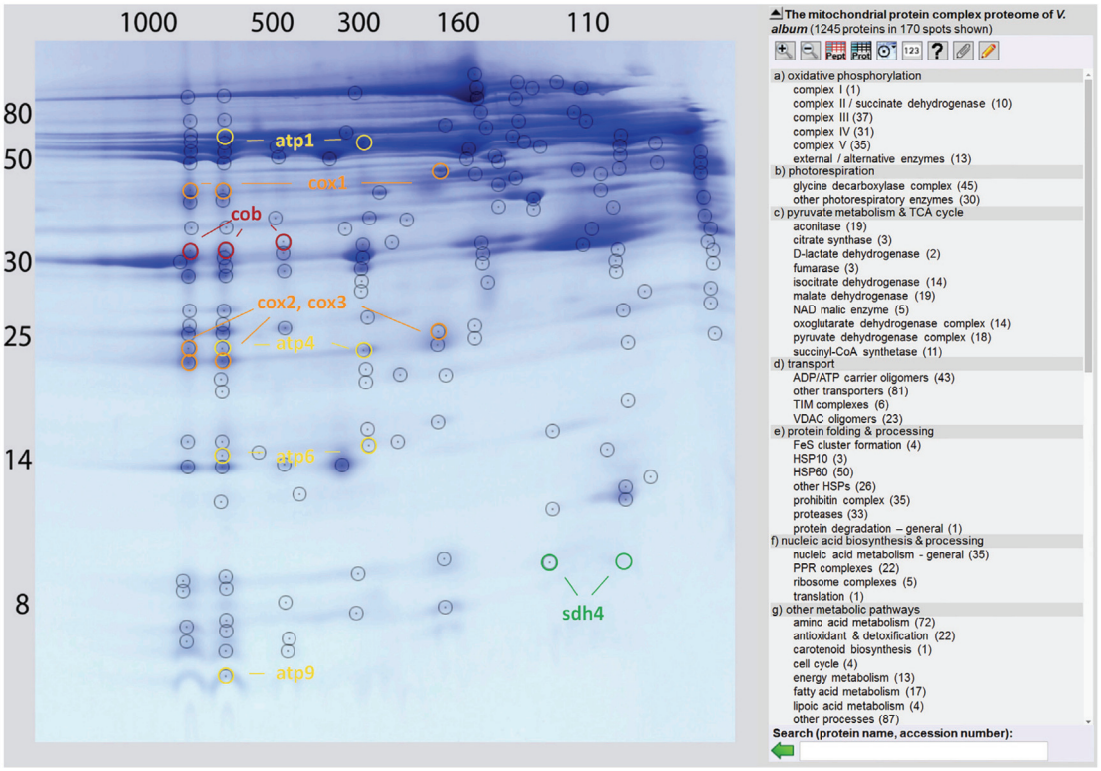

Figure 4. GelMap of Mitochondrial Proteins from *Viscum album*

The image is a screenshot from the GelMap portal (https://gelmap.de/1327). Proteins were separated by 2D BN (horizontal gel dimension)/SDS (vertical gel dimension)-PAGE. Numbers above and to the left of the gel indicate the masses of standard proteins in kDa. Proteins identified by MS are encircled. MS data were (1) evaluated using the TAIR10 database (https://www.arabidopsis.org) (spots encircled in black; see detailed gel image in Figure S2A which includes spot numbers; see corresponding MS data in Data S1) and (2) evaluated using *Viscum* protein sequences from NCBI (https://www.ncbi.nlm.nih.gov/) (spots encircled in colors; see detailed gel image in Figure S2B, which includes spot numbers; see corresponding MS data in Data S2). The identities of subunits of OXPHOS complexes as determined by (2) are indicated (cob, cytochrome b subunit of complex III; cox I, II, and III, subunits 1, 2, and 3 of complex IV; atp1, 4, 6, and 9, subunits α, b, ATP6, and ATP9 of complex V; sdh4, subunit 4 of complex II). At the GelMap portal (https://gelmap.de/1327), MS results can be directly accessed by clicking onto spots. Furthermore, all identified proteins are assigned to functional categories. Functional categories are displayed to the right of the gel image. Upon clicking a category, all protein spots that include proteins of the category are labeled. The number behind the categories indicates the number of included proteins. The GelMap portal has been introduced previously [31]. Shares of functional categories in *V. album* and *Arabidopsis* are compared in Figure S3. In the frame of the GelMap project, we identified one peptide of a complex I subunit (subunit B15) in a low-molecular-mass region of the native gel dimension. This indicates that single nuclear encoded subunits of complex I still might be synthesized but cannot assemble into a protein complex because several (most?) subunits of complex I are not made.

Finally, a large number of enzymes of the central mitochondrial metabolism were identified, such as all eight enzymes of the citric acid cycle, several members of the mitochondrial metabolite carrier family, subunits of the glycine dehydrogenase complex, heat stress proteins, and several others (Figure S3; GelMap at https://gelmap.de/1327). Interestingly, besides the absence of complex I, proteins of the functional category "Nucleic Acid Biosynthesis and Processing" are also much reduced in *V. album* in comparison to *A. thaliana* (Figure S3). This probably reflects that many proteins involved in the splicing and editing of complex I transcripts are no longer necessary in the absence of complex I.

The Alternative Oxidoreductases Form Part of 150 kDa Complexes

A complexome profiling approach was next employed to obtain even deeper insights into the *V. album* mitochondrial proteome. For complexome profiling, a stripe of a 1D BN gel is dissected into 50–70 equal-sized gel slices that all are analyzed by highly sensitive label-free shotgun proteomics [32, 33]. For *V. album* mitochondria, 54 gel slices were produced (Figure 5A). Using the TAIR10 protein database for data evaluation, overall 13.468 peptides were identified in the 54 gel slices (Data S3), allowing us to assign on average 142 proteins per gel slice (Figure S4A). The overall number of unique proteins was 477, and on average, the proteins were identified and quantified in 8.8 different gel slices. The purity of our mitochondrial preparation was assessed by assigning peptide intensities to subcellular compartments based on information at the Subcellular Localization Database for Arabidopsis Proteins (http://suba.live/). The mitochondrial fraction is highly enriched in mitochondrial proteins, but it also includes plastidial and peroxisomal proteins (21/7%). In contrast, hardly any proteins localized in the nucleus were found (>1%) (Data S3). Abundance profiles for all 477

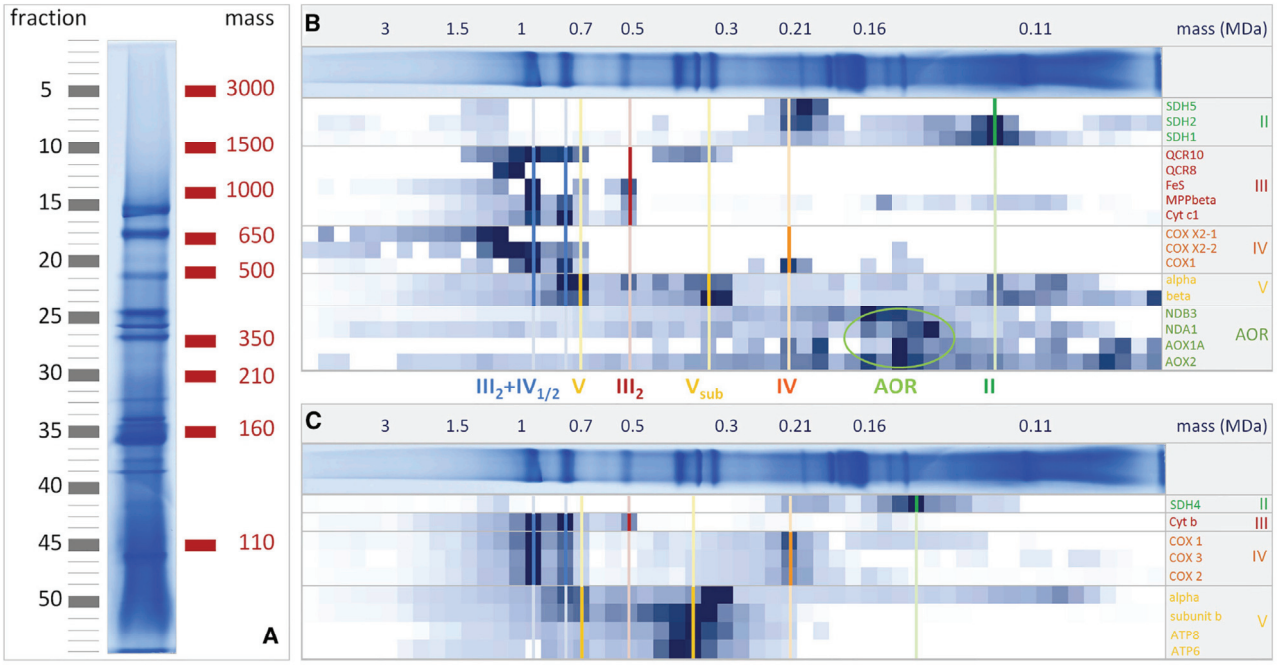

Figure 5. Complexome Profiling Analysis of *Viscum album* Mitochondria

(A) Mitochondrial protein complexes were separated by 1D BN-PAGE. The gel stripe was cut into 54 slices as indicated to the left of the gel stripe. The masses of standard proteins (in kDa) are given to the right.

(B) Quantitative profiles of subunits of complexes II to V as evaluated by using the TAIR10 database (https://www.arabidopsis.org/). All 54 gel slices were analyzed by quantitative label-free shotgun proteomics, allowing to calculate quantitative profiles of 477 proteins along the 1D BN gel stripe (for the complete dataset, see Figure S4 and Data S3; the dataset also is accessible at the ComplexomeMap portal at https://complexomemap.de/Va). The names of the subunits of the OXPHOS complexes are given to the right of the quantitative profiles. The colored bars indicate peak fractions of subunits of the complexes II to V (green, complex II; red, dimeric complex III; orange, complex IV; yellow, complex V and F_1/F_0 parts (V_{sub}) of complex V; blue, III_2IV_{1-2} supercomplexes). The light-green circle indicates the peak fractions of the alternative oxidoreductases (AOR).

(C) Same as (B), but MS data evaluation based on sequences of OXPHOS subunits encoded by the mitochondrial genomes of *Viscum* species (data from NCBI, https://www.ncbi.nlm.nih.gov/).

proteins along the 1D BN gel stripe were used for generating a heatmap. Profiles were aligned according to similarity by hierarchical clustering using the NOVA software. Subunits of protein complexes cluster on the resulting map (Figure S4B). With respect to the OXPHOS system, complexome profiling confirms presence of III_2+IV_{1-2} supercomplexes at 900 and 700 kDa, ATP synthase at 670 kDa, dimeric complex III at 500 kDa, monomeric complex IV at 200 kDa, and complex II in the 100–200 kDa range (Figures 5B and 5C). Protein complexes including AOX and alternative NAD(P)H dehydrogenases were identified in the 150 kDa region. Many further complexes are present in our dataset and can be accessed at https://complexomemap.de/Va.

Conclusions on the Energy Metabolism of *V. album*

We conclude that *V. album* mitochondria have a very special OXPHOS system. They lack complex I and have remarkably stable III+IV supercomplexes, low abundant complexes II and V, and numerous alternative oxidoreductases (Figure 6). In contrast, the protein complex composition of *V. album* chloroplasts is very similar to the one reported for *Arabidopsis* and other higher plants (Figure S5). Using densitometric gel evaluations, the stoichiometry and abundances of the mitochondrial complexes were compared between *V. album* and *Arabidopsis*. More than 80% of the complexes III and IV form part of the III_2+IV_{1-2} supercomplexes in *V. album*. Complexes III and IV are comparatively abundant in *V. album* but are still of reduced amount compared to *Arabidopsis* (Figure S6). The amount of complex V is clearly reduced in *V. album*. This is especially evident when comparing the OXPHOS systems between *V. album* and yeast (Figure S1). However, the ratios of the OXPHOS complexes might differ in other organs and developmental stages of *V. album*, which should be addressed by future investigations.

Our data indicate sharply reduced ATP formation in the mitochondria of *V. album*: (1) complex I is absent, (2) alternative oxidoreductases are present (but do not contribute to the proton gradient), and (3) complex V is of very low abundance and dimers could not be detected. Dimerization of complex V has been reported to be one of the key processes for cristae formation in mitochondria [35]. Indeed, occurrence of cristae is not very prominent in *V. album* (Figures 1D and 1E) if compared to other plants (see, e.g., [36] for reference), which also indicates reduced formation of ATP. Nevertheless, the OXPHOS system of *V. album* is very likely functional. Electron entry into the respiratory chain can take place via alternative oxidoreductases and remaining complex II. Presence of stable III-IV supercomplexes should promote efficient transfer of electrons from ubiquinol to molecular

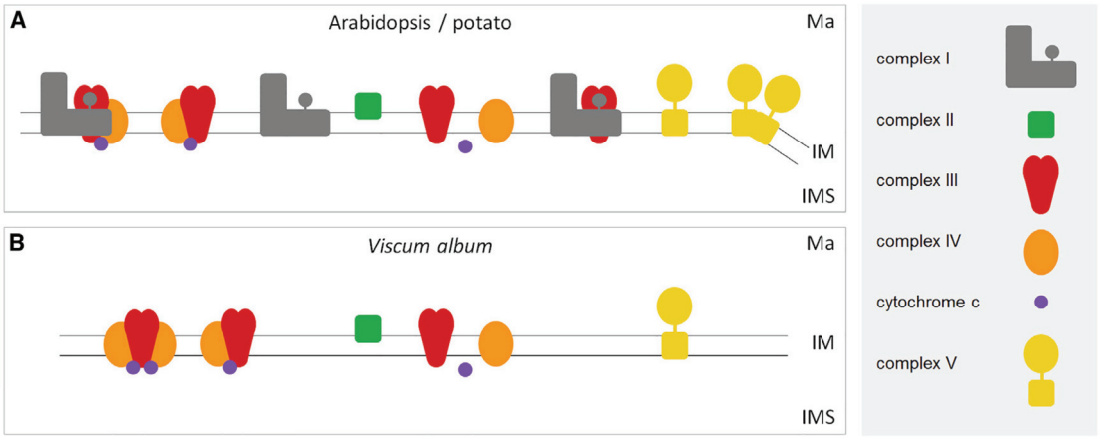

Figure 6. OXPHOS Complexes and Supercomplexes Described for the Model Plants *Arabidopsis* or Potato and in *Viscum album*

Arabidopsis or potato (A) [34] and *V. album* (B) are shown. Yellow, complex V and complex V dimers; gray, complex I; red, dimeric complex III; orange, complex IV; green, complex II; purple, cytochrome *c*. Ma, matrix; IM, inner mitochondrial membrane; IMS, mitochondrial intermembrane space. Colors correspond to those given in Figure 5 (except for the III_2IV_{1-2} supercomplexes, which are given in blue in Figure 5). Alternative oxidoreductases are also part of the OXPHOS system in all three organisms but are omitted in the figure. *V. album* protein complexes present in chloroplasts are displayed in Figure S5; a quantitative comparison of abundances of OXPHOS complexes in *Arabidopsis* and *V. album* is presented in Figure S6.

oxygen as discussed before [4, 5]. This part of the respiratory chain is coupled to proton translocation. The resulting proton gradient can be used by the ATP synthase complex for phosphorylating ADP. Additionally, the proton gradient can drive transport processes across the inner mitochondrial membrane to maintain other mitochondrial functions. Indeed, central mitochondrial metabolism is very likely functional in *V. album*, as all essential enzymes have been detected.

Our data point to a comparatively low requirement of mitochondrial ATP in *V. album* cells. Sucrose biosynthesis in the cytoplasm from triose-phosphate provided by the Calvin cycle is one of the main processes that depends on mitochondrial ATP in plants. The requirement of sucrose biosynthesis might be low in *V. album* due to its low growth rate and absence of a root system, which would need provision of sucrose from leaves. During evolution, this constellation might have promoted reduction of the respiratory chain. Due to its very large size, biosynthesis of complex I is especially expensive. Additionally, reduced formation of mitochondrial ATP might be partially compensated by increased ATP production via photophosphorylation or ATP producing processes in the cytoplasm. Alternatively, *V. album* might be supplied by the host plant not only with water and minerals, but also with assimilates. Other developmental stages of *V. album* should be investigated to obtain comprehensive information of mitochondrial functions in this and related species. Our study provides insights into energy metabolism in *V. album* leaves, but the understanding of the mistletoe mode of parasitism still is not complete.

STAR★METHODS

Detailed methods are provided in the online version of this paper and include the following:

- KEY RESOURCES TABLE
- CONTACT FOR REAGENT AND RESOURCE SHARING
- EXPERIMENTAL MODEL AND SUBJECT DETAILS
- METHOD DETAILS
  - Transmission Electron Microscopy
  - Mitochondria isolations
  - Gel electrophoresis procedures
  - Generation of a GelMap
  - Generation of a ComplexomeMap
- QUANTIFICATION AND STATISTICAL ANALYSIS
  - Data processing and heatmap generation for complexome profiling
  - Complexome profiling and ComplexomeMap generation
- DATA AND SOFTWARE AVAILABILITY
- ADDITIONAL RESOURCES

SUPPLEMENTAL INFORMATION

Supplemental Information includes six figures and three data files and can be found with this article online at https://doi.org/10.1016/j.cub.2018.03.050.

ACKNOWLEDGMENTS

We thank Michael Senkler for support with data evaluation and for developing and maintaining the GelMap and ComplexomeMap portals. We thank Claudia Probst for support in photo documentation of *V. album* in natural environment. This work was supported by Leibniz Universität Hannover and by the Deutsche Forschungsgemeinschaft (grant no. EU54/4-1 to H.E.).

AUTHOR CONTRIBUTIONS

J.S. established mitochondrial preparations from *V. album* leaves, performed protein analyses by 2D BN/SDS-PAGE and MS and data evaluation. N.R. contributed the complexome profiling dataset. H.E. performed data evaluation. J.H. performed electron microscopy analyses. H.P.B. initiated the project, performed data evaluation, and wrote the manuscript.

DECLARATION OF INTERESTS

The authors declare no competing interests.

Received: December 6, 2017
Revised: January 31, 2018
Accepted: March 21, 2018
Published: May 3, 2018

REFERENCES

1. Hatefi, Y. (1985). The mitochondrial electron transport and oxidative phosphorylation system. Annu. Rev. Biochem. *54*, 1015–1069.
2. Rich, P.R., and Maréchal, A. (2010). The mitochondrial respiratory chain. Essays Biochem. *47*, 1–23.
3. Wu, M., Gu, J., Guo, R., Huang, Y., and Yang, M. (2016). Structure of mammalian respiratory supercomplex $I_1III_2IV_1$. Cell *167*, 1598–1609.e10.
4. Letts, J.A., Fiedorczuk, K., and Sazanov, L.A. (2016). The architecture of respiratory supercomplexes. Nature *537*, 644–648.
5. Sousa, J.S., Mills, D.J., Vonck, J., and Kühlbrandt, W. (2016). Functional asymmetry and electron flow in the bovine respirasome. eLife *5*, e21290.
6. Milenkovic, D., Blaza, J.N., Larsson, N.G., and Hirst, J. (2017). The enigma of the respiratory chain supercomplex. Cell Metab. *25*, 765–776.
7. Raven, J.A., and Beardall, J. (2017). Consequences of the genotypic loss of mitochondrial complex I in dinoflagellates and of phenotypic regulation of complex I content in other photosynthetic organisms. J. Exp. Bot. *68*, 2683–2692.
8. Marcet-Houben, M., Marceddu, G., and Gabaldón, T. (2009). Phylogenomics of the oxidative phosphorylation in fungi reveals extensive gene duplication followed by functional divergence. BMC Evol. Biol. *9*, 295.
9. James, T.Y., Pelin, A., Bonen, L., Ahrendt, S., Sain, D., Corradi, N., and Stajich, J.E. (2013). Shared signatures of parasitism and phylogenomics unite Cryptomycota and microsporidia. Curr. Biol. *23*, 1548–1553.
10. Janouškovec, J., Gavelis, G.S., Burki, F., Dinh, D., Bachvaroff, T.R., Gornik, S.G., Bright, K.J., Imanian, B., Strom, S.L., Delwiche, C.F., et al. (2017). Major transitions in dinoflagellate evolution unveiled by phylotranscriptomics. Proc. Natl. Acad. Sci. USA *114*, E171–E180.
11. Flegontov, P., Michálek, J., Janouškovec, J., Lai, D.H., Jirků, M., Hajdušková, E., Tomčala, A., Otto, T.D., Keeling, P.J., Pain, A., et al. (2015). Divergent mitochondrial respiratory chains in phototrophic relatives of apicomplexan parasites. Mol. Biol. Evol. *32*, 1115–1131.
12. Vitols, E., and Linnane, A.W. (1961). Studies on the oxidative metabolism of Saccharomyces cerevisiae. II. Morphology and oxidative phosphorylation capacity of mitochondria and derived particles from baker's yeast. J. Biophys. Biochem. Cytol. *9*, 701–710.
13. Ohnishi, T., Kawaguchi, K., and Hagihara, B. (1966). Preparation and some properties of yeast mitochondria. J. Biol. Chem. *241*, 1797–1806.
14. Foury, F., Roganti, T., Lecrenier, N., and Purnelle, B. (1998). The complete sequence of the mitochondrial genome of Saccharomyces cerevisiae. FEBS Lett. *440*, 325–331.
15. Gabaldón, T., Rainey, D., and Huynen, M.A. (2005). Tracing the evolution of a large protein complex in the eukaryotes, NADH:ubiquinone oxidoreductase (Complex I). J. Mol. Biol. *348*, 857–870.
16. Millar, A.H., Whelan, J., Soole, K.L., and Day, D.A. (2011). Organization and regulation of mitochondrial respiration in plants. Annu. Rev. Plant Biol. *62*, 79–104.
17. Schertl, P., and Braun, H.P. (2014). Respiratory electron transfer pathways in plant mitochondria. Front. Plant Sci. *5*, 163.
18. Gutierres, S., Sabar, M., Lelandais, C., Chetrit, P., Diolez, P., Degand, H., Boutry, M., Vedel, F., de Kouchkovsky, Y., and De Paepe, R. (1997). Lack of mitochondrial and nuclear-encoded subunits of complex I and alteration of the respiratory chain in Nicotiana sylvestris mitochondrial deletion mutants. Proc. Natl. Acad. Sci. USA *94*, 3436–3441.
19. Yamada, K.T., and Newton, K.J. (1999). Heteroplasmy and homoplasmy for maize mitochondrial mutants: a rare case of homoplasmic nad4 deletion mutant plant. J. Hered. *90*, 369–373.
20. Remacle, C., Baurain, D., Cardol, P., and Matagne, R.F. (2001). Mutants of Chlamydomonas reinhardtii deficient in mitochondrial complex I: characterization of two mutations affecting the nd1 coding sequence. Genetics *158*, 1051–1060.
21. Kühn, K., Obata, T., Feher, K., Bock, R., Fernie, A.R., and Meyer, E.H. (2015). Complete mitochondrial complex I deficiency induces an up-regulation of respiratory fluxes that is abolished by traces of functional complex I. Plant Physiol. *168*, 1537–1549.
22. Fromm, S., Senkler, J., Eubel, H., Peterhänsel, C., and Braun, H.P. (2016). Life without complex I: proteome analyses of an Arabidopsis mutant lacking the mitochondrial NADH dehydrogenase complex. J. Exp. Bot. *67*, 3079–3093.
23. Skippington, E., Barkman, T.J., Rice, D.W., and Palmer, J.D. (2015). Miniaturized mitogenome of the parasitic plant Viscum scurruloideum is extremely divergent and dynamic and has lost all nad genes. Proc. Natl. Acad. Sci. USA *112*, E3515–E3524.
24. Petersen, G., Cuenca, A., Møller, I.M., and Seberg, O. (2015). Massive gene loss in mistletoe (Viscum, Viscaceae) mitochondria. Sci. Rep. *5*, 17588.
25. Skippington, E., Barkman, T.J., Rice, D.W., and Palmer, J.D. (2017). Comparative mitogenomics indicates respiratory competence in parasitic Viscum despite loss of complex I and extreme sequence divergence, and reveals horizontal gene transfer and remarkable variation in genome size. BMC Plant Biol. *17*, 49.
26. Braun, H.P., Binder, S., Brennicke, A., Eubel, H., Fernie, A.R., Finkemeier, I., Klodmann, J., König, A.C., Kühn, K., Meyer, E., et al. (2014). The life of plant mitochondrial complex I. Mitochondrion *19* (Pt B), 295–313.
27. Millar, A.H., Eubel, H., Jänsch, L., Kruft, V., Heazlewood, J.L., and Braun, H.P. (2004). Mitochondrial cytochrome c oxidase and succinate dehydrogenase complexes contain plant specific subunits. Plant Mol. Biol. *56*, 77–90.
28. Schikowsky, C., Senkler, J., and Braun, H.P. (2017). SDH6 and SDH7 contribute to anchoring succinate dehydrogenase to the inner mitochondrial membrane in *Arabidopsis thaliana*. Plant Physiol. *173*, 1094–1108.
29. Eubel, H., Heinemeyer, J., and Braun, H.P. (2004). Identification and characterization of respirasomes in potato mitochondria. Plant Physiol. *134*, 1450–1459.
30. Schägger, H., and Pfeiffer, K. (2000). Supercomplexes in the respiratory chains of yeast and mammalian mitochondria. EMBO J. *19*, 1777–1783.
31. Senkler, M., and Braun, H.P. (2012). Functional annotation of 2D protein maps: the GelMap portal. Front. Plant Sci. *3*, 87.
32. Heide, H., Bleier, L., Steger, M., Ackermann, J., Dröse, S., Schwamb, B., Zörnig, M., Reichert, A.S., Koch, I., Wittig, I., and Brandt, U. (2012). Complexome profiling identifies TMEM126B as a component of the mitochondrial complex I assembly complex. Cell Metab. *16*, 538–549.
33. Senkler, J., Senkler, M., Eubel, H., Hildebrandt, T., Lengwenus, C., Schertl, P., Schwarzländer, M., Wagner, S., Wittig, I., and Braun, H.P. (2017). The mitochondrial complexome of Arabidopsis thaliana. Plant J. *89*, 1079–1092.
34. Millar, A.H., Heazlewood, J.L., Kristensen, B.K., Braun, H.P., and Møller, I.M. (2005). The plant mitochondrial proteome. Trends Plant Sci. *10*, 36–43.
35. Paumard, P., Vaillier, J., Coulary, B., Schaeffer, J., Soubannier, V., Mueller, D.M., Brèthes, D., di Rago, J.P., and Velours, J. (2002). The ATP synthase is involved in generating mitochondrial cristae morphology. EMBO J. *21*, 221–230.
36. Aung, K., and Hu, J. (2011). The Arabidopsis tail-anchored protein PEROXISOMAL AND MITOCHONDRIAL DIVISION FACTOR1 is involved in the morphogenesis and proliferation of peroxisomes and mitochondria. Plant Cell *23*, 4446–4461.
37. Giese, H., Ackermann, J., Heide, H., Bleier, L., Dröse, S., Wittig, I., Brandt, U., and Koch, I. (2015). NOVA: a software to analyze complexome profiling data. Bioinformatics *31*, 440–441.
38. Hooper, C.M., Castleden, I.R., Tanz, S.K., Aryamanesh, N., and Millar, A.H. (2017). SUBA4: the interactive data analysis centre for Arabidopsis subcellular protein locations. Nucleic Acids Res. *45* (D1), D1064–D1074.

39. Tyanova, S., Temu, T., and Cox, J. (2016). The MaxQuant computational platform for mass spectrometry-based shotgun proteomics. Nat. Protoc. *11*, 2301–2319.

40. Reynolds, E.S. (1963). The use of lead citrate at high pH as an electron-opaque stain in electron microscopy. J. Cell Biol. *17*, 208–212.

41. Keech, O., Pierre Dizengremel, P., and Gardeström, P. (2005). Preparation of leaf mitochondria from Arabidopsis thaliana. Physiol. Plant. *124*, 403–409.

42. Werhahn, W., Niemeyer, A., Jänsch, L., Kruft, V., Schmitz, U.K., and Braun, H. (2001). Purification and characterization of the preprotein translocase of the outer mitochondrial membrane from Arabidopsis: identification of multiple forms of TOM20. Plant Physiol. *125*, 943–954.

43. Wittig, I., Braun, H.P., and Schägger, H. (2006). Blue native PAGE. Nat. Protoc. *1*, 418–428.

44. Neuhoff, V., Arold, N., Taube, D., and Ehrhardt, W. (1988). Improved staining of proteins in polyacrylamide gels including isoelectric focusing gels with clear background at nanogram sensitivity using Coomassie Brilliant Blue G-250 and R-250. Electrophoresis *9*, 255–262.

45. Schneider, C.A., Rasband, W.S., and Eliceiri, K.W. (2012). NIH Image to ImageJ: 25 years of image analysis. Nat. Methods *9*, 671–675.

46. Klodmann, J., Senkler, M., Rode, C., and Braun, H.P. (2011). Defining the protein complex proteome of plant mitochondria. Plant Physiol. *157*, 587–598.

47. Klodmann, J., Sunderhaus, S., Nimtz, M., Jänsch, L., and Braun, H.P. (2010). Internal architecture of mitochondrial complex I from Arabidopsis thaliana. Plant Cell *22*, 797–810.

48. Schwanhäusser, B., Busse, D., Li, N., Dittmar, G., Schuchhardt, J., Wolf, J., Chen, W., and Selbach, M. (2011). Global quantification of mammalian gene expression control. Nature *473*, 337–342.

STAR★METHODS

KEY RESOURCES TABLE

REAGENT or RESOURCE	SOURCE	IDENTIFIER
Chemicals, Peptides, and Recombinant Proteins		
Sequencing Grade Modified Trypsin	Promega, Madison (WI), USA	V5111
Deposited Data		
Lable free proteomic mass spectrometry data (complexome profiling)	this paper; ComplexomeMap; PRIDE	Table S3; https://www.complexomemap.de/va; PRIDE (https://www.ebi.ac.uk/pride/archive/) Project accession: PXD008974
Gel based proteomic mass spectrometry data (GelMap)	this paper; GelMap; Mendeley Data	Table S1; https://www.gelmap.de/1327; Mendeley link: http://dx.doi.org/10.17632/vwj4gnc5h3.1
Experimental Models: Cell Lines		
Arabidopsis thaliana Columbia 0 wild-type Suspension cell callus culture	this paper	N/A
Experimental Models: Organisms/Strains		
Viscum album	Herrenhausen Gardens, Hannover, Germany	N/A
Arabidopsis thaliana wild-type Columbia 0	this paper, NASC	N1092
Viscum album leaves	this paper	N/A
Software and Algorithms		
NOVA v0.5.7	[37]	http://www.bioinformatik.uni-frankfurt.de/tools/nova/index.php?go=overview
SUBA	[38]	http://suba.live/
MaxQuant version 1.6.0.1	[39]	http://www.biochem.mpg.de/5111795/maxquant
GelMap	[31]	https://www.gelmap.de
ComplexomeMap	N/A	https://www.complexomemap.de

CONTACT FOR REAGENT AND RESOURCE SHARING

Further information and requests for resources and reagents should be directed to and will be fulfilled by the Lead Contact, Hans-Peter Braun (braun@genetik.uni-hannover.de).

EXPERIMENTAL MODEL AND SUBJECT DETAILS

Mistletoes (*Viscum album*; also called European mistletoe) were taken from maple trees in a local garden (The Herrenhausen Gardens in Hannover/Germany, https://www.hannover.de/Herrenhausen/Herrenhäuser-Gärten) in July 2017. Wild-type *Arabidopsis* cells (Columbia 0) were cultivated in 500 mL Erlenmeyer flasks at 24°C and continuous movement (shaker, 100 rpm). The flasks initially contained 1.5 g *Arabidopsis* cells in 100 mL medium (3% (w/v) sucrose, 0.01% (w/v) 2,4-D, 0.001% (w/v) kinetin, 0.316% (w/v) Gamborg B5 medium). *Arabidopsis* cells were transferred into fresh medium weekly.

METHOD DETAILS

Transmission Electron Microscopy

A fresh *Viscum album* leaf was cut into 1 mm pieces and fixed in 150 mM HEPES, pH 7.35, containing 1.5% formaldehyde and 1.5% glutaraldehyde. After washing in water, samples were incubated 2 hr in an aqueous solution of 1% OsO_4 containing 1.5% hexacyanoferrat II, washed in water and stored in 1% aqueous uranyl acetate overnight. After washing in water and dehydration in acetone, samples were embedded in Low Viscosity Resin (Agar Scientific, Essex, UK). 60 nm ultrathin sections were mounted on formvar-coated copper grids, poststained with uranyl acetate and lead citrate [40] and observed in a Morgagni TEM (FEI). Images were taken with a side mounted Veleta CCD camera.

Mitochondria isolations

Leaves from *Viscum album* (200 g) were used as starting material for mitochondria isolations. All following steps were carried out at 4°C. Homogenization of leaves was performed in grinding buffer (0.3 M sucrose, 60 mM TES, 2 mM EDTA, 10 mM KH_2PO_4, 25 mM tetrasodium pyrophosphate, 1 mM glycine, 1% (w/v) polyvinylpyrrolidone-40, 1% BSA, 50 mM sodium ascorbate, 20 mM cysteine, pH 8.0 [KOH]) using a Waring blender (three homogenization pulses of 7 s, in between 60 s breaks, respectively). The homogenate was filtered through a single layer of Miracloth. Remaining leaf material was ground a second time in grinding buffer (see above) using mortar, pistil and quartz sand for 10 min. The second homogenate was also filtered through a single layer of Miracloth. Suspensions of the first and second homogenizations were combined. The isolation of *Viscum album* mitochondria followed a method for preparing mitochondria from *Arabidopsis* leaves ([41], Method B) with modifications: The *Viscum album* leaf suspension was centrifuged twice at 2,500 g and 4°C for 5 min (the pellets were discarded, respectively) and afterward centrifuged once at 15,000 g at 4°C for 15 min for pelletizing the mitochondria. After all centrifugation steps, whitish-viscous aggregates visible in the suspensions were removed using a Pasteur pipette. The final pellet was resuspended in 12 mL wash buffer (0.3 M sucrose, 10 mM TES, 10 mM KH_2PO_4, pH 7.5 [KOH]), homogenized by two gentle strokes in a 15 mL Dounce Homogenizator, and finally distributed onto 12 Percoll gradients (prepared with gradient buffer: 0.6 M sucrose, 20 mM TES, 2 mM EDTA, 20 mM KH_2PO_4, 2 mM glycine, pH 7.5 [KOH]; method according to [40]; each gradient had a volume of 19 mL; Percoll to buffer ratio was 1 to 3). Percoll gradient centrifugation was carried out at 10,000 g and 4°C for 30 min with minimal acceleration and deceleration speeds. As a result, chloroplasts form a band in the upper half of gradients whereas mitochondria constitute a faint white-brownish band below. The chloroplast and mitochondrial bands were carefully removed. Further washing steps (at least three) were performed in wash buffer at 17,200 g for 20 min as described in [41]. Purified mitochondria and chloroplasts were resuspended in wash buffer (final protein concentration: 10 μg/μL) and divided into aliquots à 100 μL. Aliquots were either directly used for bioanalytical investigations or shock frozen by liquid nitrogen and stored at −80°C.

Mitochondria from *Arabidopsis thaliana* cell culture were isolated as described previously [42]. All steps were performed at 4°C or on ice. Suspension cell cultures were harvested through a sieve. Cells were suspended in disruption buffer (450 mM sucrose, 15 mM MOPS, 1.5 mM EGTA, 60% (w/v) PVP40, pH 7.4; added directly before use: 20% (w/v) BSA, 10 mM sodium ascorbate, 10 mM cysteine, 0.2 mM PMSF), with a concentration of 2 mL / g fresh weight and mixed in a waring blender (1x 15 s at high speed, 2x 15 s at medium speed, 30 s break in between). The homogenized cells were then centrifuged at 2,700 g for 5 min and the supernatant was centrifuged a second time (same conditions). The supernatant was then centrifuged at 8,300 g for 5 min and the resulting supernatant was used for mitochondria pelleting (17,000 g for 10 min). Mitochondria were suspended in washing buffer (0.3 M sucrose, 10 mM MOPS, 1 mM EGTA, pH 7.2) (volume depends on capacity of ultracentrifugation tubes) and carefully treated with two strokes in a Teflon homogenizer. The suspension was loaded onto discontinuous percoll gradients (18%, 23% and 40% percoll in gradient buffer (0.3 M sucrose, 10 mM MOPS, pH 7.2)) for ultracentrifugation (70,000 g for 90 min). After centrifugation, mitochondria can be removed from the 23% - 40% interphase with a Pasteur pipette. To remove percoll, the mitochondria were washed at least two times in resuspension buffer (0.4 M mannitol, 1 mM EGTA, 10 mM tricine, pH 7.2) (centrifugation at 14,500 g for 10 min). Finally, mitochondria were suspended in resuspension buffer at a concentration of 0.1 g/mL fresh weight and either directly used for gel electrophoresis or frozen at −80°C in aliquots of 100 μL.

Gel electrophoresis procedures

Protein complexes of *Viscum album* and *Arabidopsis thaliana* mitochondria were analyzed by 1D Blue native (BN) polyacrylamide gelelectrophoresis (PAGE). For this, a gradient gel (16 × 16 × 0.15 cm) was poured using a gradient mixer MX40 with 2 chambers filled with the following solutions: Front chamber: 4.5% (v/v) acrylamide in gel buffer BN (250 mM ACA, 25 mM Bis-Tris, pH 7.0); back chamber: 16% (v/v) acrylamide, 19% (v/v) glycerol in gel buffer BN. After polymerization of the gradient gel, a sample gel (gel buffer BN, 4% acryl amide) was poured on top (leading to a total gel size of 19 × 16 × 0.15 cm) using a comp for ten sample pockets. Wash buffer was removed from mitochondrial/chloroplast samples by centrifugation and proteins were dissolved from organelles using solubilization buffer (30 mM HEPES, 150 mM potassium acetate, 10% glycerol, 5% digitonin, pH 7.4) using 100 μL per 10 μg mitochondrial protein. After 10 min incubation on ice, membrane aggregates and other insoluble materials were removed by centrifugation for 10 min at 18,300 g. Afterward, Coomassie blue was added to the sample to a final concentration of 1% (w/v). The Blue native PAGE was run using the following buffers: Anode buffer: 50 mM Bis-Tris pH 7.0; Cathode buffer: 50 mM Tricine, 15 mM Bis-Tris, 0.02% Coomassie, pH 7.0. Electrophoresis was carried out in two steps: i) maximum 100 V (current was set to 15 mA) for 45 min, ii) maximum 15 mA (voltage was set to 500 V) for 11 hr. The gel was either fixed and Coomassie-colloidal stained (fixing: 15% ethanol, 10% acetic acid, incubation for 2 hr, staining: 5% (w/v) Coomassie in 2% (w/v) ortho phosphoric acid, 10% (w/v) ammonia sulfate, incubation overnight) or used for a second dimension SDS-PAGE.

For the generation of GelMaps (see below), subunits of protein complexes were resolved by a second dimension SDS-PAGE. For this, a gel lane from the Blue-Native gel was cut out and incubated for 30 min in 1% SDS / 1% beta mercaptoethanol. Afterward the lane was washed for 30 s in water. The gel was positioned between two glass plates using 1mm spacer. Separation gel (16% (v/v) acrylamide, 12% (v/v) glycerol in gel buffer SDS (1 M Tris, 0.1% SDS, pH 8.45)) and spacer gel (10% (v/v) acrylamide in gel buffer SDS) were poured directly after each other between the plates and a thin layer of overlay solution (1 M Tris, 0.1% SDS, pH 8.45) was poured on top for producing a straight gel surface. After polymerization, the sample gel (10% (v/v) acrylamide, 10% (v/v) glycerol, 0.1% (w/v) SDS in gel buffer BN) was poured between the Blue-Native gel stripe and the SDS gel. Finally, the gel (19 × 16 × 0.1 cm) was inserted to the chamber, anode buffer (0.2 M Tris, pH 8.9) and cathode buffer (0.1 M Tris, 0.1 M Tricine, 0.1% SDS pH 8.45) were added and

the gel electrophoresis was run at 30 mA (voltage maximum: 500V) for approximately 18 hr and stopped when the blue running front entered the anode buffer.

Protocols for 1D Blue native and 2D Blue native / SDS-PAGE were taken from [43]. Protein complexes and proteins separated on the 1D and 2D gels were made visible by Coomassie colloidal staining (see above) as described in [44]. Quantifications of proteins on gels were performed by densitometric analyses using the ImageJ software tool [45].

Generation of a GelMap

For the generation of a GelMap for *Viscum album* mitochondria, protein spots from a two-dimensional Blue native / SDS gel were picked using a manual spot picker (GelPal, Genetix, diameter 1.4 mm). Proteins included in the spots were carbamidomethylated by consecutive incubation with first 20 mM dithiothreitol (30 min, 56°C) and second 55 mM iodoacetamide (30 min in the dark). After washing in 0.1M ammonium hydrogen carbonate for 15 min, in-gel digestion was carried out over night at 37°C using a prepared trypsin solution (stock solution diluted 1:10 in water; preparation of stock solution: a vial trypsin powder (Promega) was resolved in 100 μL supplied resuspension buffer (Promega) and incubated for 15 min at 30°C; afterward, 900 μL 0.1 M ammonium hydrogen carbonate were added and mixed, stored at −20°C). Between each step, gel pieces were dehydrated with 100% acetonitrile. For extraction of peptides, a 1:1 mix of water and acetonitrile was used, first with 5% formic acid, then twice with 1% formic acid. All extracts were combined and dried. For mass spectrometry (MS) analyses each sample was resuspended in 22 μL sample solution (2% acetonitrile, 0.1% formic acid in water) for 30 min at 37°C. 20μL were transferred into a 96-well plate used as sample table for nano liquid chromatography (nLC). Online nLC – ESI Q ToF (Electrospray Quadrupole Time of Flight) tandem MS analyses were carried out with an Easy nano LC (Thermo scientific) and a micrOTOF Q II (Bruker Daltonics) as described previously [46]. From each sample, 15 μL were transferred to the nLC system, included peptides were first bound onto a precolumn (Thermo Scientific, Proxeon, length = 2 cm, i.d. = 100 mm; ReproSil-Pur C18-AQ, 5 mm, 120 Å) and additionally separated via an analytical column (length = 10 cm, i.d. = 75 mm; ReproSil-Pur C18-AQ, 3 mm, 120 Å) using an acetonitrile gradient. For this, solution A (0.1% formic acid in water) and solution B (0.1% formic acid in acetonitrile) were mixed with varying ratios over the time of one LC run: First, 5% B were applied and continuously increased for 10 min until 50% B. After 3 min 50% B it was further increased for 20 min until 95% B and finally reduced within 1 min to 5% B, keeping this for column re-equilibration for again 2 min. For tandem MS, automatic intensity based MS/MS fragmentation of the three most intense peptides and a minimum intensity of 3,000 counts (precursor scan) was applied, with an exclusion of a peptide after 5 fragmentations. For data processing, the DataAnalysis software (Bruker Daltonics) was used. Data evaluation and annotation was carried out with ProteinScape (Bruker Daltonics), using an in-house Mascot server (http://www.matrixscience.com/) for database search.

Three protein databases were used for data evaluation: (i) The *TAIR10* protein database (https://www.arabidopsis.org/), (ii) a self-made database including the mitochondrially encoded proteins of Viscum [25] as well as all other protein accessions of the Viscaceae family available at NCBI (https://www.ncbi.nlm.nih.gov/; downloaded on Sep. 1st, 2017) and (iii) the UniProt all plants database (http://www.uniprot.org/; downloaded on Sep. 1st, 2017). The GelMap was created at https://gelmap.de/ following the online instructions.

Generation of a ComplexomeMap

Complexome analysis was performed following a modified version of a protocol published recently [33].

Sample preparation and liquid-chromatography

A 1D BN gel lane including separated mitochondrial protein complexes of *Viscum album* was cut horizontally into 54 slices of about 10 mm in widths and 3 mm height. Gel slices were then further processed for MS analysis by tryptic *in-gel* digestion and peptide extraction as described in [47]. Peptide extracts were taken up in 20 μL sample buffer (5% [v/v] acetonitrile 0.1% [v/v] trifluoroacetic acid) and transferred to liquid-chromatography (LC)-MS/MS analysis. For LC, an Ultimate 3000 UPLC (Thermo Fisher Scientific, Dreieich, Germany) was used. 5 μL of each sample were loaded onto a C18 reverse phase trapping column, length 2 cm, ID 75 μm, particle diameter 3 μm, pore size 100 Å (Acclaim PepMap100, Thermo Fisher Scientific, Dreieich, Germany). Subsequently, peptides were separated on a C18 reverse phase analytical column, length 50 cm, ID 75 μm, particle diameter 3 μm, pore size 100 Å (Acclaim PepMap100, Thermo Fisher Scientific, Dreieich, Germany) applying a non-linear 5% [v/v] to 30% [v/v] acetonitrile (ACN) gradient in 0.1% [v/v] formic acid at a column oven temperature of 33°C over a period of 70 min and a flow rate of 5 μL min^{-1}. Finally, the ACN concentration was increased up to 95% [v/v] within 10 min and kept for another 10 min to clean the column. Column equilibration was performed at 5% [v/v] ACN for 10 min.

Mass spectrometry

Eluting peptides were directly transferred to a Nano-Spray-Ionization (NSI) source using stainless steel nano-pore emitters of an Orbitrap Q-Exactive mass spectrometer (Thermo Fisher Scientific, Dreieich, Germany). Spray voltage was set to 2.2 kV, capillary temperature to 275°C and S-lens RF level to 50%. MS/MS spectra (top 10) were recorded from 20 to 80 min with the MS running in positive mode. For full MS scans, the number of microscans was set to 1, resolution to 70000, AGC target to $1e^6$, maximum injection time to 400 ms, number of scan ranges to 1, scan range to 400 to 1600 m/z and the spectrum data type to "Profile." For dd-MS2, the number of microscans was set to 1, resolution to 17500, AGC target to $1e^5$, maximum injection time to 250 ms, loop count to 10, MSX count to 1, isolation window to 3.0 m/z, fixed first mass to 100.0 m/z, NCE to 27 (stepped NCE deactivated) and the spectrum data type to "Profile." The data dependent (dd) settings were set to: Intensity threshold, $4.2e^3$; apex trigger, 10 to 60 s; charge exclusion, unassigned, 1, 5-8, >8; peptide match, preferred; exclude isotypes, on; dynamic exclusion 45.0 s.

QUANTIFICATION AND STATISTICAL ANALYSIS

Data processing and heatmap generation for complexome profiling

MS raw files generated by Xcalibur (Thermo Fisher Scientific, Dreieich, Germany) were evaluated via MaxQuant version 1.6.0.1 [39]. Peptide spectra were queried against the TAIR10 *Arabidopsis* protein database (https://www.arabidopsis.org/) and a set of Viscaceae protein sequences taken from NCBI (see above). Group-specific parameters were set to: Digestions mode, Specific; Enzyme, Trypsin/P; Maximum missed cleavage sides, 2; Variable modifications, Oxidation (M), Acetyl (Protein N-term); Maximum number of modifications per peptide, 5. For global parameters, Carbamidomethyl (C) was set as fixed modification, minimal peptide length was set to 7 and the maximum peptide mass [Da] to 4600. For protein identification, PSM and protein false discovery rates (FDR) were set to 5% for queries against the *Arabidopsis* database, and to 1% for queries against the Viscaceae sequences. Minimum number of peptides, razor peptides and unique peptides for protein group identification were left at the default value of 1. To accurately quantify proteins within fractions for complexome profiling, calculation of intensity based absolute quantification (iBAQ [48]) was activated. The remaining settings were left at the default values.

Complexome profiling and ComplexomeMap generation

Complexome profiling was performed using the NOVA software (Version 0.5.7 [37]) using the iBAQ values from the "proteinGroups" output file generated by MaxQuant. Values were normalized via "maximum normalization" for hierarchical clustering which was performed via the Pearson Correlation distance function and UPGMA (Unweighted Pair Group Method with Arithmetical Mean) average linkage. The *Viscum album* ComplexomeMap was created at https://complexomemap.de/ [35].

DATA AND SOFTWARE AVAILABILITY

For quantitative proteomic raw data (complexome profiling) please visit the PRIDE website (https://www.ebi.ac.uk/pride, Project accession: PXD008974). For gel-based proteomic raw data (GelMap) please visit Mendeley Data (https://data.mendeley.com/) at http://dx.doi.org/10.17632/vwj4gnc5h3.1. For GelMap data, please visit https://www.gelmap.de/1327. For ComplexomeMap data, please visit https://www.complexomemap.de/va.

ADDITIONAL RESOURCES

For subcellular localization of proteins identified in the TAIR10 *Arabidopsis* protein database, Accession numbers were searched in the SUBA database (subcellular localization database for *Arabidopsis* proteins) (http://www.suba.live/). The consensus location (SubaCon) integrating all information available for the location of a subunit present in the database was chosen for assignment.

Current Biology, Volume *28*

Supplemental Information

Absence of Complex I Implicates Rearrangement of the Respiratory Chain in European Mistletoe

Jennifer Senkler, Nils Rugen, Holger Eubel, Jan Hegermann, and Hans-Peter Braun

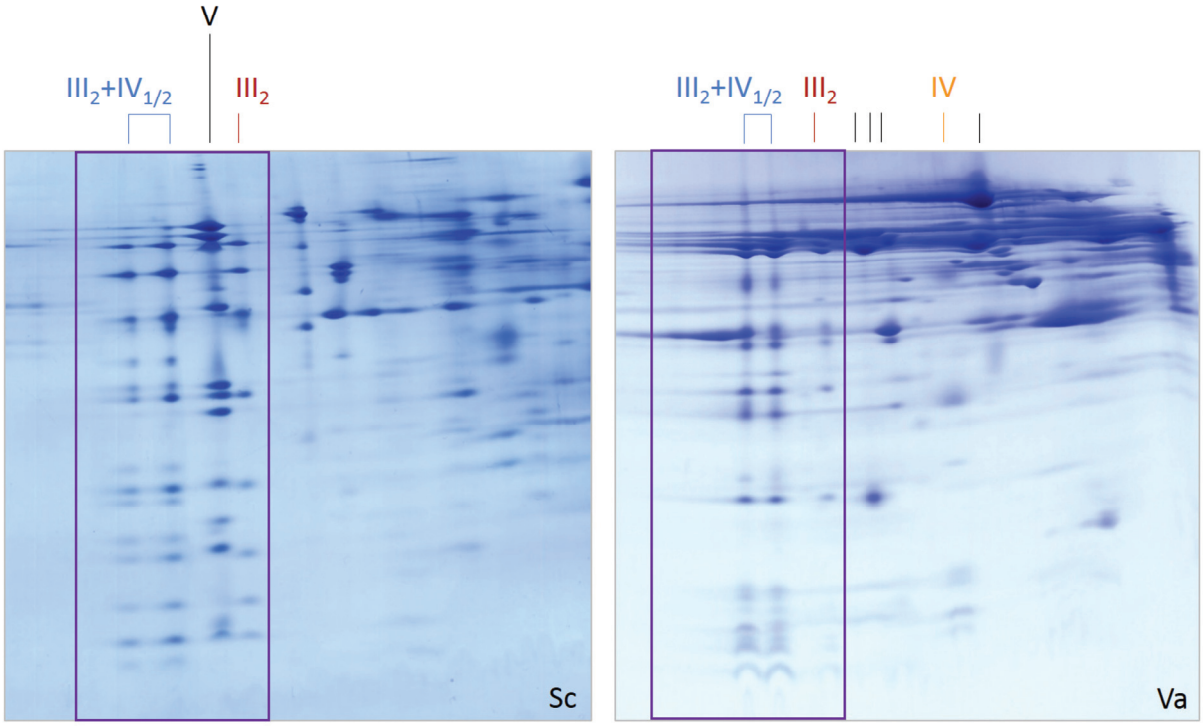

Figure S1: Two-dimensional analyses of mitochondrial protein complexes from *Saccharomyces cerevisiae* (Sc) and *Viscum album* (Va) by 2D Blue native / SDS PAGE (related to Figure 3). The 2D gels were Coomassie-stained. Identities of protein complexes are given above the 2D gels. Designations: III_2: dimeric complex III (red), IV: complex IV (orange), $III_2+IV_{1/2}$: supercomplexes composed of dimeric complex III and either one or two copies of monomeric complex IV (blue), V: complex V (black). The 2D gel for *Saccharomyces cerevisiae* is taken from [S1].

Mitochondria from yeast and from *Viscum album* both contain abundant III+IV supercomplexes. A small proportion of complexes III and IV is not involved in the formation of supercomplexes in *V. album*. This also is the case for complex III in yeast. However, complex IV from yeast seems to occur only in supercomplex-bound form. The ATP synthase complex is of high abundance in yeast under the conditions applied. In contrast, ATP synthase is not visible on the 2D gel for *V. album* (but detectable by more sensitive procedures like complexome profiling, Figure 5).

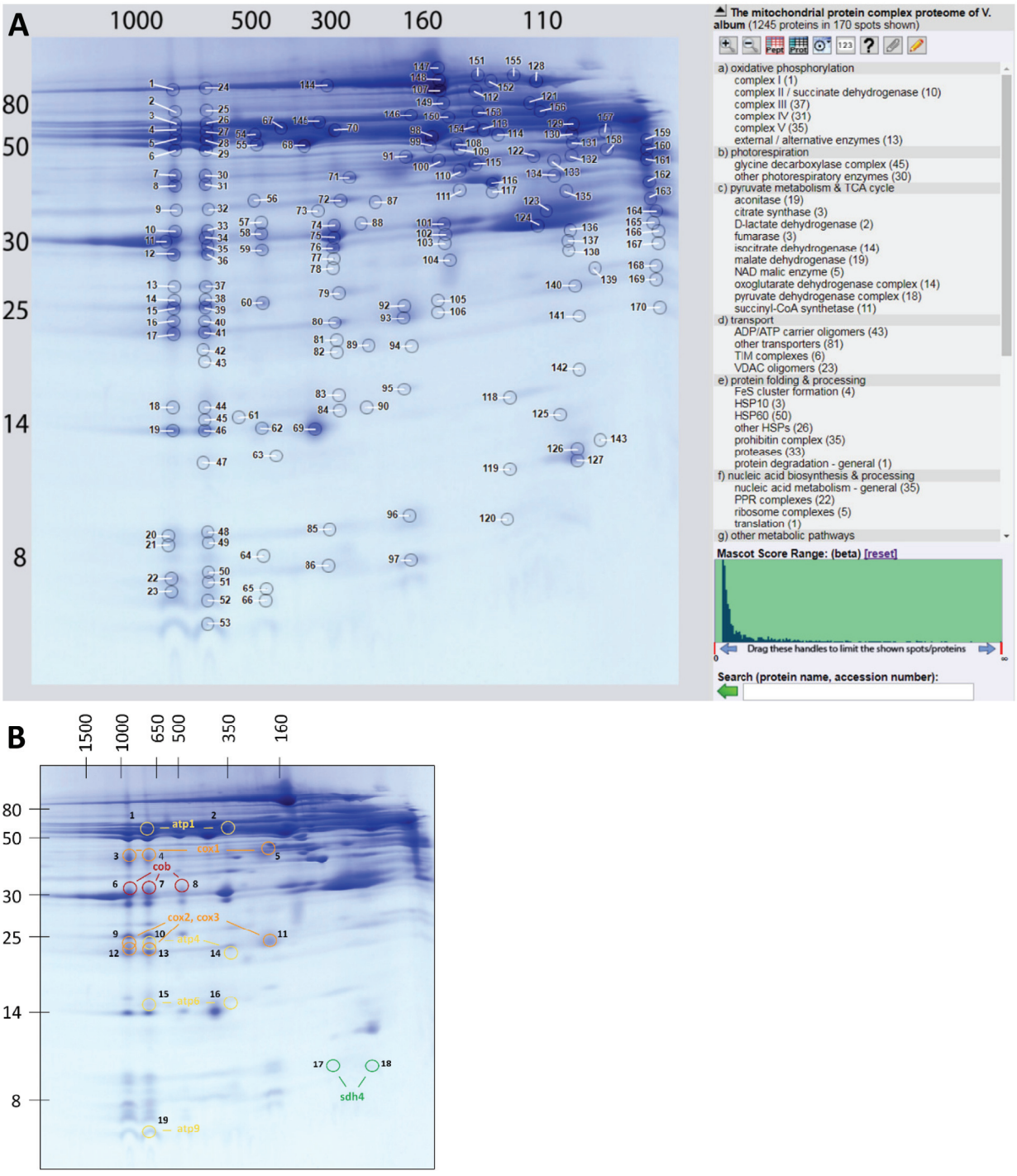

Figure S2: Protein complexes in *Viscum album* mitochondria (related to Figure 4).
A: Screenshot of the GelMap for *Viscum album* mitochondria at the GelMap-platform (gelmap.de/1327). Mitochondrial proteins of *Viscum album* were separated by 2D Blue native / SDS PAGE and identified by MS. The masses of standard proteins (and complexes) are given above and to the left of the 2D gel (in kDa). Data were evaluated using the TAIR10 database (https://www.arabidopsis.org/). On the GelMap website, all encircled spots can be clicked to access functional as well as MS data. Protein-related MS data also can be accessed by clicking functional categories in the menu to the right. MS results for all analyzed protein spots (1-170) are also presented in Table S1. Detailed information on the usage of the GelMap portal is provided at https://www.gelmp.de/howto. **B:** Identified mitochondrial proteins of *Viscum album*. Mitochondrial proteins were separated by 2D Blue native / SDS PAGE and identified by MS. The masses of standard proteins (and complexes) are given above and to the left of the 2D gel (in kDa). Data were evaluated using sequences of mitochondrial encoded proteins from Viscum species available at NCBI (https://www.ncbi.nlm.nih.gov/) (cob: cytochrome b subunit of complex III, cox I, II, III: subunits 1, 2 and 3 of complex IV, atp1, 4, 6, 9: subunits α, b, ATP6 and ATP9 of complex V, sdh4: subunit 4 of complex II). For primary MS data see Table S2.

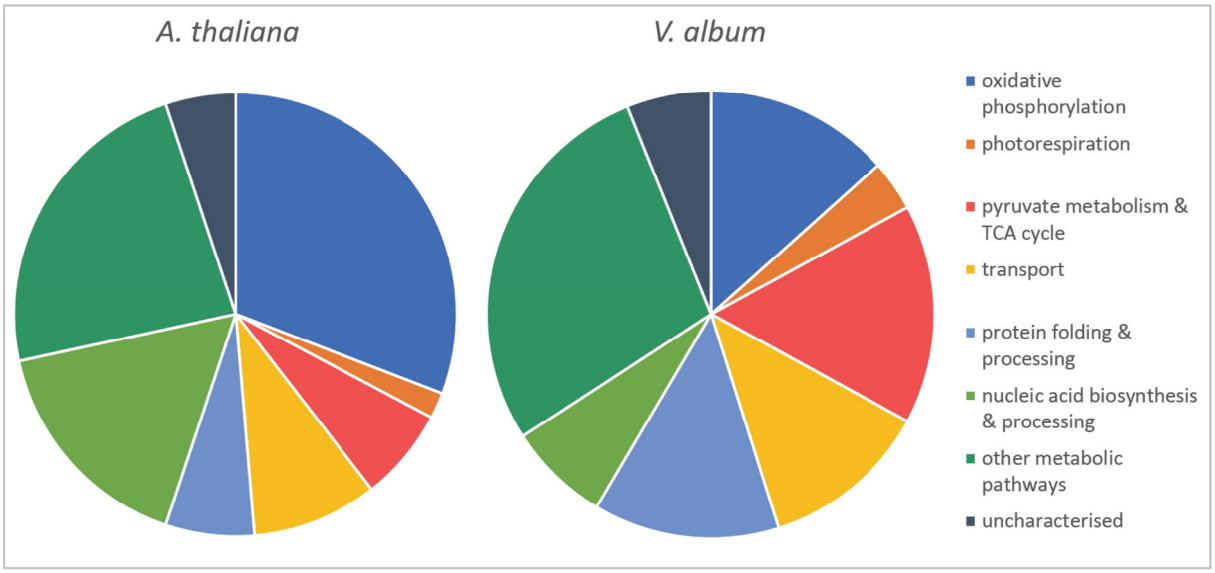

Figure S3: Composition of the mitochondrial proteomes in Arabidopsis and *V. album* (related to Figure 4; Table S1). The data are based on the GelMap projects for *V. album* (this study) and *A. thaliana* [S2]. For both projects, mitochondrial proteins were separated by 2D BN / SDS PAGE; gels were Coomassie-stained; all visible protein spots were analyzed by MS and results were evaluated using the Arabidopsis protein database at TAIR (https://www.arabidopsis.org/). Identified proteins were assigned to subcellular compartments in accordance with SUBA (http://suba.live/). Finally, all mitochondrially-localized proteins were assigned to eight functional categories for both species. The pie charts indicate the magnitude of the categories within the mitochondrial proteomes of Arabidopsis and *V. album*.

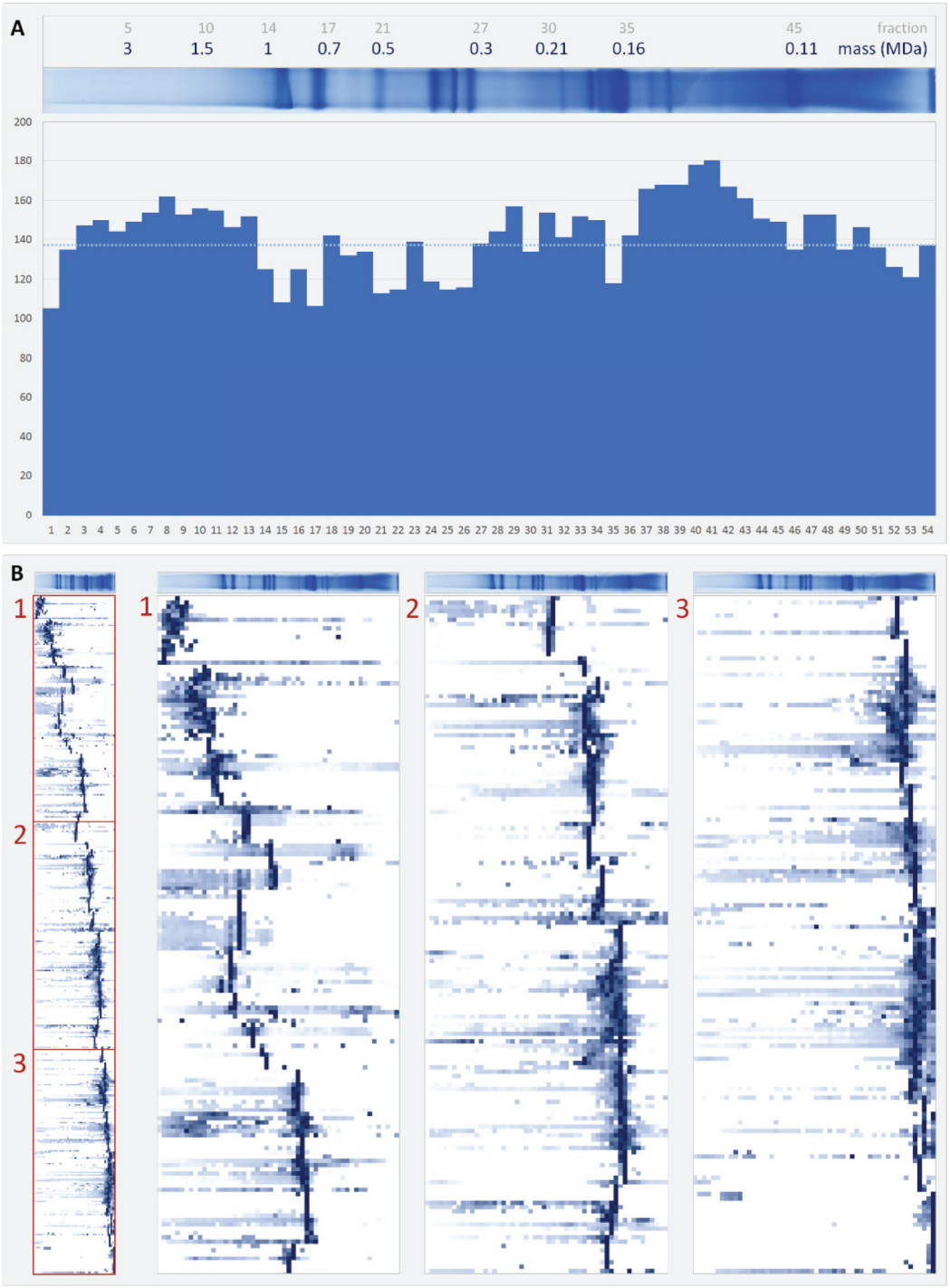

Figure S4: Complexome Map details (related to Figure 5, Table S3). A: Number of proteins (y-axis) per complexome fraction (x-axis). The *Viscum album* BN gel used for complexome profiling (Figure 5A) is shown above the diagram (fractions fit to fraction numbers on the x-axis), molecular masses are given in MDa. **B.** ComplexomeMap of *Viscum album* mitochondria. A mitochondrial fraction from *Viscum album* was separated by Blue native PAGE (Figure 5A). The gel stripe was cut into 54 fractions. All fractions were analyzed by quantitative label-free shot-gun proteomics. The heatmap displays the normalized (max) intensity profiles of all identified proteins along the 1D BN gel stripe. Profiles are aligned according to similarity by hierarchical clustering using the NOVA software (http://www.bioinformatik.uni-frankfurt.de/tools/nova/). Left: overview of the entire heat map. The map consists of 54 columns corresponding to the 54 gel slices (left: fraction of largest molecular mass, right: fraction of lowest molecular mass) and 477 lines corresponding to the 477 identified unique proteins. For better visibility, the heat map is split into three sections displayed to the right of the overview map. The original BN gel is shown on top of all three sections. The map can be accessed in full detail at https://complexomemap.de/Va.

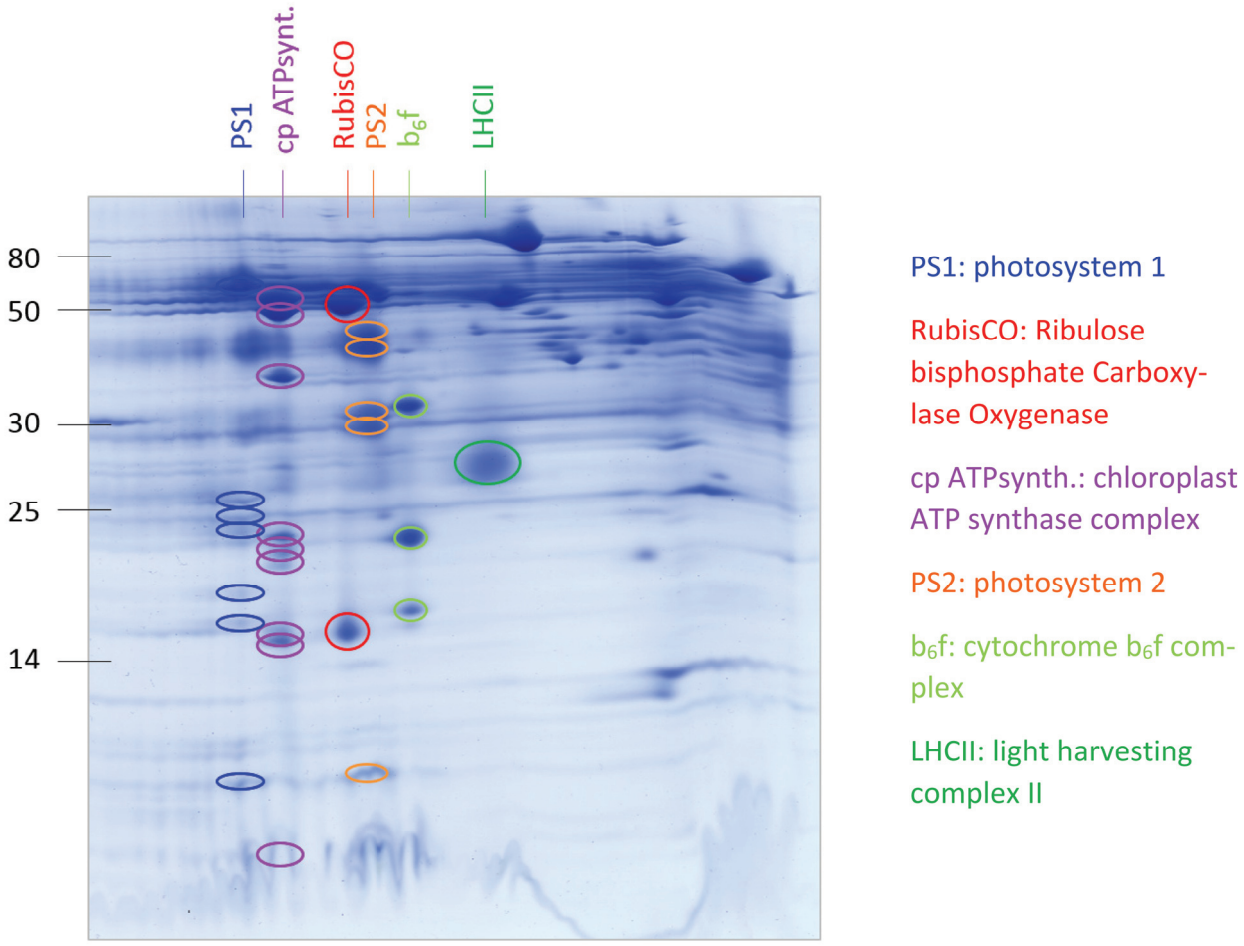

Figure S5: 2D analysis of chloroplast protein complexes from *Viscum album* by Blue native / SDS PAGE (related to Figure 6). Molecular masses (in kDa) of standard proteins are given to the left of the 2D gel. Protein complexes were identified based on their subunit compositions (see [S3] for comparison) and by MS analyses (data not shown).

In contrast to the mitochondrial compartment, 2D BN / SDS PAGE analysis of *V. album* chloroplasts did not reveal any absence or sharp reduction of any of the major chloroplast protein complexes in comparison to the chloroplasts of other plants. The chloroplast ATP synthase complex is of high abundance in *Viscum album*.

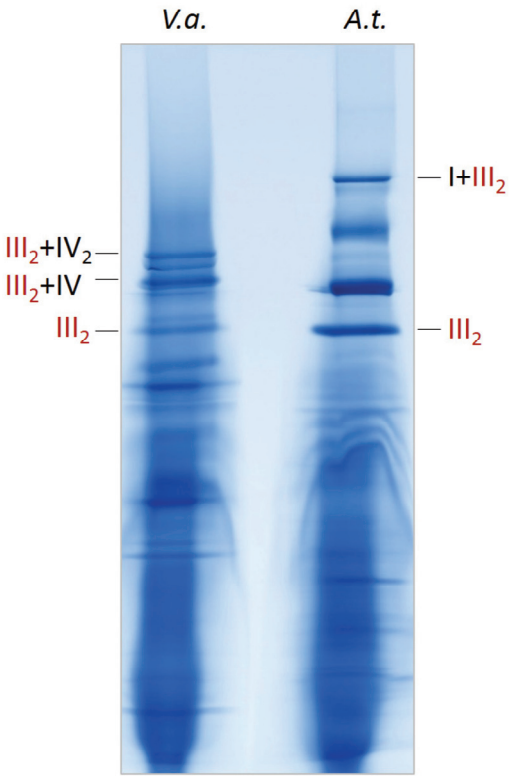

Complex	*A. thaliana*	*V. album*
I	100 %	0 %
II	100 %	<10 %
III	100 %	33 %
IV	100 %	33 %
V	100 %	<10 %

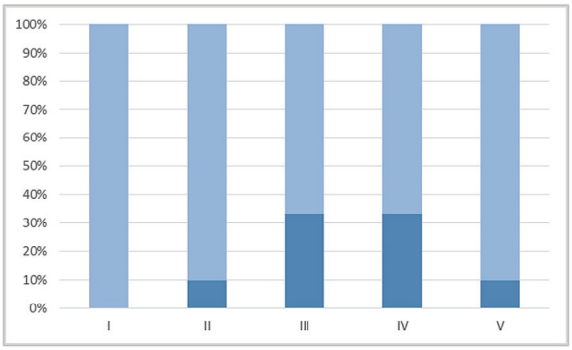

Figure S6: Comparison of protein complex quantities in *Arabidopsis thaliana* (*A.t.*) and *Viscum album* (*V.a.*) (related to Figure 6). Equal amounts of mitochondrial protein fractions from Arabidopsis and *V. album* were separated by Blue native PAGE. Gels were Coomassie-stained. Volumes of complex III-containing bands were determined by densitometric analyses using the ImageJ software tool [S4]. Quantity of complex III in *Viscum album* is given in relation to its quantity in Arabidopsis. Quantity relations for the other OXPHOS complexes are estimated (see discussion).

SUPPLEMENTAL REFERENCES

S1 Heinemeyer, J., Braun, H.P., Boekema, E.J., and Kuril, R. A. (2007). Structural model of the cytochrome c reductase / oxidase supercomplex from yeast mitochondria. J. Biol. Chem. 282, 12240-12248.

S2 Klodmann, J., Senkler, M., Rode, C. and Braun, H.P. (2011) The protein complex proteome of plant mitochondria. Plant Physiol. 157, 587-598.

S3 Heinemeyer, J., Eubel, H., Wehmhöner, D., Jänsch, L. and Braun, H.P. (2004) Proteomic approach to characterize the supramolecular organization of photosystems in higher plants. Phytochemistry 65, 1683-1692.

S4 Schneider, C.A., Rasband, W.S., and Eliceiri, K.W. (2012). NIH Image to ImageJ: 25 years of image analysis. Nat. Methods 9, 671–675.

Publication 3

2.3 Complexome Profiling Reveals Association of PPR Proteins with Ribosomes in the Mitochondria of Plants

Nils Rugen‡, Henryk Straube‡, Linda E. Franken§¶, Hans-Peter Braun‡, and Holger Eubel‡¶

‡Leibniz Universität Hannover, Institute of Plant Genetics, Herrenhäuser Str. 2, 30419 Hannover, Germany

§Heinrich Pette Institute, Leibniz Institute for Experimental Virology - Centre for Structural Systems Biology, Notkestraße 85, 22607 Hamburg, Germany

Type of authorship:	First author
Type of article:	Research article
Share of the work:	70%
Contribution to the publication:	Performed experiments, analyzed data, prepared figures, assisted in writing the manuscript
Journal:	Molecular and Cellular Proteomics
Impact factor (2018)	4.82
Number of citations (Web of Science):	0
Date of Publication:	July 01, 2019
DOI:	10.1074/mcp.RA119.001396

* Note that the supplementary files for chapter 2.3 are not included in the printed version of this dissertation (but included on the accompanied compact disc).

Complexome Profiling Reveals Association of PPR Proteins with Ribosomes in the Mitochondria of Plants

Authors
Nils Rugen, Henryk Straube, Linda E. Franken, Hans-Peter Braun, and Holger Eubel

Correspondence
heubel@genetik.uni-hannover.de

In Brief
Plant mitochondrial protein expression is complex and routinely involves pentatricopeptide repeat proteins for processing of transcripts. Although the composition and structure of the mitoribosomes in other eukaryotic kingdoms of life is well established, plant mitochondria have so far eluded a detailed analysis. Using a complexome profiling approach, this study provides an early glimpse on the composition of plant mitochondrial ribosomes and sheds new light on the process of mitochondrial gene expression in plants. Mitochondrial subunits were found to possess several additional proteins carrying pentatricopeptide repeats potentially involved in RNA editing. Other proteins are potentially involved in the processing of nascent proteins.

Graphical Abstract

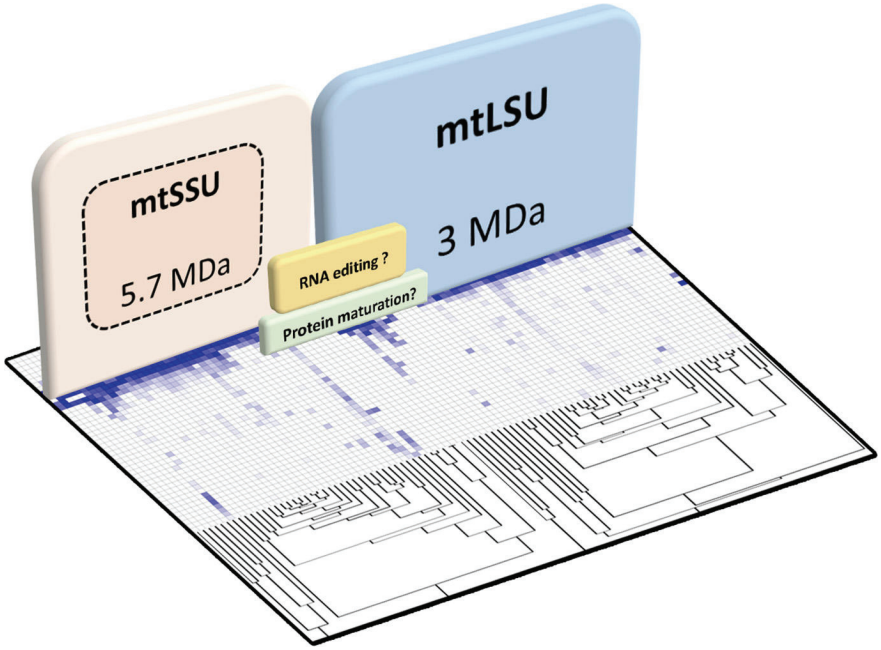

Highlights

- Plant mitoribosomes contain several pentatricopeptide repeat proteins.
- The small mitoribosomal subunit is of an exceptionally large size.
- Protein units not directly related to translation may be attached to plant mitoribosomes to confer additional functions to these molecular machines.

Rugen et al., 2019, Molecular & Cellular Proteomics *18*, 1345–1362
July 2019 © 2019 Rugen et al. Published under exclusive license by The American Society for Biochemistry and Molecular Biology, Inc.
https://doi.org/10.1074/mcp.RA119.001396

Downloaded from http://www.mcponline.org/ at LEIBNIZ UNIVERSITÄT HANNOVER on August 9, 2019

Complexome Profiling Reveals Association of PPR Proteins with Ribosomes in the Mitochondria of Plants

Nils Rugen‡, Henryk Straube‡, Linda E. Franken§¶, Hans-Peter Braun‡, and Holger Eubel‡¶‖

Mitochondrial transcripts are subject to a wealth of processing mechanisms including cis- and trans-splicing events, as well as base modifications (RNA editing). Hundreds of proteins are required for these processes in plant mitochondria, many of which belong to the pentatricopeptide repeat (PPR) protein superfamily. The structure, localization, and function of these proteins is only poorly understood. Here we present evidence that several PPR proteins are bound to mitoribosomes in plants. A novel complexome profiling strategy in combination with chemical crosslinking has been employed to systematically define the protein constituents of the large and the small ribosomal subunits in the mitochondria of plants. We identified more than 80 ribosomal proteins, which include several PPR proteins and other non-conventional ribosomal proteins. These findings reveal a potential coupling of transcriptional and translational events in the mitochondria of plants. Furthermore, the data indicate an extremely high molecular mass of the "small" subunit, even exceeding that of the "large" subunit. ***Molecular & Cellular Proteomics 18: 1345–1362, 2019. DOI: 10.1074/mcp.RA119.001396.***

Mitochondria are semi-autonomous organelles of eukaryotic cells which produce some of their proteins using innate ribosomes (mitoribosomes). Aside from ribosomal RNA-moieties (rRNAs) and dedicated tRNAs, plant mitochondria also encode proteins involved in mRNA maturation, translation, cytochrome *c* maturation and oxidative phosphorylation (1). Several of these proteins form protein complexes which also contain subunits encoded in the nucleus. Therefore, the components of these complexes are derived from two different genomes, located in the nucleus and in the mitochondria themselves, thus defining many mitochondrial protein complexes as chimeras.

Due to their α-proteobacterial origin, mitoribosomes largely resemble bacterial 70S ribosomes with respect to their sedimentation behavior, RNA content, and susceptibility to certain antibiotics (2). They also use similar initiation and elongation factors (3, 4). However, mitoribosomes have evolved considerably in the eukaryotic lineage. Reconstruction of the mitochondrial ribosomes of the Last Eukaryotic Common Ancestor (LECA)[1] revealed that mitoribosomes were initially larger and possessed more subunits than their bacterial counterpart (5). In addition, the mitoribosomal polypeptide exit tunnel possesses a more hydrophobic surface than that of bacterial ribosomes and thus caters for the high proportion of hydrophobic respiratory chain subunits produced in mitochondria (6).

The mitoribosomes of yeast, mammals, and trypanosomes are well characterized and their respective structures have been determined at near-atomic resolution using cryo-electron microscopy (7, 8, 9). The 74S yeast mitoribosomes are composed of a 54S large subunit (mtLSU) and a 37S small subunit (mtSSU). Together, they contain 73 proteins (34 in the mtSSU, 39 in the mtLSU) and two rRNAs (15S in the mtSSU and 21S in the mtLSU). Both, the 21S rRNA of the LSU as well as the 15S rRNA of the SSU consist of more nucleotides than their *E. coli* counterparts (8, 10, 11). Yeast mitoribosomes, however, lack the 5S rRNA found in the bacterial LSU, as well as the bacterial 5S rRNA binding proteins (10).

Mammalian mitoribosomes possess a lower sedimentation coefficient of 55S and dissociate into a 28S small subunit and a 39S large subunit. Together they consist of ~80 proteins, of which 30 are present in the mtSSU and 50 in the mtLSU (12, 13, 14, 15). Limited to the synthesis of respiratory subunits, a large portion of mammalian mitoribosomes interact with the inner mitochondrial membrane (16, 17). Only containing the 16S (mtLSU) and 12S (mtSSU) rRNA, mammalian mitoribosomes also lack the 5S rRNA of the bacterial LSU, instead utilizing a mt-tRNA^{Val} (18, 6). A general reduction in structural rRNA content, particularly in bridging the two subunits, is compensated for by additional proteins (19). As such, the mammalian ribosome possesses 36 proteins which are absent in its bacterial counterpart (14, 20).

From the ‡Leibniz Universität Hannover, Institute of Plant Genetics, Herrenhäuser Str. 2, 30419 Hannover, Germany; §Heinrich Pette Institute, Leibniz Institute for Experimental Virology - Centre for Structural Systems Biology, Notkestraβe 85, 22607 Hamburg, Germany

Received February 15, 2019, and in revised form, April 12, 2019

Published, MCP Papers in Press, April 25, 2019, DOI 10.1074/mcp.RA119.001396

© 2019 Rugen et al. Published under exclusive license by The American Society for Biochemistry and Molecular Biology, Inc.

Downloaded from http://www.mcponline.org/ at LEIBNIZ UNIVERSITÄT HANNOVER on August 9, 2019

The substitution of rRNA elements through the acquisition of novel ribosomal proteins, as shown for the mammalian mitoribosomes, is further perpetuated by trypanosomal mitoribosomes. Here, two extremely reduced rRNAs (9S and 12S) are joined by 127 ribosomal proteins (57 in the mtSSU and 70 in the mtLSU) in a 4.5 MDa ribonucleoprotein complex (9). A significant portion of these proteins is predicted to have functions different from those of classical ribosomal subunits. Striking features of trypanosome mitoribosomes include a small subunit of exceptionally large size and the presence of tetratricopeptide and pentatricopeptide repeat (PPR) proteins.

The latter are also present in plant mitochondria. The Arabidopsis genome encodes ~450 PPR proteins, the majority of which are predicted to be imported into mitochondria (21). While some of these proteins are involved in the processing of mitochondrial mRNAs, the functions for many mitochondrial PPR proteins are currently unknown. However, the presence of a PPR-protein in polysome fractions isolated from Arabidopsis mitochondria suggests the participation of some plant PPR proteins in mitochondrial translation (22).

Knowledge of the protein composition and structure of plant mitoribosomes is scarce. Mitoribosomes of higher plants have a sedimentation coefficient of 70–78S (depending on plant species and assay conditions) and possess 18S rRNA (mtSSU) as well as 5S and 26S rRNA (mtLSU). Furthermore, the number of proteins varies with at least 68 proteins in potato and ~80 proteins in broad bean (23–26). However, since reliable protein identification techniques such as mass spectrometry only became accessible after these studies were conducted, only a minor portion of these proteins are known. More recently, ribosomal proteins were identified as part of the plant mitochondrial proteome using shotgun and other proteomic approaches (27–31). Salvato *et al.* (30) identified more than 80 ribosomal proteins, but among these are a considerable number of cytosolic ribosomal subunits. It thus remains unclear which proteins constitute the plant mitochondrial ribosome. Due to the large extent by which mRNAs of mitochondria-encoded genes are processed, gene expression in plant mitochondria is complex and differs considerably from that of yeast and mammalian mitochondria. The sequence-specific deamination of cytosine nucleotides in mRNAs (RNA editing) is a frequently occurring process in plant mitochondria and requires a wealth of specialized RNA-binding proteins and editing factors. It is currently unclear if RNA editing occurs in the bulk phase of the mitochondrial matrix or bound to intramitochondrial structures such as mitoribosomes. However, analysis of eubacterial as well as cytosolic ribosomes showed that additional proteins involved in protein processing bind to the polypeptide exit tunnel (32). Additionally, yeast mitoribosomes are located in close proximity to the inner mitochondrial membrane, where they interact with proteins mediating the insertion of newly synthesized proteins into the lipid bilayer (33). As such, plant mitoribosomes can be expected to contain (or associate with) proteins not only directly involved in protein synthesis, but also in upstream steps (*i.e.* RNA processing) as well as downstream steps (*i.e.* protein processing) of translation.

Using a complexome profiling approach (34), we here report on the protein composition of plant mitochondrial ribosome subunits and subunit fragments. To this end, formaldehyde cross-linked protein complexes of plant mitochondria were first separated on either large-pore blue-native (lpBN) gels (35) or in sucrose velocity gradients. LpBN gel lanes were finely cut into >40 pieces of equal size, each of which was then analyzed in respect to protein composition and abundance by tandem mass spectrometry. Sucrose velocity gradients were fractionated into 29 fractions of equal volume and subsequently analyzed by the same method. For each separation approach, protein abundance profiles for approximately one thousand proteins were produced. Hierarchical clustering then allowed identification of proteins with similar abundance profiles. Co-migration of proteins within the gel or the sucrose velocity gradient is indicative of the presence of the proteins within the same protein complex. Our results suggest that the mtSSU has an unexpectedly large size, even surpassing that of the large subunit. Furthermore, the presence of several PPR-proteins and peptidases as well as proteases within the mitoribosomal subunits is observed, considerably extending our current knowledge on the protein composition of plant mitoribosomes.

MATERIALS AND METHODS

Mitochondria Isolation—preparation of organelles from Arabidopsis cell culture and leaf material was performed as described previously (31, 36), except for the isolation procedure for cross-linked leaf mitochondria, which involved an additional cross-linking step. Cross-linking was performed by adding 37% [v/v] formaldehyde solution to the filtered cell homogenate to a final concentration of 0.5% [v/v]. After differential and isopycnic centrifugation, as well as four washing steps to quantitatively remove Percoll from the isolated organelles, the mitochondrial concentration was adjusted to 3 mg protein/ml (according to Bradford). Only freshly prepared mitochondria were used for large pore Blue-Native PAGE and sucrose velocity gradient centrifugation.

Large Pore Blue-Native PAGE—lpBN-PAGE was carried out according to Strecker *et al.* (35) with minor modifications. To solubilize the membranes, 75 μg of protein (cell culture mitochondria, leaf mitochondria) or 125 μg protein (cross-linked leaf mitochondria) were treated by addition of 25 μl and 42 μl, respectively, of digitonin solubilization buffer (50 mM imidazole, 50 mM NaCl, 2 mM aminocaproic acid (ACA), 1 mM EDTA and 5% [w/v] digitonin, pH 7.0), and incubated for 20 min on ice. After addition of Coomassie G250 to 5% [w/v], protein complexes were loaded onto an acrylamide gradient gel

[1] The abbreviations used are: LECA, last eukaryotic common ancestor; iBAQ, intensity-based absolute quantification; lpBN-PAGE, large pore Blue-Native PAGE; mtLSU, mitoribosomal large subunit; mtSSU, mitoribosomal small subunit; PPR, pentatricopeptide repeat; rRNA, ribosomal RNA; SLP, stomatin-like protein; TAIR, the arabidopsis information resource.

Downloaded from http://www.mcponline.org/ at LEIBNIZ UNIVERSITÄT HANNOVER on August 9, 2019

(2% T, 20% C to 13% T, 3% C, in 0.5 M 6-aminohexanoic acid, 25 mM imidazole/HCL, pH 7.4) overlaid with a 2.5% T, 25% C (in 0.5 M 6-aminohexanoic acid, 25 mM imidazole/HCL, pH 7.4) sample gel. After 1 h at 100 V, separation continued for another 20 h at 15 mA at max. 500 V. To stabilize the fragile high molecular-mass part of the gel, the matrix was firmly attached to one of two glass plates by binding silane (GE Healthcare, Uppsala, Sweden) whereas the opposite plate was treated with releasing agent (Blueslick, SERVA electrophoresis GmbH, Heidelberg, Germany) according to the manufacturer's directions. After Coomassie staining, the gel lane was cut into ~48 fractions from top to bottom, and each of section was subsequently subjected to in-gel trypsin digestions as outlined in (31). The procedure was modified to avoid contamination of the UPLC with remnants of soft gel pieces carried over from the peptide extraction steps (now performed in two steps, first in 50% [v/v] ACN, 2.5% [v/v] formic acid, and then in 100% [v/v] acetonitrile (ACN), 1% [v/v] formic acid).

Sucrose Velocity Gradient Separation of Protein Complexes—freshly prepared mitochondria (in suspension) were subjected to protein solubilization with digitonin as described above. The sample was subsequently layered on top of a 15 ml 8% [w/v] to 40% [w/v] sucrose gradient (in 100 mm SureSpin 630 tubes, Thermo Scientific, Bremen, Germany) and centrifuged for 6 h at 125,000 × *g*. After piercing the bottom of the tube with a hot needle to create a small drain hole, fractions of 500–600 μl were collected manually, resulting in 29 fractions. Of each fraction, 75 μl were then mixed with 4x Laemmli buffer (0.2 M Tris, pH 6.8; 8% [w/v] sodium dodecylsulfate (SDS); 40% [v/v] glycerol; 20% [v/v] β-mercaptoethanol; 0.2% [w/v] bromphenol blue) and loaded onto a Tris-glycin SDS gel consisting of a 4% [w/v] acrylamide stacking gel and a 14% [w/v] acrylamide separating gel as reported previously (37). The gel run was stopped when the bromphenol blue front reached the separation gel, thus leaving the proteins concentrated in a single band at the border of the two phases. Following gel fixation and Coomassie staining, the single gel bands were excised from the gel and subjected to in-gel trypsin digestion as described in Thal *et al.* (37).

Liquid Chromatography Coupled Tandem Mass Spectrometry (LC-MS/MS)—LC-MS/MS of lpBN gel fractions and sucrose velocity gradient fractions was carried out as described in (37).

Processing of MS Data—LC-MS/MS spectra were queried against a TAIR10 database additionally containing common contaminations by using the MaxQuant software version 1.6.0.1 (38). The following parameters were selected: carbamidomethyl (C) as fixed modification, oxidation (M) and acetylation (protein N-term) as variable modifications, specific digestion mode with trypsin (P) and two missed cleavage sites. A FDR of 1% was applied on the PSM and protein level. Protein groups identified as contaminants were removed manually from the proteinGroups.txt file. The data are deposited at the ProteomeXchange Consortium using the PRIDE partner repository and carry the dataset identifier PXD011088. Abundance profiles of proteins across all gel and gradient fractions (based on iBAQ values; (39)) were produced by the NOVA software (version 0.5.9.1; (40)) and subsequently clustered hierarchically using the average linkage procedure based on the Pearson correlation distance. No normalization was performed.

Experimental Design and Statistical Rationale—the heatmaps presented in this manuscript were obtained by a complexome profiling approach. For each heatmap, more than 40 readings were performed for each of the three gel-based heatmaps and 29 for the sucrose velocity gradient based heatmap. Due to the considerable protein overlap in neighboring gel slices, the results for gel slice x are confirmed by the results obtained by slice x-1 and x+1. The different heatmaps refer to independent biological experiments.

RESULTS AND DISCUSSION

Protein Correlation Profiling and Complexome Profiling—Separation of protein complexes in combination with LC-MS/MS has been successfully employed in the past to identify stable protein complexes, either of total cell extracts or of pre-purified cellular compartments, *i.e.* organelles. Most commonly, chromatographic methods or sucrose velocity gradients have been used for the separation of native complexes (41–43). In plants, this strategy has been adopted for the analysis of chloroplasts (44) and cellular extracts (45–47). Mitochondrial ribosomes in plants have so far eluded characterization by protein correlation profiling (PCP). This is most likely due to their low abundance within the organelles and the little contribution mitochondria make toward cellular protein content. In a bid to characterize low abundant plant mitochondria protein complexes, we here use electrophoretic separation of protein complexes solubilized from isolated organelles. LpBN gels enable separation of complexes with molecular masses exceeding 30 MDa (35). In contrast to chromatography-based methods, gel separation does not lead to a dilution of protein complexes in the mobile phase, which is beneficial to the subsequent LC-MS/MS analysis.

Complexome Profiling of Arabidopsis Cell Culture Mitochondria—Mitochondria prepared from a non-green Arabidopsis suspension cell culture (36) were solubilized in 2.5% digitonin and protein complexes and proteins were subsequently separated in lpBN gels. The resulting gel lane was cut into 48 horizontal fractions of equal size and subsequently subjected to LC-MS/MS analysis (31). Protein identification and quantitation in all fractions was then performed using MaxQuant (48). Across the entire 48 fractions, 1318 proteins were identified by this approach. Based on the cumulated intensity-based absolute quantitation (iBAQ) values for each protein across the 48 fractions and the putative intracellular location of the proteins as deduced from the SUBAcon algorithm (49), it can be concluded that more than 94% of the protein abundance in the mitochondrial fraction are of mitochondrial origin (see below). Cumulated iBAQ values of all proteins within each individual gel fraction also reveal a sharp drop in protein content in the fractions above 2 MDa, consistent with the low Coomassie staining intensity in this region (Suppl. Fig. 1). Interestingly, this loss of protein abundance has no negative effect on the number of protein identifications, suggesting the presence of low abundant, high molecular mass protein complexes in the upper region of the gel lane. Based on the abundance profiles of the proteins identified across all 48 gel fractions, a complexome map was built using the NOVA software (40) (supplemental Fig. S2 and S3; supplemental Table S1 and S2). The map revealed numerous protein clusters along the whole gel lane, each of which potentially representing a stable protein complex. The validity of this approach was tested against the migration pattern of respiratory complex I (NADH/ubiquinone oxidoreductase,

Downloaded from http://www.mcponline.org/ at LEIBNIZ UNIVERSITÄT HANNOVER on August 9, 2019

(supplemental Fig. S4), which has been investigated in great detail (50). In the complexome map, 50 subunits of this respiratory complex form a cluster which has a main peak at 1 MDa and an additional peak at 1.5 MDa. The 1 MDa peak corresponds to monomeric complex I, while the 1.5 MDa peak represents a supercomplex of complex I with dimeric complex III. These results are in concordance with previous investigations (31, 51). Four confirmed complex I members are not featured in the complex I cluster shown in Suppl. Fig. 4. These include NAD6 (ATMG00270), the 13 kDa protein (AT3G03070), the B18 protein (AT2G02050), and AT3G06310, a protein of unknown function. Most of these members have a local peak at either 1 MDa (NAD6, AT3G06310, B18 protein), or at 1.5 MDa (13 kDa protein, B18 protein) and are not featured in the cluster due to additional peaks (assembly/breakdown intermediates) or due to a different weighting between individual complex I and the supercomplex.

Other protein complexes with similar migration patterns, such as the prohibitin complex, which migrates close to complex I, can clearly be distinguished from complex I. Similar results are obtained for other members of the respiratory chain, indicating that complexome profiling employing lpBN-PAGE is well suited for studying the composition of protein complexes in plant mitochondria.

Complex I, together with other respiratory protein complexes, was used for a mass calibration of the map. The Arabidopsis pyruvate dehydrogenase complex served in calibrating the gel region above 1.5 MDa. In accordance with the size of this complex from mammalian mitochondria (52), its mass is set to 9 MDa. Extrapolation of the exponential graph incorporating the respiratory complexes as well as the pyruvate dehydrogenase complex (PDC) allowed calibration of the map in the >9 kDa region (supplemental Fig. S5).

Mitochondrial ribosomes were not detected in an earlier investigation employing complexome profiling which covered the molecular mass range up to 2 MDa (31). To test if ribosomal proteins are present in the >2 MDa region of the lpBN gel lane, a list of all confirmed and potential ribosomal proteins in Arabidopsis was created from literature reports (44, 53, 54), supplemented by querying The Arabidopsis Information Resource (TAIR, www.arabidopsis.org) and NCBI (www.ncbi.nlm.nih.gov) for ribosome-related annotations. The resulting list has 824 entries including structural ribosomal proteins as well as assembly factors from the cytosol, plastids, and mitochondria (supplemental Table S3). To gain a better view on potential ribosomal subclusters in cell culture mitochondria, non-ribosomal proteins were removed from the heatmap and the residual 73 ribosomal proteins were re-clustered, forming clusters of low intensity, which are mostly found in the low molecular mass region (<1 MDa) of the gel (supplemental Fig. S6). According to the SUBAcon algorithm (49), the majority of the identified ribosomal proteins (RPs) are of mitochondrial origin (60.3%), followed by cytosolic RPs (31.5%), and only a minor portion being from the plastid compartment (5,5%). No intact ribosomes nor mtSSU or mtLSU subunits were identified in this heatmap. Despite the absence of mitoribosomal subunits, the data presented in supplemental Fig. S2 do contain a wealth of information on other potential PPIs in mitochondria of non-green tissue, which may be of interest to the reader.

Complexome Profiling of Arabidopsis Leaf Mitochondria—The experimental approach described for the cell culture was also used on slower-growing leaf material. We identified 1210 proteins across the 48 fractions. Cumulated iBAQ values, calculated in the same fashion as outlined for the cell culture, show that more than 87% of the protein abundance in the mitochondrial fraction is of mitochondrial origin and that plastids/thylakoids constitute the major contamination (see below). Like the complexome map of cell culture, protein abundance in the high molecular mass region of the lpBN gel lane dropped noticeable (supplemental Fig. S7). In contrast, protein diversity in this region is even higher than in the cell culture fraction (compare supplemental Fig. S1 and S7). This is mostly due to the presence of thylakoid photosystem assemblies which cannot be removed quantitatively from mitochondrial fractions during organelle preparations from green tissue (supplemental Figs. S8 and S9; supplemental Table S4 and S5). In total, 131 of the ribosomal or ribosome-associated proteins featured in supplemental Table S3 were detected across the 48 fractions (supplemental Fig. S10). In the leaf heatmap, the abundance profiles of these proteins differ considerably from those of the cell culture. Toward the upper end of the gel lane (at ~30 MDa), a high molecular mass cluster containing 60 ribosomal proteins is visible. According to SUBAcon (49), the bulk of these proteins is located in the cytosol, while a minor fraction is of plastid origin. Owing to the high molecular mass of the cluster (the proteins were just able to enter the gel), we speculate that it contains mainly cytosolic polysomes. A second cluster running at 3 MDa contains 14 proteins of the cytosolic 60S LSU. Some of these proteins also show weak intensities at 30 MDa, indicative of their participation in the alleged cytosolic polysomes found higher up in the gel. It is currently unknown, why cytosolic polysomes should remain stable in conditions which lead to the destabilization of mitoribosomes.

Clusters containing mitochondrial ribosomes are found at 4–5 MDa (seven proteins), 1.5 MDa (twelve proteins, two of which are being assigned to plastids by SUBAcon), and at 0.2 MDa (five proteins). Other ribosomal proteins with mitochondrial location are also present in the heatmap but migrate below 0.1 MDa and are thus most likely not assembled into protein complexes. Therefore, the leaf mitochondrial heatmap is also devoid of intact mitochondrial ribosomes or ribosome subunits. However, considerably more ribosomal subunits were detected than in its cell culture counterpart. In addition, the detected interactions are also different, giving rise to assemblies of higher molecular masses.

Downloaded from http://www.mcponline.org/ at LEIBNIZ UNIVERSITÄT HANNOVER on August 9, 2019

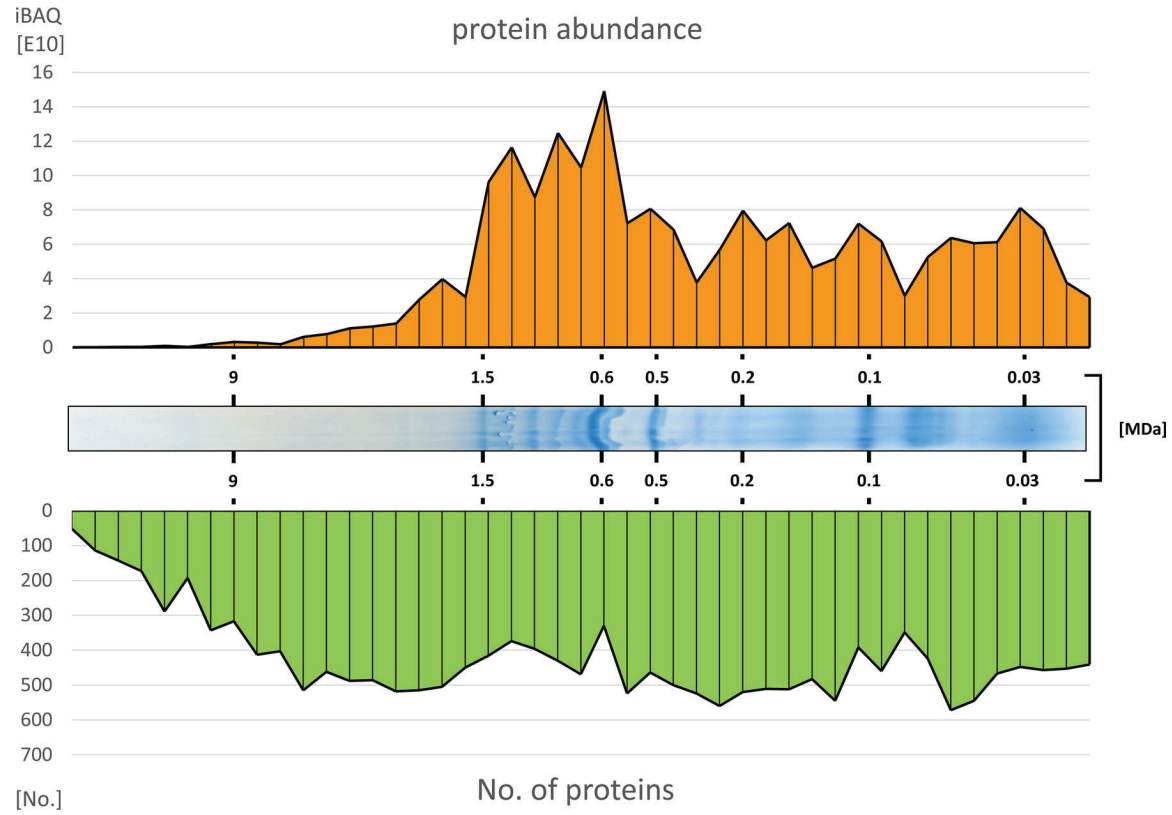

FIG. 1. **Protein abundance and protein diversity across the lpBN-PAGE of cross-linked Arabidopsis leaf mitochondria.** Digitonin solubilized leaf mitochondria were separated by lpBN-PAGE. The resulting gel lane (center panel) was cut into 48 fractions, each of which was subsequently subjected to *in gel* trypsin digestion followed by LC-MS/MS for protein identification and quantitation. Total protein abundance in each fraction (as deduced from cumulated iBAQ values) is shown in the top panel, the number of identified protein species in the bottom panel. Numbers above and below the center panel indicate molecular masses as deduced from Suppl. Fig. 5

Complexome Profiling of Cross-linked Arabidopsis Leaf Mitochondria—To improve ribosome stability, a workflow incorporating a cross-linking step early in the mitochondria isolation procedure was implemented. Protein complexes are stabilized by formaldehyde addition immediately after cell disruption, thereby freezing the state of protein complexes very shortly after ribosomal activity in the mitochondria ceases due to a lack of substrates. Complexome profiling of leaf mitochondria submitted to this experimental strategy displayed similar intensity and complexity along the gel lane when compared with its non-cross-linked counterpart (compare Fig. 1 with supplemental Fig. S7). Despite loading more protein on the gel (125 μg compared with 75 μg for not cross-linked leaf sample), the complexome map (supplemental Fig. S11 and S12; supplemental Table S6 and S7) covers less proteins (1048 compared with 1210), 77 of which are linked to ribosomes. One reason for this may be the reduced amount of plastid contamination, raising the contribution of mitochondrial proteins to more than 93% of the total protein signal. Reducing the heatmap to only the 77 ribosomal proteins, followed by re-clustering (Fig. 2) separates the bulk of the ribosomal proteins group into two clusters at ~5.7 MDa and 3.0 MDa. Less than ten predicted ribosomal proteins are not part of either of these two complexes. Fifty-nine of the 77 proteins are of mitochondrial origin but 18 entries are assigned to the cytosol, plastids, and the plasma membrane. The non-mitochondrial ribosomal proteins largely form additional clusters and none of them is embedded in the mitoribosomal clusters. A closer look reveals that the 3.0 MDa cluster is dominated by mtLSU proteins, whereas the 5.7 MDa cluster mostly consists of mtSSU proteins. Remarkably, the large cytosolic cluster in the high molecular mass region of the non-cross-linked leaf mitochondrial heatmap is missing from this map. We conclude that 1.) formaldehyde cross-linking serves in stabilizing mitochondrial ribosomal subunits and 2.) that the mtSSU has a higher molecular mass than the mtLSU in Arabidopsis.

Other Potential Subunits in the Ribosomal Clusters of Cross-linked Arabidopsis Leaf Mitochondria—To identify novel ribosomal proteins, the master heatmap containing all identified proteins was examined for proteins co-migrating with the ribosomal proteins. Based on the Pearson correlation distance, three confidence intervals for ribosome affiliation were manually defined. Proteins with a distance value of $\leq$0.05 constitute the core of a cluster, probable candidates range between $>$0.05 and $\leq$0.1, and potential candidates

Downloaded from http://www.mcponline.org/ at LEIBNIZ UNIVERSITÄT HANNOVER on August 9, 2019

FIG. 2. **Abundance profiles of ribosomal and ribosome-related proteins in cross-linked Arabidopsis leaf mitochondria.** Proteins of a mitochondrial fraction isolated from leaf material treated with formaldehyde immediately after cell disruption were separated by lpBN PAGE. The resulting gel lane was cut into 45 fractions and all fractions were subjected to label-free quantitative shotgun proteomics. The heatmap displays the abundance profiles of all potential mitoribosomal proteins detected in this approach (see Suppl. Table 3 for a list of all ribosomal and ribosome-associated proteins in Arabidopsis thaliana). Protein abundance is illustrated by color: white is absence of detection, shades of blue indicate quantities relative to the highest detected abundance (dark blue) of a particular protein across all fractions. Values on top of the heatmap indicate molecular mass as deduced from Suppl. Fig. 5. AGI, Arabidopsis genome identifier. A high resolution, interactive version of this figure enabling protein searches is found at http://complexomemap.de/ribo_fig2.

Downloaded from http://www.mcponline.org/ at LEIBNIZ UNIVERSITÄT HANNOVER on August 9, 2019

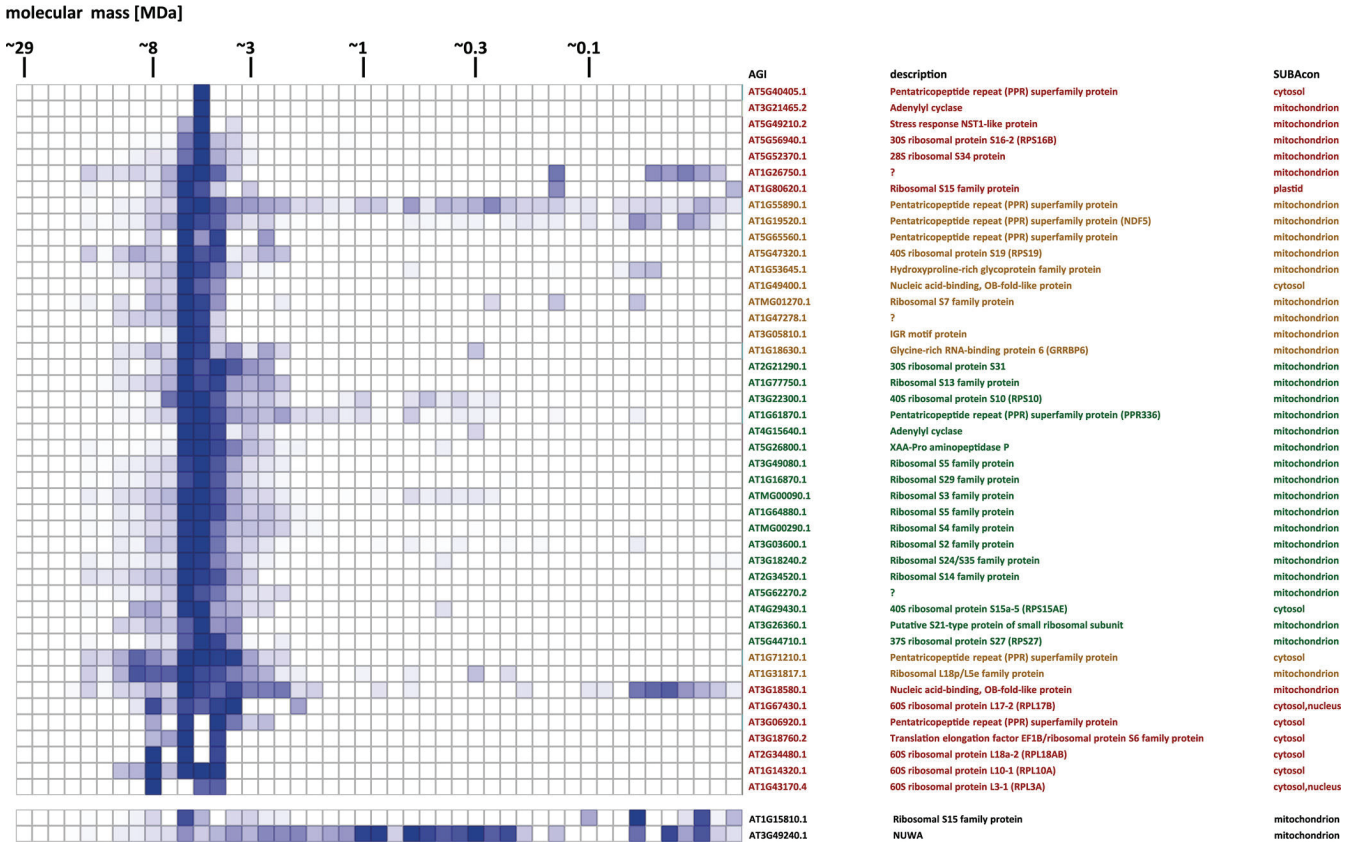

FIG. 3. **Abundance profiles of small subunit ribosomal proteins and associated proteins in cross-linked Arabidopsis leaf mitochondria.** Cutaway of the ribosomal cluster from the master heatmap (see Suppl. Fig. 11) containing small subunit ribosomal proteins and potentially associated proteins displaying similar migration patterns. Protein abundance is illustrated by color: white is absence of detection, shades of blue indicate amounts relative to the highest detected abundance of a particular protein across all fractions (dark blue). Depending on Pearson correlation distance, proteins are grouped into three classes: core proteins (green) ≤ 0.05; probable (orange) >0.05, ≤ 0.1; and potential (red) >0.1, ≤ 0.2. Ribosomal proteins found to co-migrate with the mtSSU cluster in Fig. 2, but are missing in the master heatmap cluster are shown at the bottom. AGI Arabidopsis genome identifier; SUBAcon, subcellular protein location according to the SUBAcon algorithm (Hooper *et al.* 2014). Offset heatmap row shows distribution of RPL32, which is not part of the cluster in the master heatmap but displays a migration pattern similar to other mtSSU members (see also Fig. 2). A high resolution, interactive version of this figure enabling protein searches is found at http://complexomemap.de/ribo_fig3.

have values between >0.1 and ≤ 0.2. The mtSSU contains 44 proteins across all three confidence intervals. Eighteen proteins are found in the core cluster while the residual 26 proteins are evenly distributed over the two remaining confidence intervals (twelve probable proteins and 14 potential proteins). Together, the two groups with lower confidence contain eleven proteins annotated as being ribosomal members and six proteins containing PPR motifs. In addition to the single PPR-protein found in the core cluster, this amounts to seven PPR-motif containing proteins in the small subunit (Fig. 3).

The mtLSU cluster consists of 48 proteins. Twenty are found in the core cluster, 17 are probable members, and eleven are potential members (Fig. 4). Like the mtSSU cluster, the bulk of the proteins are ribosomal proteins and PPR family members, but a higher diversity in respect to their functions is evident. A potential mtLSU subcluster (consisting of probable members) does not exactly match the pattern of the core proteins and migrates somewhat below the center of the core proteins. This subcluster contains four protease/peptidase related proteins (FTSH3, FTSH10, two S24/26 peptidases) together with stomatin-like proteins 1 and 2 (SLP1, 2), as well as a PPR-protein and a protein of unknown function.

Sucrose Velocity Gradient Centrifugation of Mitoribosomal Subunits—To test if the low electrophoretic mobility of the cross-linked small mitoribosomal subunit in lpBN gels may be related to the electrophoretic conditions, digitonin-solubilized protein complexes of cross-linked leaf mitochondria were separated in an 8% to 40% sucrose gradient. After 80 min of ultracentrifugation, the gradient was fractionated into 29 fractions of ~500 μl each, which were subsequently subjected to LC-MS/MS analysis. From this, a heatmap was built in the same fashion as described for the gel fractions (supplemental Fig. S13 and S14, supplemental Table S8 and S9). In total, 919 proteins were identified across the 29 fractions. Hierarchical clustering revealed two broad ribosomal clusters. Using

Downloaded from http://www.mcponline.org/ at LEIBNIZ UNIVERSITÄT HANNOVER on August 9, 2019

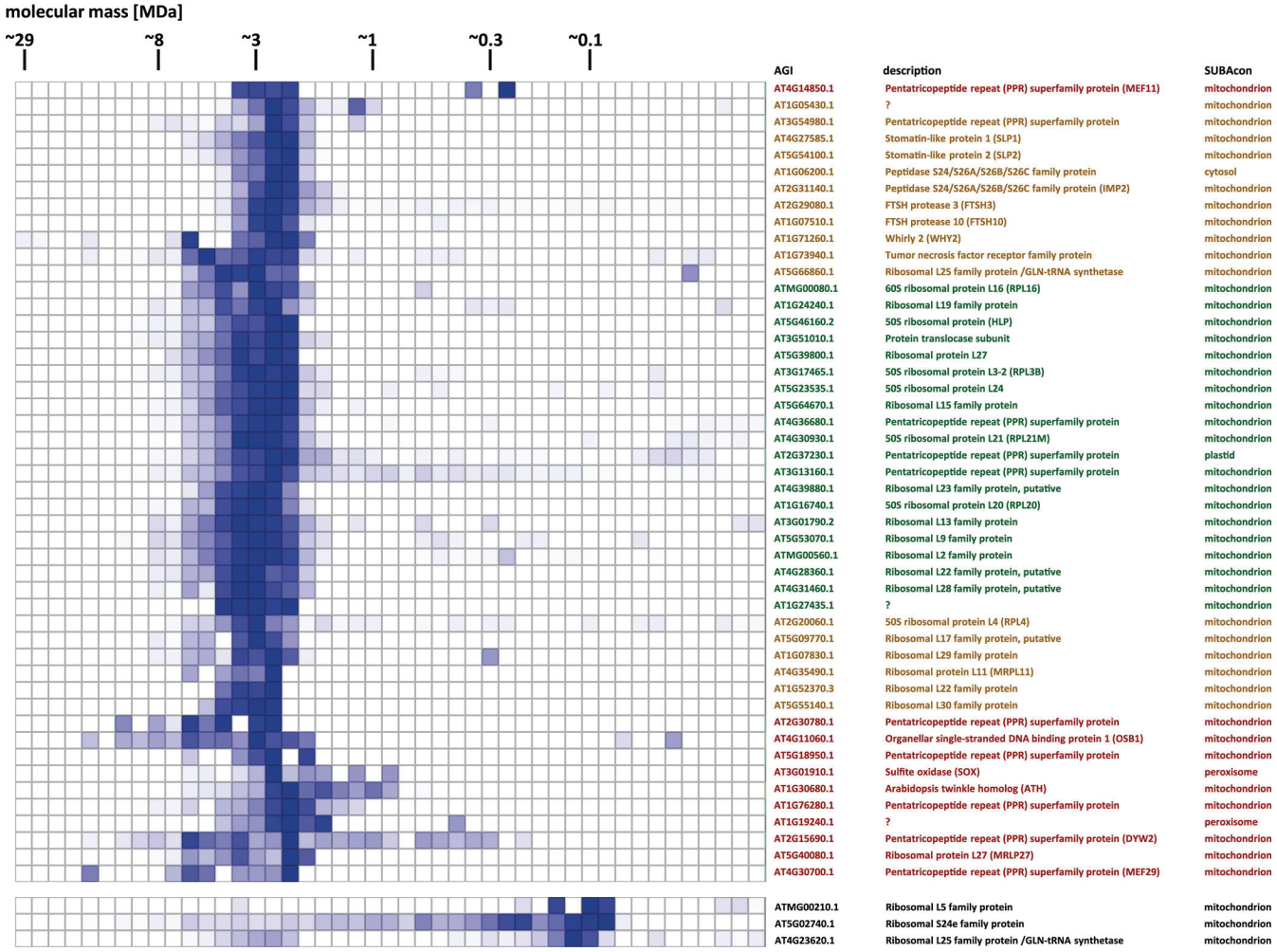

FIG. 4. **Abundance profiles of large subunit ribosomal proteins and associated proteins in cross-linked Arabidopsis leaf mitochondria.** Cutaway of the ribosomal cluster from the master heatmap (see Suppl. Fig. 11) containing large subunit ribosomal proteins and potentially associated proteins displaying similar migration patterns. Protein abundance is illustrated by color: white is absence of detection, shades of blue indicate amounts relative to the highest detected abundance of a particular protein across all fractions (dark blue). Proteins are grouped into three classes, depending on Pearson correlation distance: core proteins (green) ≤ 0.05; probable (orange) >0.05, ≤0.1; and potential (red) >0.1, ≤0.2. Ribosomal proteins found to co-migrate with the mtLSU cluster in Fig. 2 but missing in the master heatmap cluster are shown at the bottom. AGI, Arabidopsis genome identifier; SUBAcon, subcellular protein location according to the SUBAcon algorithm (Hooper *et al.* 2014). Offset heatmap rows show distribution of other mtLSU members, which are not part of the cluster in the master heatmap but display similar migration patterns (see also Fig. 2). A high resolution, interactive version of this figure enabling protein searches is found at http://complexomemap.de/ribo_fig4.

a Pearson correlation distance cutoff of 0.2, they contained 29 mtSSU and 39 mtLSU proteins (Fig. 5). Of these, 19 and 17 proteins, respectively, were also found in the two ribosomal clusters of lpBN PAGE separated cross-linked leaf mitochondria. Separation of protein complexes within the sucrose velocity gradient is inferior to that within the gel matrix of the lpBN PAGE, as indicated by the increased width of the clusters and the presence of obvious non-ribosomal proteins such as 2-oxoglutarate dehydrogenase complex (OGDC) subunits among the mtLSU cluster. Nevertheless, the comparison between sucrose velocity gradient and lpBN PAGE reveals two important aspects of mitoribosomes in plants. First, loosely attached subunits may be lost from protein complexes during lpBN PAGE as indicated by the presence of additional ribosomal proteins and PPR proteins within the ribosomal clusters of the sucrose velocity gradient. Vice versa, some proteins present in the lpBN clusters are absent from the mitoribosomal clusters in the sucrose velocity gradient. This may be due to either a different migration pattern (indicating the absence of this protein from the respective ribosomal subunit), or to the low resolution in the sucrose velocity gradient heatmap hampering hierarchical clustering. Second, the small mitoribosomal subunit migrates of a position in the sucrose velocity gradient that indicates a higher molecular mass when compared with the large subunit. Thus, the results obtained by sucrose velocity gradient separation confirm the relative

Downloaded from http://www.mcponline.org/ at LEIBNIZ UNIVERSITÄT HANNOVER on August 9, 2019

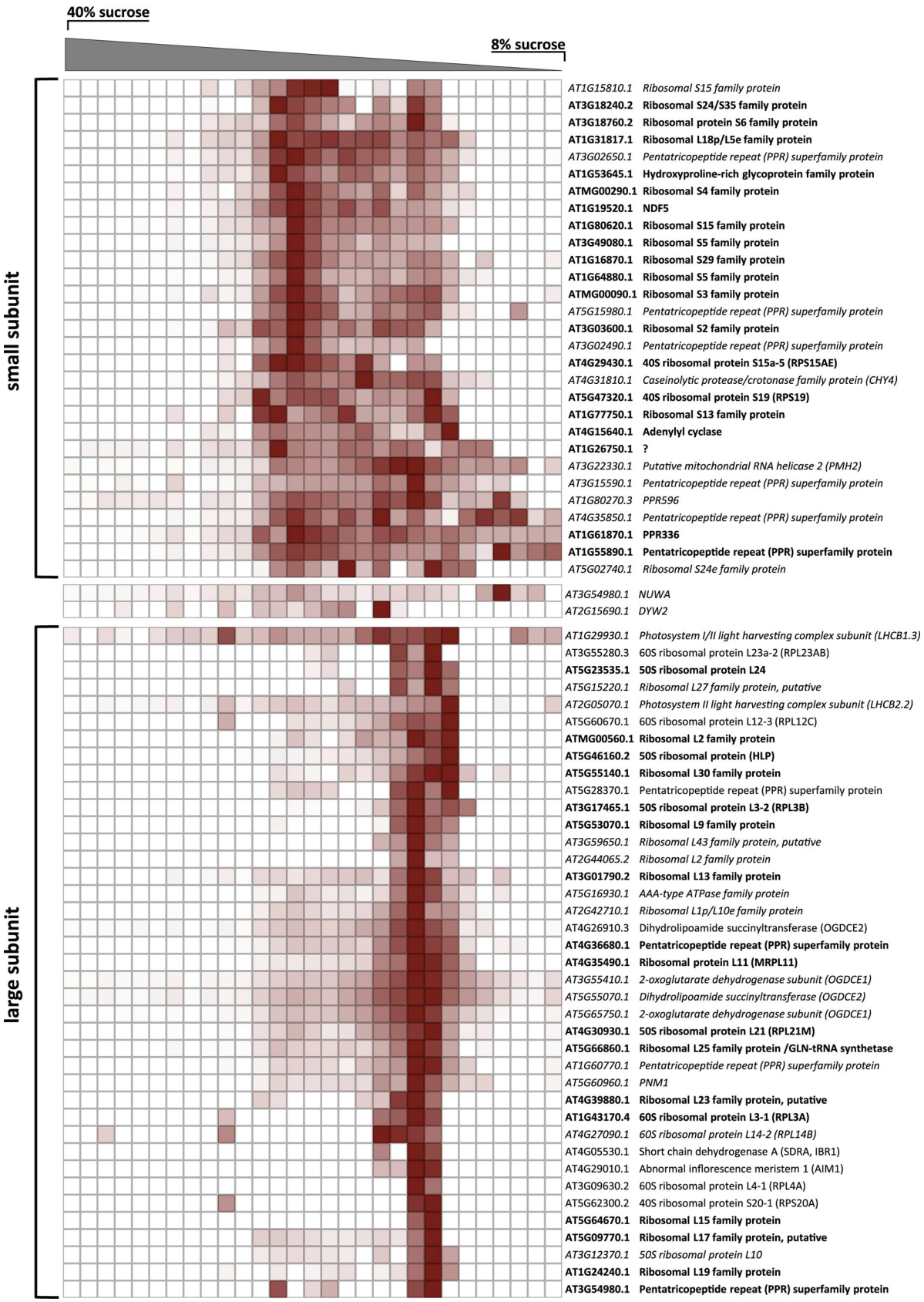

Downloaded from http://www.mcponline.org/ at LEIBNIZ UNIVERSITÄT HANNOVER on August 9, 2019

molecular masses of the plant mitoribosomal subunits and rule out an artificial, electrophoresis-related cause for the apparent molecular mass of the mtSSU in the gel-based complexome profiling approach.

Organelle Purity and Ribosome Contaminations from Other Cellular Compartments—Some of the proteins found in the four heatmaps are clearly of non-mitochondrial origin. The presence of these proteins suggest co-purification of other cellular components with the mitochondria during organelle isolation. The level of non-mitochondrial contamination within the fractions used to build the heatmaps positively correlates with the likelihood of identifying false-positive cytosolic and plastid ribosomal subunits as part of the mitochondrial ribosome. To test the purity of the mitochondrial isolates, the subcellular location of each protein was deduced by the SUBAcon algorithm. Subsequently, the cumulative abundance of each protein across the gel fractions was calculated and the resulting sums for all proteins located in the same compartment were added up. From this, relative protein abundance for each organelle was calculated (supplemental Fig. S15). Cytosolic proteins amount to ~1% in each of the four heatmaps. Contaminations of plastid proteins are generally higher, reaching 8% in the non-cross-linked leaf sample. This value is reduced to 4.3% in the cross-linked leaf sample containing the ribosomal clusters. Proteins of all other compartments amount to less than 4%. This shows that contamination of cytosolic as well as plastid proteins is low in the mitochondrial isolates used in this study. Considering that the most abundant plastid proteins are inserted into the thylakoid membranes, the likelihood of contamination of the mitochondrial ribosomes by those of plastids is judged to be very low. In contrast, a portion of the cytosolic ribosomes are attached to the mitochondrial surface (55). As such, proteins of cytosolic ribosomes may be present in mitochondrial samples despite the low abundance of cytosolic proteins in the mitochondrial isolates. Indeed, some cytosolic proteins (as described by (56)) are found in our cross-linked leaf dataset and their presence within the ribosomal clusters should be treated with caution.

The Protein Composition of the Arabidopsis Mitoribosomes—During the review-process of this manuscript, Waltz *et al.* (57) published an independent investigation of the mitochondrial ribosomes of Arabidopsis. Using two complementary approaches (epitope tagging and sucrose velocity gradient centrifugation), 94 proteins were identified as being part of the two mitoribosomal subunits in Arabidopsis flowers and a cell culture, in contrast to the 92 proteins reported here. A direct comparison of the results obtained by Waltz *et al.* (57) and those within the mtSSU and mtLSU clusters of the lpBN separated cross-linked leaf mitochondria presented here reveals an overlap of 62 proteins (66% of the 94 proteins reported by Waltz *et al.* (57), Table I). Each study also reports potential ribosomal subunit members, which are not confirmed by the other one (32 in Waltz *et al.* (57), 30 here). Within the set of the 32 Waltz *et al.* (57) specific proteins, 12 proteins were found in our complexome map to possess a second peak in the region of the mtSSU or mtLSU (indicated by the absence of a confidence interval suffix in the "lpBN PAGE" column in Table 1). These proteins are thus most likely mitochondrial riboproteins and the overlap between both data sets increases to 74 proteins (79% of the 94 proteins described by Waltz *et al.* (57)). Within the set of 74 overlapping proteins, assignment to either the mtSSU or the mtLSU is similar for all but one protein (AT3G13160, PPR superfamily protein).

The remaining 20 proteins described by Waltz *et al.* (57) were not found in the lpBN-based complexome profiling analysis. Only five of these proteins belong to the SSU. Among them are three ribosomal proteins (AT2G19720, AT4G22460, and ATMG00980) which are most likely located in mitochondria and can therefore be considered as *bona fide* mitoribosomal proteins. The remaining two SSU proteins not found by us are either of unknown function (AT1g64600) or are annotated as tyrosine sulfotransferase-like protein (At4G22000). For both proteins, experimental evidence for a mitochondrial location is missing. The majority (15 accessions) of the proteins exclusively found by Waltz *et al.* (57) are described as LSU proteins. Thirteen of the missing LSU proteins are annotated as ribosomal components and are most likely located in mitochondria. The non-ribosomal proteins include a copper ion-binding protein (AT4G05400) of unknown function and a P-class PPR protein. Both have previously been found in LC-MS/MS analyses of isolated Arabidopsis mitochondria. As such, most of the SSU and LSU proteins reported by Waltz *et al.* (57) which are missing in our clusters can be considered true mitochondrial riboproteins.

Among our list of 92 proteins which are associated with the mtSSU or mtLSU cluster in the lpBN heatmap, 30 have not been reported by Waltz *et al.* (57). Among these are ten

Fig. 5. **Abundance profiles of small and large ribosomal subunits separated by sucrose density gradient ultracentrifugation.** Digitonin-solubilized mitochondrial proteins were separated in an 8% to 40% sucrose gradient, which was subsequently fractionated. Each fraction was then subjected to LC-MS/MS and results were used to produce a heatmap in the same fashion as outlined for the lpBN PAGE (see Suppl. Figs. 2, 8, 11). Cutouts of the clusters of small (top panel) and large (bottom panel) subunits are shown. Protein abundance is illustrated by color: white is absence of detection, shades of brown indicate amounts relative to the highest detected abundance of a particular protein across all fractions. Protein names written in bold font indicate proteins which are part of the ribosomal clusters in the lpBN based heatmaps, while those written in italics represent proteins that are present in the lpBN heatmaps but are not part of the mtLSU or mtSSU clusters (Figs. 3 and 4). Please note: MS analysis of fraction 15 was hampered for unknown reasons. Protein intensities of this fraction were therefore given as the average of its two neighboring fractions. A high resolution, interactive version of this figure enabling protein searches is found at http://complexomemap.de/ribo_fig5.

Downloaded from http://www.mcponline.org/ at LEIBNIZ UNIVERSITÄT HANNOVER on August 9, 2019

TABLE I
Unified list of ribosomes as described by Waltz et al. (57) and this study

AGI	description	lpBN PAGE (Rugen)	SVC (Rugen)	Waltz	SUBAcon	GFP	MS	cytosolic ribosome	plastid ribosome
1.) components featured in Waltz et al. and lpBN ribosome clusters of Rugen et al.									
AT3G13160	rPPR3b (P-class)	mtLSU (core)	other	mtSSU	mitochondrion	+	+	-	-
AT3G26360	putative S21-type protein of small ribosomal subunit	mtSSU (core)	-	mtSSU	mitochondrion	-	-	-	-
AT2G21290	30S ribosomal protein S31	mtSSU (core)	-	mtSSU	mitochondrion	-	-	-	-
AT2G34520	ribosomal S14 family protein	mtSSU (core)	-	mtSSU	mitochondrion	-	-	-	-
AT5G44710	37S ribosomal protein S27 (RPS27)	mtSSU (core)	-	mtSSU	mitochondrion	-	+	-	-
AT5G26800	XAA-Pro aminopeptidase P	mtSSU (core)	-	mtSSU	mitochondrion	-	-	-	-
AT1G77750	ribosomal S13 family protein	mtSSU (core)	mtSSU	mtSSU	mitochondrion	+	+	-	-
AT3G03600	ribosomal S2 family protein	mtSSU (core)	mtSSU	mtSSU	mitochondrion	-	+	-	-
ATMG00290	ribosomal S4 family protein	mtSSU (core)	mtSSU	mtSSU	mitochondrion	-	+	-	-
AT1G64880	ribosomal S5 family protein	mtSSU (core)	mtSSU	mtSSU	mitochondrion	-	+	-	-
AT4G29430	40S ribosomal protein S15a-5 (RPS15AE)	mtSSU (core)	mtSSU	mtSSU	cytosol	-	+	+	-
AT3G49080	ribosomal S5 family protein	mtSSU (core)	mtSSU	mtSSU	mitochondrion	-	+	-	-
AT1G16870	ribosomal S29 family protein	mtSSU (core)	mtSSU	mtSSU	mitochondrion	-	+	-	-
AT3G18240	ribosomal S24/S35 family protein	mtSSU (core)	mtSSU	mtSSU	mitochondrion	-	+	-	-
AT1G61870	PPR336/rPPR1 (P-class)	mtSSU (core)	mtSSU	mtSSU	mitochondrion	+	+	-	-
AT4G15640	adenylyl cyclase	mtSSU (core)	mtSSU	mtSSU	mitochondrion	+	+	-	-
AT3G22300	40S ribosomal protein S10 (RPS10)	mtSSU (core)	other	mtSSU	mitochondrion	-	+	-	-
ATMG00090	ribosomal S3 family protein	mtSSU (core)	mtSSU	mtSSU	mitochondrion	-	+	-	-
AT5G62270	?	mtSSU (core)	other	mtSSU	mitochondrion	-	+	-	-
AT5G56940	30S ribosomal protein S16-2 (RPS16B)	mtSSU (pot.)	-	mtSSU	mitochondrion	+	+	-	-
AT3G21465	adenylyl cyclase	mtSSU (pot.)	-	mtSSU	mitochondrion	-	-	-	-
AT3G18760	translation elongation factor EF1B/rib. S6 family protein	mtSSU (pot.)	mtSSU	mtSSU	cytosol	-	+	-	-
AT1G80620	ribosomal S15 family protein	mtSSU (pot.)	mtSSU	mtSSU	plastid	-	+	-	-
AT1G26750	?	mtSSU (pot.)	mtSSU	mtSSU	mitochondrion	-	+	-	-
AT5G52370	28S ribosomal S34 protein	mtSSU (pot.)	other	mtSSU	mitochondrion	-	-	-	-
AT1G49400	nucleic acid-binding, OB-fold-like protein	mtSSU (prob.)	-	mtSSU	cytosol	-	-	-	-
AT1G47278	?	mtSSU (prob.)	-	mtSSU	mitochondrion	-	+	-	-
AT1G31817	ribosomal L18p/L5e family protein	mtSSU (prob.)	mtSSU	mtSSU	mitochondrion	-	+	-	-
AT5G47320	40S ribosomal protein S19 (RPS19)	mtSSU (prob.)	mtSSU	mtSSU	mitochondrion	-	+	-	-
AT1G19520	NFD5/rPPR2 (P-class)	mtSSU (prob.)	mtSSU	mtSSU	mitochondrion	-	+	-	-
AT1G55890	rPPR3a (P-class)	mtSSU (prob.)	mtSSU	mtSSU	mitochondrion	-	+	-	-
AT1G53645	hydroxyproline-rich glycoprotein family protein	mtSSU (prob.)	mtSSU	mtSSU	mitochondrion	-	+	-	-
ATMG01270	ribosomal S7 family protein	mtSSU (prob.)	other	mtSSU	mitochondrion	-	+	-	-
AT1G18630	glycine-rich RNA-binding protein 6 (GRRBP6)	mtSSU (prob.)	other	mtSSU	mitochondrion	-	+	-	-
AT1G16740	50S ribosomal protein L20 (RPL20)	mtLSU (core)	-	mtLSU	mitochondrion	-	+	-	-
AT1G27435	?	mtLSU (core)	-	mtLSU	mitochondrion	-	+	-	-
AT3G51010	protein translocase subunit	mtLSU (core)	-	mtLSU	mitochondrion	-	+	-	-
AT5G39800	ribosomal protein L27	mtLSU (core)	-	mtLSU	mitochondrion	-	+	-	-
ATMG00080	60S ribosomal protein L16 (RPL16)	mtLSU (core)	-	mtLSU	mitochondrion	-	+	-	-
AT1G24240	ribosomal L19 family protein	mtLSU (core)	mtLSU	mtLSU	mitochondrion	-	+	-	-
AT4G30930	50S ribosomal protein L21 (RPL21M)	mtLSU (core)	mtLSU	mtLSU	mitochondrion	+	+	-	-
AT5G53070	ribosomal L9 family protein	mtLSU (core)	mtLSU	mtLSU	mitochondrion	-	+	-	-
AT4G36680	rPPR7 (P-class)	mtLSU (core)	mtLSU	mtLSU	mitochondrion	-	+	-	-
AT3G01790	ribosomal L13 family protein	mtLSU (core)	mtLSU	mtLSU	mitochondrion	+	+	-	-
AT5G46160	50S ribosomal protein (HLP)	mtLSU (core)	mtLSU	mtLSU	mitochondrion	+	+	-	-
AT5G64670	ribosomal L15 family protein	mtLSU (core)	mtLSU	mtLSU	mitochondrion	-	+	-	-
AT4G39880	ribosomal L23 family protein, putative	mtLSU (core)	mtLSU	mtLSU	mitochondrion	-	+	-	-
AT5G23535	50S ribosomal protein L24	mtLSU (core)	mtLSU	mtLSU	mitochondrion	-	+	-	-
AT3G17465	50S ribosomal protein L3-2 (RPL3B)	mtLSU (core)	mtLSU	mtLSU	mitochondrion	-	+	-	-
AT4G31460	ribosomal L28 family protein, putative	mtLSU (core)	other	mtLSU	mitochondrion	-	+	-	-
AT2G37230	rPPR5 (P-class)	mtLSU (core)	other	mtLSU	plastid	-	+	-	-
AT4G28360	ribosomal L22 family protein, putative	mtLSU (core)	other	mtLSU	mitochondrion	-	+	-	-
AT5G40080	ribosomal protein L27 (MRLP27)	mtLSU (pot.)	-	mtLSU	mitochondrion	-	-	-	-
AT1G52370	ribosomal L22 family protein	mtLSU (prob.)	-	mtLSU	mitochondrion	-	+	-	-
AT5G09770	ribosomal L17 family protein, putative	mtLSU (prob.)	mtLSU	mtLSU	mitochondrion	-	+	-	-
AT5G66860	ribosomal L25 family protein /GLN-tRNA synth.	mtLSU (prob.)	mtLSU	mtLSU	mitochondrion	-	+	-	-
AT4G35490	ribosomal protein L11 (MRPL11)	mtLSU (prob.)	mtLSU	mtLSU	mitochondrion	-	+	-	-
AT5G55140	ribosomal L30 family protein	mtLSU (prob.)	mtLSU	mtLSU	mitochondrion	-	+	-	-
AT1G73940	tumor necrosis factor receptor family protein	mtLSU (prob.)	other	mtLSU	mitochondrion	+	+	-	-
AT1G07830	ribosomal L29 family protein	mtLSU (prob.)	other	mtLSU	mitochondrion	-	+	-	-
AT2G20060	50S ribosomal protein L4 (RPL4)	mtLSU (prob.)	other	mtLSU	mitochondrion	-	+	-	-
AT5G49210	stress response NST1-like protein	mtSSU (pot.)	other	unclear	mitochondrion	-	+	-	-

Downloaded from http://www.mcponline.org/ at LEIBNIZ UNIVERSITÄT HANNOVER on August 9, 2019

TABLE I—*continued*

AGI	description	lpBN PAGE (Rugen)	SVC (Rugen)	Waltz	SUBAcon	GFP	MS	cytosolic ribosome	plastid ribosome
2.) components exclusively featured in Waltz et al.									
ATMG00980	**ribosomal S12 family protein**	-	-	**mtSSU**	**mitochondrion**	-	-	-	-
AT2G19720	40S ribosomal protein S15a-2 (RPS15AB)	-	-	mtSSU	cytosol	-	+	+	-
AT1G64600	**?**	-	-	**mtSSU**	**mitochondrion**	-	-	-	-
AT4G21460	**ribosomal S24/S35 family protein**	-	-	**mtSSU**	**mitochondrion**	-	+	-	-
AT4G22000	tyrosine sulfotransferase-like protein	-	other	mtSSU	nucleus	-	-	-	-
AT5G64650	**ribosomal L17 family protein**	-	-	**mtLSU**	**mitochondrion**	-	-	-	-
AT2G16930	**50S ribosomal protein L27**	-	-	**mtLSU**	**mitochondrion**	-	+	-	-
AT5G55125	**ribosomal L31 family protein**	-	-	**mtLSU**	**mitochondrion**	-	-	-	-
AT5G18790	**ribosomal L33 family protein, putative**	-	-	**mtLSU**	**mitochondrion**	-	+	-	-
AT5G20180	**ribosomal protein L36**	-	-	**mtLSU**	**mitochondrion**	-	-	-	-
AT5G39600	**39S ribosomal protein**	-	-	**mtLSU**	**mitochondrion**	-	+	-	-
AT3G01740	**ribosomal protein L27 (MRLP27)**	-	-	**mtLSU**	**mitochondrion**	-	+	-	-
AT2G18400	ribosomal L6 family protein	-	other	mtLSU	mitochondrion	-	+	-	-
AT3G06040	ribosomal L12 family protein, putative	other	other	mtLSU	mitochondrion	-	+	-	-
AT4G37660	ribosomal L12 family protein, putative	other	other	mtLSU	mitochondrion	-	+	-	-
AT1G70190	ribosomal L7/L12 family protein	other	other	mtLSU	mitochondrion	-	+	-	-
AT4G05400	copper ion binding	other	other	mtLSU	mitochondrion	-	+	-	-
AT3G12370	**50S ribosomal protein L10**	**other**	**mtLSU**	**mtLSU**	**mitochondrion**	+	+	-	-
AT1G60770	**rPPR4 (P-class)**	**other**	**mtLSU**	**mtLSU**	**mitochondrion**	-	+	-	-
AT1G07210	**F10K1.8 protein (ribosomal)**	**other**	-	**mtSSU**	**mitochondrion**	-	+	-	-
AT5G60960	**PNM1/rPPR9 (P-class)**	**(mtLSU)**	**mtLSU**	**mtLSU**	**mitochondrion**	+	+	-	-
AT3G59650	**ribosomal L43 family protein, putative**	**(mtLSU)**	**mtLSU**	**mtLSU**	**mitochondrion**	-	+	-	-
AT2G42710	**ribosomal L1p/L10e family protein**	**(mtLSU)**	**mtLSU**	**mtLSU**	**mitochondrion**	-	+	-	-
AT2G44065	**ribosomal L2 family protein**	**(mtLSU)**	**mtLSU**	**mtLSU**	**mitochondrion**	-	+	-	-
ATMG00210	**ribosomal L5 family protein**	**(mtLSU)**	**other**	**mtLSU**	**mitochondrion**	-	+	-	-
AT4G23620	**ribosomal L25 family protein /GLN-tRNA synthetase**	**(mtLSU)**	**other**	**mtLSU**	**mitochondrion**	-	+	-	-
AT1G14620	**?**	**(mtLSU)**	**other**	**mtLSU**	**mitochondrion**	+	+	-	-
AT5G27820	**ribosomal L18p/L5e family protein**	**(mtLSU)**	-	**mtLSU**	**mitochondrion**	-	-	-	-
AT1G15810	**ribosomal S15 family protein**	**(mtSSU)**	**mtSSU**	**mtSSU**	**mitochondrion**	-	+	-	-
AT4G31810	**caseinolytic protease/crotonase family protein (CHY4)**	**(mtSSU)**	**mtSSU**	**mtSSU**	**mitochondrion**	-	+	-	-
AT3G02650	**rPPR6 (P-class)**	**(mtSSU)**	**mtSSU**	**mtSSU**	**mitochondrion**	-	+	-	-
AT5G15980	**rPPR8 (P-class)**	**(mtSSU)**	**mtSSU**	**mtSSU**	**mitochondrion**	-	+	-	-
3.) components exclusively featured in ribosome clusters from lpBN complexome map of Rugen et al.									
AT1G43170	60S ribosomal protein L3-1 (RPL3A)	mtSSU (pot)	mtLSU	-	cytosol	-	-	+	-
AT5G40405	***pentatricopeptide repeat (PPR) protein (DYW-domain)***	***mtSSU (pot.)***	-	-	***cytosol***	-	-	-	-
AT3G06920	pentatricopeptide repeat (PPR) protein (P-class)	mtSSU (pot.)	-	-	cytosol	-	-	-	-
AT2G34480	60S ribosomal protein L18a-2 (RPL18AB)	mtSSU (pot.)	-	-	cytosol	-	-	+	-
AT1G67430	60S ribosomal protein L17-2 (RPL17B)	mtSSU (pot.)	-	-	cytosol,nucleus	-	-	+	-
AT1G14320	60S ribosomal protein L10-1 (RPL10A)	mtSSU (pot.)	-	-	cytosol	-	+	+	-
AT3G18580	nucleic acid-binding, OB-fold-like protein	mtSSU (pot.)	other	-	mitochondrion	-	+	-	-
AT5G65560	pentatricopeptide repeat (PPR) protein (P-class)	mtSSU (prob)	-	-	mitochondrion	-	+	-	-
AT3G05810	IGR motif protein	mtSSU (prob.)	-	-	mitochondrion	-	-	-	-
AT1G71210	pentatricopeptide repeat (PPR) protein (P-class)	mtSSU (prob.)	other	-	cytosol	-	-	-	-
AT2G31140	***peptidase S24/S26A/S26B/S26C fam. Prot. (IMP2)***	mtLSU (prob.)	other	-	mitochondrion	-	+	-	-
AT5G54100	***stomatin-like protein 2 (SLP2)***	mtLSU (prob.)	other	-	mitochondrion	-	+	-	-
AT4G27585	***stomatin-like protein 1 (SLP1)***	mtLSU (prob.)	other	-	mitochondrion	-	+	-	-
AT2G29080	***FtsH protease 3 (FTSH3)***	mtLSU (prob.)	other	-	mitochondrion	-	+	-	-
AT1G71260	Whirly 2 (WHY2)	mtLSU (prob.)	other	-	mitochondrion	+	+	-	-
AT1G07510	***FtsH protease 10 (FTSH10)***	mtLSU (prob.)	other	-	mitochondrion	-	+	-	-
AT1G05430	?	mtLSU (prob.)	other	-	mitochondrion	-	+	-	-
AT1G06200	***peptidase S24/S26A/S26B/S26C family protein***	***mtLSU (prob.)***	-	-	***cytosol***	-	+	-	-
AT3G54980	**pentatricopeptide repeat (PPR) protein (P-class)**	**mtLSU (prob.)**	**mtLSU**	-	**mitochondrion**	-	+	-	-
AT5G18950	pentatricopeptide repeat (PPR) protein (P-class)	mtLSU (pot.)	-	-	mitochondrion	-	-	-	-
AT4G30700	***MEF29 (DYW-domain)***	***mtLSU (pot.)***	-	-	***mitochondrion***	-	-	-	-
AT4G14850	***MEF11 (DYW-domain)***	***mtLSU (pot.)***	-	-	***mitochondrion***	-	-	-	-
AT2G30780	pentatricopeptide repeat (PPR) protein (P-class)	mtLSU (pot.)	-	-	mitochondrion	-	-	-	-
AT1G76280	pentatricopeptide repeat (PPR) protein (P-class)	mtLSU (pot.)	-	-	mitochondrion	-	+	-	-
AT1G19240	?	mtLSU (pot.)	-	-	peroxisome	-	+	-	-
AT4G11060	organellar single-stranded DNA binding protein 1 (OSB1)	mtLSU (pot.)	other	-	mitochondrion	+	+	-	-
AT3G01910	sulfite oxidase (SOX)	mtLSU (pot.)	other	-	peroxisome	-	+	-	-
AT2G15690	***DYW2, (DYW-domain)***	***mtLSU (pot.)***	***other***	-	***mitochondrion***	+	-	-	-
AT1G30680	Arabidopsis twinkle homolog (ATH)	mtLSU (pot.)	other	-	mitochondrion	+	+	-	-
ATMG00560	**ribosomal L2 family protein**	**mtLSU (core)**	**mtLSU**	-	**mitochondrion**	-	+	-	-

Downloaded from http://www.mcponline.org/ at LEIBNIZ UNIVERSITÄT HANNOVER on August 9, 2019

TABLE I—*continued*

AGI	description	lpBN PAGE (Rugen)	SVC (Rugen)	Waltz	SUBAcon	GFP	MS	cytosolic ribosome	plastid ribosome
4.) components exclusively featured in ribosome clusters from sucrose velocity gradient of Rugen et al.									
AT3G55280	60S ribosomal protein L23a-2 (RPL23AB)	-	mtLSU	-	cytosol	-	-	+	-
AT5G60670	60S ribosomal protein L12-3 (RPL12C)	-	mtLSU	-	cytosol	-	-	+	-
AT5G28370	pentatricopeptide repeat (PPR) protein (P-class)	-	mtLSU	-	mitochondrion	-	-	-	-
AT4G05530	short chain dehydrogenase A (SDRA, IBR1)	-	mtLSU	-	peroxisome	-	-	-	-
AT4G29010	abnormal inflorescence meristem 1 (AIM1)	-	mtLSU	-	peroxisome	-	+	-	-
AT3G09630	60S ribosomal protein L4-1 (RPL4A)	-	mtLSU	-	cytosol	-	-	+	-
AT5G62300	40S ribosomal protein S20-1 (RPS20A)	-	mtLSU	-	cytosol	-	+	+	-
AT3G22330	putative mitochondrial RNA helicase 2 (PMH2)	other	mtSSU	-	mitochondrion	-	+	-	-
AT3G15590	pentatricopeptide repeat (PPR) protein (P-class)	other	mtSSU	-	mitochondrion	-	+	-	-
AT1G80270	PPR596 (P-class)	other	mtSSU	-	plastid, mitochondrion	+	+	-	-
AT4G35850	pentatricopeptide repeat (PPR) protein (P-class)	other	mtSSU	-	mitochondrion	-	+	-	-
AT5G02740	ribosomal S24e family protein	other	mtSSU	-	mitochondrion	-	+	-	-
AT3G49240	pentatricopeptide repeat (PPR) protein (NUWA, P-class)	other	other	-	mitochondrion	-	+	-	-
AT1G29930	photosystem I/II light harvesting complex SU (LHCB1.3)	contaminant	mtLSU	-	plastid	-	+	-	-
AT2G05070	photosystem II light harvesting complex SU (LHCB2.2)	contaminant	mtLSU	-	plastid	-	-	-	-
AT4G26910	dihydrolipoamide succinyltransferase (OGDCE2)	contaminant	mtLSU	-	mitochondrion	-	+	-	-
AT3G55410	2-oxoglutarate dehydrogenase subunit (OGDCE1)	contaminant	mtLSU	-	mitochondrion	-	+	-	-
AT5G55070	dihydrolipoamide succinyltransferase (OGDCE2)	contaminant	mtLSU	-	mitochondrion	-	+	-	-
AT5G65750	2-oxoglutarate dehydrogenase subunit (OGDCE1)	contaminant	mtLSU	-	mitochondrion	-	+	-	-
AT4G27090	60S ribosomal protein L14-2 (RPL14B)	contaminant	mtLSU	-	cytosol	-	-	+	-
AT3G02490	**pentatricopeptide repeat (PPR) protein (P-class)**	**(mtSSU)**	**mtSSU**	-	**mitochondrion**	-	+	-	-
AT5G15220	**ribosomal L27 family protein, putative**	**(mtLSU)**	**mtLSU**	-	**mitochondrion**	-	-	-	-
AT5G16930	**AAA-type ATPase family protein**	**(mtLSU)**	**mtLSU**	-	**mitochondrion**	-	+	-	-

AGI, Arabidopsis genome identifier; description, functional/structural protein annotation; lpBN PAGE (Rugen), subunit affiliation according to lpBN complexome map; SVC (Rugen), subunit affiliation according to sucrose velocity gradient complexome map; Waltz, subunit affiliation according to Waltz et al. (57); SUBAcon, subcellular location according to the SUBAcon algorithm (49); GFP, experimental evidence for mitochondrial location according to fluorescent fusion reporter protein assay; MS, experimental evidence for mitochondrial location according to MS analysis of isolated organelles; cytosolic ribosome, detection of AGI in isolated cytosolic ribosomes according to (56); plastid ribosome, detection of AGI in isolated cytosolic ribosomes according to (78). Rows shown in red indicate diverging LSU/SSU assignments; bold rows are expected to be genuine mitoribosomal proteins; rows shown in bold and italics indicate additional units potentially affiliated with mitoribosomes; subunit assignments shown in brackets indicate the absence of proteins from the subunit cluster but a local peak in either the mtSSU or mtLSU in the heatmap of cross-linked leaf mitochondria (supplemental Fig. S11); peach, mtSSU; light blue, mtLSU.

potential mtSSU components, four of which (AT2G34480, AT1G67430, AT1G14320, and AT1G43170) have annotations identifying them as eukaryotic LSU proteins. These proteins were also identified in an investigation of Arabidopsis cytosolic ribosomes (56). Although clustering with the mtSSU proteins, they show minor differences in their migration pattern and should not be regarded as mitochondrial SSU subunits. Their incorporation into the SSU cluster is more likely the result of co-migration of cytosolic LSU subunits with mtSSU subunits. Two other potential mtSSU proteins are a nucleic acid binding protein (AT3G18580) and an IGR motif carrying protein of unknown function. Their potential functions in mitochondrial translation are currently unknown.

Twenty potential mitoribosomal proteins being featured in our mtLSU cluster were not found by Waltz *et al.* (57). Of these, only one belongs to the core cluster (ATMG00560) and is annotated as a ribosomal L2 family protein. The remaining 19 proteins belong in equal parts to the probable and potential classes of LSU proteins. Six members of the LSU cluster are related to protein fate: FtsH3 and 10 (AT2G29080, AT1G07510), stomatin-like proteins 1 and 2 (SLP1/2; AT5G54100, AT4G27585), and two members of the S24/S26 peptidase family (AT2G31140, AT1G06200). FtsH3 and FtsH10 are AAA-proteases and, together with prohibitins, they form homo- and hetero-oligomeric complexes of ~2 MDa (58). In our hands, no direct correlation between FtsH3/10 and prohibitins could be detected. However, besides their main peak at ~1.1 MDa, prohibitins possess a second, minor peak close to the FtsH peak (Suppl. Fig. 11). Interestingly, the precursor polypeptide chain of RPL32 is trimmed by FtsH to yield the mature protein. RPL32 (AT1G26740) has not been identified by Waltz *et al.* (57), nor by us. It is, however, predicted to be located in mitochondria, and double knock-out mutants of FtsH3 and FtsH10 show reduced rates of mitochondrial gene expression rates (59). Hence, a potential functional connection between FtsH proteins and ribosomal proteins exists and strengthens the notion of a physical connection of these proteins. SLP, together with prohibitins belong to the band-7 family which is also referred to as SPFH superfamily. Detailed functions for the members of this protein family are unknown but seem to revolve around protein scaffolding and organization of the inner mitochondrial membrane (60). Murine SLP2 co-migrates with the mtLSU in

Downloaded from http://www.mcponline.org/ at LEIBNIZ UNIVERSITÄT HANNOVER on August 9, 2019

sucrose velocity gradients, and the protein was identified as being a key regulator of mitochondrial translation in mice (61). Hence, the presence of these proteins in the mtLSU cluster is backed by a connection to translation. No such connection between the S24/S26 peptidases and mitochondrial translation could be found. Other proteins which are found here but are missing in Waltz *et al.* (57) include two proteins of unknown function (AT1G05430, AT1G19240), an organellar single stranded DNA binding protein (AT4G11060), and an Arabidopsis twinkle homolog (AT1G30680), both of which have implicated roles in mtDNA replication (62), Whirly 2 (AT1G71260, potentially involved in DNA maturation), as well as a sulfite oxidase (AT3G01910). The remaining seven proteins are either cytosolic ribosomal subunits or PPR proteins (see below). Taken together, the proteins involved in protein maturation featured in the LSU cluster may indeed have functions in translation. Given their absence in the dataset of Waltz *et al.* (57), we speculate that they form an additional loosely bound unit which is most likely located in the inner mitochondrial membrane. Due to the cross-linking strategy employing formaldehyde, it co-migrates with the mtLSU in lpBN-PAGE. Formaldehyde has been used here in moderation and the distance it can bridge is small compared with other cross-linkers. The tendency to produce artificial protein aggregates is therefore rather small. Considering that many protein complexes, for example of the respiratory chain, remain unchanged upon its use, the additional proteins detected in the LSU and SSU clusters in the lpBN-based complexome map cannot be attributed solely to the use of formaldehyde; rather they represent candidates for ribosome members.

From the data of Waltz *et al.* (57), the heatmaps shown here, and subcellular information as well as additional information available from TAIR (Arabidopsis.org), a set of 92 proteins was extracted which constitutes the essence of the Arabidopsis mitoribosome (bold rows in Table 1). Within this set, 42 proteins are in the mtSSU, 48 in the mtLSU, and two additional proteins could not clearly be assigned to either one.

The Presence of PPR-proteins In the Ribosomal Fractions—Together, mitochondria and plastids contain several hundreds of PPR proteins. For many of them, no functional context has been identified. However, a considerable number of PPR proteins are involved in RNA processing (63). The presence of PPR-proteins has been linked to the ribosomes of plastids and mitochondria (22, 64–66) and 20 PPRs have been identified in the mtSSU and mtLSU clusters of the lpBN based complexome map or by Waltz *et al.* (57). Six of these were found in both studies, with the PPR protein used in Waltz *et al.* (57) for immune-precipitation of mitoribosomes, PPR336 (rPPR1, P-class), being among them. The remaining five PPR proteins are also members of the P-class of PPR proteins. Four PPR proteins were exclusively found by Waltz *et al.* (57) and belong to the P-class of PPR proteins. In contrast, ten PPR were exclusively identified here, of which six belong to the P-class. The other four are members of the PLS-class and contain DYW-domains (AT2G15690, DYW2; AT4G14580, MEF11; AT4G30700, MEF29; AT5G40405, unknown function; Table 1). DWY2 provides the deaminase activity to a suggested editosome protein complex, which also contains NUWA and SLO2 (67). NUWA was detected in the lpBN as well as in the sucrose velocity gradient complexome maps but did not cluster with the ribsosomal proteins. Its abundance profiles, however, show weak local highs in the area of the mtSSU clusters (please see the extra rows inserted into the heatmaps shown in Figs. 3 and 5). SLO2 was not discovered in either of the two approaches. Among the remaining three PLS-type PPR proteins are two mitochondrial editing factors (MEFs), MEF11 and MEF29. MEF11 is involved in editing three mitochondrial transcripts for respiratory chain subunits (*cox3, nad4, and ccb*), while MEF29 is required for editing respiratory protein complex subunits *nad5* and *cob* (68, 69). Information of the fourth PLS-type PPR (AT5G40405.1) is scarce and no comment on its potential functions as part of the mitoribosome can be made. The presence of these DYW-domain containing PPR proteins in the ribosomal clusters suggest a physical connection between RNA editing and translation in plant mitochondria. Analogous to the situation described for the FtsH/SLP/S-peptidase cluster described above, the presence of these mRNA editing factors within our heatmap may be due to a cross-linking event between an RNA-editing unit and the ribosome. Given that the migration pattern differs between AT5G40405 (in the SSU cluster) and MEF29, MEF11, and DYW2 (all of them in the LSU cluster), this extra subunit may be attached to both subunits. Little is known about the residual 16 PPR proteins belonging to the P-class, but some of them enhance translational activity for specific proteins (reviewed in (63)). Three P-class PPRs, however were found to interact with ribosomes/polyribosomes (PPR336, PPR 596, and PNM1; (22, 66). As such, the other P-class PPRs identified in the course of this study may also be at least temporary members of Arabidopsis mitoribosomal subunits.

Molecular Masses of mtSSU and mtLSU Clusters—The masses for the mtLSU cluster members (proteins of all three confidence intervals and 5S/26S rRNA) amount to a mass of 2.7 MDa, which is close to the apparent molecular mass of 3 MDa. However, the bulk of the abundance of the core proteins is distributed over four fractions and for most proteins the overall width of the cluster stretches over seven to nine fractions and is thus broader than the mtLSU cluster. The width of a cluster in a complexome heatmap is determined in some part by the fractionation of the gel lane and may therefore vary between replicates. However, we observed the same outcome for the mtLSU cluster repeatedly in heatmaps of cross-linked leaf mitochondria (data not shown). As such, the width of the cluster is most likely a result of some variation in molecular mass and, therefore in the composition of the mtLSU. Not all proteins of the mtLSU cluster may be present within the same large subunit at a given time point.

Downloaded from http://www.mcponline.org/ at LEIBNIZ UNIVERSITÄT HANNOVER on August 9, 2019

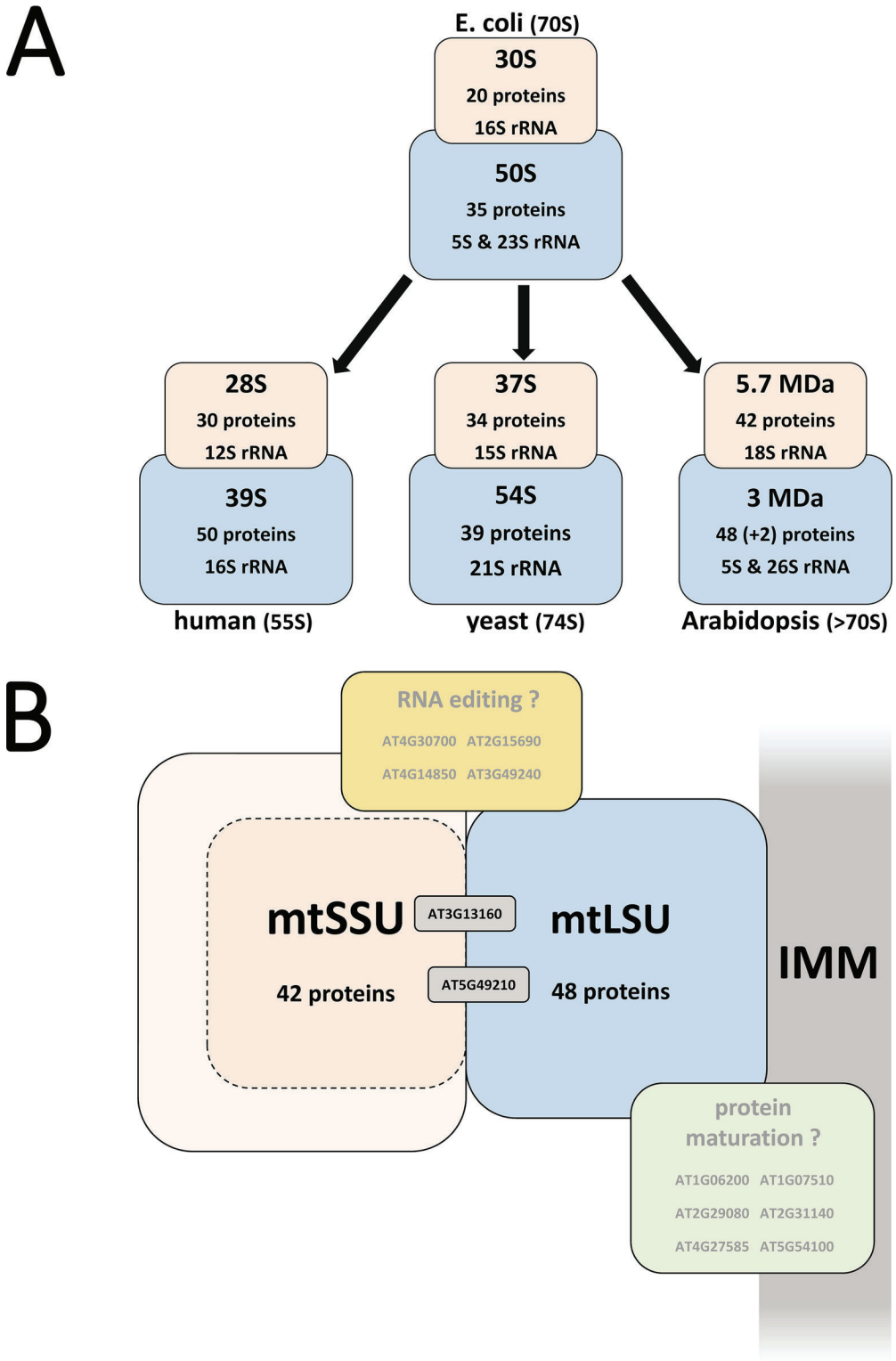

FIG. 6. **Composition of bacterial and mitochondrial RPL and RPS clusters.** *A*, general overview of the composition of LSU and SSU of *E. coli* ribosomes with that of the mtLSUs and mtSSUs of yeast (8, 10, 11) and humans (12–15), as well as the provisional Arabidopsis mtLSU and mtSSU (as deduced from the data presented by Waltz *et al.* (57) and here). *B*, the Arabidopsis mtSSU and mtLSU together with potential additional units involved in RNA editing (yellow) and protein maturation (green). The Arabidopsis mtSSU appears to be larger than the LSU, the underlying reason for this is a matter of debate. Accessions in gray boxes indicate proteins for which assignment to either of the two subunits is not clear. Peach, (mt)SSU; light blue (mt)LSU; IMM, inner mitochondrial membrane.

Downloaded from http://www.mcponline.org/ at LEIBNIZ UNIVERSITÄT HANNOVER on August 9, 2019

Intriguingly, the masses of the precursor proteins in the mtSSU cluster accumulate to ~1.6 MDa. Together with the 18S RNA, this results in a mass of ~2.2 MDa for the small subunit. Hence, its calculated mass is less than half of the apparent mass of 5.7 MDa. Waltz *et al.* (57) speculate that the high mass of the mtSSU is inflicted by the presence of additional (PPR) proteins as well as additional mRNA loops. Given that the overlap between the two studies is high for the SSU (33 proteins of 41 reported by Waltz *et al.* (57) and of 38 reported here), this may partly explain the mass difference between the plant mtSSU and the prokaryotic SSU. However, since the additional mtSSU components are already considered in our calculations, the bulk of difference between apparent and calculated mass of the ribosomes must be due to other factors. One such factor could be the shape of the particle, which may affect its electrophoretic mobility. Despite a similar molecular mass, a globular particle will face less resistance to migration in a polyacrylamide gel than an irregularly shaped particle with protrusions. MtSSU particles of the latter type have been described by Waltz *et al.* (57). Another requirement for the migration in a gel is a net negative charge, which is conferred to the complexes by a coat of the negatively charged protein dye Coomassie (70). This Coomassie-coating, however, may also impact on protein complexes in unknown ways and may thus affect their separation in the gel matrix. Both, shape and Coomassie coat, can be ruled out as major factors influencing the apparent molecular mass of the mtSSU since the sucrose velocity gradient confirms the results obtained from the lpBN gel. Alternatively, the association of the ribosomes with the inner mitochondrial membrane may affect the molecular mass of the ribosomes since lipids may remain attached to the particles upon solubilization. This, however, is unlikely since interaction of the ribosome with the membrane will most likely take place at the mtLSU surface and therefore will have little impact on the mass of the mtSSU. Instead, the apparent mass may suggest the presence of mtSSU dimers. In bacteria, inactive (hibernating) ribosomes are "stored" as dimers (100S ribosomes), the contact side of the two monomers being conferred by the SSU (71–77). As mitochondria have their origin in the bacterial kingdom, the mtSSU observed here may represent dimeric mitochondrial ribosomes which are lacking the two mtLSUs. Indeed, Waltz *et al.* (57) observed aggregation of ribosomal subunits in sucrose velocity gradients. However, dimerization of bacterial 70S ribosomes requires the presence of a ribosome modulation factor (RMF) protein and/or a hibernation promoting factor (HPF) protein, but no homologues for such proteins were found in the lpBN-based or the sucrose velocity gradient-based mitochondrial heatmaps. Further analysis of mtSSU particles, for example by crosslinking MS or cryo-EM, will be necessary to elucidate the source of the additional mass of the Arabidopsis mtSSU.

CONCLUSIONS

The data presented here shed new light on the protein composition of plant mitoribosomes. Using a combination of chemical cross-linking and complexome profiling employing both, lpBN gel electrophoresis and sucrose velocity gradients, mitoribosomal proteins were identified on a large scale. Since the ribosomal subunits were separated by this approach, the data allow a clear allocation of proteins to either the large or the small subunit. In conjunction with a recently published study using different experimental approaches, a set of 92 proteins was assembled which most likely constitute Arabidopsis mitoribosomes (Table 1). Compared with its bacterial ancestor and the mammalian as well as fungal mitoribosomes, plant mitoribosomes are thus believed to contain the highest total number of proteins (Fig. 6*A*). This is because each subunit contains non-conventional proteins, most of which belong to the PPR-class. The functions of most of these proteins in the context of translation are just beginning to emerge. However, the presence of several PPR-proteins containing DYW domains suggests that RNA editing may to some degree occur at mitochondrial ribosomes. Furthermore, proteins involved in protein maturation and protein degradation were also detected as potential components of the large subunit and may play a role in processing nascent polypeptides (Table 1, Fig. 6*B*). Remarkably, the data presented here imply an unusual molecular mass of the small ribosomal subunit, which is higher than that of the large subunit and only partly explainable by the presence of additional, plant specific components. Future efforts are necessary to investigate the roles of the newly identified, non-conventional subunits as well as the origin of the high molecular mass of the small mitoribosomal subunit.

Acknowledgments—We thank Marianne Langer and Michael Senkler for expert technical assistance and Heiko Giese for support related to NOVA data analysis.

DATA AVAILABILITY

The mass spectrometry proteomics data have been deposited to the ProteomeXchange Consortium via the PRIDE partner repository with the dataset identifier PXD011088 (http://www.ebi.ac.uk/pride/archive/projects/PXD011088; ftp://ftp.pride.ebi.ac.uk/pride/data/archive/2019/04/PXD011088).

S This article contains supplemental material.
¶ The research described in this manuscript was supported by the Deutsche Forschungsgemeinschaft (DFG, grant EU 54/4). This work was in part made possible by an EMBO long-term fellowship (ALTF 356–2018) awarded to Linda Franken.
‖ To whom correspondence should be addressed. E-mail: heubel@genetik.uni-hannover.de.
Author contributions: N.R., H.S., and L.E.F. performed research; N.R. analyzed data; H.-P.B. and H.E. designed research; H.E. wrote the paper.

REFERENCES

1. Kubo, T., and Newton, K. J. (2008) Angiosperm mitochondrial genomes and mutations. *Mitochondrion* **8,** 5–14

Downloaded from http://www.mcponline.org/ at LEIBNIZ UNIVERSITÄT HANNOVER on August 9, 2019

2. Hamilton, M. G., and O'Brien, T. W. (1974) Ultracentrifugal characterization of the mitochondrial ribosome and subribosomal particles of bovine liver: molecular size and composition. *Biochemistry* **13,** 5400–5403
3. Zhang, Y., and Spremulli, L. L. (1998) Roles of residues in mammalian mitochondrial elongation factor Ts in the interaction with mitochondrial and bacterial elongation factor Tu. *J. Biol Chem.* **273,** 28142–28148
4. Gaur, R., Grasso, D., Datta, P. P., Krishna, P. D., Das, G., Spencer, A., Agrawal, R. K., Spremulli, L., and Varshney, U. (2008) A single mammalian mitochondrial translation initiation factor functionally replaces two bacterial factors. *Mol. Cell* **29,** 180–190
5. Desmond, E., Brochier-Armanet, C., Forterre, P., and Gribaldo, S. (2011) On the last common ancestor and early evolution of eukaryotes: reconstructing the history of mitochondrial ribosomes. *Res. Microbiol.* **162,** 53–70
6. Brown, A., Amunts, A., Bai, X. C., Sugimoto, Y., Edwards, P. C., Murshudov, G., Scheres, S. H. W., and Ramakrishnan, V. (2014) Structure of the large ribosomal subunit from human mitochondria. *Science* **346,** 718–722
7. Amunts, A., Brown, A., Toots, J., Scheres, S. H. W., and Ramakrishnan, V. (2015) Ribosome. The structure of the human mitochondrial ribosome. *Science* **348,** 95–98
8. Desai, N., Brown, A., Amunts, A., and Ramakrishnan, V. (2017) The structure of the yeast mitochondrial ribosome. *Science* **355,** 528–531
9. Ramrath, D. J. F., Niemann, M., Leibundgut, M., Bieri, P., Prange, C., Horn, E. K., Leitner, A., Boehringer, D., Schneider, A., and Ban, N. (2018) Evolutionary shift toward protein-based architecture in trypanosomal mitochondrial ribosomes. *Science* **362**, eaau7735
10. Amunts, A., Brown, A., Bai, X. C., Llácer, J. L., Hussain, T., Emsley, P., Long, F., Murshudov, G., Scheres, S. H. W., and Ramakrishnan, V. (2014) Structure of the yeast mitochondrial large ribosomal subunit. *Science* **343,** 1485–1489
11. Greber, B. J., and Ban Structure, N. (2016) Function of the mitochondrial ribosome. *Annu. Rev. Biochem.* **85,** 103–132
12. O'Brien, T. W. (1971) The general occurrence of 55 S ribosomes in mammalian liver mitochondria. *J. Biol. Chem.* **246,** 3409–3417
13. Cahill, A., Baio, D. L., and Cunningham, C. C. (1995) Isolation and Characterization of rat liver mitochondrial ribosomes. *Anal. Biochem.* **232,** 47–55
14. Amunts, A., Brown, A., Toots, J., Scheres, S. H. W., and Ramakrishnan, V. (2015) The structure of the human mitochondrial ribosome. *Science* **348,** 95–98
15. Greber, B. J., Bieri, P., Leibundgut, M., Leitner, A., Aebersold, R., Boehringer, D., and Ban, N. (2015) The complete structure of the 55S mammalian mitochondrial ribosome. *Science* **348,** 303–308
16. Liu, M., and Spremulli, L. (2000) Interaction of mammalian mitochondrial ribosomes with the inner membrane. *J. Biol. Chem.* **275,** 29400–29406
17. Pfeffer, S., Woellhaf, M. W., Herrmann, J. M., and Forster, F. (2015) Organization of the mitochondrial translation machinery studied in situ by cryoelectron tomography. *Nat. Commun.* **6,** 6019
18. Greber, B. J., Boehringer, D., Leibundgut, M., Bieri, P., Leitner, A., Schmitz, N., Aebersold, R., and Ban, N. (2014) The complete structure of the large subunit of the mammalian mitochondrial ribosome. *Nature* **515,** 283–286
19. Sharma, M. R., Koc, E. C., Datta, P. P., Booth, T. M., Spremulli, L. L., and Agrawal, R. K. (2003) Structure of the mammalian mitochondrial ribosome reveals an expanded functional role for its component proteins. *Cell* **115,** 97–108
20. Greber, B. J., Boehringer, D., Leitner, A., Bieri, P., Voigts-Hoffmann, F., Erzberger, J. P., Leibundgut, M., Aebersold, R., and Ban, N. (2014) Architecture of the large subunit of the mammalian mitochondrial ribosome. *Nature* **505,** 515–519
21. Lurin, C., Andrés, C., Aubourg, S., Bellaoui, M., Bitton, F., Bruyère, C., Caboche, M., Debast, C., Gualberto, J., Hoffmann, B., Lecharny, A., Le Ret, M., Martin-Magniette, M. L., Mireau, H., Peeters, N., Renou, J. P., Szurek, B., Taconnat, L., and Small, I. (2004) Genome-wide analysis of Arabidopsis pentatricopeptide repeat proteins reveals their essential role in organelle biogenesis. *Plant Cell* **16,** 2089–2103
22. Uyttewaal, M., Mireau, H., Rurek, M., Hammani, K., Arnal, N., Quadrado, M., and Giegé, P. (2008) PPR336 is associated with polysomes in plant mitochondria. *Mol. J. Biol.* **375,** 626–636
23. Leaver, C. J., and Harmey, M. A. (1973) Plant mitochondrial nucleic acids. *Biochem. Soc. Symposia* **38,** 175–193
24. Vasconcelos, A. C., and Bogorad, L. (1971) Proteins of cytoplasmic, chloroplast, and mitochondrial ribosomes of some plants. *Biochim. Biophys. Acta* **228,** 492–502
25. Pinel, C., Douce, R., and Mache, R. (1986) A study of mitochondrial ribosomes from the higher plant Solanum tuberosum L. *Mol. Biol. Reports* **11,** 93–97
26. Maffey, L., Degand, H., and Boutry, M. (1997) Partial purification of mitochondrial ribosomes from broad bean and identification of proteins encoded by the mitochondrial genome. *Mol. General Gen.* **254,** 365–371
27. Heazlewood, J. L., Tonti-Filippini, J. S., Gout, A. M., Day, D. A., Whelan, J., and Millar, A. H. (2004) Experimental analysis of the Arabidopsis mitochondrial proteome highlights signaling and regulatory components, provides assessment of targeting prediction programs, and indicates plant-specific mitochondrial proteins. *Plant Cell* **16,** 241–256
28. Huang, S., Taylor, N. L., Narsai, R., Eubel, H., Whelan, J., and Millar, A. H. (2009) Experimental analysis of the rice mitochondrial proteome, its biogenesis, and heterogeneity. *Plant Physiol.* **149,** 719–734
29. Klodmann, J., Senkler, M., Rode, C., and Braun, H. P. (2011) Defining the protein complex proteome of plant mitochondria. *Plant Physiology* **157,** 587–598
30. Salvato, F., Havelund, J. F., Chen, M., Rao, R. S., Rogowska-Wrzesinska, A., Jensen, O. N., Gang, D. R., Thelen, J. J., and Møller, I. M. (2014) The potato tuber mitochondrial proteome. *Plant Physiol.* **164,** 637–653
31. Senkler, J., Senkler, M., Eubel, H., Hildebrandt, T., Lengwenus, C., Schertl, P., Schwarzländer, M., Wagner, S., Wittig, I., and Braun, H. P. (2017) The mitochondrial complexome of Arabidopsis thaliana. *Plant J.* **89,** 1079–1092
32. Wegrzyn, R. D., and Deuerling, E. (2005) Molecular guardians for newborn proteins: ribosome-associated chaperones and their role in protein folding. *Cell. Mol. Life Sci.* **62,** 2727–2738
33. Pfeffer, S., Woellhaf, M. W., Herrmann, J. M., and Förster, F. (2015) Organization of the mitochondrial translation machinery studied in situ by cryoelectron tomography. *Nature Commun.* **6,** 6019
34. Heide, H., Bleier, L., Steger, M., Ackermann, J., Dröse, S., Schwamb, B., Zörnig, M., Reichert, A. S., Koch, I., Wittig, I., and Brandt, U. (2012) Complexome profiling identifies TMEM126B as a component of the mitochondrial complex I assembly complex. *Cell Metabolism* **16,** 538–549
35. Strecker, V., Wumaier, Z., Wittig, I., and Schägger, H. (2010) Large pore gels to separate mega protein complexes larger than 10 MDa by blue native electrophoresis: isolation of putative respiratory strings or patches. *Proteomics* **10,** 3379–3387
36. Cavalcanti, J. H. F., Quinhones, C. G. S., Schertl, P., Brito, D. S., Eubel, H., Hildebrandt, T., Nunes-Nesi, A., Braun, H. P., and Araújo, W. L. (2017) Differential impact of amino acids on OXPHOS system activity following carbohydrate starvation in Arabidopsis cell suspensions. *Physiologia Plantarum* **161,** 451–467
37. Thal, B., Braun, H. P., and Eubel, H. (2018) Proteomic analysis dissects the impact of nodulation and biological nitrogen fixation on Vicia faba root nodule physiology. *Plant Mol. Biol.* **97,** 233–251
38. Cox, J., and Mann, M. (2008) MaxQuant enables high peptide identification rates, individualized p.p.b.-range mass accuracies and proteome-wide protein quantification. *Nat. Biotechnol.* **26,** 1367–1372
39. Schwanhäusser, B., Busse, D., Li, N., Dittmar, G., Schuchhardt, J., Wolf, J., Chen, W., and Selbach, M. (2011) Global quantification of mammalian gene expression control. *Nature* **473,** 337–342
40. Giese, H., Ackermann, J., Heide, H., Bleier, L., Dröse, S., Wittig, I., Brandt, U, and Koch, I. (2015) NOVA: a software to analyze complexome profiling data. *Bioinformatics* **31,** 440–441
41. Liu, X., Yang W. C., Gao, Q, and Regnier, F. (2008) Toward chromatographic analysis of interacting protein networks. *J. Chromatography* **1178,** 24–32
42. Kirkwood, K. J., Ahmad, Y., Larance, M., and Lamond, A. I. (2013) Characterization of native protein complexes and protein isoform variation using size-fractionation-based quantitative proteomics. *Mol. Cell. Proteomics* **12,** 3851–3873
43. Wan, C., Borgeson, B., Phanse, S., Tu F., Drew, K., Clark, G., Xiong, X., Kagan, O., Kwan, J., Bezginov, A., Chessman, K., Pal S., Cromar, G., Papoulas, O., Ni, Z., Boutz, D. R., Stoilova, S., Havugimana, P. C., Guo, X., Malty, R. H., Sarov, M., Greenblatt, J., Babu, M., Derry, W. B., Tillier,

Downloaded from http://www.mcponline.org/ at LEIBNIZ UNIVERSITÄT HANNOVER on August 9, 2019

E. R., Wallingford, J. B., Parkinson, J., Marcotte, E. M., and Emili, A. (2015) Panorama of ancient metazoan macromolecular complexes. *Nature* **525,** 339–344
44. Olinares, P. D. B., Ponnala, L., and van Wijk, K. J. (2010) Megadalton complexes in the chloroplast stroma of Arabidopsis thaliana characterized by size exclusion chromatography, mass spectrometry, and hierarchical clustering. *Mol. Cell. Proteomics* **9,** 1594–1615
45. Aryal, U. K., Xiong, Y., McBride, Z., Kihara, D., Xie, J., Hall, M. C., and Szymanski, D. B. (2014) A proteomic strategy for global analysis of plant protein complexes. *Plant Cell* **26,** 3867–3882
46. Aryal, U. K., McBride, Z., Chen, D., Xie, J., and Szymanski, D. B. (2017) Analysis of protein complexes in Arabidopsis leaves using size exclusion chromatography and label-free protein correlation profiling. *J. Proteomics* **166,** 8–18
47. McBride, Z., Chen, D., Reick, C., Xie, J., and Szymanski, D. B. (2017) Global analysis of membrane-associated protein oligomerization using protein correlation profiling. *Mol. Cell. Proteomics* **16,** 1972–1989
48. Cox, J., and Mann, M. (2008) MaxQuant enables high peptide identification rates, individualized p.p.b.-range mass accuracies and proteome-wide protein quantification. *Nature Biotechnol.* **26,** 1367–1372
49. Hooper, C. M., Tanz, S. K., Castleden, I. R., Vacher, M. A., Small, I. D., and Millar, A. H. (2014) SUBAcon: a consensus algorithm for unifying the subcellular localization data of the Arabidopsis proteome. *Bioinformatics* **30,** 3356–3364
50. Braun, H. P., Binder, S., Brennicke, A., Eubel, H., Fernie, A. R., Finkemeier, I., Klodmann, J., König, A. C., Kühn, K, Meyer, E., Obata, T., Schwarzländer, M., Takenaka, M., and Zehrmann, A. (2014) The life of plant mitochondrial complex I. *Mitochondrion* **19,** 295–313
51. Eubel, H., Jänsch, L., and Braun, H. P. (2003) New insights into the respiratory chain of plant mitochondria. Supercomplexes and a unique composition of complex II. *Plant Physiol.* **133,** 274–286
52. Patel, M. S., Nemeria, N. S., Furey, W., and Jordan, F. (2014) The pyruvate dehydrogenase complexes: structure-based function and regulation. *J. Biol. Chem.* **289,** 16615–16623
53. Bonen, L., and Calixte, S. (2006) Comparative analysis of bacterial-origin genes for plant mitochondrial ribosomal proteins. *Mol. Biol. Evolution* **23,** 701–712
54. Carroll, A. J., Heazlewood, J. L., Ito, J., and Millar, A. H. (2008) Analysis of the Arabidopsis cytosolic ribosome proteome provides detailed insights into its components and their post-translational modification. *Mol. Cell. Proteomics* **7,** 347–369
55. Suissa, M., and Schatz, G. (1982) Import of proteins into mitochondria. Translatable mRNAs for imported mitochondrial proteins are present in free as well as mitochondria-bound cytoplasmic polysomes. *J. Biol. Chem.* **257,** 13048–13055
56. Hummel, M., Dobrenel, T., Cordewener, J. J., Davanture, M., Meyer, C., Smeekens, S. J., Bailey-Serres, J., America, T. A., and Hanson, J. (2015) Proteomic LC-MS analysis of Arabidopsis cytosolic ribosomes: Identification of ribosomal protein paralogs and re-annotation of the ribosomal protein genes. *J. Proteomics* **128,** 436–449
57. Waltz, F., Nguyen, T. T., Arrivé, M., Bochler, A., Chicher, J., Hammann, P., Kuhn, L., Quadrado, M., Mireau, H., Hashem, Y., and Giegé, P. (2019) Small is big in Arabidopsis mitochondrial ribosome. *Nature Plants* **5,** 106–117
58. Piechota, J., Kolodziejczak, M., Juszczak, I., Sakamoto, W., and Janska, H. (2010) Identification and characterization of high molecular weight complexes formed by matrix AAA proteases and prohibitins in mitochondria of Arabidopsis thaliana. *J. Biol. Chem.* **285,** 12512–12521
59. Kolodziejczak, M., Skibior-Blaszczyk, R., and Janska, H. (2018) m-AAA complexes are not crucial for the survival of Arabidopsis under optimal growth conditions despite their importance for mitochondrial translation. *Plant Cell Physiol.* **59,** 1006–1016
60. Gehl, B., Lee, C. P., Bota, P., Blatt, M. R., and Sweetlove, L. J. (2014) An Arabidopsis stomatin-like protein affects mitochondrial respiratory supercomplex organization. *Plant Physiol.* **164,** 1389–1400
61. Mitsopoulos, P., Lapohos, O., Weraarpachai, W., Antonicka, H., Chang, Y. H., and Madrenas, J. (2017) Stomatin-like protein 2 deficiency results in impaired mitochondrial translation. *PloS One* **12,** e0179967
62. Zaegel, V., Guermann, B., Le Ret, M., Andrés, C., Meyer, D., Erhardt, M., Canaday, J., Gualberto, J. M., and Imbault, P. (2006) The plant-specific ssDNA binding protein OSB1 is involved in the stoichiometric transmission of mitochondrial DNA in Arabidopsis. *Plant Cell* **18,** 3548–3563
63. Barkan, A., and Small, I. (2014) Pentatricopeptide repeat proteins in plants. *Ann. Rev. Plant Biol.* **65,** 415–442
64. Williams, P. M., and Barkan, A. (2003) A chloroplast-localized PPR protein required for plastid ribosome accumulation. *Plant J.* **36,** 675–686
65. Aphasizheva, I., Maslov, D. A., Qian, Y., Huang, L., Wang, Q., Costello, C. E., and Aphasizhev, R. (2016) Ribosome-associated pentatricopeptide repeat proteins function as translational activators in mitochondria of trypanosomes. *Mol. Microbiol.* **99,** 1043–1058
66. Hammani, K., Gobert, A., Hleibieh, K., Choulier, L., Small, I., and Giegé, P. (2011) An Arabidopsis dual-localized pentatricopeptide repeat protein interacts with nuclear proteins involved in gene expression regulation. *Plant Cell* **23,** 730–740
67. Andrés-Colás N., Zhu, Q., Takenaka, M., De Rybel, B., Weijers, D., and Van Der Straeten, D. (2017) Multiple PPR protein interactions are involved in the RNA editing system in Arabidopsis mitochondria and plastids. *Proc. Natl. Acad. Sci. U.S.A.* **114,** 8883–8888
68. Verbitskiy, D., Zehrmann, A., Brennicke, A., and Takenaka, M. (2010) A truncated MEF11 protein shows site-specific effects on mitochondrial RNA editing. *Plant Signaling Behavior* **5,** 558–560
69. Sosso, D., Mbelo, S., Vernoud, V., Gendrot, G., Dedieu, A., Chambrier, P., Dauzat, M., Heurtevin, L., Guyon, V., Takenaka, M., and Rogowsky, P. M. (2012) PPR2263, a DYW-subgroup pentatricopeptide repeat protein is required for mitochondrial nad5 and cob transcript editing mitochondrion biogenesis and maize growth. *Plant Cell* **24,** 676–691
70. Schägger, H., and von Jagow, G. (1991) Blue native electrophoresis for isolation of membrane protein complexes in enzymatically active form. *Anal. Biochem.* **199,** 223–231
71. Yoshida, H., Maki, Y., Kato, H., Fujisawa, H., Izutsu, K., Wada, C., and Wada, A. (2002) The ribosome modulation factor (RMF) binding site on the 100S ribosome of Escherichia coli. *J. Biochem.* **132,** 983–989
72. Beckert, B., Turk, M., Czech, A., Berninghausen, O., Beckmann, R., Ignatova, Z., Plitzko, J. M., and Wilson, D. N. (2018) Structure of a hibernating 100S ribosome reveals an inactive conformation of the ribosomal protein S1. Nat. Microbiol. **3,** 1115–1121
73. Ueta, M., Ohniwa, R. L., Yoshida, H., Maki, Y., Wada, C., and Wada, A. (2008) Role of HPF (hibernation promoting factor) in translational activity in Escherichia coli. *J. Biochem.* **143,** 425–433
74. Franken, L. E., Oostergetel, G. T., Pijning, T., Puri, P., Arkhipova, V., Boekema, E.J., Poolman, B., and Guskov, A. (2017) A general mechanism of ribosome dimerization revealed by single-particle cryo-electron microscopy. *Nat. Commun.* **8,** 722
75. Trösch, R., and Willmund, F. (2019) The conserved theme of ribosome hibernation: from bacteria to chloroplasts of plants. *Biol. Chem.* 10.1515/hsz-2018-0436
76. Huxley, H. E., and Zubay, G. (1960) Electron microscope observations on the structure of microsomal particles from Escherichia coli. *J. Mol. Biol.* **2,** 10-IN8
77. Matzov, D., Aibara, S., Basu, A., Zimmerman, E., Bashan, A., Yap, M. N. F., Amunts, A., and Yonath, A. E. (2017) The cryo-EM structure of hibernating 100S ribosome dimer from pathogenic Staphylococcus aureus. *Nat. Comm.* **8,** 723
78. Tiller, N., and Bock, R. (2014) The translational apparatus of plastids and its role in plant development. *Mol. Plant* **7,** 1105–1120

Downloaded from http://www.mcponline.org/ at LEIBNIZ UNIVERSITÄT HANNOVER on August 9, 2019

© 2019 by The American Society for Biochemistry and Molecular Biology, Inc.
This paper is available on line at http://www.mcponline.org

Additions and Corrections

VOLUME 18 (2019) PAGES 1345–1362
DOI 10.1074/mcp.AAC119.001674

Correction: Complexome Profiling Reveals Association of PPR Proteins with Ribosomes in the Mitochondria of Plants.

Nils Rugen, Henryk Straube, Linda E. Franken, Hans-Peter Braun, and Holger Eubel

Due to publisher error, several of the symbols for the author affiliations and grant support did not indicate the correct information. This error has been corrected in the online version of this article.

Appendix

Curriculum Vitae

Personal Details

Name:	Nils Rugen
Date of Birth:	May 19, 1989
Place of Birth:	Zeven, Germany
Citizenship:	German

School Education

2006 – 2009	Oberstufe / Sekundarstufe II der Kooperativen Gesamtschule Tarmstedt **"Abitur"**, grade: 2.7
2002 – 2006	Sekundarstufe I der Kooperativen Gesamtschule Tarmstedt
2000 – 2002	Orientierungsstufe der Kooperativen Gesamtschule Tarmstedt
1996 – 2000	Grundschule Tarmstedt

Academic Education

Since June 2016	**PhD student** Institute of Plant Genetics Plant Proteomics Department Leibniz University Hannover Prof. Dr. Hans-Peter Braun
10/2013 – 10/2015	**Master of Science „Biomedicine"**, grade: 1.7 Hannover Medical School (MHH), Germany Thesis: „LFQ- and SILAC-based proteome analyses of surface attachment in *Pseudomonas aeruginosa*"
10/2010 – 09/2013	**Bachelor of Science "Biology"**, grade: 1.6 University of Göttingen, Germany Thesis: *„Interaktion von TRIM21 mit deletierter RING- und PRYSPRY-Domäne mit Salmonella enterica*"

List of Publications

- Niehaus, M. ,Straube, H.,Künzler, P., **Rugen, N**.,Giavalisco, P.,Eubel, H.,Witte, C.-P &Herde, M. (2019)

  Rapid affinity purification of tagged plant mitochondria (Mito-AP) for metabolome and proteome analyses.

  Plant Physiology **– revised version in preparation**

- Fuchs, P.[#], **Rugen, N.[#]**, Carrie, C., Elsässer, M., Finkemeiner, I., Giese, J., Hildebrandt, T.M., Kühn, K., Maurio, V.G., Ruberti, C., Schallenberg-Rüdinger, M., Steinbeck, J., Braun, H.-P., Eubel, H., Meyer, E.H., Müller-Schüssele, S.J. & Schwarzländer, M. (2019)

  Single organelle function and organization as estimated from Arabidopsis mitochondrial proteomics.

  [#] authors contributed equally

  The Plant Journal, in press, DOI: 10.1111/tpj.14534

- Batista-Silva, W., Heinemann, B., **Rugen, N.**, Nunes-Nesi, A., Araújo, W. L., Braun, H. P., & Hildebrandt, T. M. (2019).

  The role of amino acid metabolism during abiotic stress release.

  Plant Cell and Environment, *42*(5), 1630–1644.

- **Rugen, N.**, Straube, H., Franken, L. E., Braun, H.-P., & Eubel, H. (2019).

  Complexome profiling reveals association of PPR proteins with ribosomes in the mitochondria of plants.

  Molecular & Cellular Proteomics, *18*, 1345–1362.

- Senkler, J., **Rugen, N.**, Eubel, H., Hegermann, J., & Braun, H.-P. (2018).

  Absence of Complex I Implicates Rearrangement of the Respiratory Chain in European Mistletoe.

  Current Biology, *28*(10), 1606-1613.

- Krueger, J., Pohl, S., Preusse, M., Kordes, A., **Rugen, N.**, Schniederjans, M., Pich, A. & Häussler, S. (2016).

  Unravelling post-transcriptional PrmC-dependent regulatory mechanisms in *Pseudomonas aeruginosa*.

  Environmental Microbiology, 18(10), 3583–3592.

Conference Contributions

Oral Presentations

- **German Plant Mitochondria Initiative**
  November 28-29, 2016, Münster (Germany)
  Rugen N: “An introduction to large-pore native gels for identification of protein:protein interactions“.

- **German Plant Mitochondria Initiative**
  Oktober 19-20, 2017, Hannover (Germany)
  Rugen N: “Defining the subunit composition of mega-complexes in *Arabidopsis thaliana*“

- **German Plant Mitochondria Initiative**
  April 18-19, 2018, Bonn (Germany)
  Rugen N: “Ribosomal and metabolic protein complexes in plant mitochondria“

Poster Presentations

- **10th International Conference for Plant Mitochondrial Biology (ICPMB)**
  May 22-27, 2017, Hangzhou (China)
  Rugen N, Braun HP, Eubel H: “Altered micro-compartmentalization in plant mitochondria from autotrophic and heterotrophic plant tissues“

- **11th International Conference for Plant Mitochondrial Biology (ICPMB)**
  March 10-15, 2019, Ein Gedi (Israel)
  Rugen N, Braun HP, Eubel H: “Dynamic protein complexes in light-adapted and dark-adapted plant mitochondria”

Danksagung

Lieber Hans-Peter, dir möchte ich dafür danken, dass ich meine Doktorarbeit bei dir und deiner tollen Abteilung anfertigen durfte. Vielen Dank dafür, dass ich hier die Welt der Pflanzen, Mitochondrien und natürlich der Proteomik eintauchen konnte. Auch möchte ich dir dafür danken, dass ich an gleich zwei ICPMBs in China und Israel teilnehmen konnte. Das ist für einen Doktoranden nicht selbstverständlich und du sollst wissen, dass ich das absolut zu schätzen weiß.

Holger… wo fange ich da an? Erstmal danke dass du damals Klaus von der MHH eingestellt hast. Du bist ein spitzenmäßiger Betreuer und ich danke dir für alles, was ich bei dir gelernt habe, sei es Pflanzenbiologie, Proteomik, Kniffe am MS, Musikgeschichte, wie ein (Elektro-)Auto funktioniert, oder was die Turbojugend ist und wie sie feiert. Ich danke dir für deine Geduld (Gerade in den letzten Wochen) und dass du immer ein offenes Ohr für jede (noch so dumme) Frage hattest. Natürlich auch danke, dass ich mir deinen Sprinter für mein Umzugshobby leihen durfte (Schon Fast 12 Monate in der gleichen Wohnung!).

Laura. Dir möchte ich für so vieles danken, wir haben hier aber nur eine Seite Platz. Du hast mir gerade in den letzten intensiven Wochen dieser Arbeit sehr viel Rückhalt gegeben und musstest sehr viel zurückstecken. Du hast dich um die Wohnung, mich und tausend andere Dinge gekümmert und ich danke dir zutiefst, dass du das mit mir durchgestanden hast.

Allen Mitarbeitern der Abteilung Pflanzenproteomik danke ich natürlich auch. Jeder von euch hat mir in den letzten Jahren auf irgendeine Art und Weise bei meiner Arbeit geholfen. Sei es Jenny, die mir das Präpen und BN-Gele beibrachte, Marianne, die hunderte (oder tausende? Marianne?) MS-Proben für mich verarbeitet hat oder auch Michael, der in der Lösung unzähliger PC-/Daten-/Programm-und Statistik-Probleme beteiligt war. Die Bande aus Büro 007 soll natürlich nicht unerwähnt bleiben. Jungs, danke fürs Mörsern bei den unzähligen Mito-Isolationen, die gute Stimmung im Büro und die geile Zeit (Gerade in Israel). Ich danke euch allen!

Abschließend danke ich meiner Familie. Ohne eure Unterstützung in all den Jahren wäre ich nicht da, wo ich heute bin. Mutti, Andy, Lars & Lisa: Danke!